REICHHARDT F J

A PETROLOGICAL INVESTIGATION OF THE TRANSITION FROM THE LOWER TO THE UPPER CRITICAL ZONE IN THE CENTRAL SECTOR OF THE EASTERN BUSHVELD COMPLEX

PhD UP 1989

A petrological investigation of the transition from the lower to the upper critical zone in the central sector of the eastern Bushveld Complex

by

Friedrich Johannes Reichhardt

Submitted in partial fulfilment of the requirements
for the degree of
Doctor of Philosophy
in the Faculty of Science
University of Pretoria

Pretoria, 1989

If ever anyone discovers exactly how the Bushveld Complex formed and why it is here, it will instantly disappear and be replaced by something even more bizarre and inexplicable

after Douglas Adams

ABSTRACT

The transition from the lower to the upper critical zone and associated rocks (LG 6 - UG 1) has been investigated geochemically and petrographically. This well-layered and lithologically heterogeneous succession is explained by a scheme of stratified hybrid layers and by a combination of crystal/liquid slumping and crystallization of the bottom liquid. Intermittent magma influxes occurred prior to the formation of the LG 6 chromitite layer, the F and the L units.

It is proposed that the addition of relatively cool and dense tholeiitic liquid (B2/B3 type) initiated the collapse of orthopyroxene-bearing plumes from the overlying hot and less dense boninitic liquid (B1 type). The formation of chromite is attributed to a reaction process between the two chemically distinct liquids during the descent of crystal-laden boninitic plumes.

Whole rock incompatible trace element data and Sr-isotopes confirm that B1 and B2 liquids are parental liquids to the pyroxenitic lower critical zone. Addition of B2 or B3 liquid and subsequent mixing with resident hybrid liquids is believed to have formed the plagioclase-dominant cumulates of the upper critical zone.

Variations in mineral chemistry have been explained by changes in magma composition and by a series of postcumulus processes. Orthopyroxene composition has been substantially modified by re-equilibration with surrounding hybrid liquid and with chromite. Various degrees of interstitial melt fractionation and different diffusion rates for the individual elements (Fe-Mg >> Ti > Al and Cr > Ca) are indicated by the complex orthopyroxene zoning pattern. The compositional shift in orthopyroxene chemistry has been quantified and a correction method is presented to recalculate the original composition prior to the effects of re-equilibration with evolved trapped liquid and modal chromite.

Significant plagioclase variation is only found in the feldspathic pyroxenites of the lower critical zone. Limited exchange of pore liquid in the crystal pile resulted in fractionation cycles and in the development of multiple crystallization fronts. Extreme trapped liquid

fractionation is evidenced by the presence of quartz, mica, sodic plagioclase and K-feldspar with accessory rutile, loveringite, apatite and anhydrite. In contrast, liquid fractionation appears to be relatively unimportant during crystallization of the upper critical zone where changes in plagioclase composition are decoupled from variations in orthopyroxene composition.

Orthopyroxene shows distinct textural changes associated with the first occurrence of cumulus plagioclase at the lower/upper critical zone boundary (E/F boundary). Orthopyroxenes from the upper critical zone are smaller, contain numerous tiny plagioclase inclusions and have generally more evenly shaped crystal faces compared to the lower critical zone. The simultaneous change towards anhedral (intercumulus) textures with an increase in plagioclase (F and H units) is explained by the fact that orthopyroxene which was added by crystal/liquid slumping is not a stable liquidus phase in a relatively pure B2/B3 liquid. The presence of plagioclase inclusions in orthopyroxene is thought to reflect crystallization from a pyroxene-undersaturated liquid (B2/B3). The latter must have been hybridised by B1 material (crystal-bearing plumes) to account for the high modal amount of orthopyroxene in the G and J units.

A positive correlation between the thickness of individual stratigraphic units and the floor morphology has been found in the Maandagshoek area and adjoining areas: Lithological units thin out above and marginal to anticlinal floor structures and thicken in trough-like, synclinal areas. The observed changes in thickness do not display any changes in mineral composition.

The frequency of pegmatites increase significantly near anticlinal structures. It is postulated that late migrating fluids followed the palaeotopography and were therefore forced upwards at anticlinal structures. Isotopic data of metasomatically altered rocks suggest that hydrous fluids are partially sediment derived and are not simply the result of interstitial melt fractionation. Magma replenishment caused probably an increased fluid activity due to the degassing of sedimentary fragments which were draged into the chamber.

The meagre development of middle group chromitite layers (MG 1-4) throughout the central sector is explained by the additional influx of tholeiitic liquid (J and K units) to the central sector. Middle group

layers are well developed in the southern and western sectors where the J and K units are either absent or drastically reduced in thickness. The pyroxenitic L unit and associated upper middle group chromitite layers (UMG 1-3) of the central sector can be correlated with the uppermost middle group chromitite layer (MG 4) and enclosing pyroxenites of the southern and western sectors.

SAMEVATTING

Die oorgang van die onderste na die boonste kritiese sone en geassosieerde gesteentes (LG 6 - UG 1) is geochemies en petrografies ondersoek. Hierdie goed gelaagde en litologies heterogene opeenvolging word deur middel van 'n skema van gestratifiseerde hibriede lae en deur 'n kombinasie van insinking van 'n kristal-vloeistofmengsel en kristallisasie van die onderste vloeistoflaag verklaar. Inplasing van nuwe magma het voor die ontstaan van die LG 6 chromitietlaag, die F eenheid en die L eenheid plaasgevind.

Dit word aan die hand gedoen dat die toevoeging van relatief koel en digte tholeiitiese magma (B2/B3 tipe) die insakking van ortopirokseendraende vloeistof van die oorliggende warm en minder digte boninitiese B1-tipe magma geïnisieer het. Die vorming van chromiet word toegeskryf aan 'n reaksieproses tussen die twee chemies kenmerkende vloeistowwe tydens die versakking van die kristalbelaaide boninitiese magma.

Onversoenbare spoorelementgegewens van heelgesteentes en Sr-isotope bevestig dat B1 en B2 magmas die moedermagmas van die piroksenitiese, laer kritiese sone was. Toevoeging van B2 of B3 magma en daaropvolgende vermenging met residerende hibriede vloeistowwe word veronderstel om oorsprong aan die plagioklaas oorheersende kumulate van die boonste kritiese sone te gegee het.

Variasies in die mineraalchemie is verduidelik d.m.v. veranderings in magmasamestelling en 'n verskeidenheid van nakumulus prosesse. Ortopirokseensamestellings is aansienlik gemodifiseer deur herekwilibrasie met omgewende, hibriede vloeistof en met chromiet. Verskeie grade van fraksionering van die tussenkorrelrige vloeistof, en verskillende diffusietempo's vir die individuele elemente (Fe-Mg >> Ti > Al en Cr > Ca) word deur ingewikkelde soneringspatrone in ortopirokseen aangedui. Die verandering in samestelling van die ortopirokseen is gekwantifiseer en 'n korreksiemetode word aan die hand gedoen om die oorspronklike samestelling voor die effekte van herekwilibrasie met ontwikkelde interstisiële vloeistof en modale chromiet te bereken.

Noemenswaardige variasie in die samestelling van die plagioklaas is slegs in die veldspatiese pirokseniete van die laer kritiese sone teëgekom. Beperkte uitruiling van porieë vloeistof in die kristal-

massa het aanleiding gegee tot fraksioneringsiklusse en die ontwikkeling van veelvuldige kristallisasiefronte. Uiterste fraksionering van vasgevangde tussenkorrelrige vloeistof word aangedui deur die teenwoordigheid van kwarts, glimmer, Na-plagioklaas en K-veldspaat, met rutiel, loveringiet, apatiet en anhidriet as aksessoriese minerale. In teenstelling hiermee blyk die fraksionering van vloeistof van minder belang tydens kristallisasie van die boonste gedeelte van die kritiese sone te wees, waar verandering in die samestelling van kumulus plagioklaas ontkoppel is van variasies in die ortopirokseensamestelling.
Ortopirokseen vertoon duidelike teksturele veranderinge geassosieer met die eerste voorkoms van kumulus plagioklaas by die E-F grens, d.w.s. tussen die onderste en boonste kritiese sone. Ortopirokseen van die boonste kritiese sone is kleiner, bevat talle klein insluitsels van plagioklaas en het oor die algemeen meer egalige kristalvlakke in vergelyking met die laer kritiese sone. Die gelyktydige verandering van anhedrale (interkumulus) tekstuur met 'n toename in plagioklaas (F- en H-eenhede) word verklaar deur die feit dat ortopirokseen wat deur kristal-vloeistof insinking toegevoeg is, nie 'n stabiele liquidusfase in 'n relatief suiwer B2/B3 magma is nie. Die teenwoordigheid van plagioklaasinsluitsels in ortopirokseen word beskou om kristallisasie van 'n pirokseen onderversadigde vloeistof (B2/B3) te reflekteer. Laasgenoemde moes deur B1 magma gehibridiseer gewees het om die lae modale hoeveelheid ortopirokseen in die G en J eenhede te verklaar.
'n positiewe korrelasie tussen die dikte van die individuele stratigrafiese eenhede en die vloermorfologie is in die Maandagshoek- en aanliggende gebiede erken. Litologiese eenhede is dunner bokant en langs antiklinale vloerstrukture en word dikker in die trogagtige sinklinale gebiede. Die waargenome veranderinge in dikte gaan nie gepaard met enige verandering in mineraalsamestelling nie.
Die hoeveelheid pegmatiete neem aansienlik toe naby antiklinale struktuure. Daar word gepostuleer dat laat, migrerende vloeistowwe die paleotopografie gevolg het en dus langs die antiklinale strukture opwaarts geforseer is. Isotoopgegewens van metasomaties veranderde gesteentes dui daarop dat water-ryk fluïdum gedeeltelik van sedimente afkomstig is en nie slegs die gevolg is van fraksionering van interstisiële smeltsel nie. Deur magmatoevoeging is die aktiwiteite van 'n

fluïede fase vermoedelik ook verhoog vanweë die ontgassing van sedimentfragmente wat ingesleep is in die magmakamer.
Die ondergeskikte ontwikkeling van die middelste groep van chromitietlae (MG 1 - 4) deur die hele sentrale sektor word verklaar deur die toevoeging van tholeiitiese vloeistof (J en K eenhede) tot hierdie sektor. Die middelste groep van chromitietlae is goed ontwikkel in die suidelike en westelike sektore waar die J en K eenhede of afwesig is of aansienlik dunner is. Die proksenitiese L eenheid en geassosieerde boonste middelgroep van chromitietlae (UMG 1 -3) van die sentrale sektor kan met die boonste chromitietlaag (MG 4) van die middelste groep en omsluitende pirokseniete in die suidelike en westelike sektore gekorreleer word.

CONTENTS

CHAPTER I: INTRODUCTION AND REVIEW Page 1

I.1. The Bushveld Complex 1
I.2. The eastern Bushveld Complex 2
I.3. The critical zone 2
I.4. The critical zone in the study area 5
I.5. Previous work in the critical zone 6
I.6. Previous work in the study area 8
I.7. Scope and aims of present study 9

CHAPTER II. FIELD RELATIONSHIPS, STRATIGRAPHY AND LITHOLOGY 11

II.1. Introduction 11
II.2. Rock nomenclature 12
II.3. The lower critical zone 13
II.3.1. Sequence below the LG 6 13
II.3.2. The D_2 unit 16
II.3.3. The E unit 16
II.4. The upper critical zone 17
II.4.1. The F unit 17
II.4.2. The G unit 18
II.4.3. The H unit 18
II.4.4. The J unit 19
II.4.5. The K unit 20
II.4.6. The L unit 21
II.4.7. The M unit 23
II.5. Summary 24
II.6. Lateral correlation of the LG 6 - UG 1 sequence 25
II.7. Distribution and proposed structural control of pegmatite formation 31

CHAPTER III: COMPLEX ZONING PATTERNS IN LOWER CRITICAL ZONE SILICATES 34

III.1. Introduction 34
III.1.1. Analytical procedures 35
III.2. Orthopyroxene 36
III.2.1. Orthopyroxene textures 36
III.2.1.1. Large grains 36
III.2.1.2. Small grains 38
III.2.2. Intra-grain compositional variation - orthopyroxene traverses 39
III.2.3. Inter-grain compositional variation 43
III.3. Plagioclase 49
III.3.1. Plagioclase traverses and inter-grain variation 49
III.4. Clinopyroxene 51
III.4.1. Textural features 51
III.4.2. Grain traverses and inter-grain variation 51
III.4.3. Clinopyroxene zoning - fractionation or re-equilibration ? 54

III.4.4. Crystallization temperature - an estimate 57
III.4.5. Proposed origin of clinopyroxene oikocrysts 59
III.5. Discussion of complex zoning patterns in orthopyroxene - evidence for subliquidus disequilibrium 60
III.5.1. Primary magmatic zoning and subsolidus re-equilibration 60
III.5.2. Reaction of orthopyroxene with intercumulus liquid 60
III.5.3. Element behaviour during re-equilibration 62
III.5.3.1. Calcium 62
III.5.3.2. Aluminium 63
III.5.3.3. Chromium 66
III.5.3.4. Titanium 66
III.5.3.5. Magnesium and Iron 68

CHAPTER IV: PLAGIOCLASE VARIATION - FRACTIONATION PROCESSES IN A CUMULATE PILE 70

IV.1. Sampling 70
IV.2. Plagioclase variation 70
IV.3. Intercumulus fractionation cycles - a model for intercumulus feldspar variation 76
IV.3.1. Cyclic plagioclase variation 76
IV.3.2. Physico-chemical considerations - accumulation rate, porosity and adcumulus growth 77
IV.3.3. Thermal considerations - diffusion rate versus crystallization rate 79
IV.3.4. Porosity and its elimination and the build-up of multiple crystallization fronts 81

CHAPTER V: PYROXENE VARIATION - THREE STAGE MODIFICATION OF MG# 82

V.1. Introduction 82
V.2. Stage one: Orthopyroxene - liquid reaction 83
V.3. Stage two: Orthopyroxene - trapped liquid reaction 89
V.4. Stage three: Orthopyroxene - chromite subsolidus re-equilibration 91
V.5. Stratigraphic variation after recalculation of Mg# 92
V.6. Summary of results derived from mineral variations 100

CHAPTER VI: MINERAL CHEMISTRY OF THE UPPER CRITICAL ZONE 102

VI.1. Plagioclase 102
VI.1.1. Plagioclase inclusions in orthopyroxene - evidence for magma mixing ? 105
VI.2. Orthopyroxene 112
VI.2.1. Mg# in orthopyroxene 112
VI.2.2. Chromium in orthopyroxene 116
VI.2.3. Aluminium in orthopyroxene 119
VI.2.4. Titanium in orthopyroxene 121
VI.2.5. Calcium in orthopyroxene 123
VI.3. Conclusions 125

CHAPTER VII: WHOLE ROCK CHEMISTRY 127

VII.1. Sampling 127
VII.2. Trace element abundance - indications for parental magma composition 127
VII.3. Sulphur and Copper 136
VII.4. Strontium 137

CHAPTER VIII: STRONTIUM ISOTOPES 139

VIII.1. Previous Sr isotope work on the Bushveld Complex 139
VIII.2. Sr isotope systematics of the proposed parental liquids 140
VIII.3. Sampling 141
VIII.4. Results 142

CHAPTER IX: DISCUSSION OF SR ISOTOPES AND PROPOSED MODEL FOR THE FORMATION OF THE LG 6 - UG 1 SEQUENCE 147

IX.1. The lower critical zone 147
IX.1.1. Introduction 147
IX.1.2. Crystal/liquid slumping - two phase convection 148
IX.1.3. Viscosity effects and crystallization in crystal/liquid plumes 151
IX.1.4. Formation of the D_2 and E units 152
IX.2. The transition from lower to upper critical zone 153
IX.2.1. Geochemical and lithological features - a review 153
IX.2.2. Magma replenishment - physico-chemical considerations 156
IX.2.3. Formation of the F unit 157
IX.2.4. Formation of middle group chromitite layers 158
IX.2.5. Formation of the G unit 160
IX.2.6. Formation of the H unit 160
IX.2.7. Formation of the J unit 161
IX.2.8. Formation of small-scale layering in the K unit 162
IX.2.9. Formation of the L unit 163
IX.2.10. Formation of the M unit 164
IX.2.10.1. Possible origin of the very fine grained gabbronorites in the M unit 165
IX.3. Summary 167

CHAPTER X: COMPOSITIONAL FEATURES AND SR ISOTOPES SYSTEMATICS OF CHEMICALLY ALTERED SEQUENCES 169

X.1. Mineral-chemical features 169
X.1.1. Proposed origin of chemically altered sequences 173
X.2. Sr isotopes systematics of chemically altered sequences 175
X.2.1. Sr isotopes of unusually calcic (high An) plagioclase separates 175

X.2.2. Sr isotopes of Rb-rich plagioclase separates 177
X.3. Summary 181

CHAPTER XI: SUMMARY AND CONCLUSIONS 182

ACKNOWLEDGEMENTS 186

REFERENCES 187

APPENDIX 198

A.I. Electron Microprobe Analyses 198
A.II. X-Ray Fluorescence Spectrometry 199
A.III. Sulphur Determination 199
A.IV. Analytical Procedures of Sr Isotopes 200

ANALYTICAL RESULTS 202

Mineral Analyses 202

Orthopyroxene 203
Plagioclase 215

Whole Rock Analyses 229

CHAPTER I: INTRODUCTION and REVIEW

I.1. THE BUSHVELD COMPLEX

The Bushveld Complex is an assemblage of Proterozoic plutonic and volcanic rocks covering roughly 65000 km² in the Eastern Transvaal, RSA. The outcrop pattern and geophysical data of the basic and ultra-basic plutonic rocks has led to the recognition of four compartments (Molyneux and Klinkert, 1978; Sharpe and Chadwick, 1982). Figure I.1 displays the localities of the compartments and adjacent rocks.

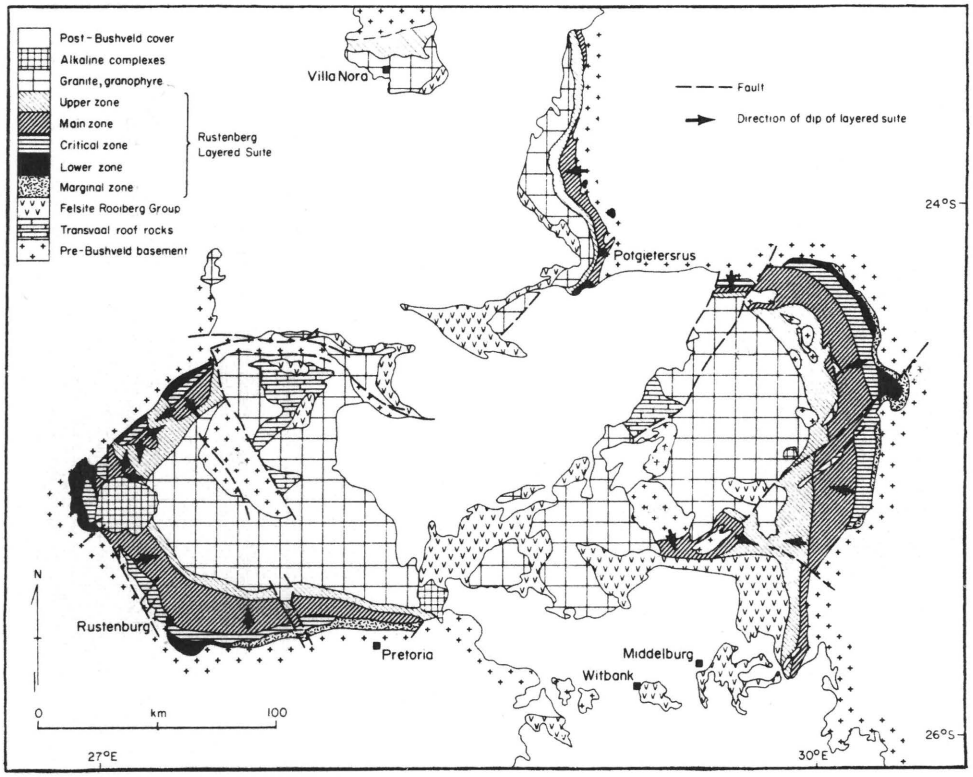

Figure I.1: Locality map of the Bushveld Complex showing the distribution of mafic rocks and adjacent rocks (after Tankard et al., 1982). The western, eastern, and northern (Potgietersrus and Villa Nora) compartments are displayed. The fourth lobe (far western compartment) is about 100 km to the west of the large alkaline intrusion (Pilanesberg) in the western compartment.

Hall (1932) subdivided the layered sequence into four major stratigraphic zones. Detailed work by various authors (e.g. Willemse, 1959, 1969; Molyneux, 1974 ; Cameron, 1964, 1978, 1980, 1982) has subsequently led to a further subdivision into subzones and units (Fig. I.2). A compilation of the most recent lithostratigraphic classification is given by the South African Committee for Stratigraphy (Kent, 1980).

I.2. THE EASTERN BUSHVELD COMPLEX

The Wonderkop and Steelpoort faults divide the eastern Bushveld compartment into three sectors (western, central and southern sector). The absence of lower zone rocks above the Schwerin anticline and the Derde Gelid pericline (Fig. I.3) has led to a further subdivision of the central sector into three geographically separated regions. These three troughs are referred to as the Jagdlust-, Clapham- and Winterveld sections. The rock sequence above the lower zone is continuous throughout the entire central sector.

I.3. THE CRITICAL ZONE

Cameron (1963) subdivided the critical zone in the eastern Bushveld Complex into a lower (pyroxenitic) and an upper (anorthositic) subzone. He (1964, 1980, 1982) further subdivided the entire zone into 16 principal units (B - Y), excluding the sequence from the base of the Merensky Reef to the top of the Bastard Reef (Fig. I.2). Each unit is characterized by an abrupt change in lithology, generally accompanied by changes in mineral chemistry, or by the appearance or disappearance of a mineral phase.

Feldspathic pyroxenites, norites and leuconorites (mottled and spotted anorthosites) are the predominant rock types; harzburgite, gabbronorite, anorthosite and chromitite represent less than 10 per cent of the sequence. Although chromitite layers and stringers are present throughout the critical zone they are localized in three distinct settings; viz. the lower group (LG), the middle and upper middle group (MG and UMG) and the upper group (UG) (classification after Cousins and Feringa, 1964; and Gain, 1981 (UMG)).

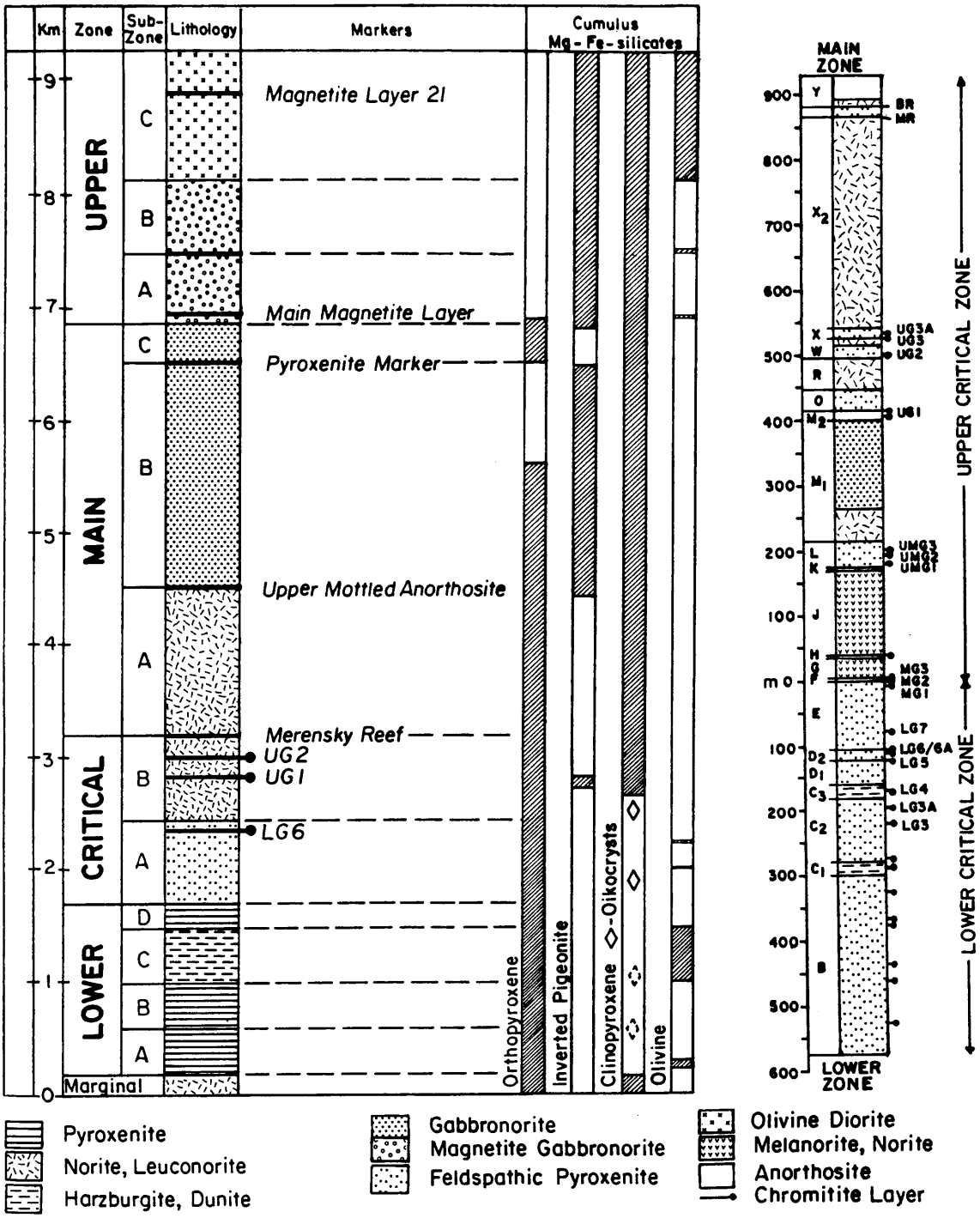

Figure I.2: Generalized stratigraphic section of the Bushveld Complex with detailed columnar section of the critical zone. Data compiled from South African Committee for Stratigraphy (Kent, 1980) and Cameron (1980, 1982). Distribution of cumulus Mg-Fe silicates is compiled from Cameron (1978, 1980, 1982), von Gruenewaldt (1971) and Molyneux (1970).

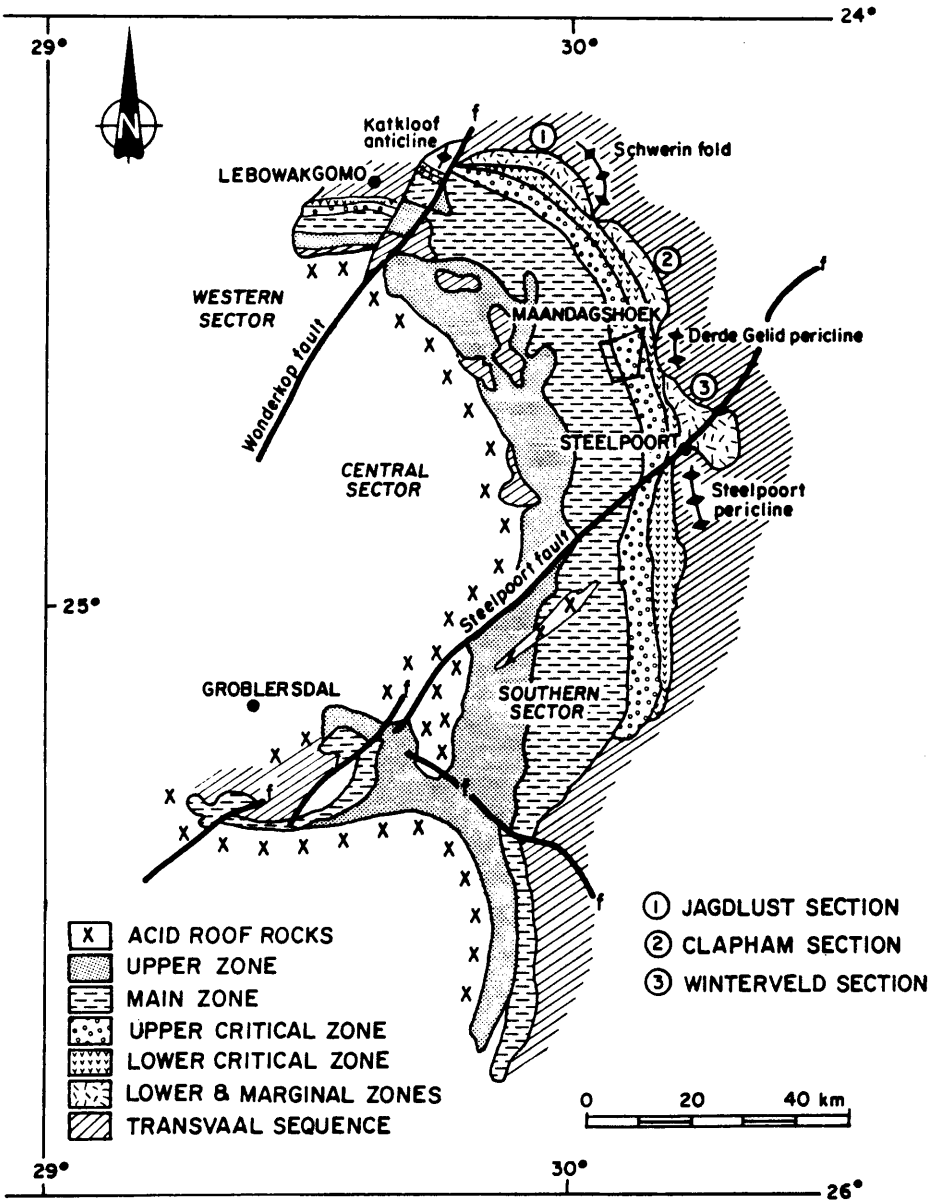

Figure I.3: Geology of the eastern Bushveld compartment showing the geographic position of floor folds and the study area. Data modified after the 1:1 000 000 map of the Geological Survey of South Africa.

Exposure of critical zone rocks in the central sector is generally good. Apart from the central area (Clapham section), the critical zone forms a continuous mountain range stretching for about 70 km from the Steelpoort River in the south to the Olifants River in the north. The homogeneous and rather fine grained leuconorites of the M-unit usually form prominent ridges which protect the underlying sequence from denudation.

The fact that the two highest peaks (1440 and 1400 m) in the critical zone are found where the floor folds protrude the layered sequence indicates that the quartzitic metasediments have protected the layered mafic rocks from erosion. The lack of exposure in the Clapham section can be explained by the large lateral distance (> 7 km) to the floor rocks.

I.4. THE CRITICAL ZONE IN THE STUDY AREA

The Maandagshoek area is situated adjacent to the Derde Gelid pericline, which separates the Clapham section from the Winterveld section (Fig. I.3). The topography in the Maandagshoek area is dominated by the north-south trending Lebalelo Mountain. This mountain range exhibits an almost complete section from below the C unit (LG 3) up to the base of the X unit (UG 3) (Fig. I.2). The remainder of the critical zone, including the Merensky Reef, is covered by scree and eluvial deposits. The lower part of the critical zone and the contact of the layered sequence with the floor rocks are also not exposed.

The updomed Transvaal sediments, mainly of the Lakenvalei Quartzite Formation border the layered sequence to the east, while in the west the steep cliffs of the Leolo Mountains, formed by norites and anorthosites of subzone A of the main zone, rise sharply for more than 800 m above the valley floor.

The Steelport chromitite layer (LG 6) is presently mined at several localities in the area, e.g. on the farm Hendriksplaats (Montrose Mine) just south of Maandagshoek, on Mooihoek/Maandagshoek itself (Dilokong Mine) and on Groothoek (Groothoek Mine) adjoining to the north. Local mining of the LG 3 and/or LG 3A has ceased long ago. The platiniferous "Mooihoek pipe" (see Viljoen and Scoon, 1985) situated in the area was mined out more than 20 years ago. Large scale mining

of the UG 2 and the Merensky Reef is planed to commence on Maandagshoek in the near future (The Star, 1988).

I.5. PREVIOUS WORK ON THE CRITICAL ZONE

The critical zone has long attracted interest for its chromitite layers which constitute the world's largest known chromite deposits. Although earliest reports of chromite in the Bushveld Complex date back to the year 1865 (Huebner, 1872), mining only started in 1917 on the farm Mooihoek (Kupferbürger et al., 1937). Since then the demand for chromite has increased production from 200 tons in 1917 to 100000 tons in 1935 and to about 3,3 Mio tons in 1985 (data from Kupferbürger et al., 1937; Minerals Bureau of S. A., 1986)

A similar development followed the discovery of platinum in 1923. The Merensky Reef, the platiniferous UG 2 chromitite layer and some ultramafic pegmatites are the main platinum-bearing units. No further specific reference to literature dealing with the Upper Group chromitite layers and the Merensky Reef will be made as this stratigraphic sequence falls outside the scope of this investigation.

The earliest reported studies on the chromite ore and its country rocks were carried out by Molengraaf (1901) and by Hall and Humphrey (1908). Detailed investigations on the chromite deposits were subsequently presented by Wagner (1923), Sampson (1932), Kupferbürger et al. (1937), van der Walt (1941) and by de Wet (1952). Most of the earlier work concentrated on the chromite ore and its economic aspects.

The unique variety of host rocks of the chromitite layers resulted in a number of systematic studies of these rocks by e.g. Henderson, (1898), Reuning (1928), Wagner (1929), Hall (1932), Lombaard (1934) and Kuschke (1939). Detailed fieldwork along with petrographic studies was carried out by Schwellnus (1956), Cameron and Emerson (1959), Schwellnus et al. (1962) and by Cameron (1963).

The primarily field orientated and more descriptive nature of the earlier studies and the limited amount of analytical data available, are likely reasons that the proposed genetic models for the critical zone were very much alike. They all follow the basic principles of fractional crystallization combined with crystal settling, with or

without periodic magma influxes at the bottom of the magma chamber. This standard model was modified by certain authors who advocated successive pulses of separate magmas, which had undergone differentiation at greater depths (Reuning, 1928; Lombaard, 1934; Coertze, 1958; Feringa, 1959; Cousins, 1959).

During the last 20 years many features of the critical zone were re-examined and re-interpreted as more and more geochemical and experimental data became available. The complex processes of crystallization, cooling, convection and periodic magma influxes into a stratified magma chamber have been subjected to numerous experiments (e.g. Turner, 1973, 1978, 1980; O'Hara, 1977; Turner and Gustafson, 1978, 1981; Chen and Turner, 1980; Irvine 1980a, b; McBirney, 1980; Huppert and Sparks, 1980; Huppert and Turner, 1981; Huppert et al., 1983; Sparks and Huppert, 1984;). The Rustenburg Layered Suite and the critical zone in particular have since become a testing ground for the validity and applicability of these new concepts. The following only summarizes the most pertinent work on the critical zone itself and the models which were applied to explain its diversity of rock types.

Jackson (1970) developed a concept whereby a cyclical repetition of rock units is explained by periodic magma convection, followed by closed system fractionation and crystal settling. In 1959 Cameron and Emerson already proposed a genetic model for the chromitite layers, which combined the effects of magma currents and differential rates of magmatic sedimentation.

The most complete documentation of critical zone lithology was presented by Cameron (1980, 1982), whose detailed petrographic studies together with mineral analyses of more than 1100 thin sections have since become a benchmark for critical zone stratigraphy. Cameron (1980) suggested that sudden changes in pressure and successive pulses of parental magma (1982) are the controlling mechanism for at least some of the observed mineralogical and chemical variations. However, a change in pressure was subsequently refuted by Hatton (1984) as a feasible mechanism to produce the observed chemical and mineralogical trends on the grounds of experimental results.

Petrological and geochemical evidence for at least two contrasting parental liquids to the critical zone, was given by Cawthorn and co-workers (1979, 1981), Davies et al. (1980) and by Sharpe (1981). The

earlier B1-type liquids (Sharpe, 1981) were SiO_2- and MgO-rich magmas similar to olivine boninites, whereas the other liquids were tholeiitic and referred to as B2 and B3 by Sharpe (1981). Irvine et al. (1983) termed the two lineages U and A because of their ultramafic (orthopyroxene) and anorthositic (plagioclase) rock products. Compositional differences between the two series in terms of Sr isotopic ratio and REE concentration are discussed in Chapter VIII.2.

Subsequently, Sharpe and Irvine (1983) carried out a series of melting experiments on mixtures of the postulated two parental compositions which showed that mixing of two magma types is a likely mechanism for producing chromitite layers (Irvine and Sharpe, 1986).

In 1983, Irvine et al. presented an elaborate and comprehensive model, whereby a stratified column of A and U type liquid layers separated by numerous diffusive interfaces, is visualized. According to this model lateral accretion of cumulate layers leads to internal fractionation and to "finger mixing" across the interfaces.

Eales et al. (1986) and Naldrett et al. (1987) presented petrogenetic models specifically concerned with the formation of the cyclic units in the upper critical zone and the Merensky Reef in particular. The authors used existing and new geochemical data to constrain genetic models and independently came to the conclusion that the cyclic units are caused by periodic injections of primitive magma, which subsequently fractionated and mixed with magma in the chamber to form hybrid liquid layers.

I.6. PREVIOUS WORK IN THE STUDY AREA

Kuschke (1939) optically determined orthopyroxene and plagioclase compositions in samples from below the LG 6 up to the Merensky Reef. The data presented show a general upward decrease in the Mg/Fe ratio of orthopyroxene, with an abrupt reversal at the level of the upper group chromitite layers. He interpreted the observed variation as being due to two separate and chemically distinct influxes of magma, each pulse undergoing in situ fractionation and possibly mixing with the previously emplaced magma. Kuschke also demonstrated that orthopyroxenes adjacent or closely associated with chromitite layers have

higher Mg/Fe ratios than those some distance above or below. The composition of the plagioclase shows no systematic variation and varies within a very restricted range between An 75 and An 84 with an average of An 81.

Detailed mapping in the Maandagshoek area and selective sampling allowed Heckroodt (1958) to determine the inter-relationship of the various rock types. With the aid of orthopyroxene chemistry, he could demonstrate an intimate relationship between the Mg/Fe ratio and the lithology, and points out that, although orthopyroxene exhibits an overall upward enrichment in iron, the absolute Mg/Fe values depend on the particular rock type. Bronzite in norite is generally richer in iron than bronzite in pyroxenite. This he interpreted as reflecting the existence of two different parental liquids. The intermediate iron content of orthopyroxene in melanorite is related to mixing between the two endmembers. Although Heckroodt's conclusions are based on a very limited data set, they are consistent with data from Schwellnus (1956) who investigated two comparable stratigraphic profiles to the north of Maandagshoek.

Cameron (1964) included two profiles from areas just north (Twyfelaar/Driekop) and south (Hendriksplaats) of Maandagshoek in his lateral correlation of critical zone lithology. These two columnar sections show that all the principal rock units of his type section in the Jagdlust-Wintersveld area are present in the Maandagshoek-Mooihoek area, although they vary considerably in thickness along strike. Cameron also briefly describes the chromitite layers in the two areas adjacent to the Maandagshoek-Mooihoek area.

Gain (1981, 1985) carried out a comprehensive study on the UG 1 - UG 3A interval, focussing on the geological setting and the geochemistry of the platinum-group elements in the UG 2. The observed modal variations of the major silicate minerals allowed him to define 4 cyclic units which were confirmed by the cryptic variation displayed in the mineral chemistry.

I.7. AIMS OF PRESENT STUDY

The above reviews of the critical zone and the evolution in the interpretation of geochemical features suggest that considerably more

detailed information is necessary for a better understanding of the complex processes that gave rise to the critical zone cumulates. The primary purpose of this investigation is to explain the chemical and textural features of the cumulates which straddle the transition from the lower to the upper critical zone in terms of magmatic and post-magmatic processes. The study also includes a re-examination of the lateral consistency of silicate and chromitite layers of the lower/upper critical zone transition within the eastern Bushveld compartment.

In order to achieve this, lithological changes, systematic variations in whole rock and mineral chemistry, the appearence and disappearence of mineral phases and textural changes are the main geological features which were studied in great detail.

This entailed the compilation of a comprehensive record of the chemistry and textures of the various silicates present in a 700 m section of the LG 6 - UG 1 sequence from the farm Maandagshoek in the central sector of the eastern Bushveld Complex. Chromite chemistry was not included, because this would expand this thesis beyond reasonable limits.

The mineral chemical data are supported by whole rock analyses and a strontium isotope study carried out on plagioclase separates. The latter was done to characterize the involvement of isotopically distinct liquids and to attempt a reconstruction of the presence of liquid layers.

To evaluate lateral variation in mineral chemistry, several stratigraphic units from adjacent drill-core material were also investigated and correlated.

Particular emphasis is given to those post-cumulus processes which most likely modified the original cumulus composition, such as those involving re-equilibration with interstitial liquid, subsolidus cation exchange between adjacent or enclosed mineral phases and late- or post-magmatic migration of hydrous fluids.

Mineral chemical, whole rock and isotopic data together with petrographic observations are synthesized in a petrogenetic model which attempts to link the facts to existing theoretically and experimentally derived concepts.

CHAPTER II: FIELD RELATIONSHIPS, STRATIGRAPHY AND LITHOLOGY

II.1. INTRODUCTION

Lithological information derived from drillcore material was supplemented by detailed mapping (1:20,000) on the farms Maandagshoek-254KT, Mooihoek-255 KT and Hendriksplaats-281 KT. Mapping was not confined to the stratigraphic sequence intersected by drillcores (LG 6 - UG 1) but also included the succession below the LG 6. In order to present a complete picture of the local geology, the presented map (Folder 1) was compiled from data on the floor and marginal rocks (Willemse, unpubl. map), from the farms Driekop-253 KT, Clapham-118 KT and Twyfelaar-119 KT (Heckroodt, 1959) and the farm Maandagshoek (Gain, 1981). The farm boundary between Maandagshoek and Mooihoek can be approximately taken as the western boundary of the area mapped by the author as part of this study.

Mapping of rock units was carried out in accordance with the lithological units defined by Cameron (1980, 1982). The fact that all units are present as mappable entities emphasizes the lateral consistency of the layering, bearing in mind that the units were originally identified by Cameron from a profile some 40 km along strike to the north.

A pronounced increase in the thickness of individual units from south to north was established from the field relationships.

Mapping revealed the presence of more than 30 ultramafic pegmatites varying in diameter from less than 10 m to over 100 m. By far the largest pegmatite body is found on Hendriksplaats where it forms the core of a prominent steep hill (Tshidintshi). The affected portion represents approximately 200 m of the layered sequence including the upper group chromitite layers UG 1 and UG 2. Chromitites within the pegmatitic part have undergone a process of severe magnetitization (Merkle, 1988).

The discordant bodies are invariably coarse-grained and consist almost exclusively of mafic minerals, irrespective of the surrounding lithology. Pegmatites in the studied area show no preference for any particular stratigraphic horizon, but do not seem to be developed below the LG 6 chromitite layer. Pegmatites are absent in the central and

northern parts of Mooihoek where the thickness of the layered sequence reaches its maximum in this area.
The possible genetic link between the formation of pegmatites and the geometry of the magma chamber will be discussed in Chapter II.7, together with some geochemical and mineral chemical aspects.
The striking lithological similarities between rock units in the Maandagshoek-Mooihoek area and the section studied by Cameron (1980, 1982) necessitates only a brief description, as a very detailed description of all the characteristic lithological features of the various units is given by Cameron (1980; 1982). The following chapters therefore only highlight the principal features of the individual units and serve to emphasize differences from the established type section.
The following descriptions of the various rock types are based on over 300 polished thin sections from continuous drillcore material which intersected the 700 m thick stratigraphic sequence from the base of the LG 6 up to the UG 1. The rock succession below the LG 6 has been investigated from outcrops during detailed mapping on the farm Mooihoek.
The minimum and maximum thicknesses quoted for chromitite layers below the LG 5 were established from outcrops. Values for the remaining chromitites were taken from a total of 21 borehole logs from the Maandagshoek area, which includes the farms Hendriksplaats in the south and Twyfelaar in the north.

II.2. ROCK NOMENCLATURE

Rocks are classified according to the terminology employed by Cameron and Desborough (1969). Thus, a feldspathic pyroxenite is a rock containing cumulus orthopyroxene (bronzite) and postcumulus feldspar, whereas a norite has cumulus orthopyroxene and cumulus plagioclase. The terms leuco- (modal plag >65 %) and mela- (modal plag <35 %) are applied according to the definitions used by Streckeisen (1976).
The subdivision of the critical zone and the alphabetical nomenclature of units by Cameron (1980, 1982) is maintained throughout the dissertation.

II.3. THE LOWER CRITICAL ZONE

II.3.1. SEQUENCE BELOW THE LG 6

Rocks underlying the LG 6 are generally poorly exposed and largely covered by scree and alluvial deposits. A strict classification according to Cameron's stratigraphic units is therefore difficult, as his subdivision is exclusively based on two relatively thin olivine-rich horizons.

The information derived from scattered outcrops and the two isolated hills, Difataneng and Ga-Mathipa (Folder 1) revealed that feldspathic pyroxenite predominates and that it contains several intercalated chromitites and one correlatable olivine-bearing layer (Figs. II.1 and II.2). The stratigraphic position of the latter corresponds to the upper harzburgite (C_3 unit) from the type section of the eastern compartment (Cameron, 1980). The associated chromitite layer is consequently labelled LG 4, although the terminology of the lower chromitite layers was established from the western compartment (Cousins and Feringa, 1964) and was not applied by Cameron to the chromitites of the eastern lobe. The LG 4, as defined by Cousins and Feringa (1964), is hosted by olivine-bearing cumulates. The chromitites below the upper harzburgite are, by analogy referred to as the LG 3 and LG 3A although only one layer (LG 3) is developed at the corresponding stratigraphical position in the western lobe. LG 2 in the western compartment occurs below the lower harburgite unit, and although this unit could not be found in outcrop, its presence in the studied area is confirmed by results from recent drillcores (McCloud, personal communication 1987).

LG 4 has a maximum thickness of about 15 cm; it may be massive or split by silicate partings in a series of thin chromitite stringers.

LG 3A has a sharp upper and lower contact with a maximum thickness of about 20 - 25 cm; the layer is very fine grained and less impure than the LG 3, which makes the LG 3A more resistent to weathering.

LG 3 is a 40 - 45 cm thick friable, finely crystalline chromitite layer situated in a fine-grained pyroxenite. Its lower contact is gradational over 8 - 10 cm and the upper contact gradational over 2 - 5 cm.

Figure II.1: Columnar sections of the lower group chromitite layers and their relationship to the enclosing lithologies as found on the farm Mooihoek. Data derived from outcrops. For localities of the sections see Figure II.2

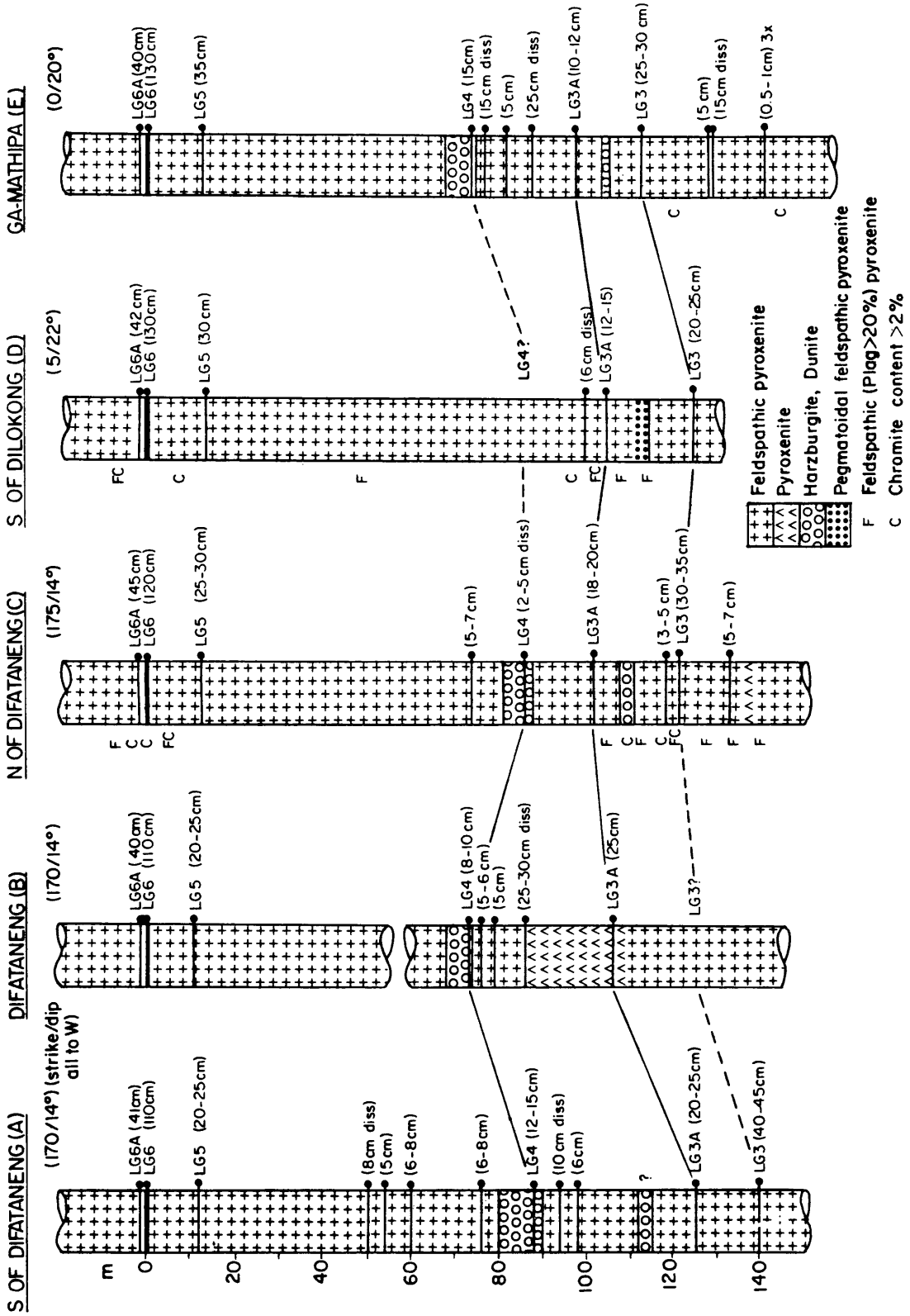

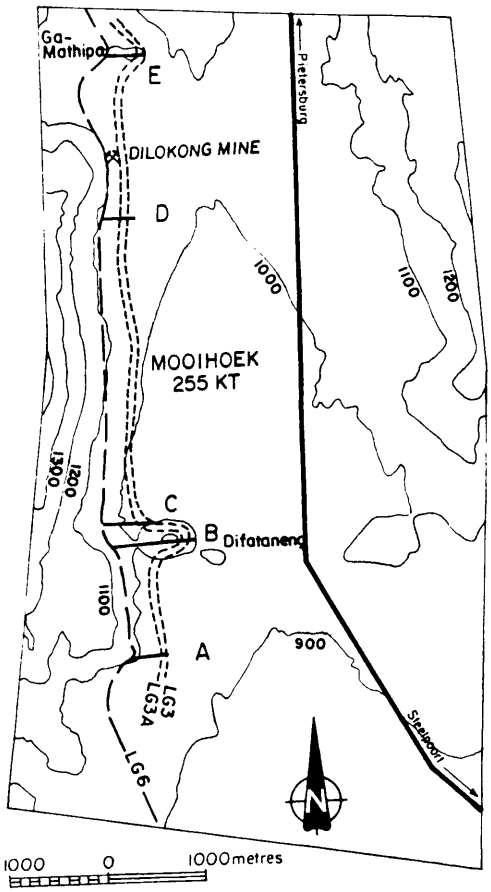

Figure II.2: Positions of lower group chromitite layers and of the five traverses shown in Figure II. 1.

LG 3 and LG 3A are situated approximately 100 to 140 m below the LG 6. Field evidence leads to the interpretation that both layers have a maximum thickness in the southernmost outcrops and thin towards the northern part of Mooihoek. It is of particular interest that they were not intersected in a borehole on Clapham further north (Lee and Wadsworth, unpublished data) whereas they have been found on Winterveld-293 KT to the south (Bristow, personal communication 1987).

The feldspathic pyroxenite is generally medium to coarse grained with varying amounts of intercumulus feldspar. Large, randomly orientated clinopyroxene oikocrysts are found throughout the sequence although they occasionally increase in number below chromitite layers.

The olivine-bearing unit which hosts the LG 4 is usually intensely weathered and serpentinized and can be easily recognized by a distinct morphological depression. Extensive alteration of olivine has locally formed layers of magnesite.

The fact that the stratigraphically lowest exposures (350 m below LG 6) within the studied area consist of pyroxenite with considerable amounts (5 - 15 %) of intercumulus plagioclase suggest that these rocks are still part of the lower critical zone. Lower zone pyroxenites characteristically lack abundant intercumulus feldspar (0 - 4 %; Cameron, 1978). It is not obvious from field relations whether the lower zone is developed on Mooihoek, or if the lower critical zone is directly overlying floor sediments. If the lower zone is present then its thickness cannot be more than the 400 m thick unexposed sequence between floor rocks and the critical zone. Lower zone rocks are well developed to the north and south of Mooihoek which suggests that deformation of the floor rocks to form the Derde Gelid pericline either predated or accompanied the intrusion and subsequent crystallization of lower zone magma.

II.3.2. THE D_2 UNIT

The D_2 subunit hosts the massive, 96 - 128 cm thick Steelpoort chromitite layer (LG 6), the overlying 25 - 47 cm thick Leader layer (LG 6A) and the underlying 12 - 24 cm thick LG 5 chromitite layer. All three chromitites occur in feldspathic pyroxenite rich in disseminated chromite. Clinopyroxene oikocrysts and phlogopite are common postcumulus mafic silicates, while K-feldspar and quartz are present in varying amounts. Variations in the modal proportions (Folder 2) of late-magmatic phases are discussed in Chapter IV.

II.3.3. THE E UNIT

The E unit forms the top of the lower critical zone. Lithologically the unit resembles the underlying feldspathic pyroxenite, although the amount of intercumulus plagioclase increases slightly upward. Orthopyroxene grains are commonly embayed and can have thin rims of clinopyroxene along their corroded margins (Plate 1.D).
Phlogopite, poikilitic clinopyroxene, quartz and K-feldspar are principal postcumulus minerals. Rutile, loveringite (Ti-Fe-Zr-REE oxide),

1A: Intercumulus anhydrite (centre) surrounded by orthopyroxene (beige to brown colours) and phlogopite (red and green colours) in feldspathic pyroxenite of the E unit; diametre of anhydrite is about 0.6 mm. Crossed nicols.

1B: Intercumulus anhydrite (centre) surrounded by orthopyroxene (beige to brown colours), minor quartz (grey and black) and phlogopite (top right) in feldspathic pyroxenite of the E unit; length of anhydrite is about 1.5 mm. Crossed nicols.

1C: Enlargement of central portion of anhydrite in 1B. Note the numerous tiny grains of pyrrhotite (opaque) along the margin of anhydrite and the fluid inclusions in anhydrite. Plane polarized light.

1D: Feldspathic pyroxenite of the E unit. Note the corroded margins of orthopyroxenes (beige to brown colours) which are partially rimmed by clinopyroxene (blue and orange colours). Interstitial plagioclase (centre) shows albite twinning. Width of photo equals 3 mm. Crossed nicols.

1E: Middle group chromitite layer 3 above chromiferous anorthosite (top of F unit). The melanorite overlying the chromitite layer marks the bottom of the G unit. Length of hammer is 30 cm.

1F: Central part of clinopyroxene oikocryst with abundant orthopyroxene exsolution lamellae. Melanorite of the G unit. Note the numerous plagioclase and orthopyroxene inclusions which are partly resorbed. Width of photo equals 3 mm. Crossed nicols.

1G: Norite of the J unit with irregular schlieren of anorthosite. Note coin for scale.

2A: Norite of the upper J unit which typically shows slumping features. Length of hammer is 30 cm.

PLATE 1

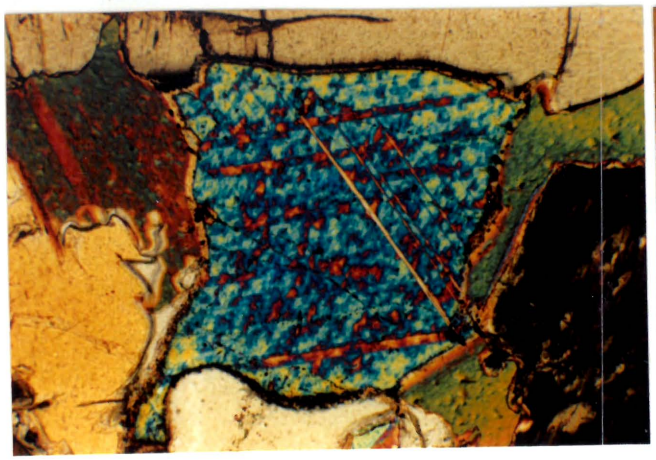

A

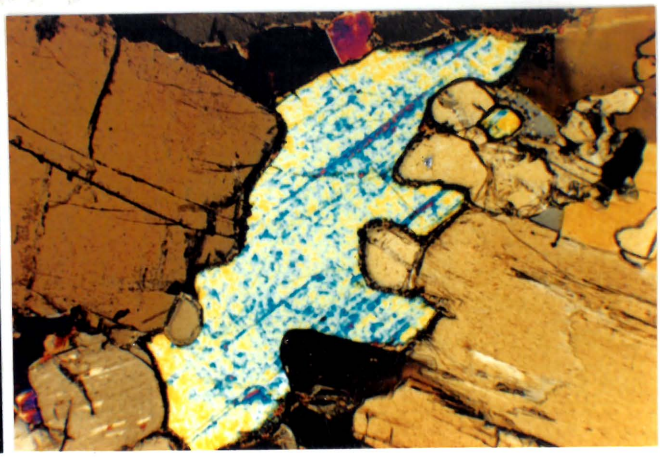

B

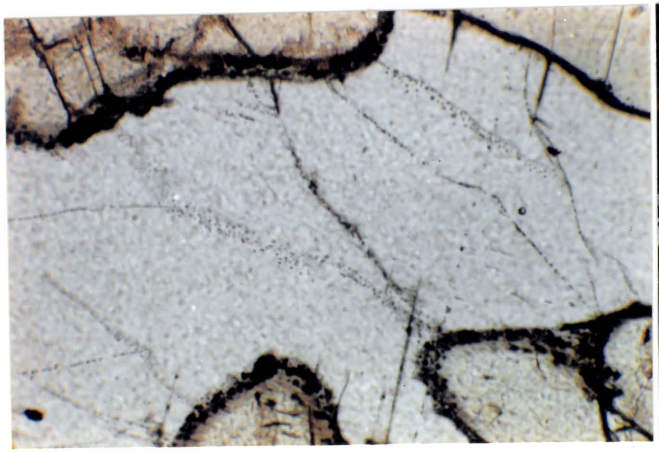

C

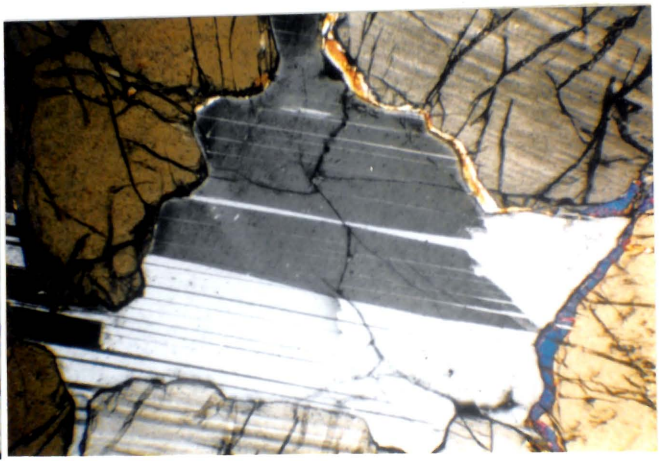

D

E

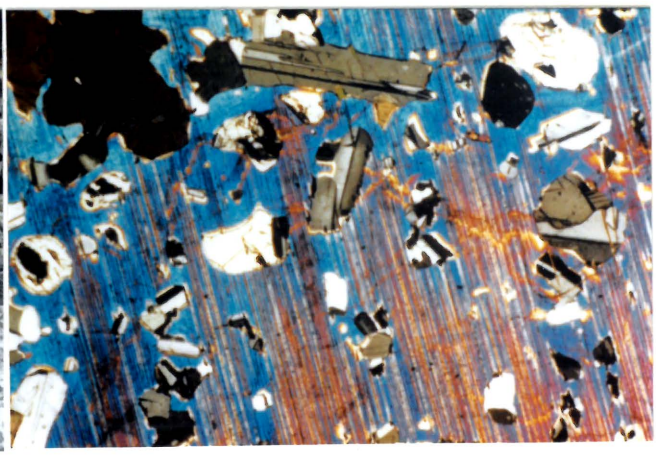

F

G

H

apatite and anhydrite occur in rocks enriched in intercumulus quartz, sodic plagioclase and K-feldspar. The presence of anhydrite (Plate 1.A-C) in this assemblage is particularly interesting and indicates a strong increase in the volatile content during melt fractionation.

The 25 - 56 cm thick Marker chromitite layer (LG 7) occurs about 25 - 40 m above the LG 6. Two further chromitite layers, the 20 - 46 cm thick MG 1 layer and the 6 - 15 cm thick MG 2A layer appear about 5 - 7 m and 0 - 3 m below the top of the unit. Accessory chromite is only found above and below the LG 7 and in the upper 30 m, where it increases towards the top.

The terminology for the middle group chromitites (MG 1 - 4) was adapted for chromitites in the studied area because of the close resemblance of the sequence that hosts these chromitite layers with that which hosts the MG 1 - MG 4 chromitite layers in other parts of the Bushveld Complex (Hatton and von Gruenewaldt, 1987).

II.4. THE UPPER CRITICAL ZONE

II.4.1. THE F UNIT

The unit consists principally of two chromiferous anorthosite layers separated by melanorite. Both anorthosites contain various amounts of intercumulus orthopyroxene and are terminated at their tops by chromitite layers (Plate 1.E).

The lower MG 2B chromitite layer is not always present and usually much thinner (6 - 20 cm) than the upper 10 - 30 cm thick MG 3 layer. The bottom anorthosite can thin out or disappear completely, in which case the F unit starts with the MG 2B chromitite. In borehole MDH 29 (up-dip section) the bottom anorthosite is present as a 3 mm thick stringer underlying the MG 2B, which contains an unusually large amount of intercumulus plagioclase.

In the F unit melanorite the orthopyroxene becomes more and more corroded (Plate 3.A) concomitant with an upwards increase in modal plagioclase content (Folder 2). The transition to anorthosite is gradual over about one metre, and marked by small-scale fluctuations

in the amount of orthopyroxene. Within the anorthosite the texture of orthopyroxene changes from cumulus to intercumulus as the amount of pyroxene decreases upwards (Plate 3.B). Both anorthosites are modally layered due to an uneven distribution of chromite, commonly as thin horizontal chains, with individual stringers containing as little as one row of crystals. Distortion of chromite chains produces characteristic "flow"-structures, which probably resulted from disturbance in a semi-consolidated stage. Similar textures described by Lee (1981) from other areas of the Complex were equated by him to plastic deformation textures in soft sediments.

The majority of orthopyroxene grains in the melanorite have a grain size ranging between 0.2 and 1.2 mm with only a very few grains larger than 2 mm. The latter grains resemble orthopyroxenes from the lower critical zone in size and shape. The anorthosite layers contain large orthopyroxene grains (2 - 6 mm) except in the upper part where orthopyroxene is intercumulus. Cumulus orthopyroxene throughout the unit contains tiny inclusions (5 - 200 um) of plagioclase (see Chapter VI.1), which increase in frequency upwards. Clinopyroxene is present as oikocrysts which contain corroded grains of orthopyroxene and plagioclase (Plate 1.F).

II.4.2. THE G UNIT

The G unit has a thin feldspathic pyroxenite layer at the base which grades upwards into melanorite. The amount of plagioclase increases gradually with stratigraphic height, but does not exceed 35 % of the rock. Plagioclase inclusions in orthopyroxene increase upwards in the melanorite (Plate 3.C-D), but are absent in the basal felspathic pyroxenite. The latter commonly contains small amounts of chromite and resembles rocks from the upper E unit.

II.4.3. THE H UNIT

The H unit is similar to the F unit in that it consits of a norite, with interlayered leuconorites, sandwiched between two plagioclase-

rich layers which form the bottom and the top of the unit. Chromite is an abundant phase in the lower anorthosite, resulting in a well layered texture. The central noritic part and the upper anorthosite contain only small amounts of chromite. A very thin chromitite layer (1 - 5 cm) is sporadically found at the contact between the upper anorthosite and the overlying norite of the J unit.
Particularly the upper portion of the unit seems to have been deformed in the semi-consolidated stage, as can be seen by a patchy intermingling of anorthositic and (mela-)noritic material in outcrops as well as in boreholes.
Intercumulus orthopyroxene is present in only one sample, while the rest of the sequence contains cumulus orthopyroxene. Very uneven and strongly embayed grain boundaries together with numerous inclusions of plagioclase suggest an early state of disequilibrium and resorbtion.

II.4.4. THE J UNIT

The J unit consists of fine- to medium-grained norites with an overall upward increase in the amount of orthopyroxene. A maximum in mafic minerals is encountered about 2/3 up in the unit with the brief reappearance of feldspathic pyroxenite and traces of chromite. The remainder of the unit shows no systematic variation in modal proportions and is extremely heterogeneous. Thin and sometimes fragmented layers of anorthosite and intercalated leuconorites are frequently found in the upper J unit (Plate 1.G). Disturbed accumulation is also indicated by patches of chromitite and anorthosite as well as by macroslumping structures (Plate 1.H).
Mineral and textural relationships are identical to those in the (mela-)norites of the preceeding units.
A thin layer (< 1 m) of feldspathic pyroxenite and local increases in the chromite concentrations are occasionally present at the very base of the unit. Apart from in this and the earlier mentioned feldspathic pyroxenite the unit appears to be free of chromite. Phlogopite is restricted to the lower half of the unit.

IG:
: Cm - scale layering of orthopyroxene-rich and plagioclase-rich layers of the upper K unit. Note the partially irregular layering and the cross-cutting relationship of the pyroxene-rich layers to the left of the hammer (30 cm). Hanging wall marks the bottom of the pyroxenitic L unit.

2B: Orientated rutile needles in the marginal area of an orthopyroxene grain of a feldspathic pyroxenite from the E unit. Width of rutile needles is about 1 micron. Crossed nicols.

2C: Feldspathic pyroxenite of the E unit with evolved interstitial mineral assemblage. Orthopyroxenes (beige to brown colours) are surrounded by quartz (white), phlogopite (green and blue) and plagioclase (grey to brown, near top right). Note the orientated rutile needles in the centre of dark-brown orthopyroxene (centre). Long axis of dark-brown pyroxene is about 0.7 mm. Crossed nicols.

2D: Feldspathic pyroxenite of the E unit. Note the orientated rutile needles in plagioclase (light grey) adjacent to orthopyroxene (left side). Width of photo equals 400 microns. Plane polarized light.

2E: Feldspathic pyroxenite of the E unit. Orthopyroxene (high relief), plagioclase (light grey) and phlogopite (light brown) enclosing rutile (dark brown). Length of upper rutile is about 250 microns. Plane polarized light.

2F: Feldspathic pyroxenite of the E unit. Note the change in plagioclase extinction angle along the contacts with orthopyroxene indicating a sharp decline in the An content of plagioclase. Length of small orthopyroxene below centre is 300 microns. Crossed nicols.

2G: Central portion of clinopyroxene oikocryst (grey-green) of feldspathic pyroxenite from the E unit. Note inclusions of orthopyroxene (beige to dark brown) and euhedral chromite (black) surrounded by plagioclase (centre and lower right) which shows albite twinning (white and black). Diametre of chromite grains varies between 50 and 300 microns. Crossed nicols.

2H: Feldspathic pyroxenite of the E unit with evolved interstitial mineral assemblage. Orthopyroxene (light to dark brown), quartz (grey white), clinopyroxene (blue) and phlogopite (red brown) enclosing loveringite (black). Note the radioactive halo around loveringite. Loveringite has a length of 600 microns. Crossed nicols.

PLATE 2

A

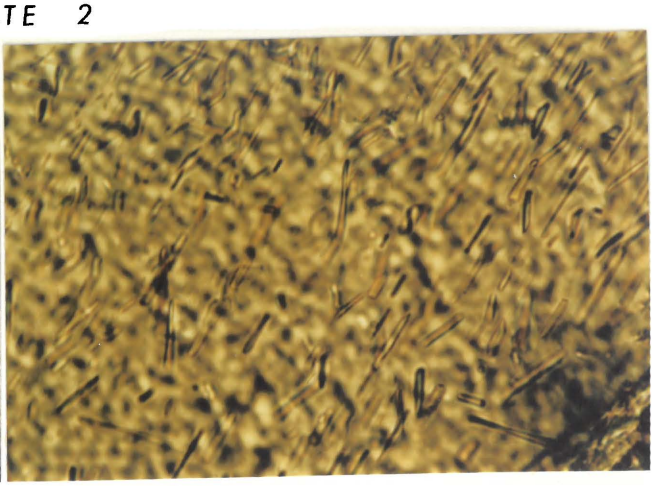

B

C

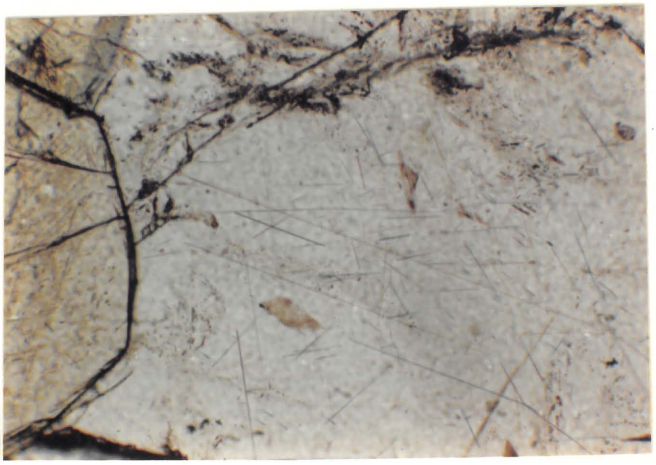

D

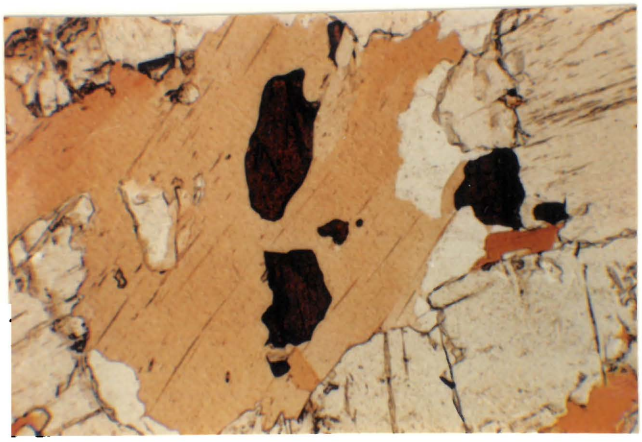

E

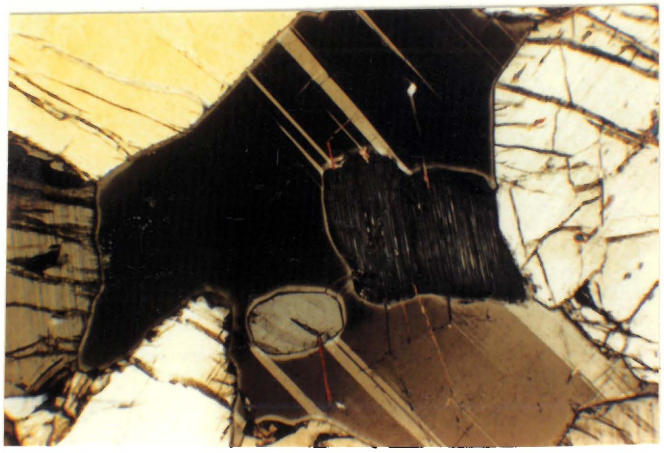

F

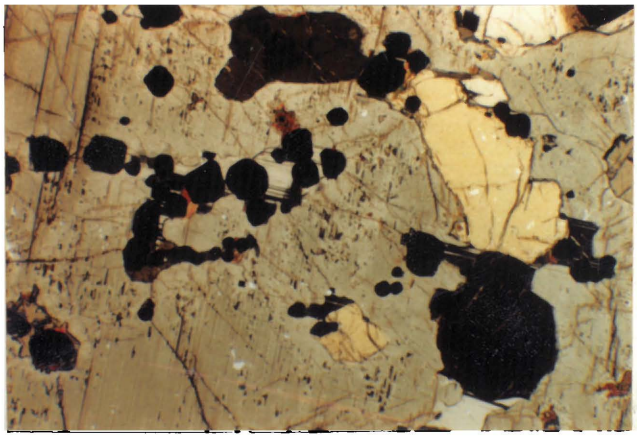

G

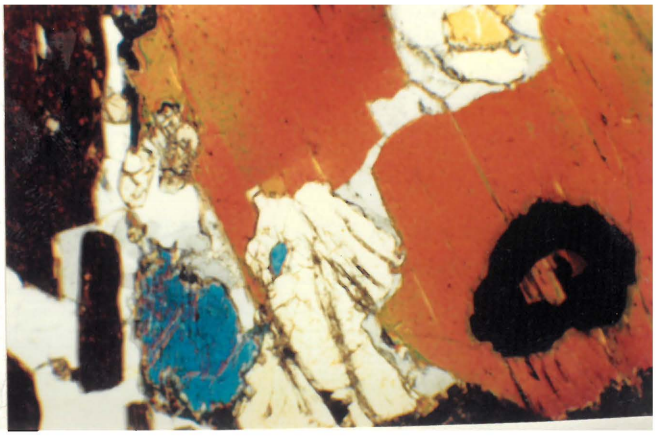

H

II.4.5. THE K UNIT

The base of the K unit is marked by an increase in the plagioclase content although the contact is locally gradational. Norites and leuconorites with macro-textural features, similar to the underlying upper part of the J unit, persist up to about 5 m from the top. The upper part, which is readily recognized in drillcores and outcrops, consists of intercalated layers (1 - 20 cm) of melanorite and chromite-bearing anorthosite (Plate 2.A, Fig. II.3). Plagioclase is intercumulus in particularly pyroxene-rich layers (feldspathic pyroxenite). The amount of pyroxene varies for individual mafic and felsic layers but contacts are exceptionally sharp. The thickness of layers changes rapidly along strike and individual layers can only be followed for a few metres. Pyroxenite layers often bifurcate or form series of separated and elongated lenses. All these features appear to have originated during accumulation of the K unit rather than being the result of physical disturbance and re-arrangement of the still unconsolidated material.

Plagioclase commonly shows myrmekitic textures along mutual grain boundaries (Plate 3.E). Similar features were described from the main- and upper zones (e.g. von Gruenewaldt, 1971; Reichhardt, 1984) and were seen as evidence for a late-stage migration of hydrous fluids (Dymek and Schiffries, 1987).

Chromite first appears about halfway up in the K unit and increases to the top. The well-layered upper part is generally chromite-rich (>3 %) with maximum chromite concentrations in the pyroxene-rich layers.

Orthopyroxene in the norite and leuconorite occurs as stubby, subhedral, medium-sized crystals with numerous plagioclase inclusions, but is usually inclusion-free in the pyroxene-rich layers.

Some melanorite layers are characterized by an abundance of elongated (3 - 10 mm) subhedral orthopyroxene grains orientated parallel to the plane of igneous layering. A similar concentration of orthopyroxene needles has not been encountered in any other layer of the studied sequence. However, orthopyroxene with a length/width ratio of about 8:1 is occasionally present in samples from the lower critical zone.

A thin lithologically distinct layer (< 1 m) of very fine grained (< 0.3 mm) norite was intersected above the uppermost plagioclase-rich

3A: Melanorite of the F unit. Note the numerous plagioclase inclusions in orthopyroxene (light to dark grey) and the corroded shape of central orthopyroxene grain. Crossed nicols.

3B: Chromiferous anorthosite with intercumulus orthopyroxene of the upper F unit. Plane polarized light.

3C: Melanorite of the lower G unit. Note the almost complete absence of plagioclase inclusions in orthopyroxene. Crossed nicols.

3D: Melanorite of the upper G unit. Note the abundant plagioclase inclusions in orthopyroxene. Orthopyroxenes (high relief) are mostly surrounded by interstitial clinopyroxene (light grey) which contains cumulus plagioclase (mostly twinned). Crossed nicols.

3E: Norite from the K unit. Plagioclase shows corrosion features and myrmekitic rims. Crossed nicols.

3F: Very fine-grained norite from the top of the K unit. Large orthopyroxene crystal with clinopyroxene exsolution lamellae and blebs is surrounded by small orthopyroxenes (high relief) and plagioclase grains. Crossed nicols.

3G: Gabbronorite of the lower M unit. Inverted pigeonite (black) shows bleb-like exsolutions of clinopyroxene. Crossed nicols.

3H: Gabbronorite of the upper M unit. Inverted pigeonite (black) shows lamellar exsolutions of clinopyroxene. Crossed nicols.

PLATE 3

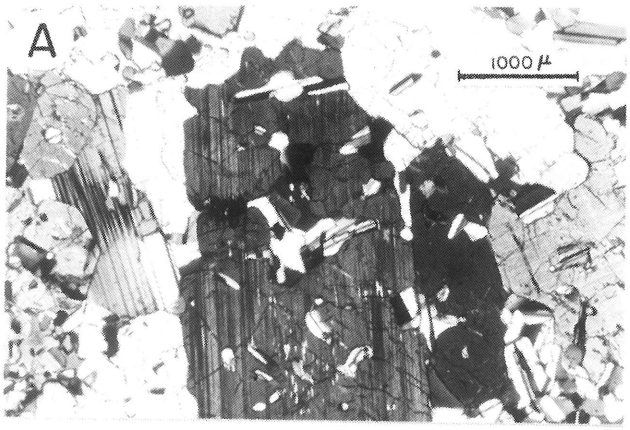

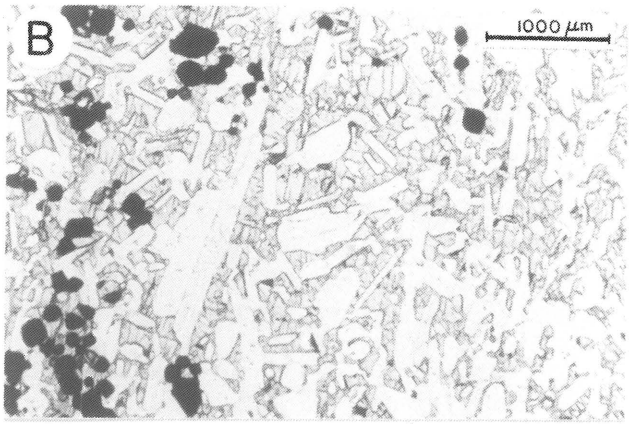

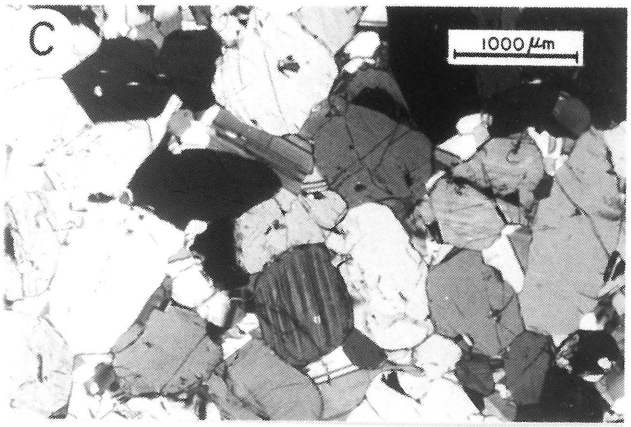

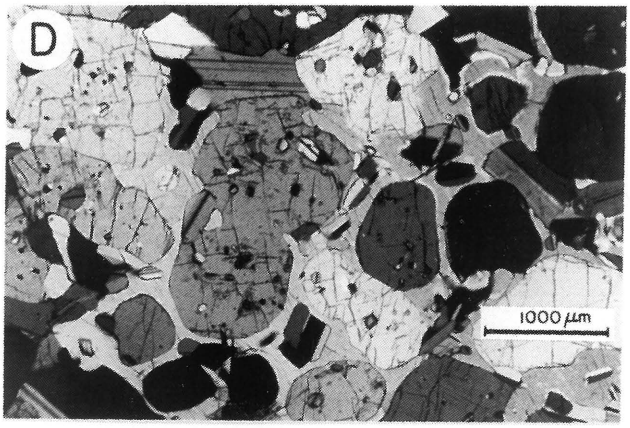

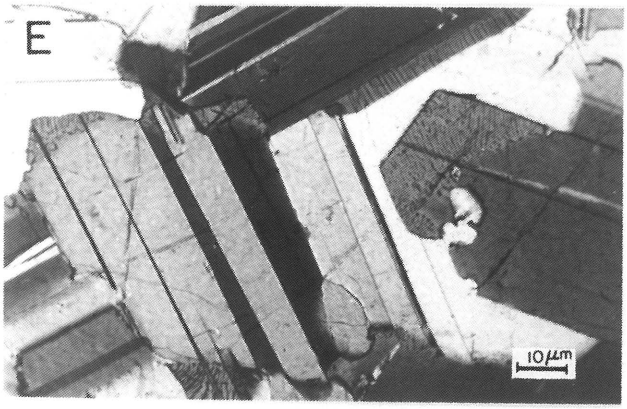

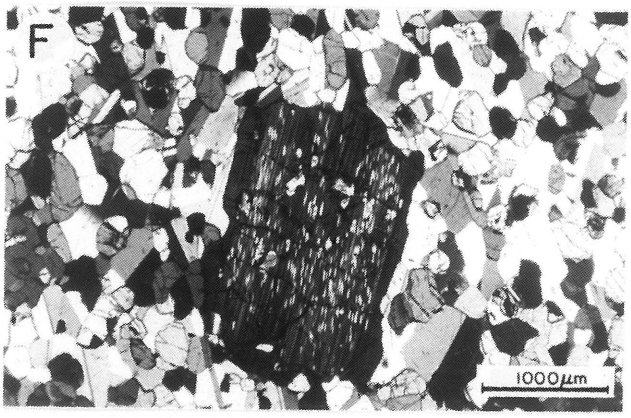

layer of the K unit and was taken as the top of the K unit. The norite is very homogenous and evenly grained and has a sharp lower and upper contact. Cumulus clinopyroxene and chromite are both present in accessory amounts. Orthopyroxene crystals (2 - 3 mm) similar in size to those in the over- and underlying rocks are sporadically found as insets (Plate 3.F).

Inverted pigeonite was found in a 20 cm thick, very fine grained portion about 20 metres below the top of this unit. Thus, the K unit marks the lowest stratigraphic occurrence of cumulus clinopyroxene and inverted pigeonite. It must be emphasized, however, that both minerals occur only over a very restricted interval and in lithologically distinct rocks. Similar fine grained rocks are a common feature of the M unit (see also Chapter IX.2.10.1).

II.4.6. THE L UNIT

The L unit consists of melanorite and feldspathic pyroxenite with thin interlayered chromitites (1 - 8 cm) at three well defined intervals within the feldspatic pyroxenite (Fig. II.3). These layers can be conveniently grouped as UMG 1 to 3 in accordance with the suggestion of Gain (1981) who proposed the stratigraphic term "Upper Middle Group" chromitites. Disseminated chromite is absent in the lower melanorite and in the upper portion of the unit.

The contact between feldspathic pyroxenite and melanorite is always transitional over less than 0.5 m, with plagioclase changing from intercumulus to cumulus. Tiny inclusions of plagioclase in the orthopyroxene appear simultaneously with cumulus plagioclase.

A diagnostic feature of the L unit and the feldspathic pyroxenite in particular, is the abundance of clinopyroxene oikocrysts. The latter are more resistant to weathering and are readily recognized in outcrops as sharp protuberances.

Phlogopite and quartz are occasionally present in the feldspathic pyroxenite as additional postcumulus minerals.

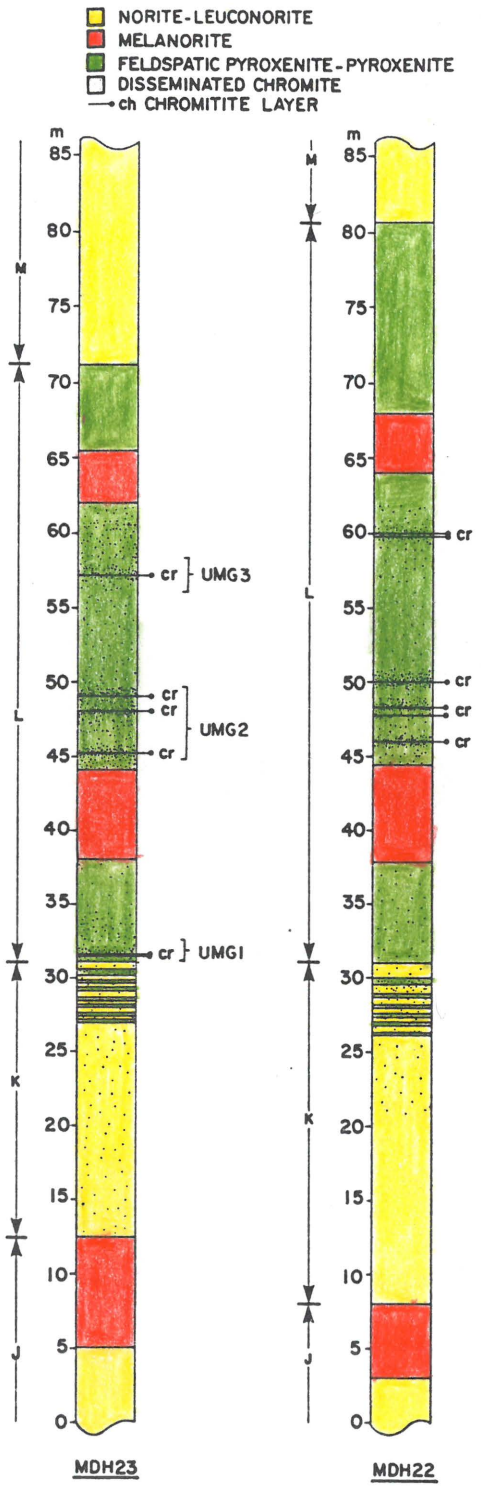

Figure II.3: The upper middle group chromitite layers and their relationship to the enclosing lithologies. Data from boreholes MDH 23 and MDH 22.

II.4.7. THE M UNIT

The M unit consists of three principal rock types. Norite and gabbronorite to leuconorite and leucogabbronorite, with generally low but varying amounts of medium-sized ortho- and clinopyroxene grains are the most abundant rock types. Pyroxene only predominates over plagioclase in a 15 m thick interval about 30 m above the base of the unit. Leuconorite and leucogabbronorite occur at at least 11 stratigraphic horizons. Both rock types are also known as spotted anorthosite due to their characteristic spotted appearance. The former terms are mineralogically more precise and are therefore prefered.

The next most abundant rock type is mottled gabbronorite (also known as mottled anorthosite) in which the characteristic mottled texture is caused by the scattered distribution of poikilitic orthopyroxene aggregates which are up to 1.5 cm in diameter. Clinopyroxene is present as small (< 0.5 mm) and evenly distributed cumulus grains. Depending on the relative proportion of enclosed plagioclase orthopyroxene appears either as subhedral sieve-textured grains with irregular margins or as anhedral intercumulus aggregates. The more subhedral grains tend to have an inner core free of plagioclase inclusions. The change in pyroxene texture from subhedral to intercumulus is gradual, with intercumulus textures typically confined to the almost pure anorthosites.

The third rock type is a very fine grained gabbronorite, which consists of plagioclase, inverted pigeonite and clinopyroxene. Very fine grained gabbronorites increase in frequency towards the top and commonly overlie mottled gabbronorites. The contact between the latter rock types is commonly not very sharp and patches of very fine grained gabbronorite occur in the underlying mottled gabbronorite.

The textural habit of inverted pigeonite, only absent in the bottom most very fine grained gabbronorite, changes with stratigraphic height. In the lower part of the M unit inverted pigeonite appears as individual grains with similar orientated bleb-like exsolutions of clinopyroxene (Plate 3.G), while lamellar exsolution and the formation of optically continuous units prevails in the upper gabbronorites. Unlike inverted pigeonite from the main- and upper zone (e.g. von Gruenewaldt, 1970) only one set of exsolution lamellae (parallel 100)

4A: Gabbronorite from the lower M unit. Clinopyroxene (centre) contains relics of optically uniform orthopyroxene. Crossed nicols.

4B: Feldspathic pyroxenite of the E unit. Orthopyroxene shows lamellar clinopyroxene exsolutions which terminate near the margin at exsolution droplets. The outer rim of orthopyroxene is almost free of exsolution products. Crossed nicols.

4C: Feldspathic pyroxenite of the E unit. Clinopyroxene oikocryst (centre) shows orthopyroxene exsolution lamellae and contains numerous corroded orthopyroxene grains. Crossed nicols.

4D: Norite from the upper F unit. Orthopyroxene grains (high relief) contain plagioclase inclusions. Plagioclase grains in the large orthopyroxene (centre) have crystallized in embayments. Crossed nicols.

4E: Melanorite of the F unit. Orthopyroxene grains contain numerous plagioclase inclusions, while the central part of the large orthopyroxene grain (centre) is free of plagioclase incusions. Crossed nicols.

4F: Feldspathic pyroxenite of the chemically altered upper E unit from borehole MDH 23. Orthopyroxene is partially replaced by olivine (high relief and irregular cleavage). Chromite (black) shows "inclusions" of orthopyroxene which probably indicate an incomplete annealing process of several smaller chromite grains. Plane polarized light.

4G: Back scattered electron image (BEI) of feldspathic pyroxenite from the E unit. Orthopyroxene (light grey) is enclosing interstitial plagioclase (medium grey), quartz (black) and K-feldspar (light grey). Note the patchy occurrence and the microscopic intergrowth of K-feldspar and plagioclase. Various shades of grey within plagioclase indicate chemical zoning (Na-rich plagioclase is slightly darker than Ca-rich feldspar).

4H: Back scattered electron image (BEI) of melanorite from the F unit. Orthopyroxene (light grey) and plagioclase (dark grey). Note that plagioclase is partially replaced and rimmed by K-feldspar (medium grey). Black spot at bottom centre is a hole in the thin section.

PLATE 4

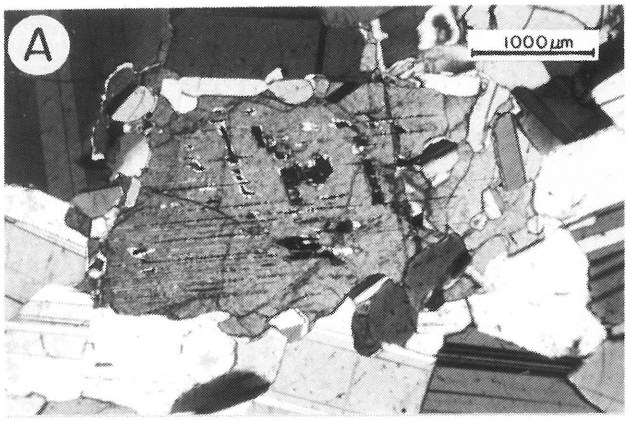

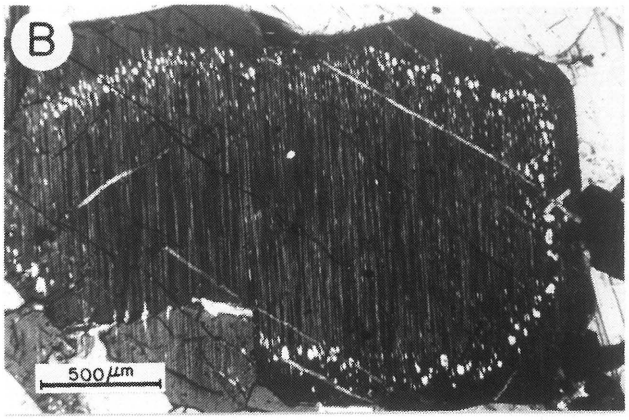

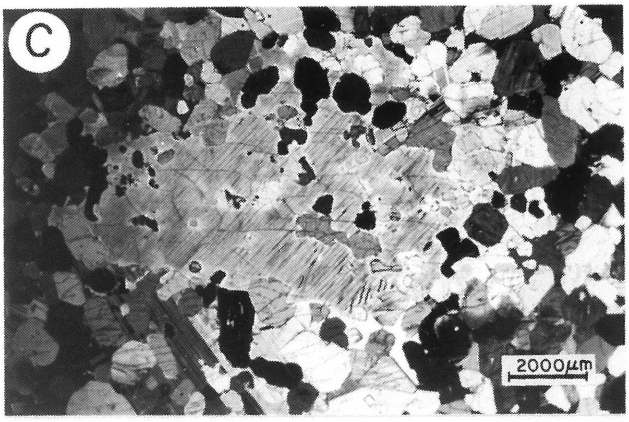

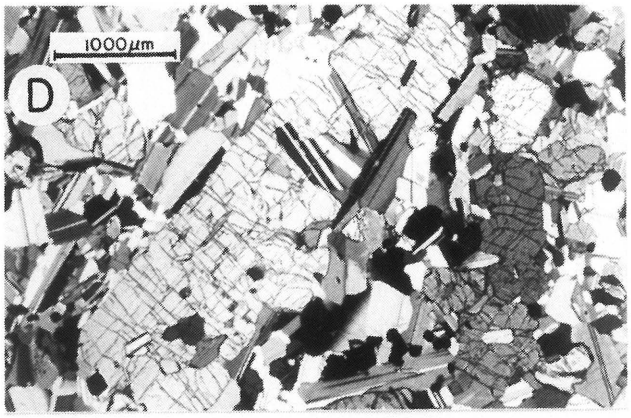

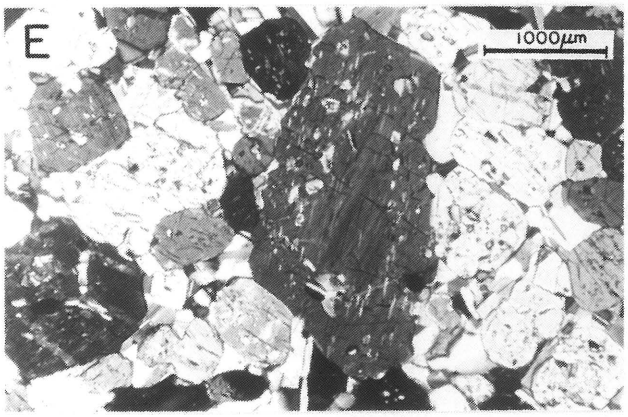

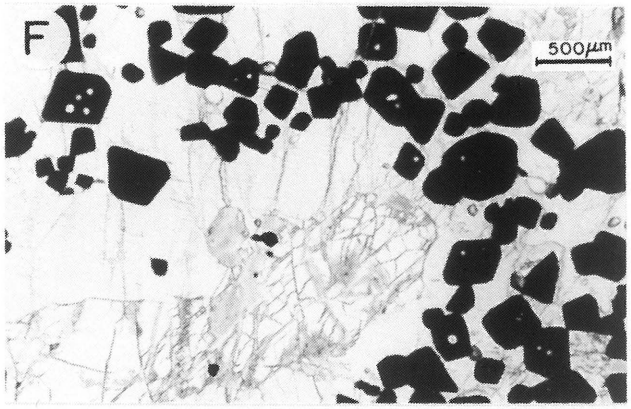

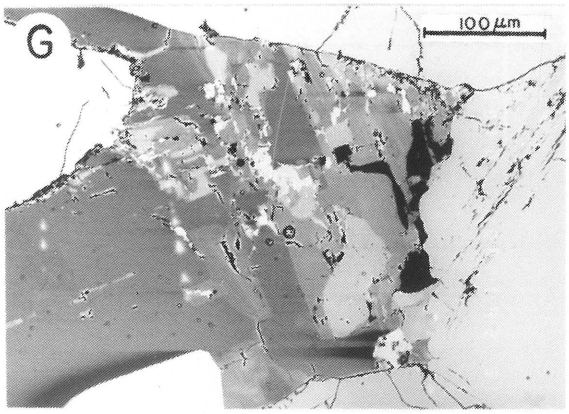

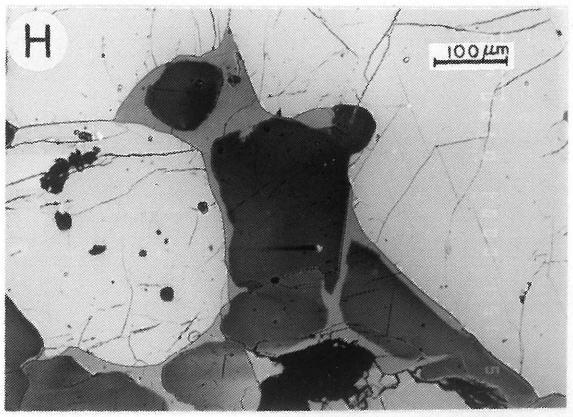

is developed (Plate 3.H). Large sieve-textured orthopyroxene grains occur frequently in the very fine grained gabbronorite.
Euhedral grains of clinopyroxene appear about 40 m above the base, just below the first layer of fine grained gabbronorite. Particularly in the lower leucogabbronorite layers clinopyroxene seems to have formed as a result of an orthopyroxene/liquid reaction (Plate 4.A). This is indicated by the small relic cores of orthopyroxene (inverted pigeonite ?).
Clinopyroxene oikocrysts are occasionally present in the M unit, while phlogopite and chromite are invariably absent.

II.5. SUMMARY

The described sequence of the lower critical zone consists predominantly of massive feldspathic pyroxenite, which is commonly coarse grained and chromite-bearing. Chromite-rich horizons and chromitite layers (LG chromitites) appear at several intervals, while olivine occurs in one unit. The amount of intercumulus feldspar increases gradually from the LG 6 chromitite towards the top of the lower critical zone. Within the same stratigraphic interval the amount of interstitial quartz, K-feldspar and phlogopite show multi-cyclic variations in modal content (Fig. IV.1).
The complex lithological succession of the upper critical zone can be divided into a predominantly melanoritic lower portion (units F - L) and an upper part, which consists mainly of norites and gabbronorites and their leucocratic equivalents in the M unit. Thin layers of chromiferous anorthosite occur within the F, H and K units of the lower mafic portion, which is terminated by the feldspathic pyroxenite of the L unit. Chromitite layers are restricted to the lower - upper critical zone transition (MG chromitites) and to the L unit (UMG chromitites).
Rocks of the upper critical zone are, with the exception of the gabbronorites of the upper M unit, fine- to medium grained two-phase assemblages of orthopyroxene and plagioclase. The F and G units show a systematic upward decrease in modal orthopyroxene, a trend that is reversed in the J unit. The other units show multi-cyclic variations,

with the amount of pyroxene generally decreasing in individual cycles. Apart from the feldspathic pyroxenites of the L unit, all the orthopyroxenes from the upper critical zone contain small inclusions of plagioclase. The size and frequency of inclusions increases in plagioclase-rich rocks resulting in an ophitic texture in the mottled gabbronorite.
A gradual change-over from orthopyroxene to orthopyroxene plus clinopyroxene and finally to a three pyroxene assemblage which includes inverted pigeonite is recorded in the M unit.

II.6. LATERAL CORRELATION OF THE LG 6 - UG 1 SEQUENCE

The correlation of thicknesses of individual units in drillcores from the farm Maandagshoek revealed some substantial differences (Fig. II.4). These differences are too large to be entirely due to changes in dip or deflections of the boreboles. The apparent thicknesses in each borehole were therefore not corrected and taken as "true" thicknesses.
The intersected units thicken systematically up-dip (W to E) and northwards along strike. Figure II.5 shows an east-west section with an inferred lower zone sequence and morphology of the floor contact.

The layered sequence in the Mooihoek/Maandagshoek area appears to be canoe-shaped with the position of the long axis approximately coinciding with the present erosion level of the Lebalelo ridge. The thinning towards the south and west is presumably a result of the underlying floor morphology which suggests an anticlinal structure in this case. It is thought that the thinning of the layered sequence to the south is caused by an anticlinal structure which is physically linked with the NNE - trending Derde Gelid pericline, while the inferred anticlinal structure below borehole MDH 20 in Figure II.5 to the west strikes presumably parallel to the latter.
It is of interest that only the silicate portions display differences in thickness, whereas chromitite layers have an almost constant thickness or even tend to decrease when the silicate host-rock thickens.

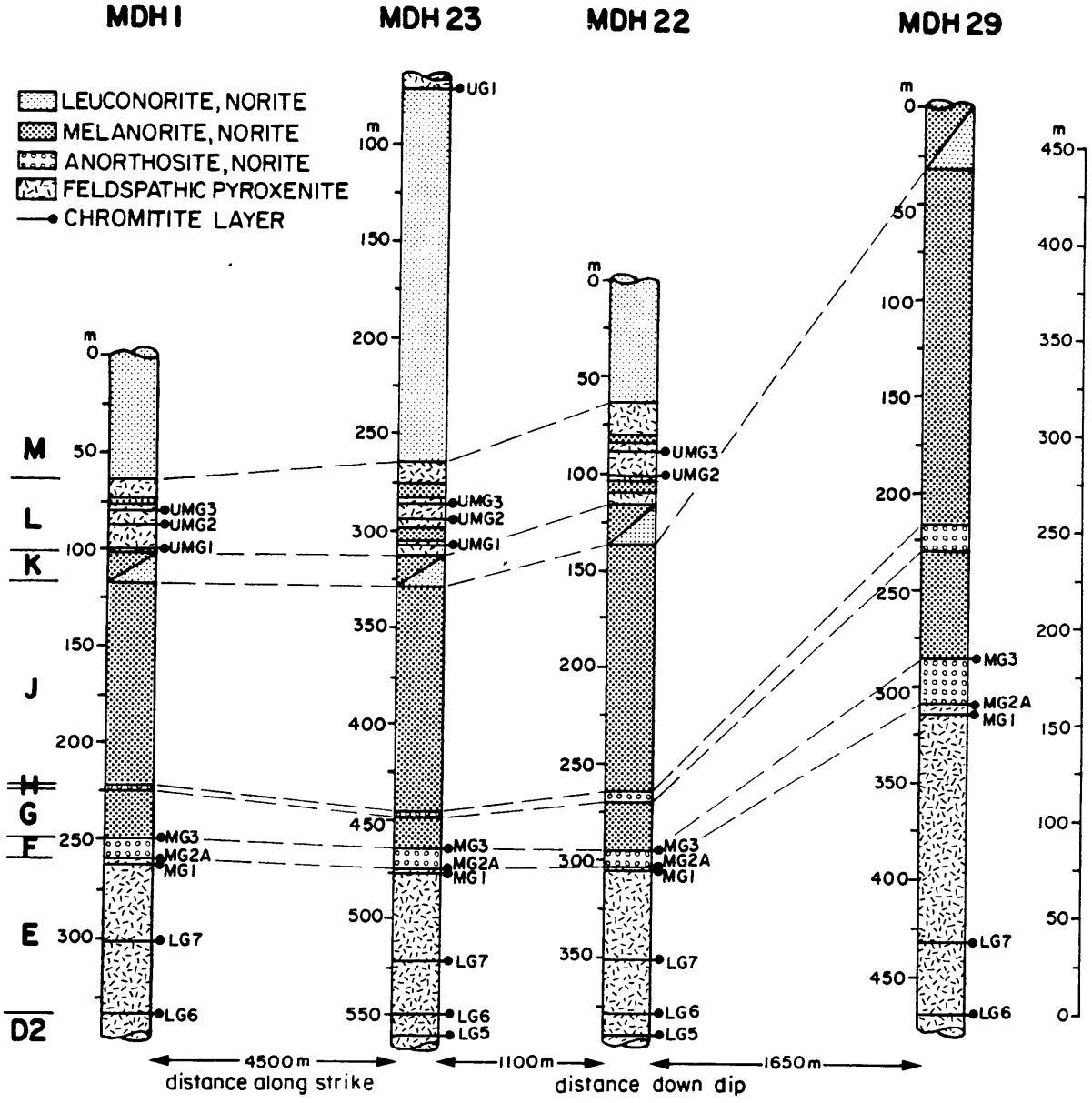

Figure II.4: Correlation of the lower/upper critical zone interval for the four investigated drill-cores. Note the decrease in thickness of individual units from MDH 29 to MDH 23 (down-dip). The shown distances along strike and down-dip are horizontal distances. The particular borehole depths are given for each drillcore.

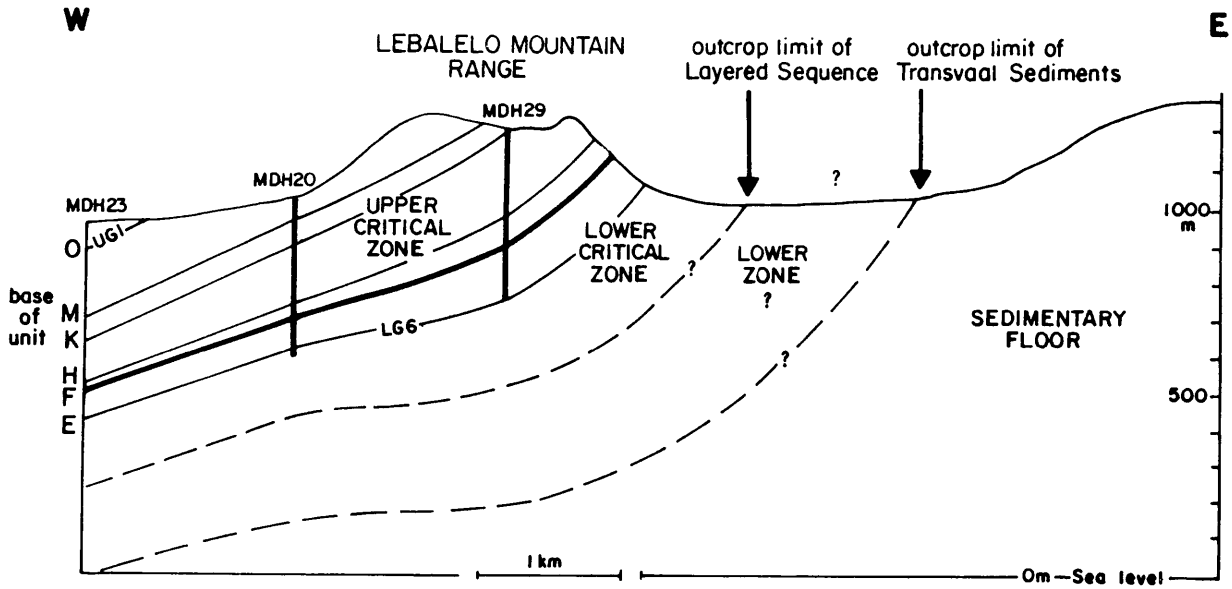

Figure II.5: East-west cross-section of the Maandagshoek-Mooihoek area. The cross-section is based on drillcore data and on outcrops. The hypothetical position of lower zone is derived from the outcrop limits of the layered sequence and Transvaal sediments.

The geometric relationship between visible physical structures exposed in the floor and the thickness of the layered sequence has been subsequently investigated on a larger scale. The displayed section (Fig. II.6) covers the western, central and southern sectors and is based on published and unpublished data from drillcores and geological maps. Figure II.6 clearly shows the close relationship between floor structures and the relative thickness of individual layered units. It is particularly interesting that this relationship also applies to most of the LG 6 - UG 1 sequence, despite its considerable stratigraphic distance from the floor, with only the M unit at the top of this sequence maintaining a fairly constant thickness throughout the area. A further interesting feature is the thinning of individual units towards the western sector and the total disappearance of the H, K and J units in the southern sector. The overlying L and M units are developed throughout the eastern compartment.

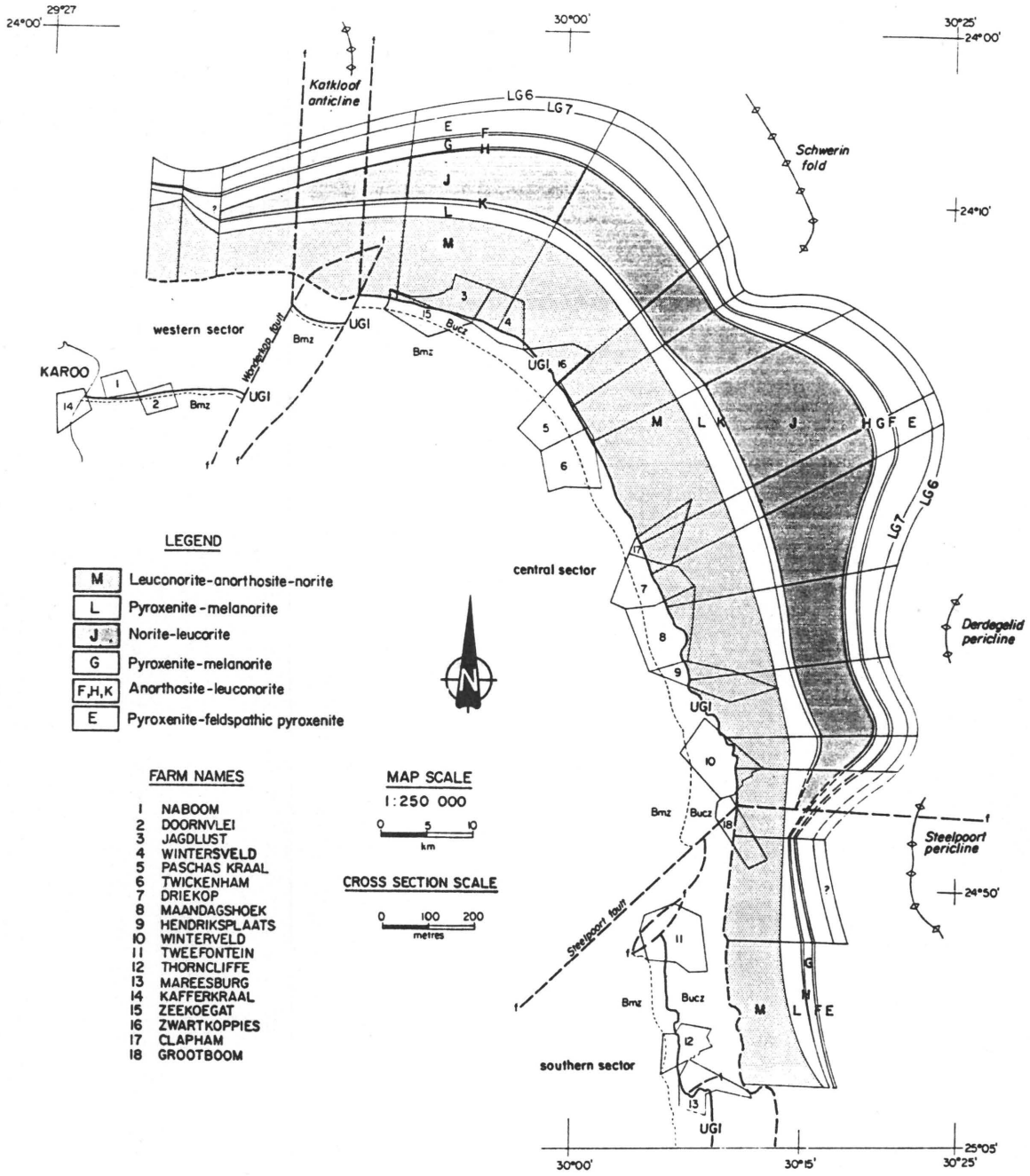

Figure II.6: Cross-section of the western, central and southern sectors of the eastern Bushveld Complex illustrating the changes in thickness of the layered sequence associated with floor-rock structures. Data for the relevant sequence (LG 6 - UG 1) were compiled from literature (Cameron and Desborough, 1969; De Villiers, 1968) and from logs kindly provided by the mining division of S.A. Development Trust, Rand Mines, Gencor and Messina Ltd. Displacement caused by faults were eliminated for clarity and to obtain a continuous section.

Figure II.7 displays a very detailed and laterally closely spaced correlation of the lower/upper critical zone interface (E/F boundary) and associated chromitite layers and siliceous rocks. All stratigraphic columns were derived from drillcore data. Several features can be recognized in this figure:

The first appearance of plagioclase-rich rocks can be correlated throughout the eastern compartment. This anorthositic layer of the F unit is underlain by at least two chromitites (MG 1 and 2A). The lithology of the F unit changes laterally from almost pure anorthosite in the southern and western sectors to an anorthosite base and top with intercalated norite and melanorite in the central sector. Such a heterogeneous F unit is characteristically found in the geographically marginal areas (Winterveld/Doornbosch and Jagdlust/Wintersveld troughs) of the central sector. The F unit, which in the central sector commonly hosts an additional chromitite (MG 2B) close to its base, is invariably topped by the MG 3 chromitite layer.

The thickness of MG chromitite layers increases abruptly from the central sector to the southern and western sectors, where the nature of the individual chromitite bearing intervals intersected in the boreholes changes laterally over very short distances. This is probably due to local bi-furcating of individual layers, similar to the classic exposure of the UG 1 chromitite layer at Dwars River (see Cameron and Emerson, 1959).

Figure II.7 shows the MG 4 chromitite layer(s) only for the boreholes from the southern and western sectors. The individual columns from these sectors cover the E/F interface including the G unit and the bottom of the L unit, whereas columns from the central sector cover the sequence from the E/F interface up to the bottom of the J unit. This difference in the succession is readily explained by the almost complete absence of the H, J and K units and reduced thicknesses of the F and G units in the southern and western sectors (Fig. II.6).

The pyroxenitic L unit and the associated chromitite layers (UMG) are however present in the central sector although here this lithologically distinct unit occurs about 100 - 300 m above the E/F contact. The upper middle group chromitite layers (UMG) in the central sector are therefore considered to be the stratigraphic equivalent of the MG 4 layer(s) in the southern and western sectors.

CORRELATION OF THE MIDDLE GROUP CHROMITITE LAYERS IN THE EASTERN BUSHVELD COMPLEX

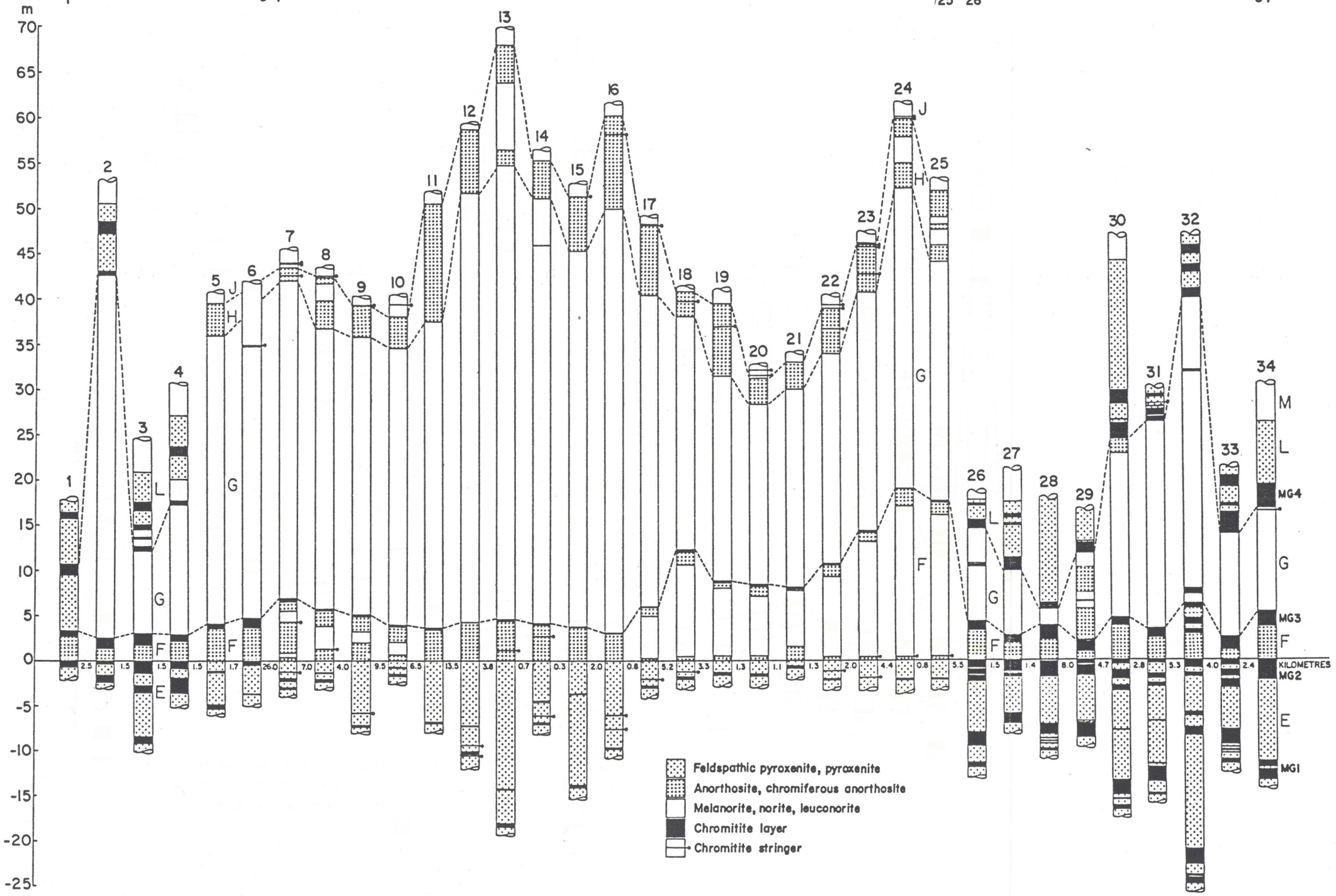

1 KAFFERKRAAL - 163 KS
2 NABOOM (WEST) - 451 KS
3 NABOOM (CENTRAL) - 451 KS
4 NABOOM (EAST) - 451 KS
5 DOORNVLEI (CENTRAL) - 456 KS
6 DOORNVLEI (EAST) - 456 KS
7 ZEEKOEGAT - 421 KS
8 JAGDLUST - 418 KS
9 WINTERSVELD - 417 KS
10 ZWARTKOPPIES - 413 KS
11 MECKLENBURG - 112 KT
12 CLAPHAM - 118 KT
13 DRIEKOP (NORTH) - 253 KT
14 DRIEKOP (CENTRAL) - 253 KT
15 DRIEKOP (CENTRAL) - 253 KT
16 MAANDAGSHOEK (NORTH) - 254 KT
17 MAANDAGSHOEK (CENTRAL) - 254 KT
18 MAANDAGSHOEK (SOUTH) - 254 KT
19 HENDRIKSPLAATS (CENTRAL) - 281 KT
20 HENDRIKSPLAATS (SOUTH) - 281 KT
21 ONVERWACHT - 292 KT
22 DOORNBOSCH (NORTH) - 294 KT
23 DOORNBOSCH (CENTRAL) - 294 KT
24 WINTERVELD (CENTRAL) - 293 KT
25 WINTERVELD (SOUTH) - 293 KT
26 GROOTBOOM (NORTH) - 366 KT
27 GROOTBOOM (CENTRAL) - 366 KT
28 ANNEX GROOTBOOM - 335 KT
29 TWEEFONTEIN (NORTH) - 360 KT
30 TWEEFONTEIN (SOUTH) - 360 KT
31 DE GROOTEBOOM - 373 KT
32 THORNCLIFFE - 374 KT
33 HELENA - 6 JT
34 MAREESBURG - 8 JT

Figure II.7: Correlation of the lower/upper critical zone boundary and associated chromitite layers along the western, central and southern sectors of the eastern Bushveld Complex. Data compiled from literature (Cameron, 1963, 1964; Cousins, 1964; De Villiers, 1968; Cameron and Desborough, 1969) and from logs kindly provided by Messina Ltd., S.A. Development Trust, Rand Mines, Gencor and Lavino Ltd.

II.7. DISTRIBUTION AND PROPOSED STRUCTURAL CONTROL ON PEGMATITE FORMATION

More than 30 ultramafic pegmatites have been located in the studied area (Folder 1), and their actual stratigraphic position is shown on the schematic cross-section in Figure II.8. Pegmatites in this area appear to be restricted to that portion of the layered sequence which is closest to the underlying floor rocks. The thining of individual lithological units and the absence of lower zone rocks in the vicinity of the Derde Gelid pericline has been described in Chapter II.6. It is of particular interest that a similar cluster of pegmatites is found close to the Schwerin fold (see Schwellnus, 1956). Pegmatites appear to be absent further away from anticlinal floor structures, where a relatively thick sequence is developed.

In the Stillwater Complex, Raedeke and McCallum (1984) reported a similar relationship between the occurrence of discordant ultramafic bodies and the thickness of lithological units. Replacement of earlier formed cumulates is particularly abundant in the Chrome Mountain area, where the total thickness of the Peridotite and Bronzitite zones is about half of that in the Mountain View area, where discordant pipes are rare (Raedeke and McCallum, 1984). The authors explain the large difference in thickness between the two sections by differential subsidence of the floor during deposition.

Although one cannot exclude the possibility that at least some floor structures existed prior to the emplacement of the Complex (see Sharpe and Chadwick, 1982), plastic deformation during magma emplacement appears to have formed subsiding basins and adjacent platforms in the Bushveld magma chamber. Thus, regional variations in the relative thickness of the cumulate sequence mirror the resulting floor morphology.

The common setting of pegmatite bodies at basin margins and over "palaeohighs" such as the Derde Gelid pericline and the Schwerin anticline, may then be largely a consequence of these structures.

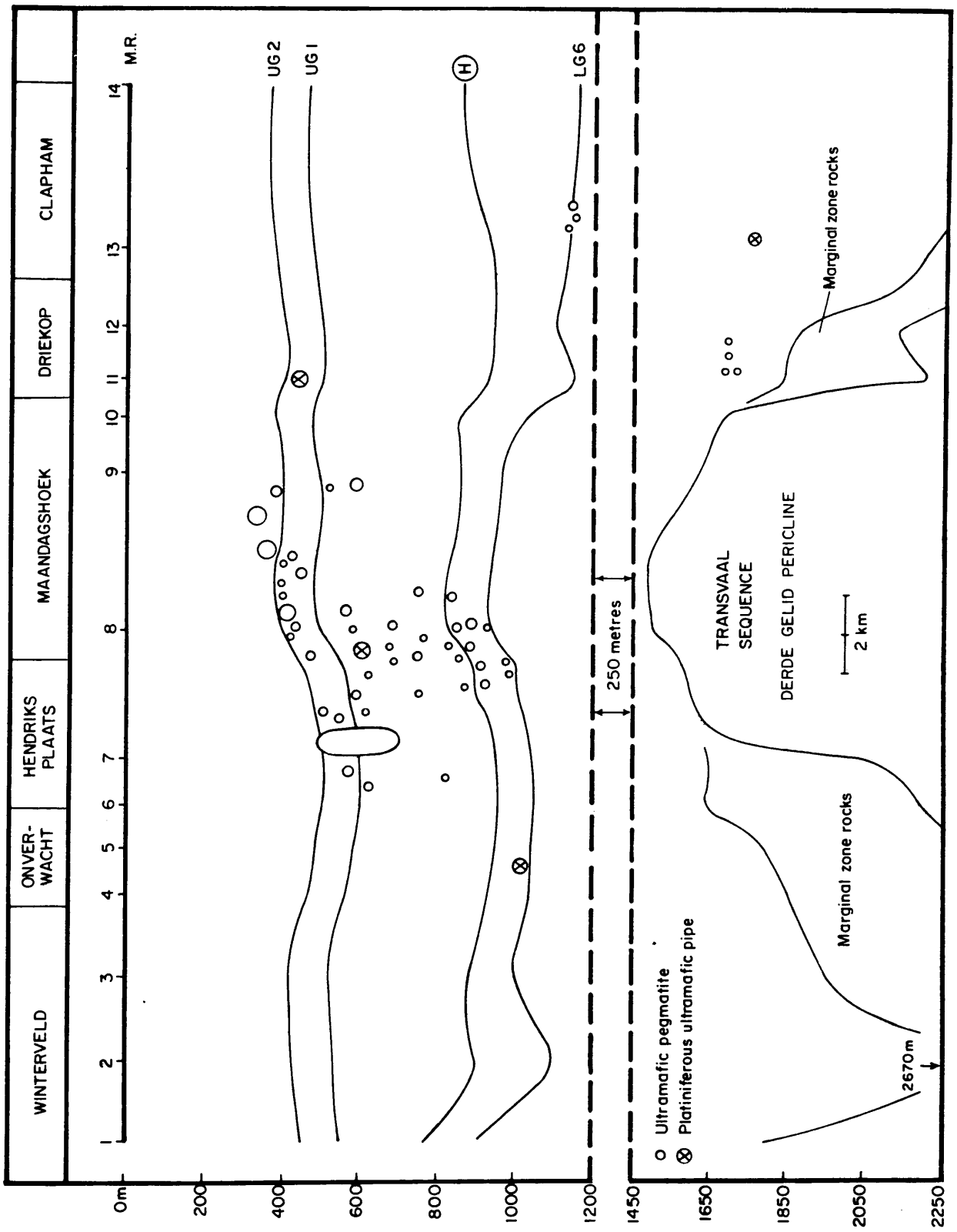

Figure II.8: Cross-section of the Maandagshoek area showing the lower and critical zone sequence in relation to the morphology of the floor. Reconstruction of the LG 6 - UG 1 sequence is mostly based on 14 boreholes, while the relative thicknesses of the sequence up to the Merensky Reef are estimated from outcrops; the Merensky Reef is taken as datum. The cross-section shows the positions of ultramafic pipes in their actual stratigraphic position and incorporates data from Viljoen and Scoon (1985). H marks the base of the H unit as defined by Cameron (1964).

Based on a first-order modelling of flow regimes in sedimentary orebodies, Holocombe (1985) showed that the fluid path and the flow velocity critically depend on the particular morphology and conductivity within a sedimentary environment. Consequently the flow direction closely follows the palaeotopography. Similar to such sedimentary environments, it is suggested that pegmatitic fluids, derived from within the crystallizing pile and/or from devolatilization of floor sediments migrated preferentially laterally but were forced upwards at anticlinal structures.

Viljoen and Scoon (1985) recently proposed that fluids were channelled into areas of structural weakness. It is quite possible that a subvertical fracture pattern developed within the relatively thin cumulate sequence above the updomed structures which in turn facilitated the upward migration of fluids. However, the preferred occurrence of pematites in disturbed areas characterized by faulting and post-Bushveld dykes (Viljoen and Scoon, 1985) does not necessarily imply that pegmatite formation was controlled by (pre-)existing faults. It seems more likely that at least some fractures developed after complete solidification and preferentially in those areas where floor folds caused the deposition of a relative thin cumulate pile. The lithological heterogeneity due to the presence of pegmatites and the reduced thickness of lithological units create a natural weakness and make these areas more prone to tectonic stress.

CHAPTER III: COMPLEX ZONING PATTERNS IN LOWER CRITICAL ZONE SILICATES

III.1. INTRODUCTION

Complex zoning pattern in Mg-Fe silicates have been described in many magmatic rocks from various geological settings. Mineral zoning has been attributed amongst others to magma mixing (Barton et al., 1982) and to high pressure crystallization followed by a low pressure stage, with or without mixing (Emslie, 1975; Kontak et al., 1986; Nabelek and Langmuir, 1986; Dobosi and Horvarth, 1988). Zoning has also been explained by a change in magma composition due to supercooled crystallization (Maaloe and Hanson, 1982), by different cooling rates (Lally et al., 1975; Coish and Taylor, 1979), by subsolidus re-equilibration (Wilson, 1982), or by diffusion controlled growth (Eriksson, 1985).
Zoned orthopyroxenes have previously been described from the Bushveld Complex (Kruger, 1982; De Klerk, 1982; Naldrett and von Gruenewaldt, 1988), and were also found in other layered intrusions like the Great Dyke (Wilson, 1982), the Jimberlana Intrusion (Roeder and Campbell, 1985) and the Stillwater Complex (Barnes and Naldrett, 1986).
Crystal zoning provides an excellent opportunity to reconstruct the magmatic and postmagmatic processes a particular grain has undergone during growth, subsequent solidification and final cooling. During each stage the initial composition might be altered, the extent of which depends largely on the degree of equilibrium attained. Any interpretation has to consider the kinetic parameters governing each stage in the complex history from crystallization to final cooling. The whole process can be schematically divided into a solid/liquid and a solid/solid stage, although the transition is by no means sharp. The solid/liquid stage can be further subdivided into an early stage where crystals coexist with relatively unevolved liquid (open system) and into a late stage where grains are surrounded by trapped fractionating liquid (an essentially closed system).
The results of detailed microprobe traverses across orthopyroxenes, plagioclases and clinopyroxenes are presented and discussed in the following subchapters. The investigations focus mainly on intra-grain compositional variations of orthopyroxene as a function of the parti-

cular composition of the adjoining mineral phase(s). For this reason microprobe traverses were carried out across grain boundaries between orthopyroxenes and intercumulus plagioclases of varying An contents. The investigation also includes a detailed study on the grain size-dependence of orthopyroxene composition. For this purpose more than 100 individual orthopyroxene grains were analyzed in a single thin section and the composition of each grain was plotted against the particular size. To establish distinct size populations the size of more than 300 orthopyroxene grains were determined for three thin sections.

Finally, several small intercumulus clinopyroxenes were analyzed and two detailed traverses were carried out across a large clinopyroxene oikocryst. Compositional variations were related to the adjoining or enclosed silicate phases. The composition of several different sized orthopyroxenes which are fully enclosed by clinopyroxene were additionally analyzed for this particular study.

The purpose of these detailed studies is to quantify the extent to which the primary composition of cumulus minerals has been modified due to subliquidus and subsolidus equilibration processes. It is particularly important to evaluate which element abundance or element ratios in the cumulus phases are likely to have changed or remained constant during postcumulus processes. It is for this reason that detailed mineral-chemical studies were carried out first and that the results are discussed prior to the results of stratigraphic compositional variations (Chapters IV and V).

III.1.1. ANALYTICAL PROCEDURES

All analyses were performed with a Jeol JCXA 733 electron microprobe. The beam diameter was fixed at 10 um (micrometres). Grain traverses were carried out with 10 um spacing for orthopyroxene, 25 um for plagioclase and 50 um for clinopyroxene. Analyzing conditions, reproducibilities and detection limits are given in the Appendix.

III.2. ORTHOPYROXENE

III.2.1. ORTHOPYROXENE TEXTURES

The sizes of more than 300 orthopyroxene grains from feldspathic pyroxenite (E unit) were determined for three different thin sections cut parallel to the drillcore axis (Fig. III.1). This was done by measuring the long axes of each orthopyroxene prism irrespective of the orientation of the grain.
Although thin section measurements do not provide actual grain sizes, such measurements should reflect relative differences in grain size.
Grain size analyses revealed two distinct size populations for each investigated sample, viz. "small" grains with long axis < 1 mm and "large" grains with long axis > 1 mm.

III.2.1.1. LARGE GRAINS

The feldspathic pyroxenites are characterized by large sub- to euhedral orthopyroxene grains which vary in size from 700 * 1000 um to 1500 * 3500 um. They form a loosely packed framework, and account for between 75 and 95 % of the volume of the rock.
Abundant Ca-rich exsolution lamellae are microscopically discernable; the presence of the latter generally being obscured in grains cut parallel to (100). The small width of the lamellae (< 0.5 um) makes quantitative analyses with standard microprobe techniques impossible.
Although the density of lamellae per mm cross-section differs within individual grains, the density in the outermost 50 - 150 um of the grains is generally greatly reduced. This is most clearly shown in several grains where exsolution lamellae terminate at exsolution droplets near the margin, thereby clearly defining an outer rim almost free of exsolution products (Plate 4.B).
Although the large size of the orthopyroxene gives the impression of an almost perfect rhombic shape in hand specimen, individual grains show irregular and embayed crystal faces under the microscope (Plate 1.D). These textures cannot be explained by primary crystal growth

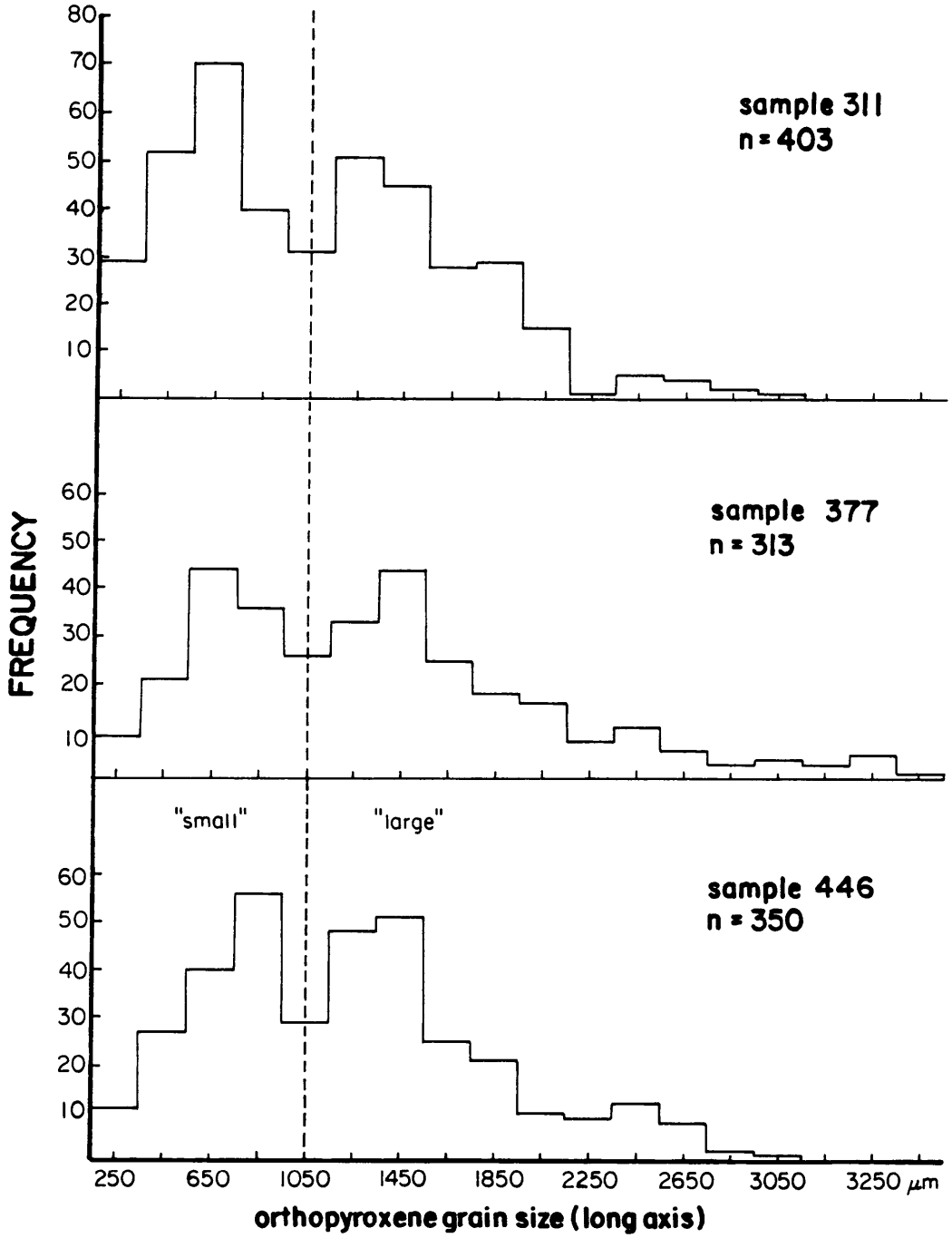

Figure III.1: Histogramms of the grain-size variation (long axis) for 3 different samples from the E unit (lower critical zone). Note the presence of two relative maxima for each studied sample which allows a grouping of "large" and "small" grains.

from the magma and are most likely caused during a postcumulus stage of disequilibrium with surrounding liquid. The degree of resorption is not related to the amount of intercumulus minerals, but is more severe where orthopyroxene is closely associated with interstitial quartz, phlogopite, K-feldspar or sodic plagioclase (An < 50).

A further distinguishing feature of large grains is the presence of numerous orientated rutile needles (Plate 2.B). These are strictly confined to the marginal areas of the host but are absent in the outermost 10 - 30 um of the grain. Needles are less obvious in grains cut parallel to the (100) plane (exsolution plane of the Ca-rich lamellae), indicating that they are confined to the (100) plane. The rutile needles vary in length from 10 um to 100 um, with the breadth not exceeding 1 um. They increase in size and frequency where orthopyroxene is in contact with highly fractionated intercumulus phases.

III.2.1.2. SMALL GRAINS

Small grains commonly cluster in the spaces interstitial to the large grains and are either fully surrounded by plagioclase or, less commonly, in direct contact with large grains. In the latter case they tend to be subhedral and to fill the space between large grains; this can even lead to triple junction texture. The same textural relations have been described from the lower critical zone in the western Bushveld (McDonald, 1967).

The small grains usually range from 400 to 800 um in size, and are mostly euhedral. Ca-rich exsolution lamellae are less abundant and seem to be absent in very small grains (< 300 um).

Unlike the cores of large grains, which are optically free of rutile needles, small grains contain abundant rutile needles (Plate 2.C). The size and density of the needles increases in grains which are near evolved mineral phases such as phlogopite, quartz and K-feldspar. The outermost 30 um are generally free of rutile needles.

III.2.2. INTRA-GRAIN COMPOSITIONAL VARIATION - ORTHOPYROXENE TRAVERSES

Detailed microprobe traverses across several pyroxenes were carried out on thin section 311 29 (upper E unit) to document chemical zoning. Figure III.2 shows 8 grain traverses for Ca, Al, Cr and Ti (all as oxide wt %) concentrations and for the Mg# (mol % 100*Mg/(Mg+Fe)). Both grain types show the same zoning characteristics for Ca, Al, and Cr.

No systematic change is found for Mg#, except in grain 10 where Mg# decreases towards the rim in contact with K-feldspar. Large grains (2 and 13) are marked by a systematic increase in Ti from core to rim with the outermost rim again depleted. Rims of small grains tend to be rather depleted in Ti compared to their cores. Grains 7, 10 and 11 show this effect particularly well.

The extent of zoning for Al and Cr seems to be related to the adjoining mineral phase and to its particular composition. Grains 1 and 2 are in contact with plagioclase of varying composition, reflecting different stages of crystal fractionation. The particular side of a grain which is in contact with more evolved plagioclase (lower An content) shows a stronger depletion in refractory elements (Cr and Al). The same relationship is found in grain 10 where zoning for Al is more pronounced towards the side in contact with K-feldspar.

Orthopyroxene grains in direct contact with either orthopyroxene (grains 12 and 13) or clinopyroxene (grain 4) show normal zoning patterns, although Al and Cr depletion of the rim differs for the three grains, probably indicating variable liquid compositions from which overgrowth and the formation of mutual grain boundaries took place.

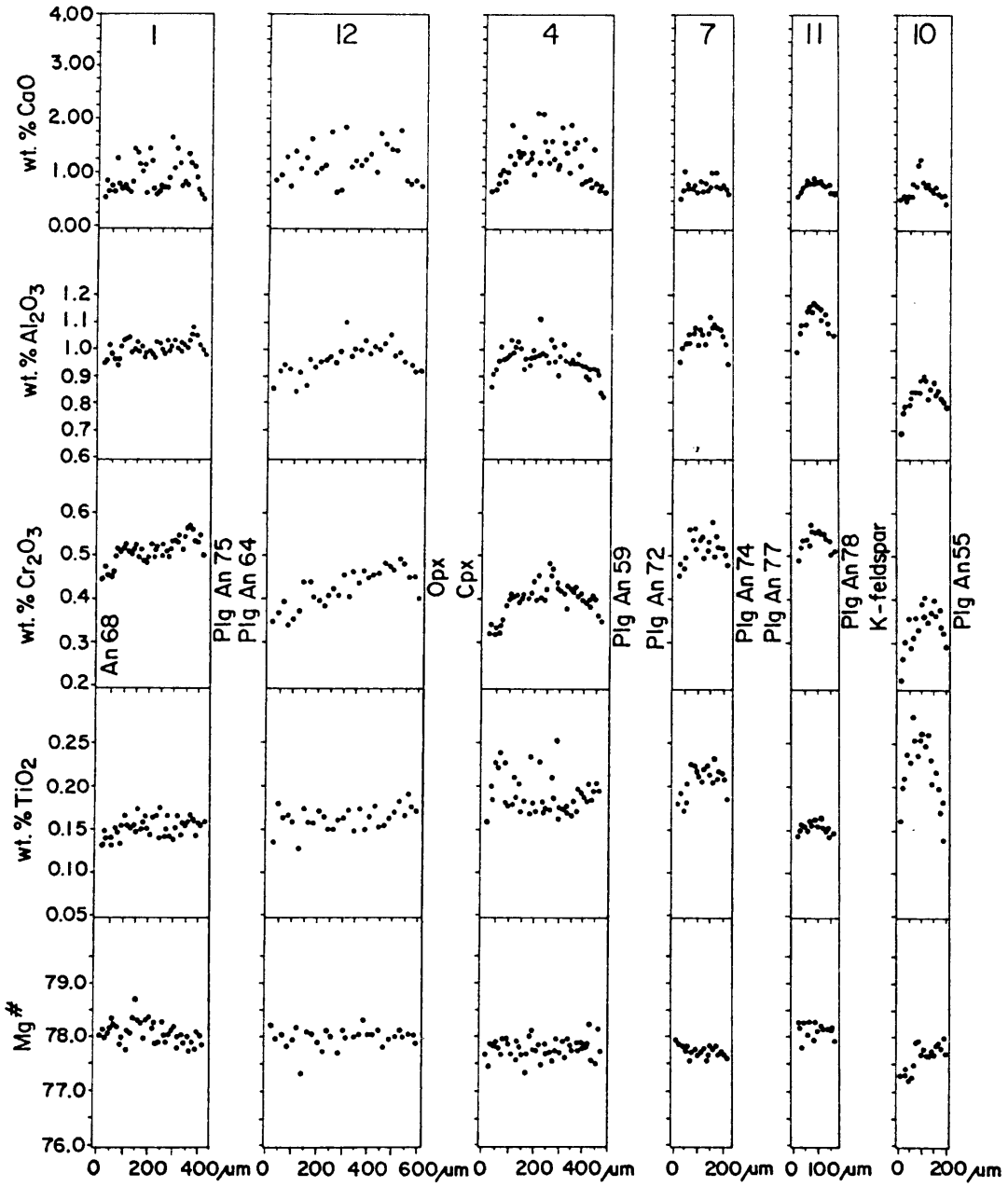

Figure III.2: Intra-grain variation of eight different-sized orthopyroxenes. The remaining two grains and element ratios are shown on the following two pages. The quoted plagioclase compositions (mol % An) refer to the adjoining feldspar grains at a distance of 100 um from the mutual contact. Investigated grains are in contact with either Opx (orthopyroxene), Cpx (clinopyroxene) or K-feldspar where indicated. Distance between each point of analysis is 10 um except for grain 12 where it is 20 um.

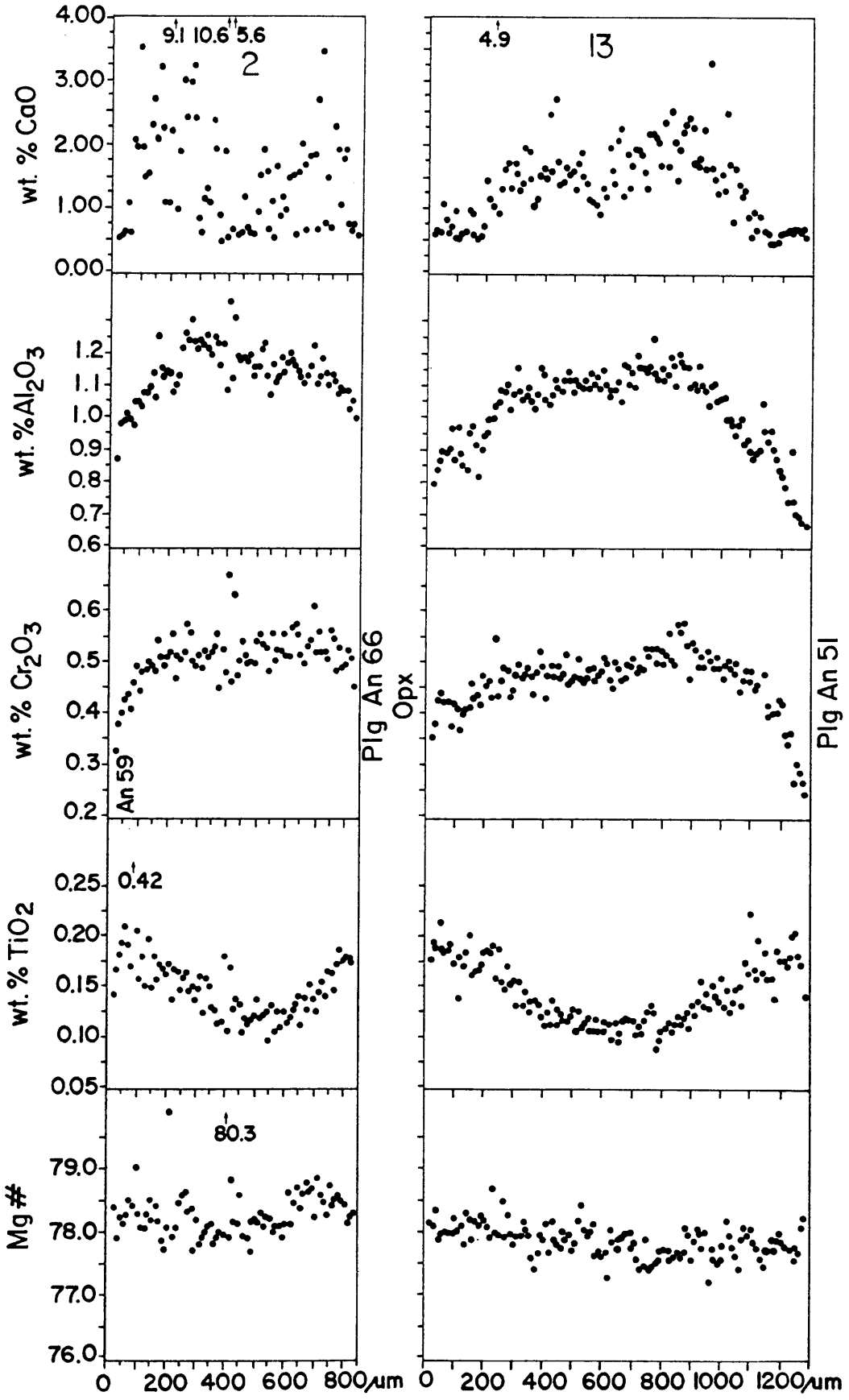

Figure III.2: Intra-grain variation of orthopyroxene. For further information see previous page and text.

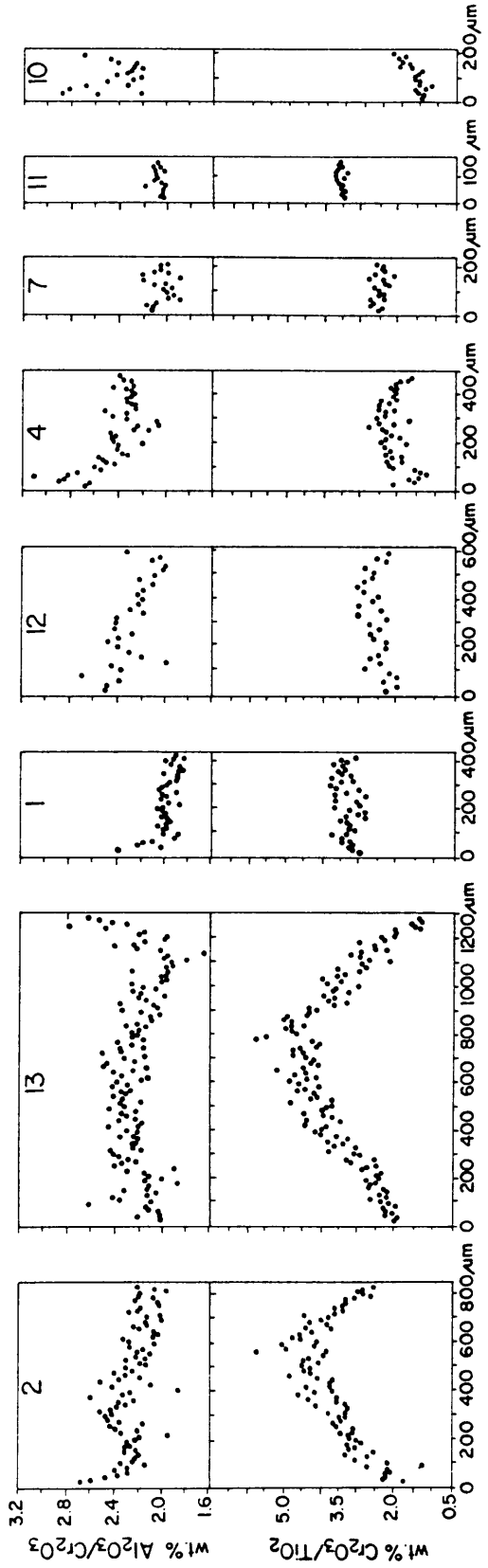

Figure III.2: Intra-grain variation of orthopyroxene. For further information see previous page and text.

III.2.3. INTER-GRAIN COMPOSITIONAL VARIATION

To quantify chemical variation within one sample (311 29) microprobe analyses of 116 orthopyroxene grains were carried out and related to the grain size. For every grain 10 analyses were taken, 5 in the center, and 5 around the margin. The resulting analyses were then averaged for core and rim and plotted against the grain-size (Fig. III.3).

The averaged **calcium** content shows an overall decrease with decreasing grain size. Establishing the absolute Ca content in heavily exsolved pyroxenes generally presents an analytical problem. The observed scatter (0.5 - 5.5 wt % CaO), caused by the presence and the uneven distribution of exsolution lamellae in the grain, can only be overcome by averaging a large number of analyses (n = 10-15). Scatter in the Ca content between individual grains of similiar size is probably the result of an insufficient number of analysed points per grain. The variation in Ca between large and small grains complements the difference in the amount of exsolution lamellae. Rims of large and small grains have identical low Ca values.

The **aluminium** content in the cores shows a similar grain-size dependence as Ca, with small grains relatively depleted in Al. Rims have lower Al concentrations compared to cores.

Cores of small and large grains have comparable **chrome** values while rims tend to have slightly lower Cr concentrations compared to cores. **Al/Cr** ratios define a relatively narrow range despite the considerable range in Al_2O_3 (0.8 - 1.25 wt %) and Cr_2O_3 (0.36 - 0.56 wt %) concentrations. The gradual decrease in the Al/Cr ratio with decreasing grain-size reflects the fact that small grains have generally lower Al but identical Cr concentrations compared to large grains. Al/Cr ratios of the rims show the same principal trend as the cores although with a much larger overall variation.

The observed spread in Al and Cr either reflects inherent properties or it could be due to the orientation of a particular grain (Pearce, 1984). Seeing that Al and Cr decrease from core to rim it follows that the apparent core (grain centre) of a grain cut closer to the rim

Figure III.3: Inter-grain variation of 116 orthopyroxenes from a single sample. Individual data points are average compositions of 5 analyses from the centre and from the rim. The grain sizes were determined by measuring the long axis of each crystal.

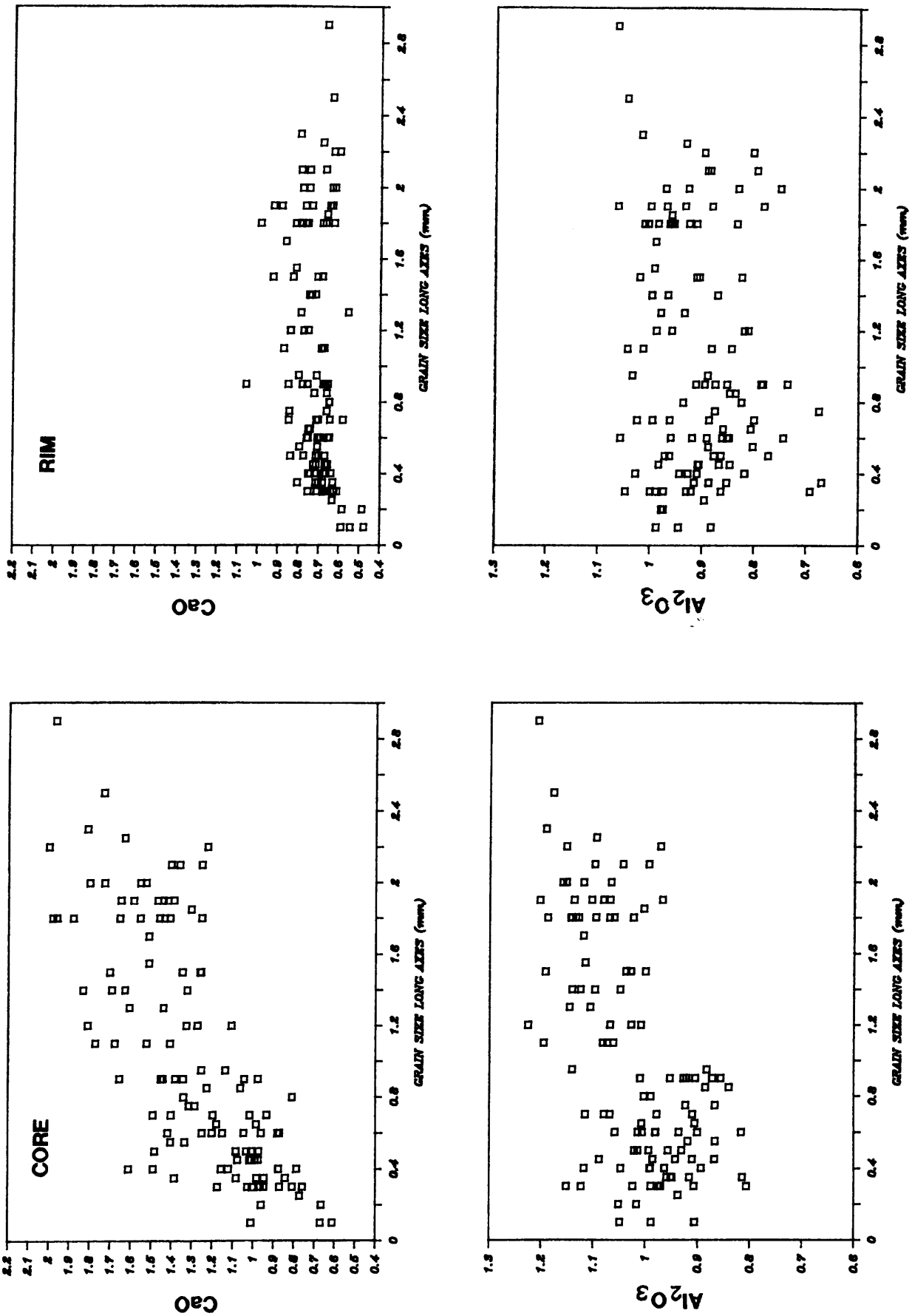

Figure III.3: Inter-grain variation of 116 orthopyroxenes from a single sample. Individual data points are average compositions of 5 analyses from the centre and from the rim. The grain sizes were determined by measuring the long axis of each crystal.

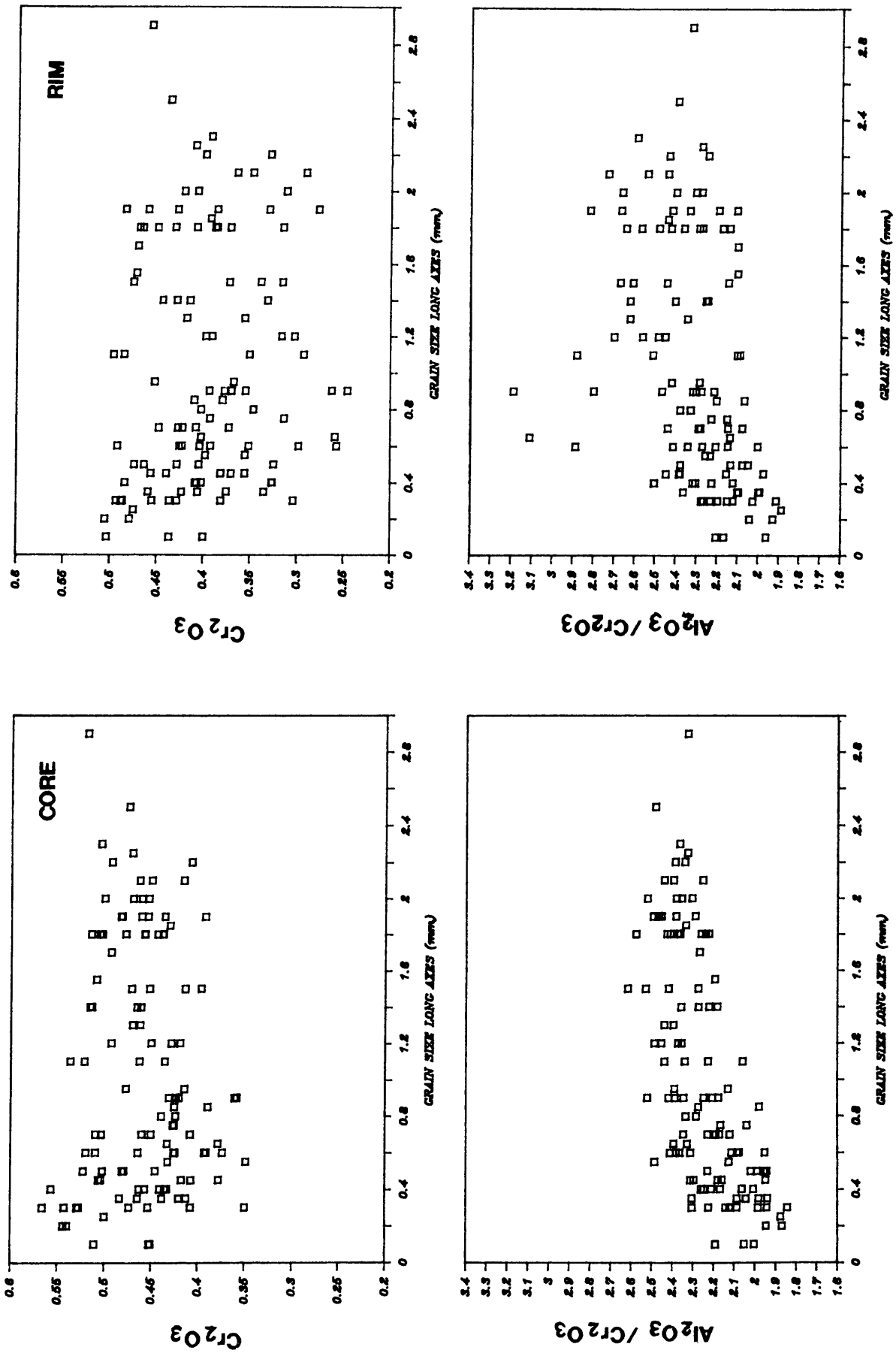

must have lower Al and Cr concentrations. On the other hand, if marginal cuts were included in the core compositions, they should display some elevated TiO_2 and some lower CaO concentrations (Fig. III.2) which was not found to be the case. The observed variation in Al and Cr for large grains is therefore not caused by marginal cuts.
The same argument can not be applied for cores of small grains, as small grains show no pronounced zonation for Ti and Ca. Their total range for Al_2O_3 (0.8 - 1.15 wt %) and Cr_2O_3 (0.35 - 0.57 wt %) is similiar to large grains, although small grains have generally lower Al/Cr ratios.

The **Mg#** (100*Mg/(Mg+Fe)) for different grain sizes and for cores displays considerable scatter over the same compositional range. However, slightly lower Mg# tend to be restricted to both core and rim of small grains.

The **titanium** content shows a strong size dependence, with small grains invariably enriched. This feature is optically expressed by the presence of numerous rutile needles in the cores of small grains, whereas cores of large grains are devoid of needles. Rims of large grains are relatively enriched compared to cores, while small grains show the reverse trend. The pronounced difference in the TiO_2 content between cores of large and small grains is also well illustrated by plotting the Cr/Ti ratio against the grain size (Fig. III.3).
It must be mentioned that the analyzed Ti values represent the host composition only. Occasional high TiO_2 values (0.4 - 1.0 wt %), the lack of pronounced scatter in grain traverses and no apparent TiO_2 depletion next to the rutile needles confirm this. It is not obvious whether the rutile needles exsolved from the orthopyroxene (Moore, 1968) or resulted from epitaxial growth. It should be mentioned that rutile is present in the sample as orientated needles in plagioclase (Plate 2.D) and interstitial clinopyroxene, as well as a discrete euhedral accessory phase (Plate 2.E). These observations could indicate an origin by epitaxial growth of the rutile needles. However, Shatsky et al. (1986) suggested that with decreasing temperature oxidation of Ti^{3+} could lead to the exsolution of rutile.

Figure III.3: Inter-grain variation of 116 orthopyroxenes from a single sample. Individual data points are average compositions of 5 analyses from the centre and from the rim. The grain sizes were determined by measuring the long axis of each crystal.

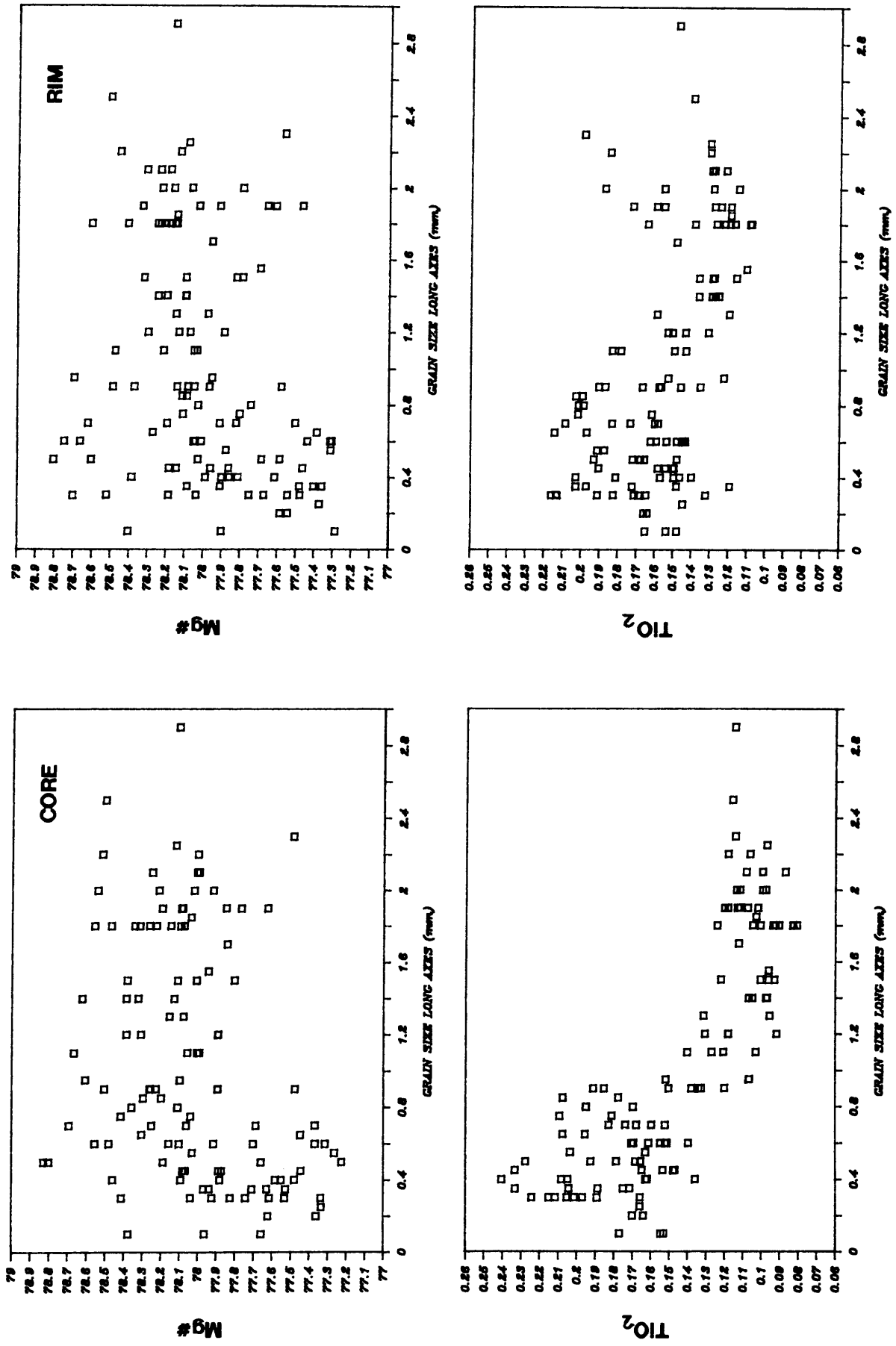

Figure III.3: Inter-grain variation of 116 orthopyroxenes from a single sample. Individual data points are average compositions of 5 analyses from the centre and from the rim. The grain sizes were determined by measuring the long axis of each crystal.

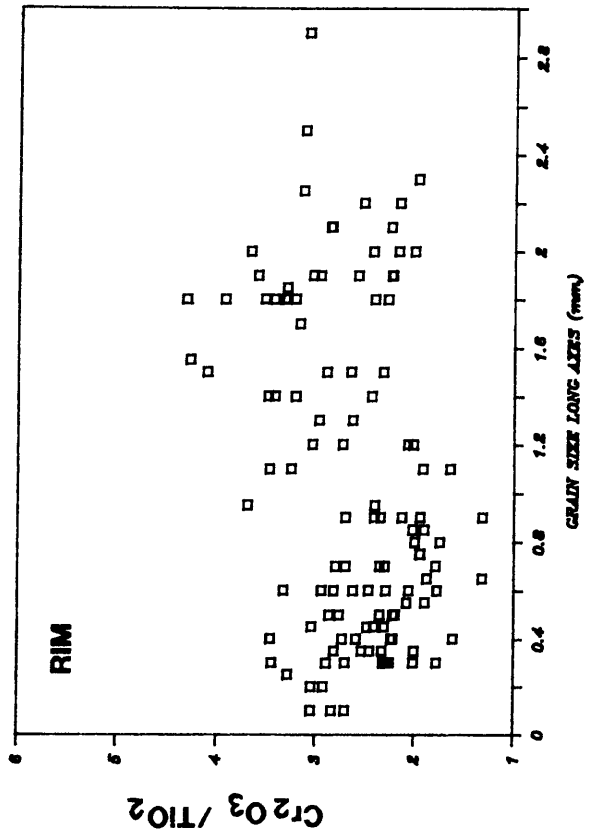

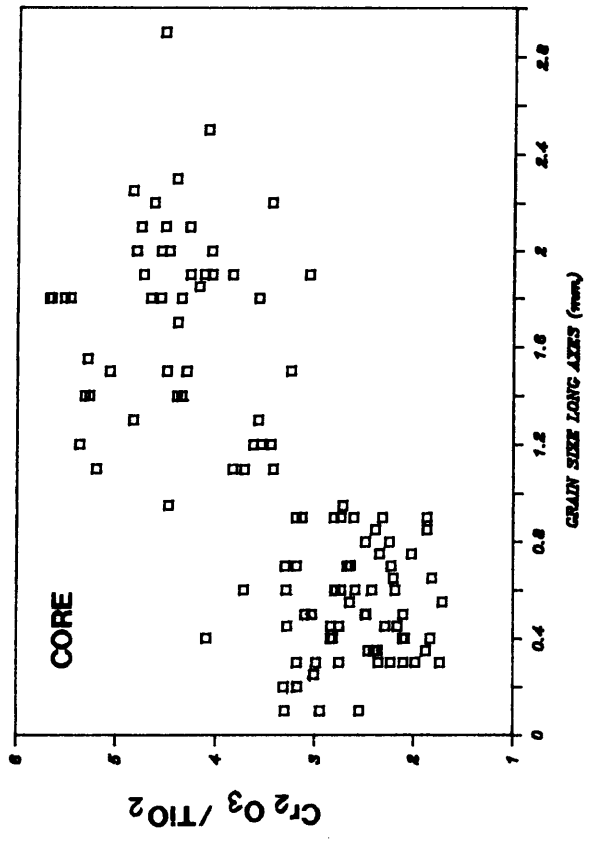

III.3. PLAGIOCLASE

III.3.1. GRAIN TRAVERSES AND INTER-GRAIN VARIATION

Microprobe traverses on the intercumulus plagioclase are linear extensions from the orthopyroxene traverses into plagioclase (Fig. III.4). Several features are noteworthy. Firstly, compositions of the apparent cores (geometrical centres) are relatively uniform over distances as much as 600 um, with their absolute An content (mol % 100*Ca/(Ca+Na)) ranging from An 78 in grain 11 to An 51 in grain 13.

Secondly, plagioclases show a distinct decline in An content towards the contact with orthopyroxene, indicating that crystallization and fractionation of pore liquid started somewhere in the pore space and progressed towards orthopyroxene grains. Pore liquid was therefore free to migrate around pyroxenes and to equilibrate with the latter until it solidified. Various stages of trapped liquid fractionation are indicated by the observed range in mantling plagioclase composition.

Thirdly, a sharp drop in the An content towards the contact is found in plagioclase grains with a high average An content (grains 7L and 11), a feature that is also optically discernable by a sudden change in plagioclase extinction angle (Plate 2.F). This abrupt decline over less than 40 um cannot be explained by continuous growth from a slowly evolving liquid under internal equilibrium conditions. Possible reasons for the sudden drop in An content towards the contact with orthopyroxene will be discussed in Chapter III.5.3.2 together with the respective zoning patterns of the adjoining orthopyroxene grains.

FeO and K_2O show a broadly sympathetic behaviour and increase with decreasing An content.

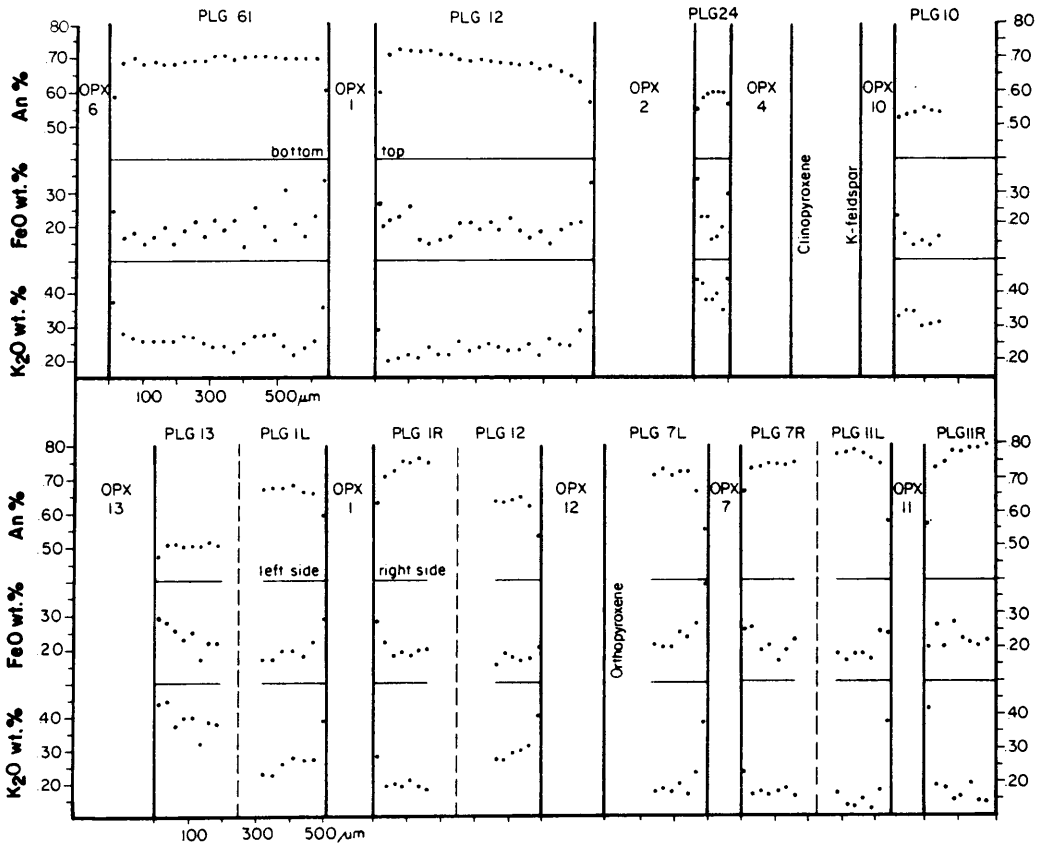

Figure III.4: Interstitial plagioclase composition plotted against the distance from the grain boundaries. Traverses are linear extensions of the orthopyroxene traverses (Fig. III.2). The shown pyroxenes are identical with the ones from Figure III.2. Orthopyroxenes 4, 10, 12 and 13 are only on one side in contact with plagioclase. Vertical (bottom - top) and horizontal (left-right) traverses were carried out in feldspar surrounding orthopyroxene 1; the horizontal traverse for grain 1 joins up with the pyroxene traverse from Fig. III.2. Distance between each point of analyses is 25 um.

III.4. CLINOPYROXENE

III.4.1. TEXTURAL FEATURES

Postcumulus clinopyroxene oikocrysts occur throughout the lower critical zone. Oikocrysts appear to be evenly distributed on an outcrop scale but can increase in frequency in individual layers. Field evidence and thin sections indicate that clinopyroxenes have no preferred orientation. Individual euhedral crystals are up to 3 cm in diameter, display well developed exsolution textures and invariably enclose numerous irregularly shaped orthopyroxene grains (Plate 4.C). The width of the orthopyroxene exsolution lamellae (up to 5 um) require more than 25 analyses with a 10 um beam diameter in order to obtain an average grain composition within an error of 0.2 wt % CaO. The following results were therefore obtained from a single thin section (311 29) and no attempt was made to evaluate possible compositional variations within the studied sequence. It should be mentioned that clinopyroxene is also found as very small (< 0.5 mm) anhedral and typically interstitial grains.

III.4.2. GRAIN TRAVERSES AND INTER-GRAIN VARIATION

Table III.1 shows the core and rim compositions of a clinopyroxene oikocryst. Two detailed traverses across the same oikocryst are presented in Figure III.5. Both the bulk analyses and the traverses reveal a decrease in Al and an increse in Mg# (mol % 100*Mg/(Mg+Fe)), Ca and Ti towards the rim. Except for Ti, element zoning is more obvious towards the side which is in contact with plagioclase than towards adjoining orthopyroxene. Cr shows no pronounced change, although a slight decrease towards adjoining and enclosed orthopyroxene can be seen.

Table III.1 Averaged bulk core and rim composition of a single clinopyroxene oikocryst; analyses were taken randomly in the centre and along the margin.

SiO_2	Na_2O	Al_2O_3	MgO	CaO	TiO_2	FeO	MnO	Cr_2O_3	Total	Mg#
clinopyroxene oikocryst core (n = 60)										
52.49	0.17	1.89	16.68	19.46	0.23	6.90	0.18	0.87	98.90	81.2
same oikocryst rim (n = 90)										
52.77	0.21	1.72	16.67	20.60	0.30	6.42	0.16	0.85	99.74	82.2

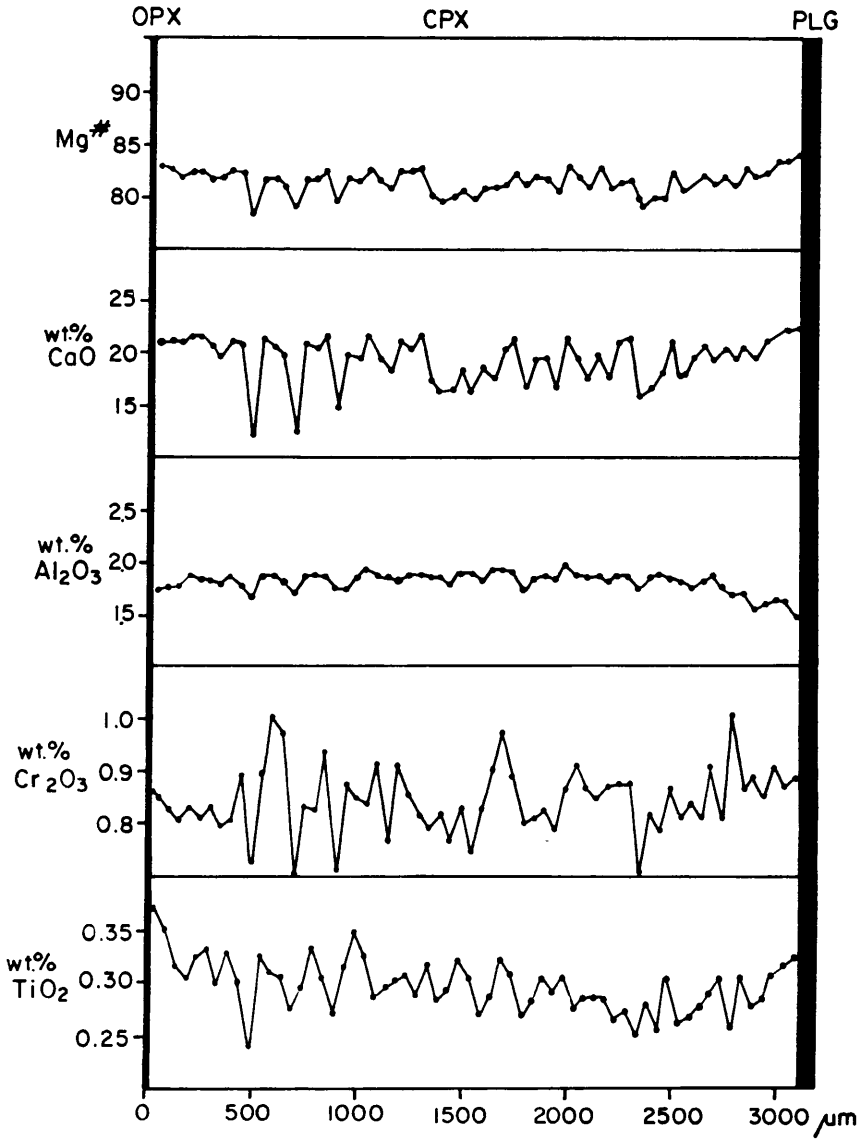

Figure III.5: Line profile across a clinopyroxene oikocryst. Clinopyroxene is in contact with plagioclase and orthopyroxene. Low Ca-contents are caused by orthopyroxene exsolution lamellae. Distance between each point of analysis is 50 um. See also traverse on following page.

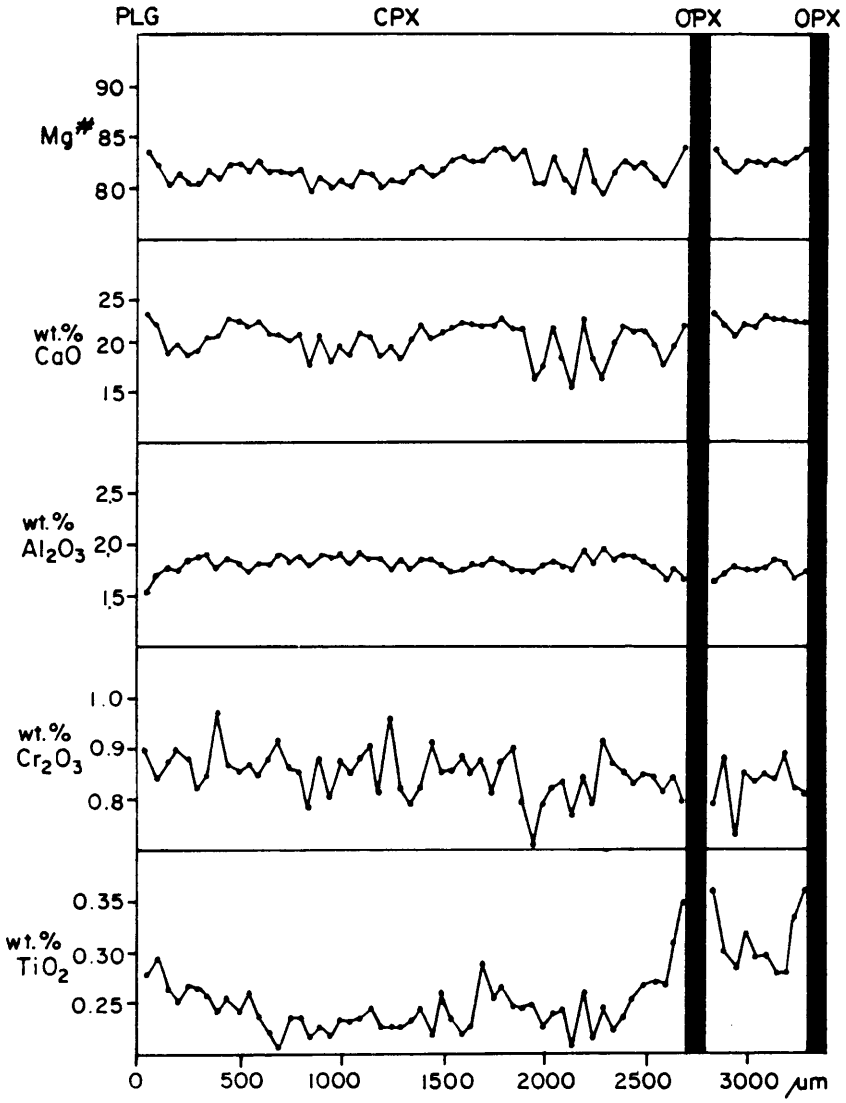

Figure III.5: Line profile across a clinopyroxene oikocryst. Clinopyroxene is in contact with plagioclase and orthopyroxene. Profile intersects an enclosed orthopyroxene grain. Low Ca-contents are caused by orthopyroxene exsolution lamellae. Distance between each point of analysis is 50 um. See also traverse on previous page.

A comparison of different sized clinopyroxene grains reveals that individual grains differ in their element concentrations as a function of the grain size. Table III.2 lists bulk core analyses of two oikocrysts and five interstitial clinopyroxene grains of different size. The latter are mostly surrounded by orthopyroxene. The analyzed grains show a systematic increase in Mg# and Ca with decreasing grain size. Ti also increases in smaller grains but decreases again in very small grains (< 100 um). Al and Cr decrease with decreasing grain size.

Table III.2. Bulk analyses of seven clinopyroxene grains. All analyses are from the same thin section and were performed with 10 um beam diameter in the core of each grain. Note the systematic increase in Mg# and CaO with decreasing grain size, whereas Al_2O_3 and Cr_2O_3 decrease.

SiO_2	Na_2O	Al_2O_3	MgO	CaO	TiO_2	FeO	MnO	Cr_2O_3	Total	Mg#
clinopyroxene oikocryst > 3 mm (n = 30)										
52.44	0.31	2.07	16.81	19.46	0.24	7.17	0.18	0.86	99.64	80.7
clinopyroxene oikocryst 1100 um (n = 11)										
52.36	0.34	1.99	16.79	19.36	0.36	6.83	0.18	0.92	99.13	81.4
interstitial clinopyroxene 550 um (n = 6)										
52.88	0.33	1.58	16.05	21.62	0.39	5.86	0.18	0.69	99.56	83.0
interstitial clinopyroxene 400 um (n = 14)										
53.12	0.32	1.47	15.66	22.28	0.36	5.38	0.14	0.55	99.28	83.8
interstitial clinopyroxene 200 um (n = 3)										
52.94	0.31	1.51	15.49	22.48	0.37	5.12	0.14	0.74	99.10	84.5
interstitial clinopyroxene < 100 um (n = 2)										
52.96	0.33	1.37	15.60	23.18	0.29	4.56	0.12	0.79	99.20	85.9
interstitial clinopyroxene < 100 um (n = 2)										
53.07	0.31	1.20	15.93	23.63	0.25	4.27	0.12	0.70	99.48	86.9

III.4.3. CLINOPYROXENE ZONING - FRACTIONATION OR RE-EQUILIBRATION ?

The systematic element variations within a single clinopyroxene grain and between individual grains is the result of interstitial liquid fractionation and/or subsolidus re-equilibration with surrounding orthopyroxene. The fact that Ti concentrations are higher in medium sized grains and lower in very small grains reflects crystallization of a Ti-rich phase during progressive liquid fractionation and that the Ti-poor clinopyroxenes crystallized very late as indicated by their high Ca content (Table III.2) after the liquid was relatively depleted in Ti. The same two-stage fractionation behaviour for Ti is also found in orthopyroxene traverses and is attributed to the crystallization of Ti-rich phases such as phlogopite and rutile. Evidence

for subsolidus re-equilibration is provided by the differential behaviour of Ti in grain traverses, i.e. a Ti increase is more pronounced towards orthopyroxene (adjacent and enclosed) than towards feldspar.
It is particularly difficult to evaluate which of the two processes is more important for the final clinopyroxene composition, as both processes i.e. liquid fractionation and re-equilibration will produce the same trends. A decline in temperature during progressive fractionation is expected to result in higher Ca concentrations (e.g. Wood and Banno, 1973; Kretz, 1982; Lindsley, 1983). The increase in Ca with decreasing grain size is coupled with a decrease in Fe while Mg stays relatively constant. This can be attributed to the fact that both Ca and Fe show a strong preference for the same lattice site (M2) whereas Mg partitions preferentially into the smaller M1 sites (e.g. Virgo and Hafner, 1970; Bertrand and Mercier, 1985).
Subsolidus re-equilibration between clinopyroxene and orthopyroxene will also increase Ca, Mg# and Ti in clinopyroxene. The systematic change in clinopyroxene composition towards adjoining orthopyroxene is shown in Figure III.6. The trends displayed were derived from a large number of individual analyses which were taken radially to an enclosed orthopyroxene grain.
To document a cation exchange process (re-equilibration) between the two pyroxenes, several enclosed orthopyroxenes were also analysed. Figure III.7 shows various element concentrations and the Mg# of 12 centrally enclosed orthopyroxene grains and 10 marginally enclosed orthopyroxene grains versus size of each particular grain. The averaged composition of orthopyroxene (> 0.6 mm^2) not enclosed by clinopyroxene is plotted within each compositional field, while the composition of orthopyroxene exsolution lamellae in clinopyroxene is plotted on the vertical axis.
Centrally enclosed grains show a systematic change in composition with grain size which is consistent with a subsolidus re-equilibration process. The extent of compositional change is controlled by the volume of a particular orthopyroxene which equilibrated with surrounding clinopyroxene. The smaller a particular orthopyroxene grain is, the closer its composition becomes to the composition of an exsolution lamellae. The latter must be regarded as the ultimate equilibrium composition between clinopyroxene and coexisting orthopyroxene.

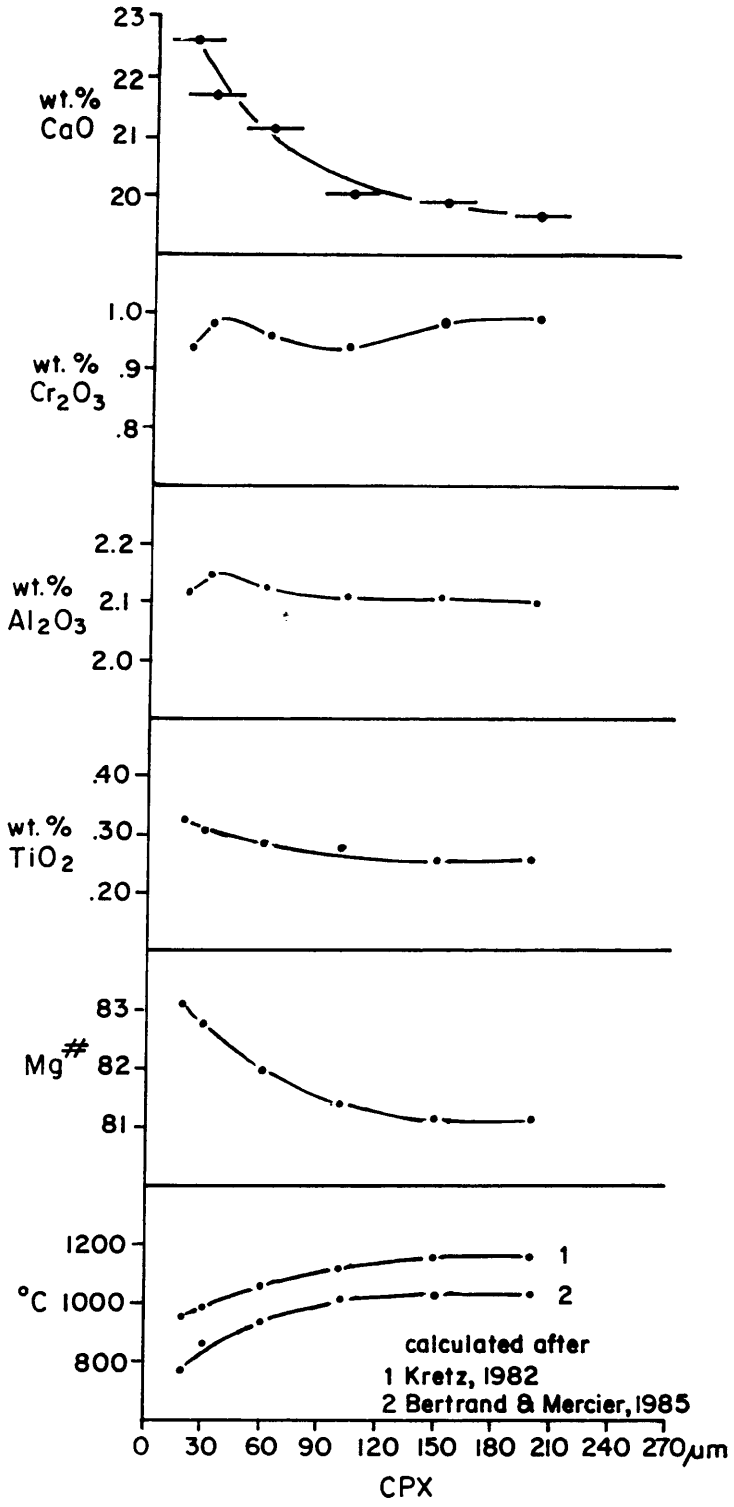

Figure III.6: Clinopyroxene traverse around an enclosed orthopyroxene. Individual data points are averages from individual analyses which were taken radially at various distances (20, 30, 60, 100, 150 and 200 um) to the enclosed orthopyroxene. The beam diameter used was 30 um. Mg# is mol % 100*(Mg/(Mg+Fe)). Temperatures were calculated by using a constant orthopyroxene composition and the various clinopyroxene compositions.

Marginally enclosed grains are relatively depleted in Al and Cr and enriched in Ti and show no obvious correlation between grain size and these elements. The different compositional behaviour of marginally enclosed grains possibly reflects enclosure by clinopyroxene at a late stage so that these grains were still free to react with surrounding liquid. The composition of the latter has therefore changed according to the degree of interstitial melt fractionation. The compositional shifts (Al and Cr depletion, Ti enrichment) are consistent with trapped liquid fractionation, and the compositions of marginally enclosed grains are similar to the compositions of small orthopyroxene grains not enclosed by clinopyroxene (Chpts. III.2.2 and III.2.3). Continuous clinopyroxene growth presumably caused the trapped liquid to evolve further.

It can be assumed that the composition of marginally enclosed grains also changed subsequently to enclosure. However, the compositional effects due to subsolidus re-equilibration appear to be relatively small compared to the observed change in centrally enclosed grains. One can therefore speculate that, because of the strong temperature dependance of diffusion rates, which decrease with decreasing temperature, temperature had dropped considerably by the time marginal grains became enclosed. Evidence for subsolidus re-equilibration in marginal grains is provided by their zoning pattern. Rims are generally richer in Al and Cr and poorer in Ti than cores (Fig. III.7), which is contrary to the zoning trends found in non-enclosed orthopyroxene grains.

III.4.4. CRYSTALLIZATION TEMPERATURE - AN ESTIMATE

The calculated crystallization temperatures for clinopyroxene (Fig. III.6) are comparable to the experimentally determined data (Cawthorn and Davies, 1983; Sharpe and Irvine, 1983). The latter authors have shown that for most B1/B2 mixtures clinopyroxene becomes a stable liquidus phase after spinel, olivine, orthopyroxene and plagioclase at about 1130°C. The temperatures calculated at a distance of 150 - 200 um can be seen as a clinopyroxene crystallization temperature, while the lower temperature values towards the contact with orthopyroxene

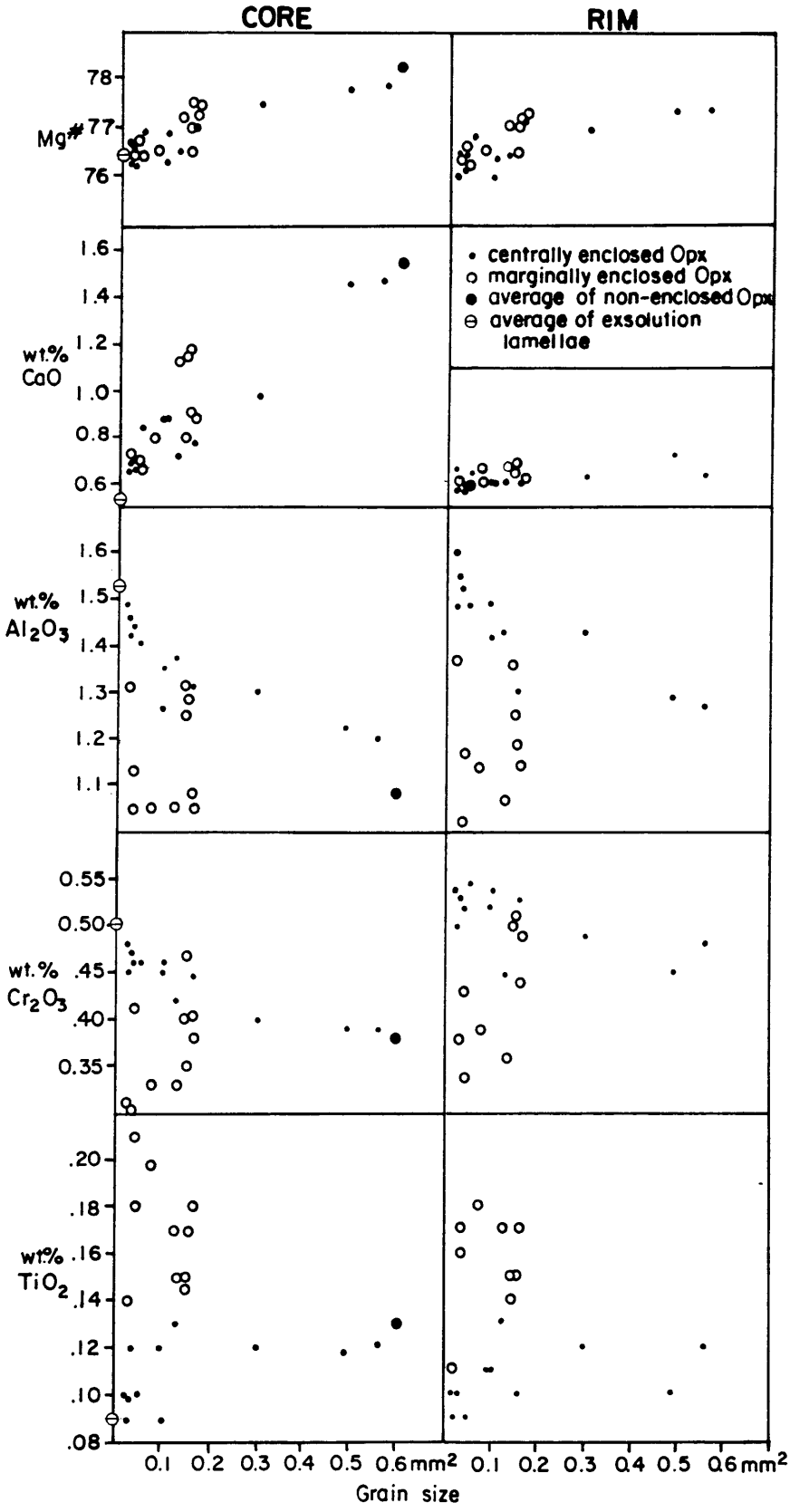

Figure III.7: Composition of 22 orthopyroxenes enclosed in a clinopyroxene oikocryst. Core and rim compositions are averages from 4-10 individual analyses. Centrally and marginally enclosed grains are marked by different symbols. The average compositions of 10 orthopyroxene exsolution lamellae are indicated on the vertical axis; the compositional average of 25 orthopyroxene grains (> 0.6 mm²) which are not enclosed by clinopyroxene are plotted for comparison.

probably reflect various blocking temperatures during subsolidus re-equilibration. Although the calculation methods proposed by Kretz(1982) and Bertrand and Mercier (1985) result in different temperatures, the resulting range clearly confirms that clinopyroxene crystallized after orthopyroxene and calcic plagioclase (see Fig. V.1a and b). Crystallization of clinopyroxene is therefore restricted to growth from interstitial liquid within the cumulus pile.

III.4.5. PROPOSED ORIGIN OF CLINOPYROXENE OIKOCRYSTS

The characteristic textural occurrence of clinopyroxene as postcumulus sub- to euhedral oikocrysts can be explained by a late magmatic process whereby, on a very local scale, pre-existing orthopyroxene is partially and plagioclase almost completely re-dissolved (Plate 2.G) by the interstitial liquid.

Re-fusion of already crystallized phases and subsequent growth of large clinopyroxene crystals could have been aided by an increase in the volatile content during progressive trapped liquid fractionation. The latter seems to be substantiated by an increased number of oikocrysts in samples with strongly evolved interstitial phases and by the fact that phlogopite commonly occurs in close vicinity to clinopyroxene. The tendency of clinopyroxene to form large sub- to euhedral grains could have resulted from different growth mechanisms for clinopyroxene and plagioclase, as growth rates for clinopyroxene are higher at a given undercooling than those for plagioclase (Kirkpatrick et al., 1976).

The observed chemical zoning resulted from subsolidus re-equilibration with enclosed or adjacent orthopyroxene as well as from continuous crystallization from an evolving interstitial liquid.

III.5. DISCUSSION OF COMPLEX ZONING PATTERNS IN ORTHOPYROXENES - EVIDENCE FOR SUBLIQUIDUS DISEQUILIBRIUM

III.5.1. PRIMARY MAGMATIC ZONING AND SUBSOLIDUS RE-EQUILIBRATION

Zoning as a result of disequilibrium conditions during primary growth crystallization has not been recorded for cumulus pyroxenes in large layered intrusions (e.g. Wager and Brown, 1967). Ideal equilibrium conditions can be assumed due to the high atomic diffusivities in the melt and to the slow growth rate (Hart, 1981; Lindstrom, 1983, Tsuchiyama, 1985). Thus, it can be assumed that zoning resulted from disequilibrium between cumulus grains and interstitial liquid. The efficiency of grain-boundary diffusion was recently documented by various authors (Roeder and Campbell, 1985; Barnes, 1986; Bodinier et al., 1987).

Subsolidus re-equilibration between orthopyroxene and an adjoining silicate mineral phase can be discarded as an alternative process because it can not explain the overall similarities in the zoning pattern, whether orthopyroxene is in contact with orthopyroxene, clinopyroxene, plagioclase or K-feldspar.

III.5.2. REACTION OF ORTHOPYROXENE WITH INTERCUMULUS LIQUID

Disequilibrium conditions between large orthopyroxenes and intercumulus liquid are indicated by abundant uneven and embayed crystal faces. As these features are not restricted to grains associated with evolved phases one can assume that disequilibrium was not the result of progressive fractionation of interstitial liquid. Disequilibrium conditions, resulting in pyroxene resorbtion, must have existed prior to the crystallization of intercumulus liquid and persisted on a local scale of micrometres to fairly low temperatures. As was shown by Roeder and Campbell (1985) crystallization of trapped liquid can take place over a range as large as 300°C.

It is very difficult to determine whether grains have attained their zoning pattern by re-equilibrating with trapped liquid, or by adcumulus overgrowth, because data on partition coefficients and element diffusion rates are very limited and secondly because trapped liquid composition can only be estimated. Although overgrowth and re-equilibration are physically different processes, both will result in similar zoning patterns, reflecting various compositions of a slowly evolving liquid.

A primarily overgrowth-controlled origin of the zoning should result in similar volumes (although not necessarily of similar composition) being added onto pre-existing grains of similar size. In the case of large grains, however, the volume of the zoned part is far too large to have been caused by zoned overgrowth alone. This discrepancy is best shown in grain 13 (Fig. III.2) where the unzoned core accounts for about 30 % of the diameter or less than 10 % of its total volume. The fact that very small grains are zoned shows that the effects of subsolidus homogenization are negligible. A smoothing of an overgrowth related stepped chemical profile seems therefore not likely. The observed zoning gradients for large and small grains are remarkably similar which suggests that pore spaces filled with interstitial liquid remained interconnected to assure internal equilibrium.

The large volume of the zoned part of large grains shows clearly that the origin of zoning is not related to fractionated overgrowth, although it cannot be ruled out that limited overgrowth and the nucleation of further grains took place. The relatively small volume of liquid required for the growth of small grains make a primary zoned growth unlikely because constant equilibrium between solid and liquid can be assumed in a slow cooling environment.

The zoning characteristics therefore reflect various stages of disequilibrium with a continuously evolving liquid. This is not to say that small grains did not crystallize from an already evolved liquid. Zoning itself, however, is caused by postcumulus reaction with interstitial liquid irrespective of the time a particular pyroxene formed. The attained composition can therefore be used to reconstruct the fractionation path of the interstitial liquid.

III.5.3. ELEMENT BEHAVIOUR DURING RE-EQUILIBRATION

III.5.3.1. CALCIUM

The high Ca values found in large orthopyroxene grains undoubtedly reflect a high temperature origin. The dependence of Ca concentration on liquidus temperature has been shown by numerous authors (Boyd and Schairer, 1964; Saxena, 1976; Kretz, 1982; Lindsley, 1983; Nabelek et al., 1987). Ca depleted rims can therefore be attributed to re-equilibration of high temperature orthopyroxene in a low temperature environment.

The interdiffusion coefficient for Ca in pyroxene ranges between 10^{-15} cm^2/s at 1200°C (Brady and McCallister, 1983) and 10^{-20} to 10^{-17} cm^2/s at about 900°C (Rietmeijer, 1983). Although the data were determined from clinopyroxenes, they might semi-quantitatively be applied to orthopyroxene as well. A cooling period of 20000 years provides for a temperature decrease from 1200 to 1000°C for a 3 km thick intrusion (after Wilson, 1982; Fig. 22 curve 5); this would result in Ca diffusion in pyroxene over a distance of approximately 50 um (after Tsuchiyama, 1985; Fig. 12B).

Hence, the sluggishness of Ca diffusion will invariably cause pyroxenes to become chemically zoned even at relatively high temperatures.

If Ca concentrations are solely diffusion controlled then the final pattern should be a function of grain size. A positive correlation between grain size and Ca content can in fact be shown (Fig. III.2 and III.3). The uniform Ca content of the outermost rim (0.5 - 0.7 wt % CaO) of all the grains (Fig. III.2) can then be regarded as an equilibrium composition. Of interest is the fact that the same low Ca values (0.5 - 0.7 wt % CaO) are occasionally found in the central portion of grain traverses (grain 1, 2 and 12; Fig. III.2). These low Ca values are interpreted to reflect the composition of the orthopyroxene host after the exsolution of Ca- rich lamellae.

Thus, the systematic decrease in Ca content from core to rim and with grain size is most likely the result of subliquidus re-equilibration with interstitial liquid in response to decreasing temperature.

III.5.3.2. ALUMINIUM

The controlling parameters on the solubility of Al in orthopyroxene are too manifold and complex to draw unambiguous conclusions about liquidus temperature or melt composition. Temperature and pressure (Green, 1963; Anastasiou and Seifert, 1972; Wood and Banno, 1973; Gasparik, 1987), a change in the SiO_2 activity (Campbell and Borley, 1974; Campbell, 1977) presumably as a result of a change in the water content in the melt (Kushiro, 1975) and the influence of coexisting spinel (Obata, 1976; Gasparik and Newton, 1984) have all been demonstrated to affect the Al content of pyroxene. The erratic scatter in the Al content of Bushveld orthopyroxenes with stratigraphic height (Cameron, 1978, 1980, 1982) and along strike (Chpt. V.5) highlights these complications and require further research.

Nevertheless, the uniform behaviour of Al in the grain traverses requires a process which has affected all grains in a systematic manner. The almost linear relation of Al content in orthopyroxene at the rim and the composition of plagioclase at a distance of about 50 to 100 um (Fig. III.8) can only be explained by a diffusional process, controlled by the degree of trapped liquid fractionation. It is assumed in Figure III.8 that the composition of adjoining plagioclase at various distances from the contact with orthopyroxene is directly related to the interstitial liquid composition. This is based on the assumption that any compositional change in the interstitial liquid due to fractionation is recorded by the respective interstitial plagioclase composition.

The relatively narrow range in plagioclase composition at the immediate contact (< 15 um) with orthopyroxene and the fact that the best fit between Al in orthopyroxene and An content is found at greater distance (100 um) make it doubtful whether some plagioclase rims were in equilibrium with the adjoining orthopyroxenes. As some pyroxenes (grains 10 and 13 in Fig. III.4) were able to maintain equilibrium with an even more evolved liquid than pyroxene grains 7 and 11 (Fig. III.4) which are adjoined by more calcic plagioclase, it is likely that the outermost rim of this plagioclase (grains 7L, 7R, 11L and 11R) formed very late and under conditions not suitable for re-adjustment of orthopyroxene composition.

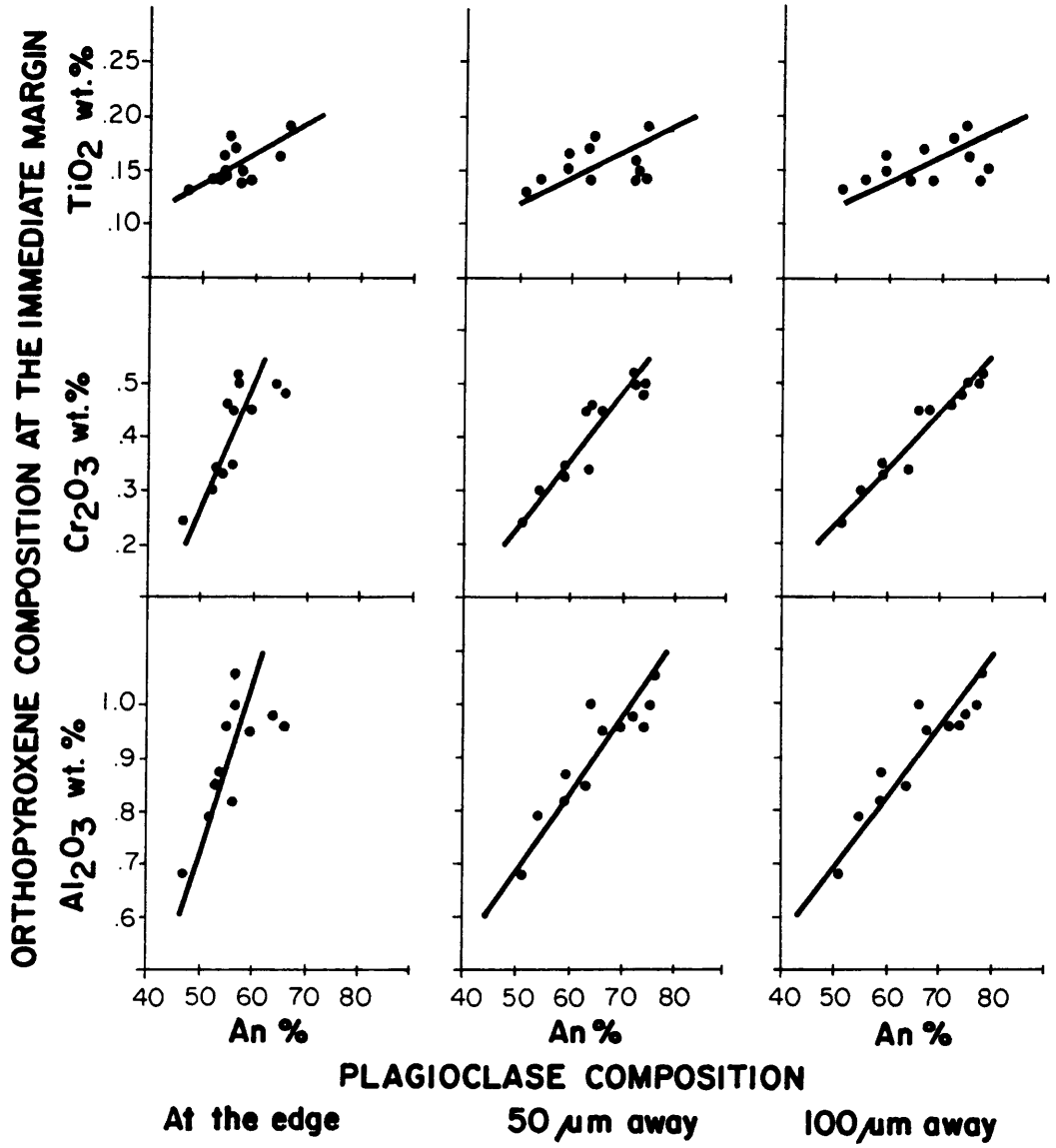

Figure III.8: Composition of orthopyroxene at the immediate margin versus the composition of adjoining plagioclase at the edge, 50 um and 100 um away for 12 orthopyroxene/plagioclase pairs. Data are compiled from orthopyroxene traverses (Fig. III.2) and plagioclase traverses (Fig. III.4). Regression lines have been calculated.

It is suggested that some orthopyroxenes were mantled by early formed, high An plagioclase which was subsequently partly replaced by late stage low An plagioclase. Evidence for this process is provided by the sharp drop in An content (grains 7 and 11 in Fig. III.4) at the immediate contact with orthopyroxene. The high Al core values, found in some small pyroxenes (7 and 11) can then be explained as well. If these grains were free to equilibrate with a continuously evolving liquid, one would expect the final Al core concentrations to be close to those of grain 10. Although one does not know the original Al content of grain 10, it can be assumed that the starting composition gradually changed in response to a continuously evolving liquid. At high temperatures the Al content in small grains will initially decrease, affecting the whole grain, until at lower temperatures the grain radius exceeds the diffusion distance, resulting in a bell-shaped zoning pattern (Fig. III.9). High preserved Al concentrations in the core can therefore be seen as evidence that a particular grain re-equilibrated only at a very late stage to produce the marginal depletion.

It can only be speculated whether microfractures developed due to crystal contraction during progressive cooling, or whether trapped liquid was forced to migrate along grain boundaries due to compaction. Considering the temperature range over which trapped liquid crystallization occurs, grain contraction seems a likely process. Cooling from 1200°C to 800°C would result in a 1.5 % decrease in volume for pyroxene and about 0.5 % for plagioclase (Skinner, 1966). Refusion of early formed plagioclase along grain boundaries due to a change in equilibrium conditions is a further possible process. Remnants of interstitial plagioclase around orthopyroxene and chromite are found where the latter are poikilitically enclosed by late stage clinopyroxene oikocrysts (Plate 2.G). This can be seen as evidence that trapped liquid was capable of remelting plagioclase. One possible reason for remelting is a progressive increase in H_2O-content during fractionation (Roeder and Campbell, 1985) which would result in corrosion of previously formed plagioclase (Adams, 1968; Dymek and Schiffries, 1987). The presence of late stage mica would favour a proposed increase in volatile content.

III.5.3.3. CHROMIUM

The sympathetic behaviour of Al and Cr (Figs. III.2 and III.8) clearly indicates the intimate relationship between these two elements. Although diffusion coefficients are not known for either of the two one can assume that they are very similar. However, the observed increase in the Al/Cr ratio towards the rim in most grain traverses (Fig. III.2) shows that Cr diffusion is not directly coupled to Al diffusion or vice versa. The decoupling could either reflect differences in diffusion rates or different fractionation trends for Al and Cr. The latter possibility is favoured because an increased Al/Cr ratio at the margins is in good agreement with the expected composition of a strongly fractionated liquid. The highest Al/Cr values are found in rims in contact with strongly evolved plagioclase and K-feldspar. The initial decrease in the Al/Cr ratio towards the margin (e.g. grains 2 and 13; Fig. III.2) followed by an increase at the outer rim indicates a complex equilibration history. Declining Al/Cr ratios in the melt can be explained by plagioclase crystallization (high An), which causes the liquid to become depleted in Al relative to Cr. This is possibly followed by an equilibration stage, which affected only the outermost rims, when Cr was effectively removed from the melt by crystallizing clinopyroxene and phlogopite. Intercumulus phlogopite contains more than 1 wt % Cr_2O_3 (Tab. III.3), interstitial clinopyroxene about 0.7 wt % Cr_2O_3 (Tab. III.2).
The final Cr concentration at a particular edge of an individual grain depends on whether the edge remained in contact with liquid or was sealed off by early formed plagioclase. The close dependence of the marginal Cr content of pyroxene and the An content of adjoining plagioclase is shown in Figure III.8. The plagioclase composition is again taken as an indicator of the relative degree of interstitial liquid fractionation.

III.5.3.4. TITANIUM

Ti in large grains is negatively correlated with both Al and Cr (Fig. III.2, grains 2 and 13). In small grains however (Fig. III.2 grains 1, 7, 10, 11 and 12), all three elements show a positive correlation,

Table III.3: Phlogopite analyses from two different rock samples. First three analyses are from sample 353 29, the other two from 473 29. Mg# is 100*(Mg/(Mg+Fe)).

SiO_2	Al_2O_3	TiO_2	FeO	MnO	MgO	Cr_2O_3	Na_2O	K_2O	total	Mg#
38.71	13.66	3.08	8.66	0.04	18.38	1.19	0.41	7.99	92.12	79.1
39.13	13.43	2.96	8.21	0.03	19.31	1.06	0.59	8.19	92.91	80.7
37.68	12.98	3.76	8.27	0.03	19.32	1.13	0.50	8.27	91.94	80.6
39.60	15.39	3.06	3.56	nd	22.16	1.33	0.44	9.06	94.61	91.7
38.76	15.72	2.94	3.50	nd	21.57	1.31	0.55	8.18	92.52	91.7

ruling out a coupled cation exchange. Ti increases from the centre to the margin in large grains, while a decrease in Ti is found from core to rim in small grains and at the outermost margin (< 50 um) of large grains where the latter are in contact with low An plagioclase (grain 2 left side and grain 13 right side). These features are best explained by a two stage fractionation history. Predominant plagioclase crystallization will initially increase Ti concentration until clinopyroxene and phlogopite become liquidus phases which will cause a decrease in Ti in the interstitial liquid. Late stage clinopyroxene contains about 0.3 wt % TiO_2, phlogopite about 3.0 wt % TiO_2 (Tab. III.3).

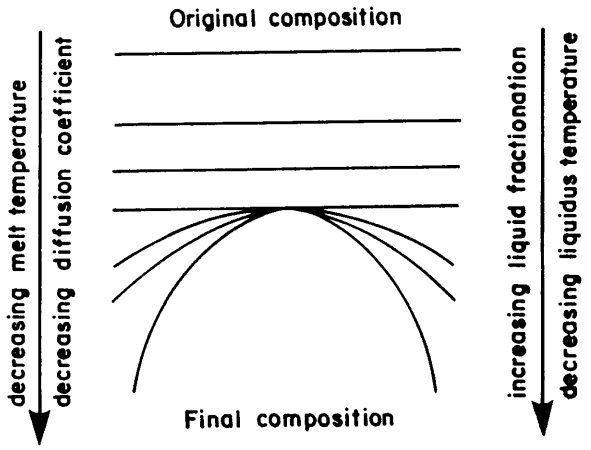

Figure III.9: Schematic illustration of the proposed evolution of orthopyroxene zoning. At higher temperatures the whole grain equilibrates, while with decreasing temperature and hence decreasing diffusion distances only the marginal portion stays in equilibrium with interstitial liquid.

The Ti content at the margin of orthopyroxene indicates when an individual grain or a particular side of a grain last equilibrated. This is confirmed by grain 1 (right side) and grain 2 (right side) where the adjoining plagioclase composition (Fig. III.4) suggests an earlier cut-off and therefore no Ti depletion at the margin. Ti depletion at the margin is found where the grain is in contact with low An plagioclase (e.g. grain 2 left side, grain 13 right side, grain 10 right side). The relatively high Ti content (> 0.20 wt % TiO_2) in the centre of grains 7 and 10 is seen as evidence that these grains grew during the stage where Ti became progressively enriched in the interstitial liquid (prior to cpx and mica crystallization), while the depleted margins reflect a subsequent stage of re-equilibration with a Ti poor liquid (after cpx and mica crystallization).

Differences in orthopyroxene rim concentrations therefore reflect different liquid compositions, which in turn are a function of temperature and time at which equilibrium was last attained. The fact that the best correlation between Ti concentrations at the margins of orthopyroxene and the An content of adjoining plagioclase is found at the immediate margin of feldspar (Fig. III.8) suggests that Ti equilibration in orthopyroxene continued to lower temperatures than Cr and Al equilibration. This is also supported by experiments which showed that Ti has a higher diffusional rate than Cr (Bodinier et al., 1987).

III.5.3.5. MAGNESIUM AND IRON

The relatively flat Mg# zoning pattern in orthopyroxene is in sharp contrast to all the other analyzed elements. Not only are individual grains homogenous, but even grains of various sizes and with different adjoining phases have comparable Mg#. Thus, maintaining internal equilibrium with surrounding liquid must have been extremely efficient during solidification. Although grain homogeneity due to intra-grain diffusion in the solid state might have played a part in gaining grain homogeneity, it cannot explain the overall similarities between individual grains. However, the Mg/Fe zoning pattern in grain 10 (Mg# in Fig. III.2) and the slightly lower Mg/Fe ratios in several small grains (Mg# in Fig. III.3) are an indication that intra-grain diffu-

sion and magmatic re-equilibration are finite processes, which probably ceased during the stage when K-feldspar was a liquidus phase (the zoned portion of grain 10 is in contact with K-feldspar).

The only published data on Mg - Fe interdiffusion (Wilson, 1982) were established from natural orthopyroxene - chromite pairs which equilibrated at subsolidus temperatures (1000 - 800°C). By extrapolating Wilson's data to 1200°C, interdiffusion coefficients of the order of 10^{-11} cm^2/s at 1200°C and 10^{-15} cm^2/s at 1000°C are obtained.

This indicates that the Mg - Fe ratio of a grain with a diameter of about 1 mm will homogenize by re-equilibration if it cools from 1200 to 1000°C (Tsuchiyama, 1985 Fig. 12B and Rietmeijer, 1983 Fig. 6) over a minimum timespan of 20000 years (Wilson, 1982 Fig. 22, curve 5). At 800°C, maximum diffusion distance for Mg and Fe is reduced to less than 10 um (Tsuchiyama, 1985 Fig. 12B and Rietmeijer, 1983 Fig. 6) allowing 35000 years for further cooling from 1000°C to 800°C. At 900°C and for a cooling period from 1000°C to 900°C of about 15000 years, a maximum distance of about 70 um (op. cit.) can be assumed, which would still homogenize a grain with a diameter of 140 um.

Although these bulk diffusion distances are only estimates, because of the infinite small increments of diffusion with decreasing temperature, they can be used to define reasonable limits of the effects of Mg-Fe diffusion through the crystal lattice.

From the Mg/Fe - homogeneity of large grains it can be assumed that equilibrium with interstitial liquid with respect to Mg/Fe was maintained until 1000°C. The volume of trapped liquid must have been so small at this stage that further fractionation affected an insignificantly small volume of crystals, which would be difficult to detect.

The Mg/Fe zoning in grain 10 ($Mg^{\#}$ in Fig. III.2) can be seen as evidence that fractionation of trapped liquid continued on a very local scale. Free migration of liquid must therefore have ceased at temperatures still high enough (+- 900°C; Tsuchiyama, 1985 Fig. 12B and Rietmeijer, 1983 Fig. 6) to allow for the observed diffusion distance of about 60 um. 900°C can then be regarded as a minimum solidus temperature for most plagioclases rims in contact with orthopyroxene, as their crystallization probably caused the interconnected pore spaces to break up into isolated pockets.

CHAPTER IV: PLAGIOCLASE VARIATION - FRACTIONATION PROCESSES IN A CUMULATE PILE

IV.1. SAMPLING

To document cryptic variation of cumulus orthopyroxene and interstitial plagioclase within the lower critical zone the stratigraphic succession from the footwall of the LG 6 up to the E - F boundary was investigated in great detail. About 3000 orthopyroxene and plagioclase analyses were performed on over 70 thin sections from drill-core MDH 29 with an average sampling interval of approximately 2.5 m. In addition, the lower/upper critical zone transition was investigated from drillcores MDH 23 and MDH 22.
Cores (geometric centre) and rims of 8 to 15 individual pyroxene and plagioclase grains were analysed for each sample. The average core and rim compositions for plagioclase and orthopyroxene are shown in Folder 2. The overall range in the An content of plagioclase is presented in Figure IV.1.

IV.2. PLAGIOCLASE VARIATION

All plagioclase in the lower critical zone is texturally post-cumulus. Plagioclase in individual samples shows a compositional range from as little as 3 mole percent anorthite (An = 100*(Ca/(Ca+Na))) to as much as 33 mole % An with an average range of about 20 % An (Fig. IV.1). Cameron (1980) quotes a maximum range of 29 % An for the lower critical zone. The smallest variation in the An content is found in chromitites (Fig. IV.1). Cores (geometric centre) of plagioclase are invariably more calcic than rims (Folder 2). The wide range in composition for individual samples (up to 33 % An) is caused by the variation of the An content between individual grains with the zoning within single grains normally not exceeding 10 to 15 mole % An. However, detailed grain traverses revealed within-grain zoning of up to 25 % An (Fig. III.4), which is attributed to a late migration of strongly fractionated liquid which resulted in the replacement of the marginal portion of plagioclase by more sodic plagioclase (see Chpt. III.5.3.2)

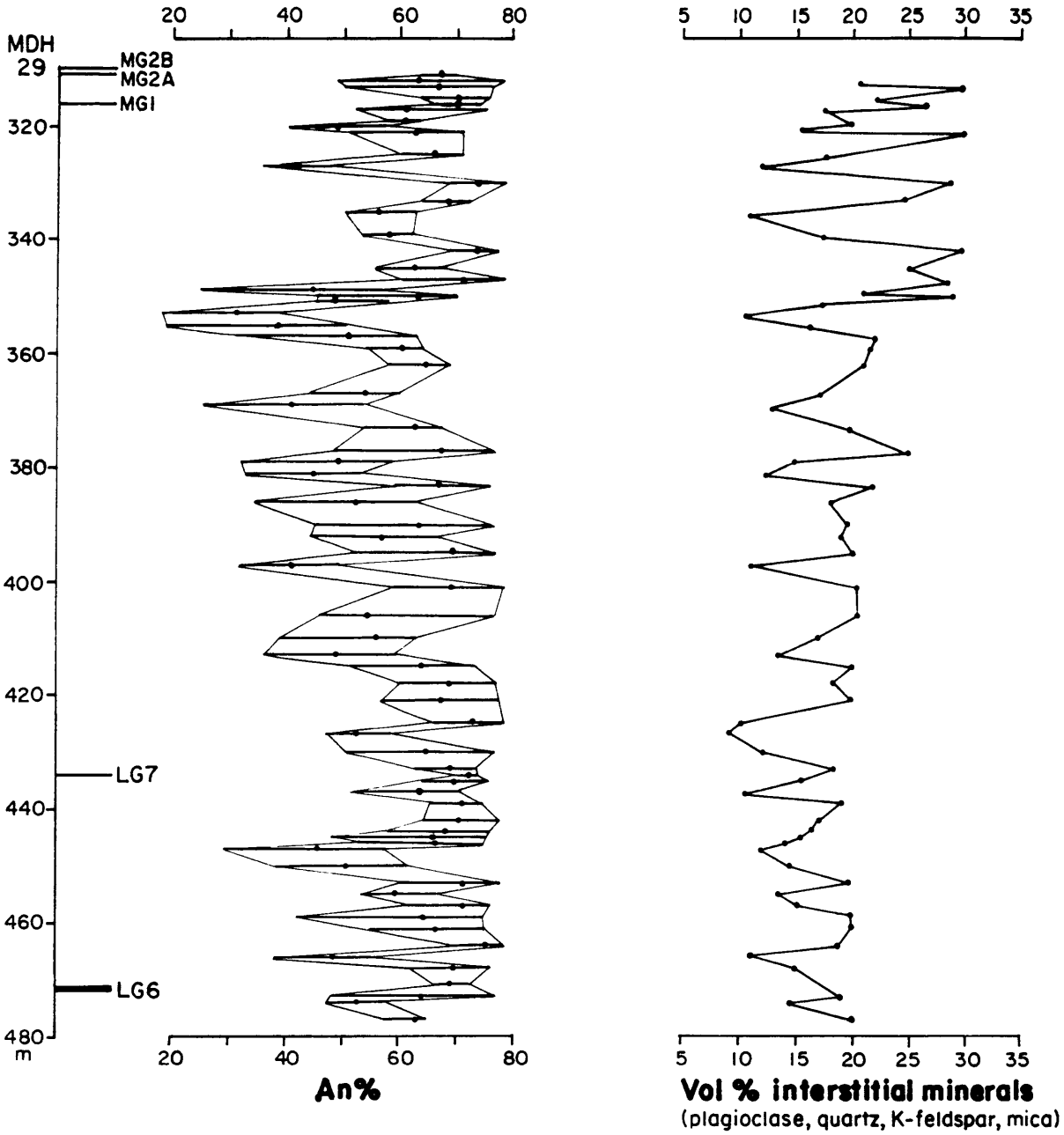

Figure IV.1: Variation in plagioclase composition and modal amount of intercumulus phases in the D_2 and E units in borehole MDH 29. Variation in An content (mol % 100*Ca/(Ca+Na)) within each sample was established from 8-15 individual core and rim analyses. The mean compositions are calculated averages. Modal proportions were established from point counting (1000 counts per thin section) and include all major intercumulus phases (plagioclase, quartz, K-feldspar and phlogopite) except clinopyroxene.

The range in plagioclase composition and the maximum and minimum values fluctuate considerably in the D_2 and E units. However, the An maxima in the samples with the more calcic plagioclase remain fairly constant between An 75 and An 79. This more calcic plagioclase is interrupted at regular intervals with more sodic plagioclase, with minimum An values as low as An 18. Samples with Na - rich feldspar invariably contain quartz and K-feldspar (Folder 2).

The **potassium** content of plagioclase shows a negative correlation with the An content (Fig. IV.2a). However, rims of very low An plagioclase (An < 40) show no increase in potassium, despite decreasing An values from core to rim (Fig. IV.2b). This feature can be explained by the simultaneous crystallization of low An plagioclase and potassium - rich phases such as K-feldspar and phlogopite during late stage crystallization.

Plagioclase in chromitites and chromite-rich rocks is typically depleted in potassium (Fig. IV.2), relative to the An content of feldspar from chromite-poor rocks. The same relationship between the K - content of plagioclase and the amount of cumulus chromite has been described by Cameron (1980) and holds for the entire lower critical zone.

The **iron** content of plagioclase is positively correlated with the An content (Fig. IV.3), confirming the known tendency for total iron to increase with An content and crystallization temperature (Smith, 1983).

Longhi et al. (1976) noted a possible increase in iron at grain margins due to secondary fluorescence effects. All plagioclase rim analyses were therefore carried out at a "safety" distance of about 30 um from grain boundaries and the analytical results should represent the real iron concentrations at that particular distance from the adjoining phase (orthopyroxene; chromite in chromitites).

Plagioclase rims have generally higher Fe concentrations than the cores (Fig. IV.4). However, feldspar from chromitites and chromite - rich samples show the reversed trend or are virtually unzoned. The observed increase in iron at the rim is a common feature in basaltic plagioclase (Longhi et al., 1976) and, together with the decrease in An content, is an indication of outward growth.

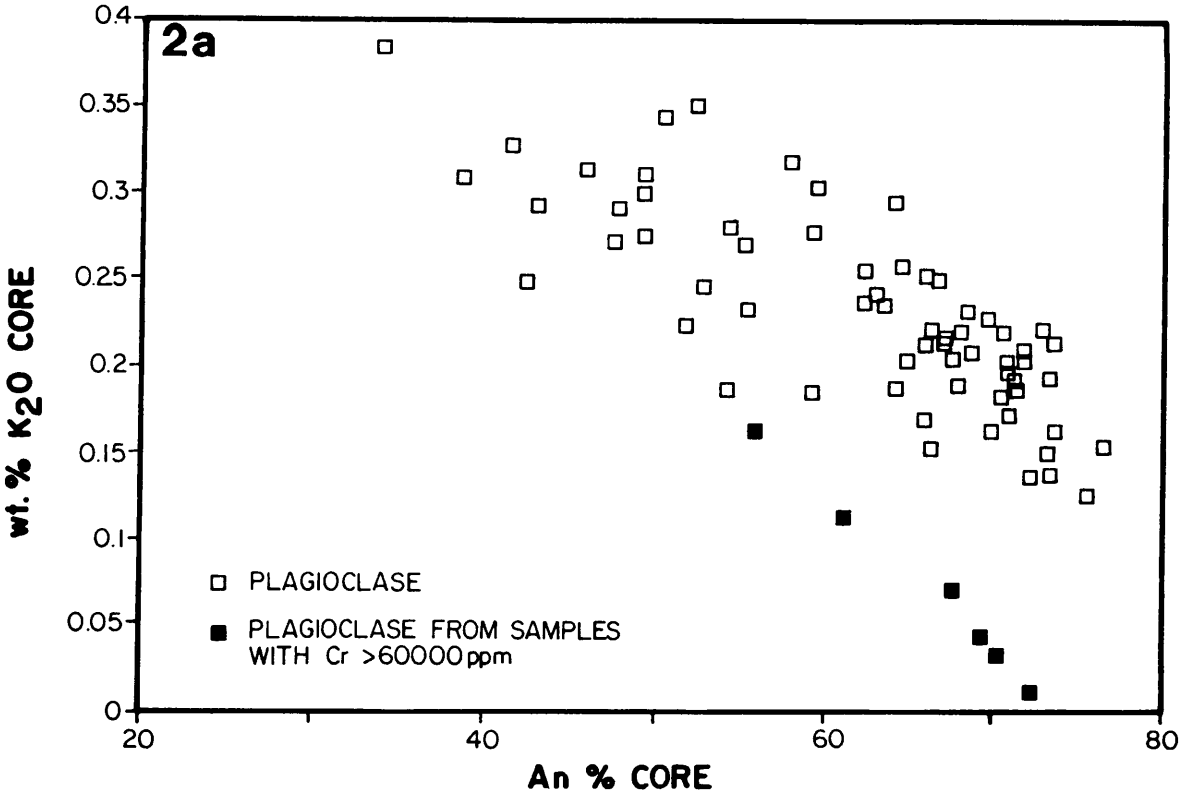

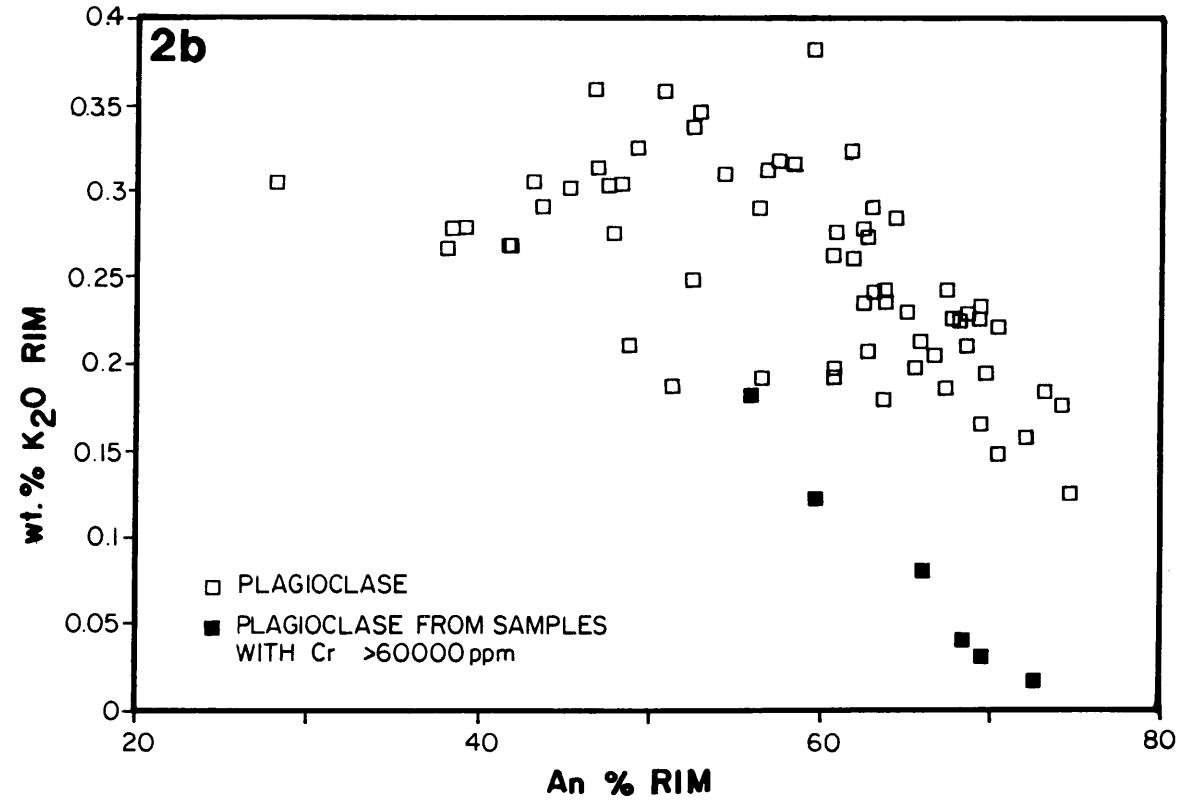

Figures IV.2a and 2b: Potassium versus An content of plagioclase cores (2a) and rims (2b) from the D_2 and E units of MDH 29. Feldspar from rocks with more than 60000 ppm chromium (XRF whole-rock) are marked by a different symbol. Each data point is the calculated average of 8-15 individual analyses.

The increase in iron could either reflect a progressive Fe - enrichment during liquid fractionation, or an increase in the oxidation state (fO_2) of the fractionating interstitial liquid. Increasing fO_2 during fractionation was documented by Roeder and Campbell (1985).
The partition coefficient for Fe between plagioclase and liquid is dominated by the amount of ferric iron and therefore increases with increasing oxygen fugacity (Longhi et al., 1976). According to these authors, between two-thirds and three-fourths of the iron in basaltic plagioclase is ferric. This dependence of the Fe partitioning on the oxidation state of the melt could explain the reversed Fe zoning found in plagioclase from chromitites. The abundance of chromite evidently buffered the oxygen fugacity by constant re-equilibration with the interstitial liquid.

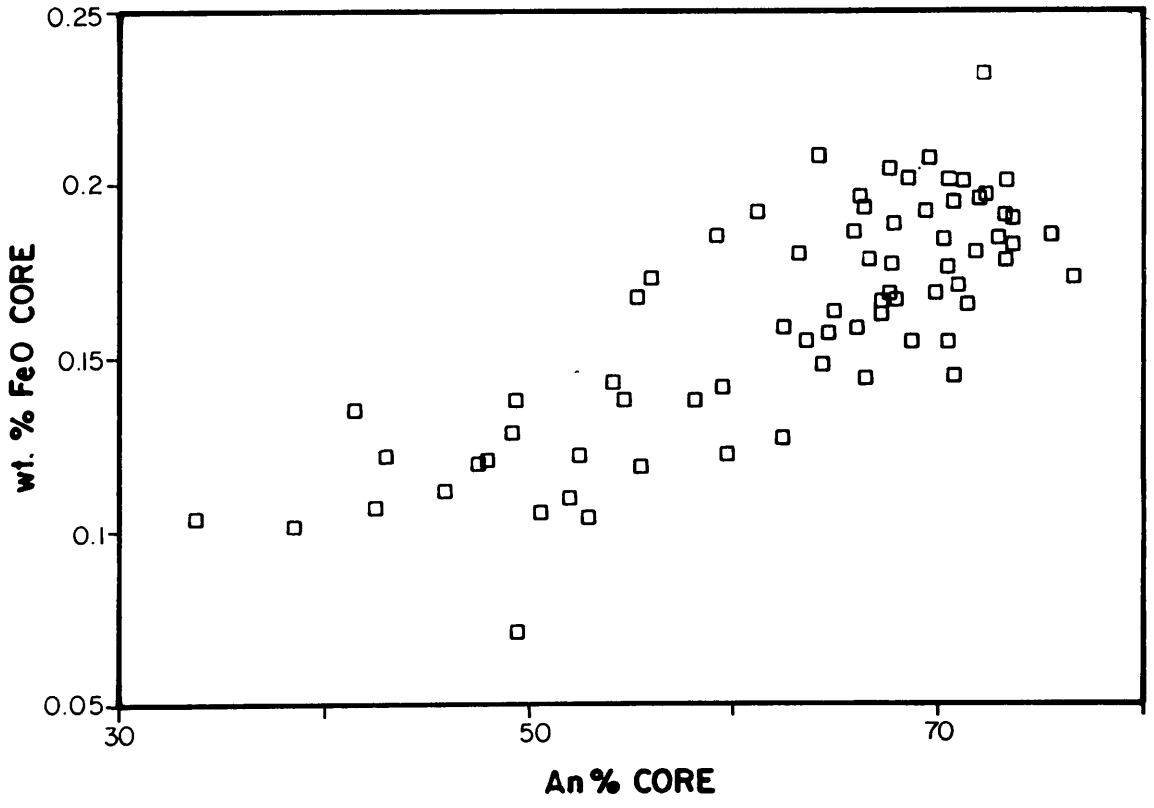

Figure IV.3: Total iron (FeO) versus An content of plagioclase cores from the D_2 and E units. Each data point is the calculated average of 8-15 individual analyses.

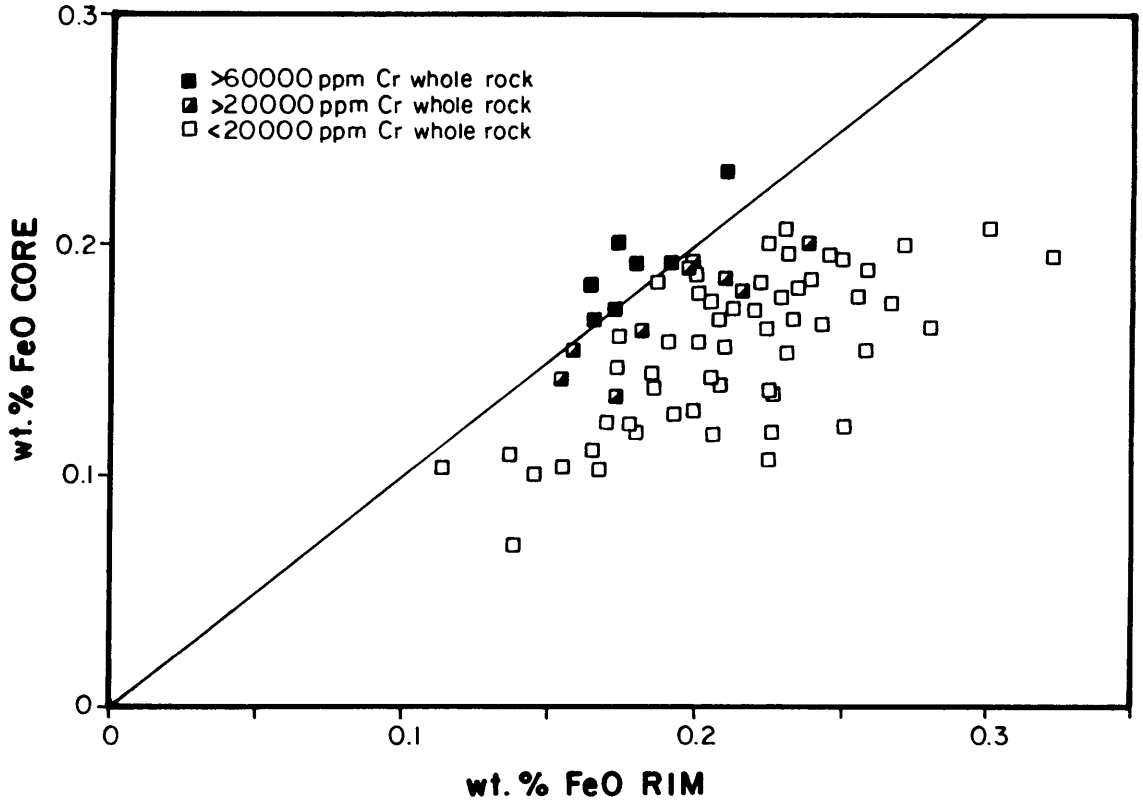

Figure IV.4: Total iron (FeO) of plagioclase cores versus total iron of plagioclase rims from the D_2 and E units. Each data point is the calculated average of 8-15 individual analyses. Samples which contain in excess of 20000 ppm Cr in the whole-rock analyses are shown with different symbols.

IV.3. INTERCUMULUS FRACTIONATION CYCLES - A MODEL FOR INTERCUMULUS FELDSPAR VARIATION

IV.3.1. CYCLIC PLAGIOCLASE VARIATION

The An content of plagioclase shows a strong positive correlation with the modal amount of plagioclase (Fig. IV.5). Thus, rocks with highly fractionated plagioclase (low An) are generally poor in plagioclase (Fig. IV.1), but contain considerable amounts of quartz, K-feldspar and phlogopite.

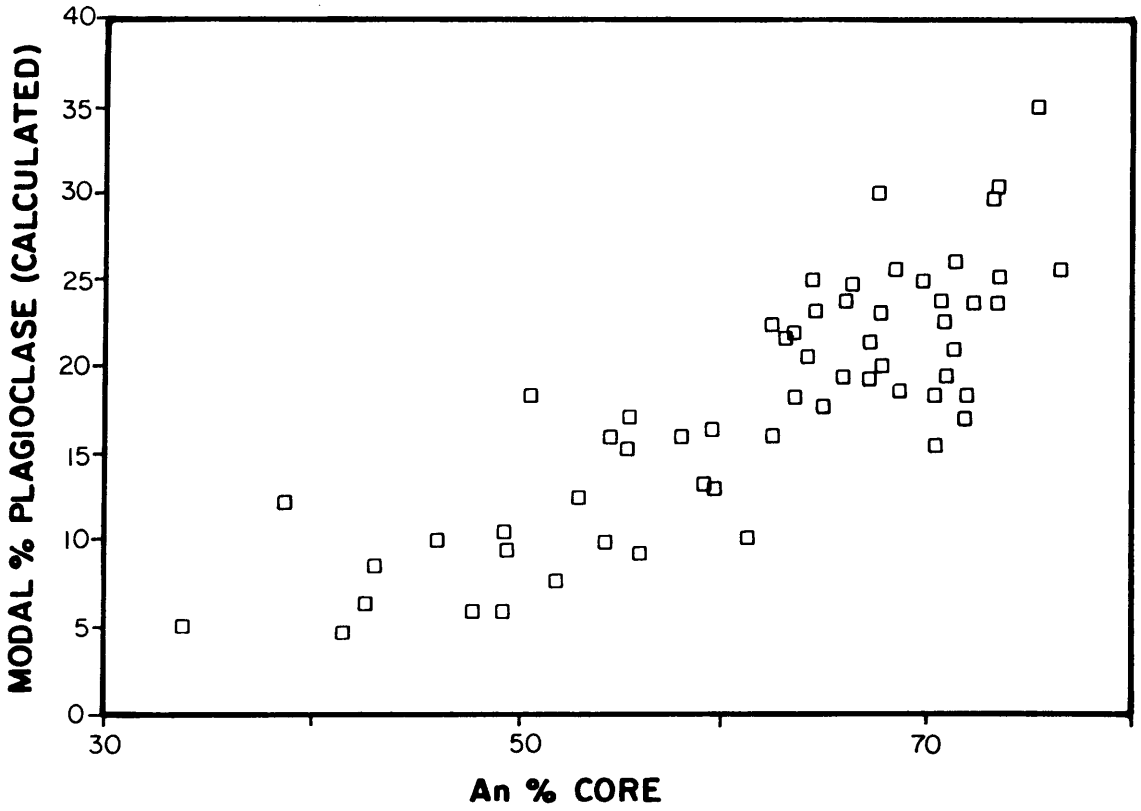

Figure IV.5: Normative content of plagioclase versus An content of plagioclase cores from the D_2 and E units. Normative content is calculated from whole-rock Na_2O concentrations (XRF) and Na_2O concentrations of plagioclase (microprobe). Each data point is the calculated average of 8-15 individual plagioclase analyses.

The cyclic variation in the An content with stratigraphic height and the simultaneous change in the modal amount of plagioclase (Fig. IV.1) are indications that crystallization and solidification of the lower critical zone was not a continuous, steady state process. The variation in the An content can only be explained by a slow cooling process which allowed the pore liquid to fractionate. However, progressive crystallization and simultaneous fractionation did not result in a continuous fractionation but gave rise to intermittent cycles. This is attributed to limited exchange of pore liquid and to the particular rate by which the isotherms pass through the crystallizing system, i.e. the cooling rate. Both parameters are expected to change as a function of the initial porosity and with progressing solidification. A fast cooling rate or a low initial porosity are likely to limit movement of interstitial liquid within the cumulus pile.

IV.3.2. PHYSICO-CHEMICAL CONSIDERATIONS - ACCUMULATION RATE, POROSITY, AND ADCUMULUS GROWTH

It is believed that accumulation of orthopyroxene resulted initially in a loosely packed, self-supporting network with an average porosity of about 50 % (e.g. Wager and Brown, 1967; Irvine, 1980c). The observed differences in the thickness of lithological units (Chpt. II.6) are thought to reflect different accumulation rates, which must have been about twice as high for the thick sequence intersected in borehole MDH 29 (Fig. II.4) compared to the two thin intersections in MDH 23 and MDH 1. The particular rate of accretion might have fluctuated in each individual case depending on the mode and cause of "sedimentation", such as crystal settling or slumping, magma mixing or replenishment. Hence an initially heterogeneous pile with varying (initial) porosities can result. However, only the residual (final) porosity can be directly estimated from the modal amount of intercumulus phases.

Morse (1986a) has demonstrated convincingly for the Skaergaard and Kiglapait intrusions that the accumulation rate and the residual porosity are related to each other in as far as the accumulation rate determines the path length for exchange of interstitial liquid. Rapid

accumulation produces a longer path length for liquid migration, with the result that the chances of entrapment of some pore liquid are enhanced. Morse, however, assumed very limited crystal pile thicknesses which allowed communication of pore liquid through the mush with overlying, supernatant liquid. Migration of pore liquid within the cumulate pile must also be governed by the relative permeability of the pile.

Phase relations for chilled marginal rocks (related to the lower and lower critical zone) have shown that plagioclase only starts to crystallize about 100°C below the liquidus temperature (Sharpe and Irvine, 1983). Thus, the build-up of a thick pile of pyroxenes has to be assumed before the temperature of the pore liquid can have dropped sufficiently to allow feldspar to crystallize.

Evidence for adcumulus growth deep within the cumulus pile has been provided by several authors (Irvine, 1980c; Wadsworth, 1985; Sparks et al., 1985) but this process is of no immediate concern in the studied case as only variations in interstitial minerals such as plagioclase are evaluated here.

It must be mentioned that the textural term "adcumulate" is generally used in a descriptive sense for rocks which contain less than 7 % interstitial minerals (Irvine, 1981). However, the term also implies continuous growth at an almost constant and near-liquidus composition (unzoned crystals) until virtually all the pore space is eradicated (Sparks et al., 1985). Paradoxically, rocks in the studied sequence with the least amount of intercumulus minerals, i.e. adcumulates, contain the most fractionated minerals, while relatively unzoned high An plagioclase is found in rocks with the highest percentage of interstitial phases (orthocumulate). For this reason, a classification of the investigated rocks in ad-, meso- and orthocumulates would be misleading as these terms do not distinguish whether texturally intercumulus minerals have a primitive composition or are strongly fractionated, regardless of their total amount. The rocks, therefore, are collectively considered to be orthocumulates in which intercumulus phases have either a "primitive" (high An) or a "fractionated" (low An) composition.

IV.3.3. THERMAL CONSIDERATIONS - DIFFUSION RATE VERSUS CRYSTALLIZATION RATE

The fact that the layers with the highest amount of interstitial plagioclase have also the least evolved starting composition (An +- 75), indicates that these layers represent the sites where plagioclase started to crystallize. Crystallization of initially high An plagioclase continues as long as the growing crystals are supplied by the appropriate refractory components. The transport of elements towards the crystallization site can be controlled either by static diffusion or by compositional convection; the latter being more effective than molecular diffusion (Sparks et al., 1985). As the temperature can be assumed to stay nearly constant at the crystallization site, the only limitation to continuous growth of high An plagioclase (An +- 75) will be set by limited supply of fresh liquid. Continuous growth is indicated by virtually unzoned plagioclase cores (Fig. III.4).

The maximum possible volume from which a high An component can be drawn is defined by the transport distance (path length) over which exchange of pore liquid takes place. When surrounding pore liquid is depleted in refractory components, no further crystallization can occur until temperature decreases to the liquidus temperature of the evolved liquid. As cooling is controlled by downward heat loss through the underlying pile and the floor contact, the isotherm which corresponds to the plagioclase An 75 liquidus temperature (+- 1190°C; Sharpe and Irvine, 1983) has to pass through the immediately overlying partially fractionated liquid. No crystallization can occur within this partially fractionated liquid, whereas the unfractionated zone immediately above (i.e. beyond the path length) will start to crystallize plagioclase when the 1190°C isotherm passes through (Fig. IV.6). Again growth continues until the liquid is depleted in its high An component and requires further cooling. This leads to an alternating series (fractionation cycles) of layers in which the intercumulus plagioclase has partially crystallized and plagioclase-free layers containing fractionated liquid. As cooling and fractionation proceed progressively lower An feldspar crystallizes. The more fractionated liquid is continuously concentrated above each crystallizing front.

A very slow stepwise cooling and solidification process is indicated by the fact that individual plagioclase aggregates from one sample differ considerably in their core compositions, while individual crystals are virtually unzoned over most parts of the grain (Fig. III.4).

The constantly decreasing permeability will eventually cause the crystallizing system to break up into isolated pockets. McKenzie (1984) and Tait and co-workers (1984) have shown that free migration is still possible at porosities as low as 4 %. The minimum value for free communication will, however, strongly depend on the extent to which pore spaces remain interconnected with decreasing temperature. The surprisingly constant range in the An content (+- 20 mol %) for the great majority of samples from the D_2 and E units would indicate a uniform closing porosity at which effective communication ceased.

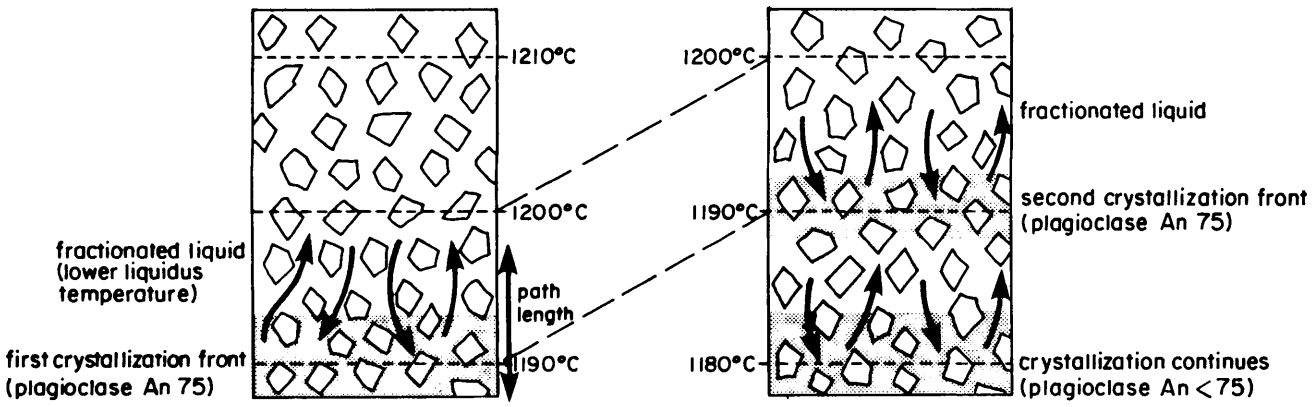

Figure IV.6: Schematic illustration of the thermal profile within cumulus pile and the evolution of intercumulus fractionation cycles. High An plagioclase crystallization (1190°C) releases fractionated liquid and depletes the layer immediately above the crystallizing front. The lower liquidus temperature of the fractionated liquid in the overlying layer inhibits crystallization and the 1190°C isotherm passes through. Once the 1190°C isotherm reaches unevolved liquid (beyond the diffusion path length) a second crystallization front develops further up in the pile. Progressive cooling leads to a series of crystallizing layers, while fractionated liquid is continuously concentrated in the overlying layers (higher temperature regime).

IV.3.4. POROSITY AND ITS ELIMINATION, AND THE BUILD-UP OF MULTIPLE CRYSTALLIZATION FRONTS

Accretion of cumulus grains creates an imbalance of hydrostatic and lithostatic pressures in the cumulate pile (Sparks et al., 1985), which causes the crystalline matrix to deform and part of the pore liquid to be expelled. Lithostatic pressure is likely to increase with progressive solidification, and to affect those horizons still containing liquid. Layers dominated by early formed plagioclase are less compacted as most of the initial pore liquid had already crystallized. The relatively low abundance of interstitial minerals in those layers with very late phases could be explained in this way. Upward expulsion of highly fractionated residual liquid might also be the cause for the unusually low An values occasionally found marginal to high An feldspar (Chapters III.3.1 and III.5.3.2).

Alternatively, a change in porosity can result from an annealing process of pyroxene solution and reprecipitation (Hunter, 1986; Campbell, 1987) or simply from a loss in volume due to the transformation from liquid to solid state (Petersen, 1986). To accomplish the observed variation in the final porosity requires that both processes preferentially affect the more fractionated horizons.

As layers with strongly evolved (low temperature) interstitial minerals are invariably over- and underlain by rocks with high An plagioclase (high temperature), it is evident that crystallization of interstitial liquid occurred simultaneously at several horizons. This build-up of multiple crystallization fronts contrasts with the standard model of a single upwards moving crystallization front (e.g. Morse, 1986a) and could provide interesting consequences for the migration paths of late magmatic or genetically unrelated fluids/liquids. Given the case that percolating fluids/liquids contain appreciable concentrations of gold or platinum, then preferential trapping and precipitation in these low temperature horizons might lead to local strata-bound enrichment of these elements.

CHAPTER V: PYROXENE VARIATION - THREE STAGE MODIFICATION OF MG#

V.1. INTRODUCTION

Examination of the Mg# (mol % 100*Mg/(Mg+Fe)) of orthopyroxene versus height in the lower critical zone (Folder 2) reveals two prominent features. Firstly, the Mg# decreases systematically with the degree of plagioclase fractionation. Secondly, the Mg# shows a positive correlation with the modal amount of chromite (given as whole rock ppm Cr). Hence, the Mg# decreases in rocks with strongly evolved interstitial phases and increases in samples rich in modal chromite. An increase in Mg# with modal chromite has been documented by several authors (e.g. Cameron and Desborough, 1969; Jackson, 1969; Cameron, 1970) and is attributed to subliquidus (Jackson, 1969; Roeder and Campbell, 1985) and subsolidus re-equilibration (Irvine, 1967; Wilson, 1982) of Fe^{2+} and Mg.

A number of authors (Jackson, 1961; Henderson, 1970; Raedeke and McCallum, 1984) have qualitatively addressed the compositional effect of trapped intercumulus liquid on the composition of cumulus minerals. Barnes (1986) quantified this effect which he called "trapped liquid shift", and related the final cumulus composition to the proportion of crystallized trapped liquid. He argued that the magnitude of the decrease in the Mg# increases systematically with the amount of trapped liquid and presented a method to recalculate the original cumulus composition. However, Barnes's method is based on the assumption that the degree of trapped liquid fractionation is constant within each individual crystallizing unit (closed system). Thus, his calculations can not be applied to quantify the relative shift in Mg# caused by different degrees of trapped liquid fractionation as proposed in Chapter V.3. Furthermore, his calculations require a considerable variation in the amount of cumulus pyroxene within a stratigraphic unit such as the modal variation from pyroxenite to anorthosite which is commonly found within a cyclic unit. Nevertheless, the basic concept of his calculations, namely the compositional effect of interstitial liquid on early formed cumulus crystals, appears to be of great importance for the final composition of cumulus minerals and will be evaluated in the following subchapters.

V.2. STAGE ONE: ORTHOPYROXENE - LIQUID REACTION

To evaluate the compositional history of orthopyroxene in the feldspathic pyroxenite of the lower critical zone one has to constrain several genetic parameters, based on petrographic evidence and experimentally derived petrological data.

It is assumed that cumulus pyroxene crystallization took place from a liquid of known composition, represented by the chilled marginal rocks of the Complex (Sharpe, 1981), and that crystal settling was responsible for the build-up of an initially loosely packed crystal pile, an assumption that will be justified later. The initial amount of intercumulus liquid is estimated to be between 50 and 60 %. It should be mentioned, that compaction (Richter and McKenzie, 1984; Shirley, 1986), mineral contraction (Petersen, 1986) or a density driven upward migration of evolved liquid (Tait et al., 1984; Morse, 1986a) can modify the initial porosity prior to final solidification.

Two cases will be considered, first where cumulus crystals have formed and settled within the same liquid, and second, where crystals formed from one liquid and subsequently settled into a liquid layer of different composition. In both cases orthopyroxene is assumed to have formed from a liquid of boninitic composition (B1-type, Sharpe, 1981). Based on field evidence and mineral chemical considerations, a B1-type liquid is generally accepted as parental to lower and lower critical zone cumulates (Cawthorn and Davies, 1983; Irvine et al., 1983; Sharpe, 1985; Naldrett et al., 1986,).

Modelled trends for orthopyroxene composition during fractional crystallization for a B1 starting composition show a decrease in Mg# from about 91 to 87 after 20 % fractionation (Barnes, 1986a). 20 % fractionation can be regarded as a maximum value for a B1 liquid in order to keep the liquid above the orthopyroxene-plagioclase cotectic. Melting experiments on B1-chills (Sharpe and Irvine, 1983) have shown that orthopyroxene crystallizes alone between 1300°C and 1180°C before it is joined by plagioclase at 1180°C for QFM - 1.7 (Fig. V.1a). The observed range in Mg# for chromite-poor samples in the investigated interval is however between 83 and 78. Thus, to explain the discrepancy between observed and modelled composition, orthopyroxene crystallized either from a more iron-rich B1 and B2 hybrid liquid or

re-equilibrated with a more evolved liquid.

An origin from a hybrid liquid is however not indicated by the mineral chemistry. Trace element concentrations in cores of large orthopyroxene (0.45-0.53 wt % Cr_2O_3 and 0.07-0.13 wt % TiO_2) from the D_2 and E units are similar to those from lower zone pyroxenites (0.48-0.52 wt % Cr_2O_3 and 0.09 wt % TiO_2; Cameron, 1978) and therefore favour a common, B1-type parental liquid. This is also supported by Cr and Ti concentrations of orthopyroxene from the lower critical zone which show no systematic upwards decrease or Mg# dependance (Cameron, 1980), and is consistent with experimental results for a B1 melt which showed that Cr concentrations in orthopyroxene remain almost constant until plagioclase becomes a liquidus phase (Barnes, 1986a).

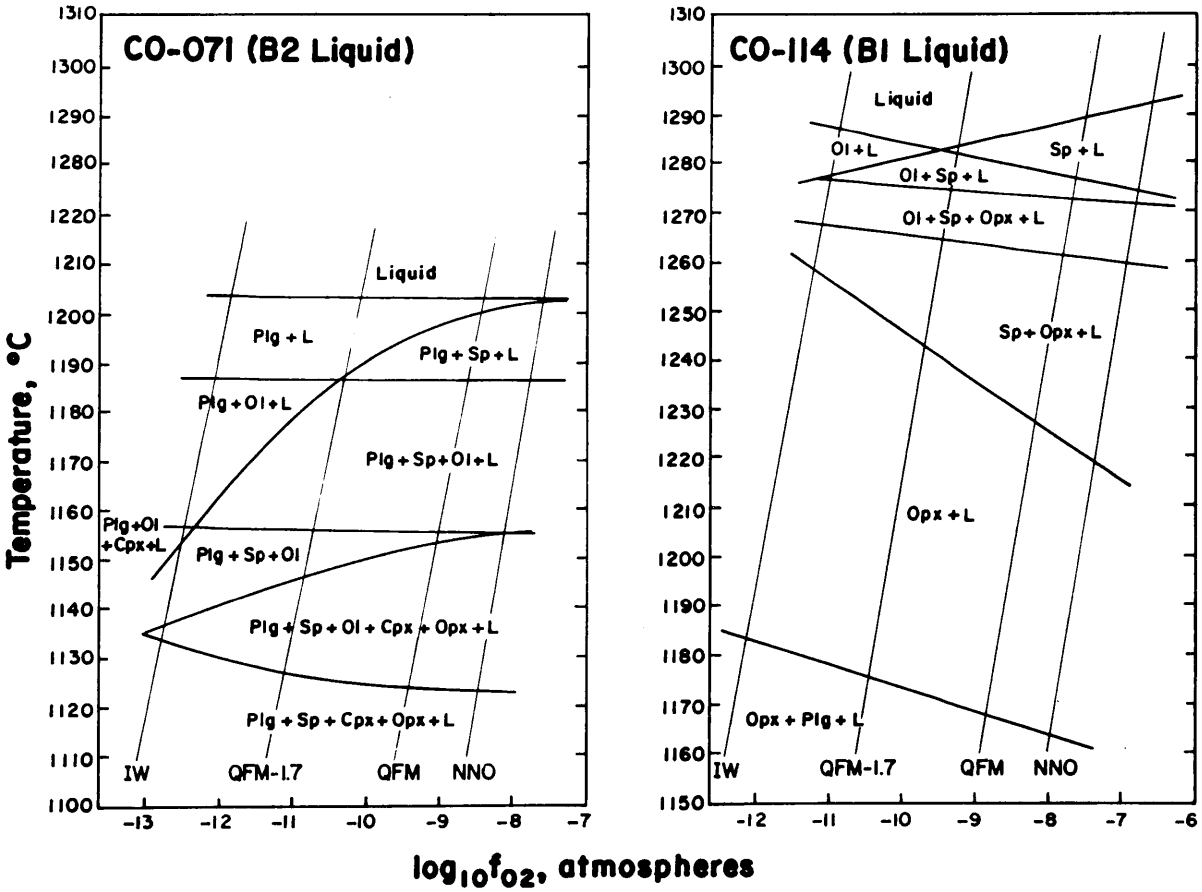

Figure V.1a: Phase relations for the 1-atm melting of chilled marginal rocks CO-114 (B1) and CO-071 (B2) as functions of temperature and fo_2. All data from Sharpe and Irvine (1983).

Furthermore, orthopyroxene crystallization from a hybrid liquid (B1 - B2 mixture) seems unlikely because olivine is the sole silicate liquidus phase for most B1-B2 mixtures and is only replaced by orthopyroxene after the plagioclase cotectic is reached (Fig V.1b). Only mixtures with a B1 component of more than 90 % have orthopyroxene as the dominant phase prior to plagioclase crystallization (Fig. V.1b). Although the presented data from Sharpe and Irvine (1983) in Figure V.1 were derived from 1 atm experiments, 3 kbar experiments on B1-chills by Cawthorn and Davies (1983) show no significant increase in the stability field of orthopyroxene. Formation of orthopyroxene from a B1/B2 hybrid (B2 > 10 %) would therefore be restricted to a magmatic (< 1190°C) reaction between olivine and liquid within the cumulus pile. The presented textural and mineral chemical evidence strongly argue against a peritectic replacement of olivine by orthopyroxene. Particularly the high Ca concentrations of orthoproxene cores (> 1.5 wt% CaO) are difficult to explain by a late formation at reduced temperatures.

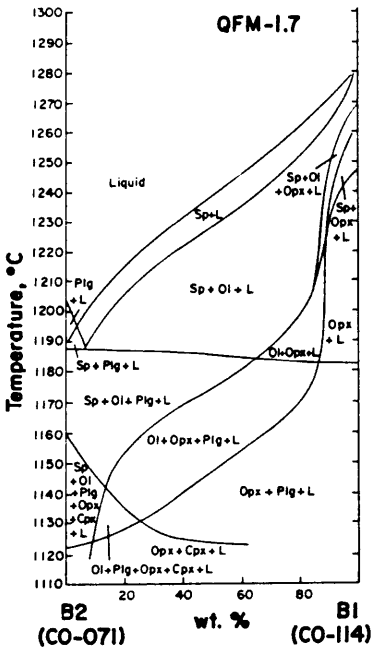

Figure V.1b: Phase relations of B2 - B1 mixtures as functions of temperature and fo_2 at 1-atm . Phase relations were established on T-fo_2 curves equivalent to the QFM - 1.7. All data from Sharpe and Irvine (1983).

The liquidus temperature of the melt (B1) could also not have been close to the orthopyroxene-plagioclase cotectic (1180°C), because experiments (Sharpe and Irvine, 1983) on a B1 melt composition show that, depending on fo_2, chromite ceases to crystallize below temperatures ranging from 1260°C (IW buffer) to 1220°C (NNO buffer) (Fig. V.1a). The disappearance of chromite is attributed by Irvine (1967) to a reaction relationship whereby Cr_2O_3 enters orthopyroxene. Chromite, however, is a common cumulus phase throughout the lower critical zone (Cameron, 1980).

From the evidence presented above it seems more likely that orthopyroxenes attained their relatively low Mg/Fe ratios by re-equilibration with interstitial liquid. The fact that orthopyroxenes have a higher Mg# in plagioclase-rich samples implies that a compositional shift is not simply a function of the relative amount of intercumulus liquid (initial porosity). The lack of late mineral phases such as quartz and K-feldspar, together with the relatively primitive composition of plagioclase in plagioclase-rich samples (see Chpt. IV.3.1) indicate a restricted degree of intercumulus liquid fractionation. Hence, a pronounced shift in Mg# due to trapped liquid fractionation can be ruled out for those samples.

The compositional effect of trapped liquid fractionation is evaluated in the following chapter. It will be shown that within individual stratigraphic intervals (LG 6 - LG 7 and LG 7 - MG 1) orthopyroxene had a fairly uniform composition (83-82 and 81-80) prior to the stage where interstitial liquid fractionated.

It is proposed that the Mg# of orthopyroxene within the LG 7 and MG 1 interval has decreased from originally more than 87 to about 83 as a result of re-equilibration with a liquid which was less Mg-rich than primitive B1. A B1 liquid would have to undergo about 50 % fractionation to be in equilibrium with Mg# 83 (Barnes, 1986a). A pure B2 liquid is, at its liquidus temperature, in equilibrium with Mg# of close to 79. Figure V.2 shows the respective equilibrium orthopyroxene compositions (Mg#) for various hybrids produced by mixing between B2 and B1. Fractionation path of B1 liquid (0, 10, 15 and 20 % fractionation) and the respective orthopyroxene compositions are those calculated by Barnes (1986a). B1 starting composition is from Cawthorn and Davies (1983) B2 from Harmer and Sharpe (1985). From this figure it

can be seen that the B1 component in the hybrid has to be between 30 to 50 % to be in equilibrium with orthopyroxene Mg# 84 - 83 and that the hybrid must have undergone 15 - 20 % fractionation.
Similarly, a Mg# of 81 (LG 6 - LG 7) could be explained by a hybrid with a B1 component of less than 20 %. This value, however, appears to be unreasonably low and is not consistent with whole-rock (Chpt. VII) and Sr isotope data (Chpt. IX). The two stratigraphic intervals show a similar range in the amount and composition of intercumulus phases and in orthopyroxene trace element concentrations (Cr and Ti). One can therefore assume that the low Mg# of orthopyroxene from the LG 6 - LG 7 sequence is not simply a function of a lower B1 component in the hybrid.

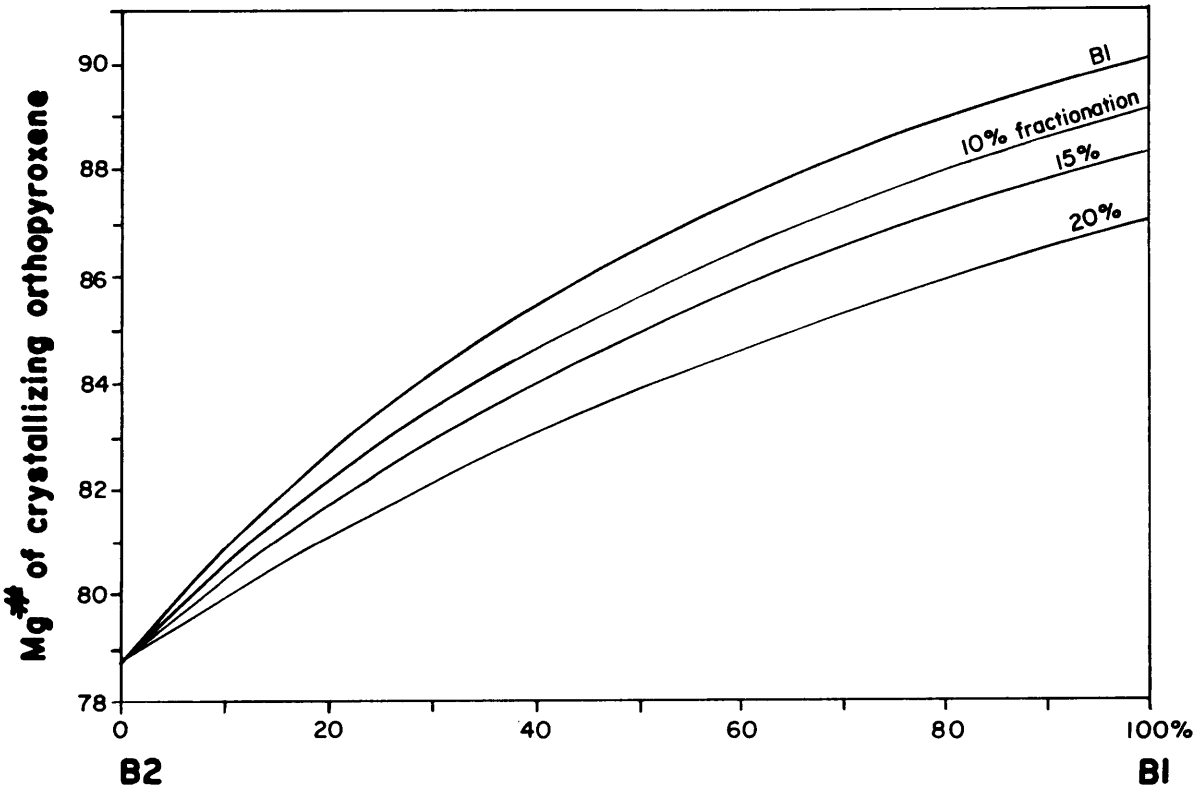

Figure V.2: Calculated Mg# of orthopyroxene in equilibrium with various B2 - B1 mixtures. Hybrids were calculated for various B1 compositions (0, 10, 15 and 20 % fractionation). B2 composition after Harmer and Sharpe (1985), B1 after Cawthorn and Davies (1983). Mg# for the four B1 endmembers are from Barnes (1986a).

Mixing of B2 liquid and B1 liquid plus orthopyroxene crystals has a complicating effect on the bulk Mg/Fe ratio of the hybrid melt. The presence of orthopyroxene in the B1 component is neglected in Figure V.2 which shows various B2-B1 mixtures with their respective orthopyroxene liquidus compositions. It is obvious that the addition of pyroxene increases the bulk Mg/Fe ratio of the hybrid melt and hence the final Mg# of the pyroxene. Thus, a large amount of orthopyroxene carried within the added B1 liquid will result in a relatively high Mg#, while a small amount of pyroxene will cause a proportionally smaller increase in Mg#. The compositional effect of added pyroxene on the hybrid liquid is independent from the total volume proportion (crystal and liquid) of B1 in the hybrid. Thus, for a quantitative calculation of the final Mg# one would have to know the proportion of B1 in the hybrid, the degree of fractionation of B1 prior to mixing and the relative proportion of orthopyroxene in the B1 component. It is particularly difficult to assess the latter variable as the proportions in a two-phase (crystal-liquid) system are expected to change with the thermal conditions in the magma chamber.

The low Mg# of the LG 6 - LG 7 interval possibly indicates a relatively low crystal/liquid ratio in the B1 component. A low crystal proportion within plumes descending from a B1 layer into an underlying B2 layer is expected during the early stages of magma emplacement where thermal differences between individual liquid layers are more pronounced (The thermodynamic principles of crystal/liquid slumping are discussed in Chapter IX.1.2). It is assumed that intermittent replenishment by B2 liquid (+- 1190°C; Sharpe and Irvine, 1983) led initially to rapid crystallization in the overlying B1 layer (+- 1290°C; Sharpe and Irvine) and hence to a chaotic descent of crystal-bearing plumes. As the two liquids approach thermal equilibrium, crystallization slows down and gravitative settling proceeds in a more orderly manner with a higher crystal/liquid ratio. A decrease in the proportion of liquid relative to the amount of crystals is consistent with the observed increase in Mg# above the LG 7. The subsequent decrease in Mg# towards the top of the lower critical zone is presumably related to a further magma addition and hence a repetition of the decrease in Mg# associated with the LG 6.

V.3. STAGE TWO: ORTHOPYROXENE - TRAPPED LIQUID REACTION

In order to evaluate the relative shift in Mg# caused by chemical interaction between cumulus orthopyroxene and fractionating interstitial liquid, the Mg# of orthopyroxene was plotted against the An content of corresponding plagioclase (Fig. V.3). While the Mg# is well defined due to the almost constant pyroxene composition within individual samples (Chpt. III.5.3.5), the bulk An content for surrounding feldspar was determined by calculating the weighted average of all analyzed feldspar cores for each sample.

The resulting diagram shows a fairly good correlation between the Mg# and the An content. The fact that the data plot as two distinct groups (labelled as A and B) indicates that the starting composition of pyroxene differed for each group. However, both groups form an almost parallel trend which is seen as further evidence that the shift in Mg# is systematic irrespective of the pyroxene starting composition.

Samples in group A cover the stratigraphic sequence between MG 1 and LG 7 (342 - 421 m in drillcore MDH 29), whereas group B consists of samples from LG 7 to LG 6 (430 - 461 m in MDH 29). In order to document a direct relationship between the Mg# and the An content it is important that only samples are used for which a constant initial Mg# can be assumed. For this reason samples from the hangingwall of LG 7 (422 - 428 m) and from the top of the investigated sequence (311 - 321 m) were excluded as pyroxenes of those samples show a systematic change in Mg# with stratigraphic height which can not be related to interstitial melt fractionation or to the presence of modal chromite, and is therefore considered to be a primary feature.

Furthermore, only chromite-poor samples are displayed in Figure V.3 and used for the two regression lines. Samples with a whole rock Cr content of more than 6000 ppm were excluded to eliminate the compositional change in Mg# caused by orthopyroxene-chromite re-equilibration.

Regression of the two groups resulted in the following coefficients: 0.065 (STD 0.006) for line A and 0.061 (0.011) for line B, with an average value of 0.063 (0.009).

The Mg# of orthopyroxene with most calcic plagioclase in set A is about 82 and the difference in the Mg# and that determined for samples

with less calcic plagioclase can be taken as the reduction caused by re-equilibration with trapped liquid.

Recalculation of the "original" Mg# was done for each sample by subtracting the particular An content from a constant An value of 75. The difference was then multiplied with the correction factor (0.063) and added to the Mg#. A constant An value of 75 was used because this value is the highest observed averaged An content in the investigated sequence. Normalizing the feldspar composition of each sample to An 75 is solely based on the assumption that pyroxenes surrounded by plagioclase An 75 have not changed their Mg# due to trapped liquid fractionation. A maximum correction of 2.6 Mg# units was made for sample 353 29 which has an An content of 34.

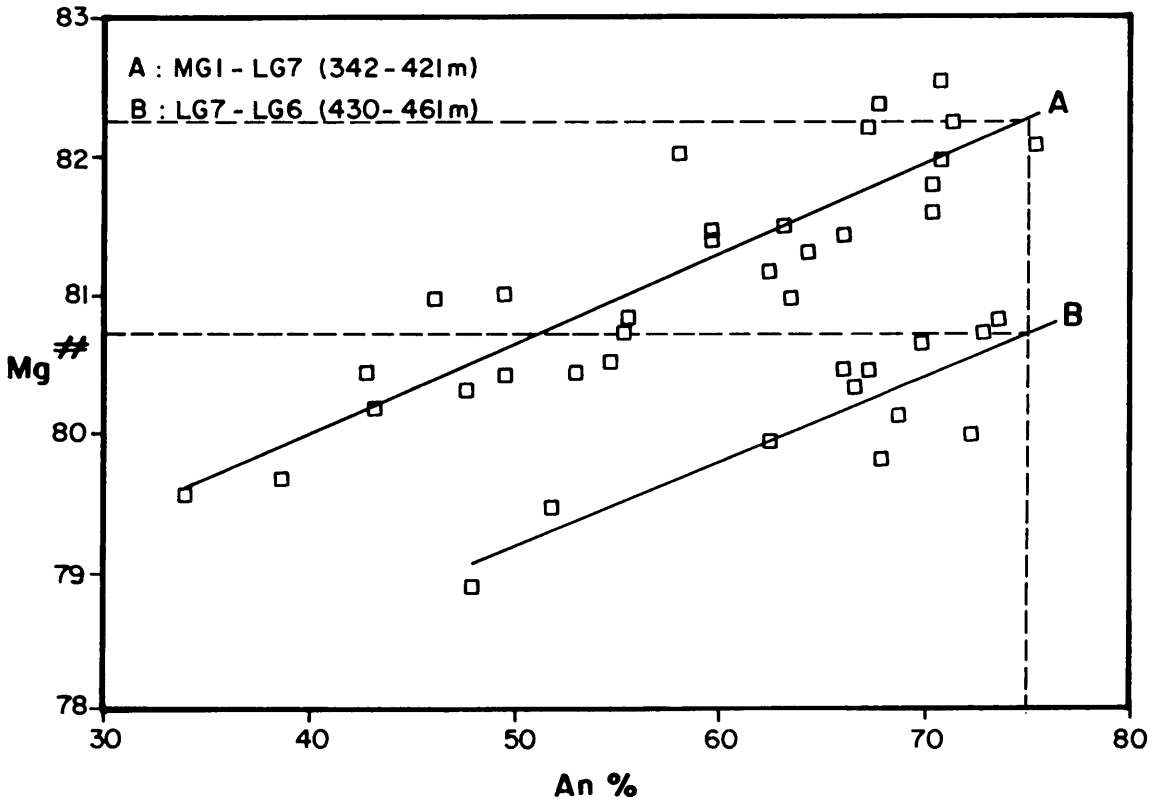

Figure V.3: Mg# of orthopyroxenes versus the An content of co-existing plagioclase from the E unit (MDH 29). Mg# and An content of each sample are the calculated averages of 8-15 individual grains (core compositions). Regression lines for the two stratigraphic intervals (A and B) are calculated (coefficients are quoted in the text). Mineral data from rocks with more than 6000 ppm Cr (whole-rock XRF) are excluded.

V.4. STAGE THREE: ORTHOPYROXENE - CHROMITE SUBSOLIDUS RE-EQUILIBRATION

A similar method was used to correct for the apparent shift in Mg# caused by the Fe^{2+} - Mg exchange between pyroxene and chromite. Figure V.4 shows the increase in Mg# as a function of modal chromite. For simplicity the normative chromite content was derived from the whole rock Cr concentration (ppm). 3000 ppm was subtracted from the Cr concentration of each sample as this is the amount of chromium considered to be present in the orthopyroxene (chromite-free analyses, Folder 2).

The two populations A (330-415 m) and B (430-468 m) correspond to the stratigraphic sequences as described above. However, the number of individual samples is greatly reduced as only samples with interstitial plagioclase of An content between 75 and 67 were considered. The exclusion of samples with more fractionated interstitial minerals was necessary to eliminate the compositional effect on pyroxene caused by trapped liquid fractionation.

The following coefficients were computed: 0.00005 (STD 0.00001) for A and 0.00006 (0.00001) for group B with a calculated average of 0.000055. The Mg# of each sample was then recalculated by multiplying the Cr content (apparent Cr minus 3000 ppm) with the factor (0.000055) and the resulting value was subtracted from the Mg#. The corresponding normative amount of chromite is shown in Figure V.4 and was calculated from whole rock data by assuming that chromite contains a constant amount of 45 % Cr_2O_3.

The maximum individual Mg# correction is 4.5 units for sample 319 29 which contains 85000 ppm Cr (+- 16 vol % chromite). The corrected Mg# (79) appears to be too low by about one unit relative to the Mg# of adjacent rocks (Fig. V.5a). It is quite possible that the established correction factor tends to overcorrect the Mg# in chromite-rich samples. This indicates that Fe^{2+} - Mg exchange between pyroxene and chromite is a finite process and that the presented regression line might flatten towards higher Cr concentrations. Caution should therefore be taken when recalculating the Mg# of chromite-rich samples (> 10 vol % chromite).

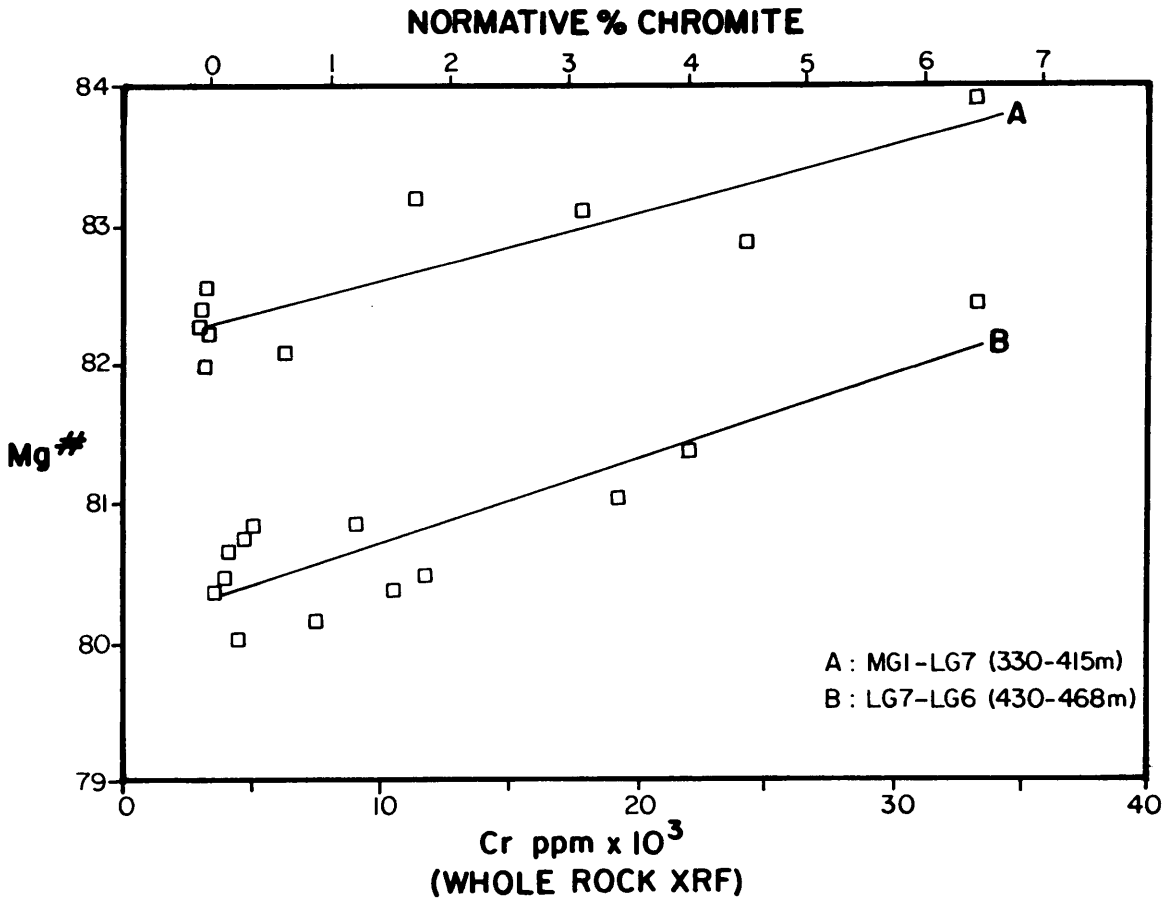

Figure V.4: Mg# of orthopyroxene versus the whole-rock chromium content (XRF) of samples from the E unit (MDH 29). Mg# is the calculated average of 8-15 individual grains. Regression lines for the two stratigraphic intervals (A and B) are calculated (coefficients are quoted in the text). Pyroxene data are from samples with coexisting plagioclase compositions between An 77 and 67. Upper scale shows the calculated normative abundance of chromite.

V.5. STRATIGRAPHIC VARIATION AFTER MG# RECALCULATION

Figures V.5a and 5b show the uncorrected Mg# and the Mg# corrected for modal chromite and trapped liqid fractionation for drillcore MDH 29. The modal amount of chromite in samples from MDH 23 and MDH 1 has been estimated by comparing the thin sections with sections of samples from MDH 29 for which the Cr concentrations were analytically determined. Only the corrected Mg# is presented in Figure V.6 for the three drillcores MDH 29, 23 and 1.

Figures V.5a and 5b: Stratigraphic variation of analyzed (5a) and corrected (5b) Mg# of orthopyroxene from the D_2 and E units (MDH 29). Mg# is corrected for trapped liquid shift and subsolidus re-equilibration with chromite. Recalculation methods are outlined in the text. Each data point is the calculated average of 8-15 individual grains.

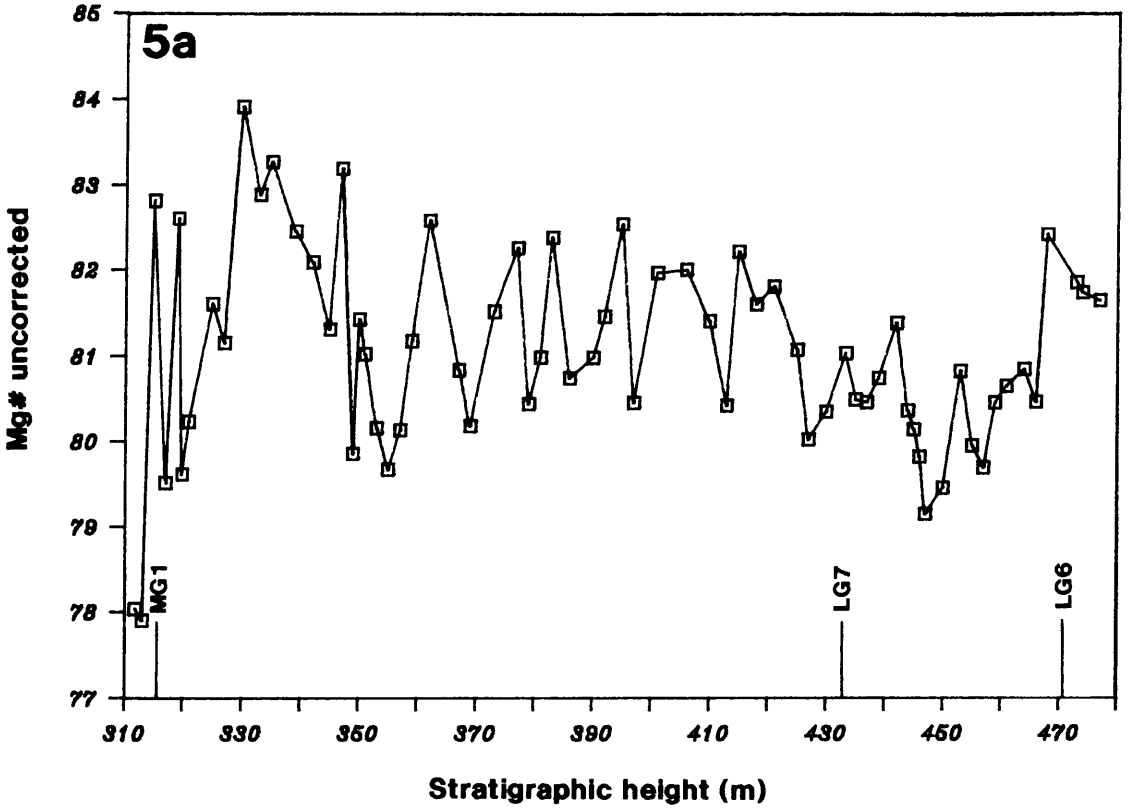

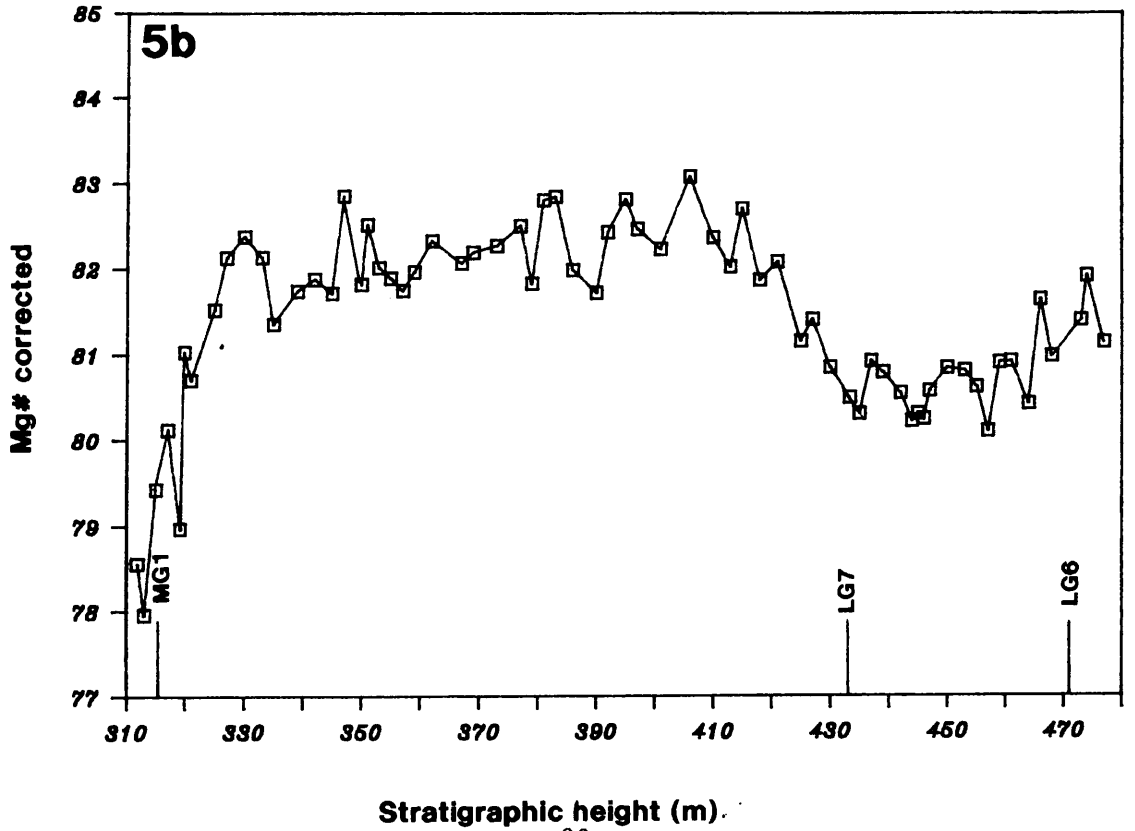

The correction method has eliminated the irregular variation in the E unit to a large extent (Fig. V.5a and 5b). An apparently non-systematic variation in Mg# in E was also noted by Cameron (1980).

Several systematic changes in pyroxene composition emerge from these three drillcores (Fig. V.6). Mg# decrease across the LG 6 and relatively low values (Mg# 80 - 81) continue up to the stratigraphic position of the LG 7. Subsequently Mg# increase to a relative maximum of about 83 followed by a gradual upward decrease to 82. The top of the unit is characterized by a decline in Mg# to values below 80. The apparently systematic decrease occurs over an interval of less than 20 m and starts about 10 to 20 m below the MG 1 in MDH 29. Absolute thicknesses for this interval will obviously vary according to the particular thickness of the unit intersected in each borehole. In MDH 23 the variation in the Mg# towards the top is quite different, because this stratigraphic interval coincides with the bottom of an abnormal and chemically extensively altered sequence that is discussed in greater detail in Chapter X.1.

The observed trends in Mg# compare well with published data (Cameron, 1980) from the Jagdlust - Wintersveld area. Cameron's section is about 40 km along strike to the north. Of further interest is the fact that trends and the absolute range in Mg# are similar in all three investigated drillcores despite the considerable differences in stratigraphic thicknesses. The averaged orthopyroxene compositions for this particular succession for the three drillcores are presented in Table V.1 in order to emphasize the close mineral-chemical correspondence between the three boreholes.

Trace element concentrations (Cr and Ti) in orthopyroxene cores show considerable scatter with no systematic variation with stratigraphic height (Folder 2). Only Al displays a gradual upwards increase (Fig. VI.9). Detailed orthopyroxene grain traverses revealed that the abundance of these elements is also critically dependent on the degree of interstitial melt fractionation (Chpt. III.5.2), which is expressed by the variation in actual Mg#. Plots of Al, Cr and Ti versus Mg# should therefore be useful in demonstrating a systematic variation in these elements with trapped liquid fractionation.

Figures V.7a and 7b to V.9a and 9b show the averaged core and rim concentrations for Cr, Al and Ti versus actual Mg# for the three

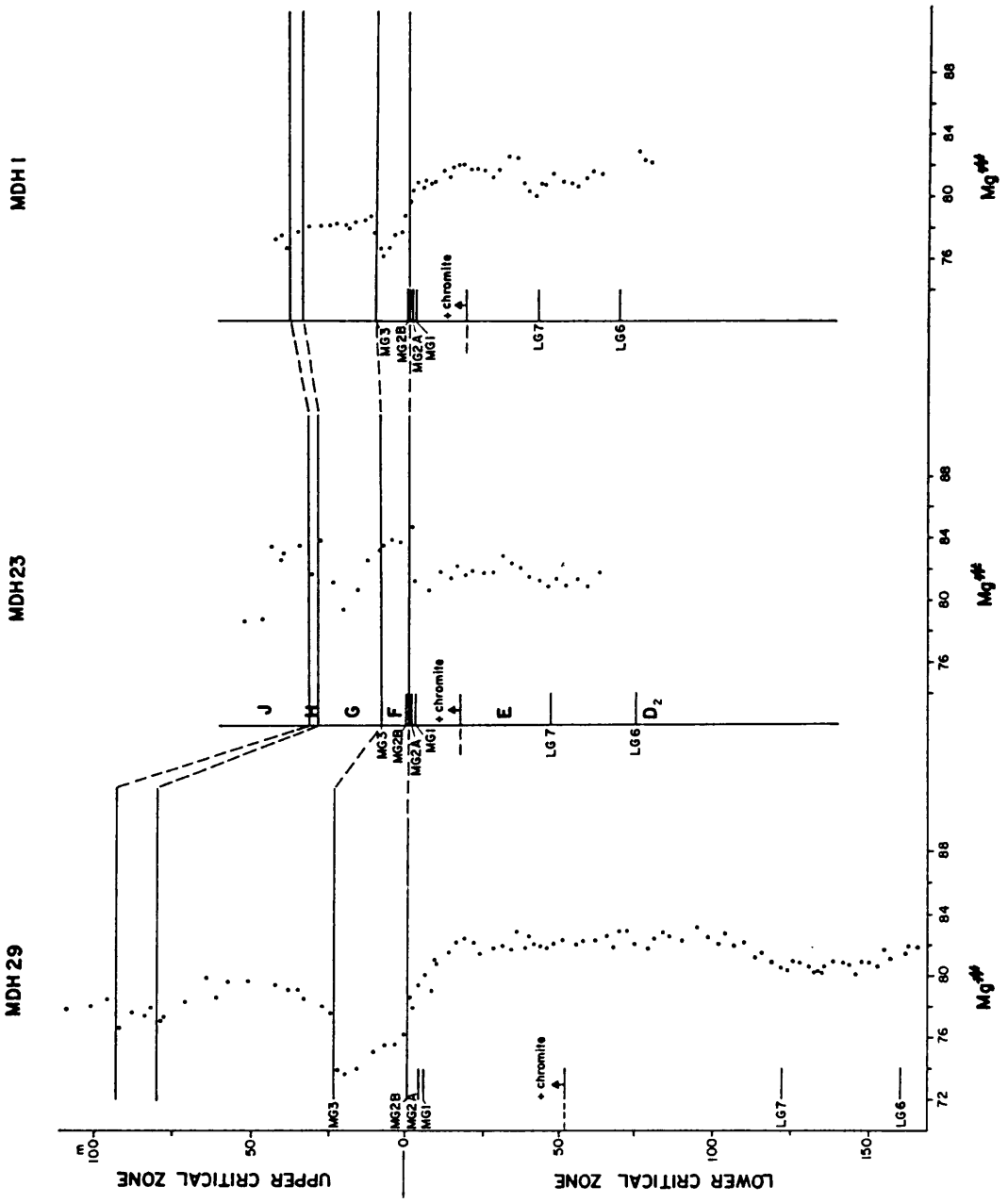

Figure V.6: Stratigraphic variation of corrected Mg# of orthopyroxene for the three drillcores MDH 29, 23 and 1. Recalculation methods are outlined in the text. Datum marks the lower-upper critical zone boundary (E/F). The aberrant pyroxene composition from MDH 23 between the upper E and lower J units is discussed in Chapter X.1. Each data point is the calculated average of 8-15 individual grains. The arrow in the upper E unit indicates the re-occurrence of abundant modal chromite.

Table V.1: Averaged element concentrations of orthopyroxene from two stratigraphic sequences for the three drillcores.

Orthopyroxene from the		MDH 29	MDH 23	MDH 1
		n = 44	n = 14	n = 20
MG 1 - LG 7 sequence	CaO	1.55 +- 0.18	1.53 +- 0.15	1.61 +- 0.19
	Al_2O_3	1.21 +- 0.10	1.22 +- 0.11	1.20 +- 0.07
	Cr_2O_3	0.47 +- 0.03	0.45 +- 0.02	0.44 +- 0.03
	TiO_2	0.12 +- 0.02	0.12 +- 0.02	0.12 +- 0.01
	Mg#	81.5 +- 1.66	81.8 +- 0.87	80.9 +- 1.12
		n = 20	n = 6	n = 13
LG 7 - LG 5 sequence	CaO	1.55 +- 0.11	1.46 +- 0.15	1.54 +- 0.09
	Al_2O_3	1.10 +- 0.05	1.14 +- 0.11	1.14 +- 0.04
	Cr_2O_3	0.48 +- 0.02	0.48 +- 0.02	0.47 +- 0.03
	TiO_2	0.11 +- 0.02	0.11 +- 0.02	0.10 +- 0.01
	Mg#	81.3 +- 2.25	81.8 +- 1.99	81.3 +- 1.88

investigated drillcores. Only samples between LG 7 and the top of the unit were considered as an originally uniform Mg# has been shown for this stratigraphic interval.

Rim concentrations of all three elements are reasonably well correlated with actual Mg# (Fig. V.7b - V.9b). Samples from chromite-rich rocks have been included and can be identified by their higher Mg# (Mg# > +- 82). Orthopyroxene rims from chromite-rich samples have commonly increased Al and decreased Ti concentrations, while no systematic change is found in the Cr content. Pyroxenes from chromite-free samples show the already established trends, namely an increase in Ti and a decrease in Cr and Al with progressing trapped liquid fractionation.

Cores of pyroxenes show a poor correlation between Mg# and both Cr and Al (Fig. V.7 and V.8). Similar to the rims, cores of high Mg# pyroxene from chromite-rich samples have elevated Al concentrations, but show no systematic correlation with Cr. The particularly poor fit for Mg# and Al of pyroxenes from chromite-free samples is caused by the observed increase in Al with stratigraphic height. The gradual increase

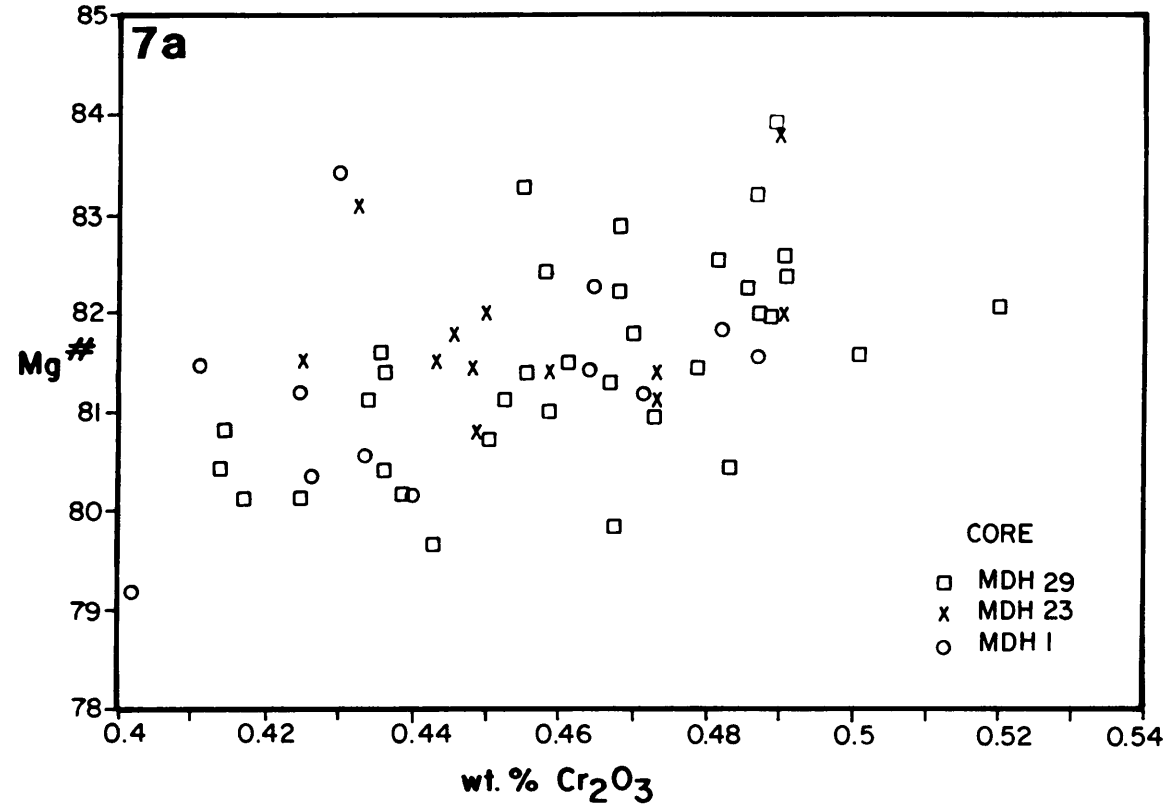

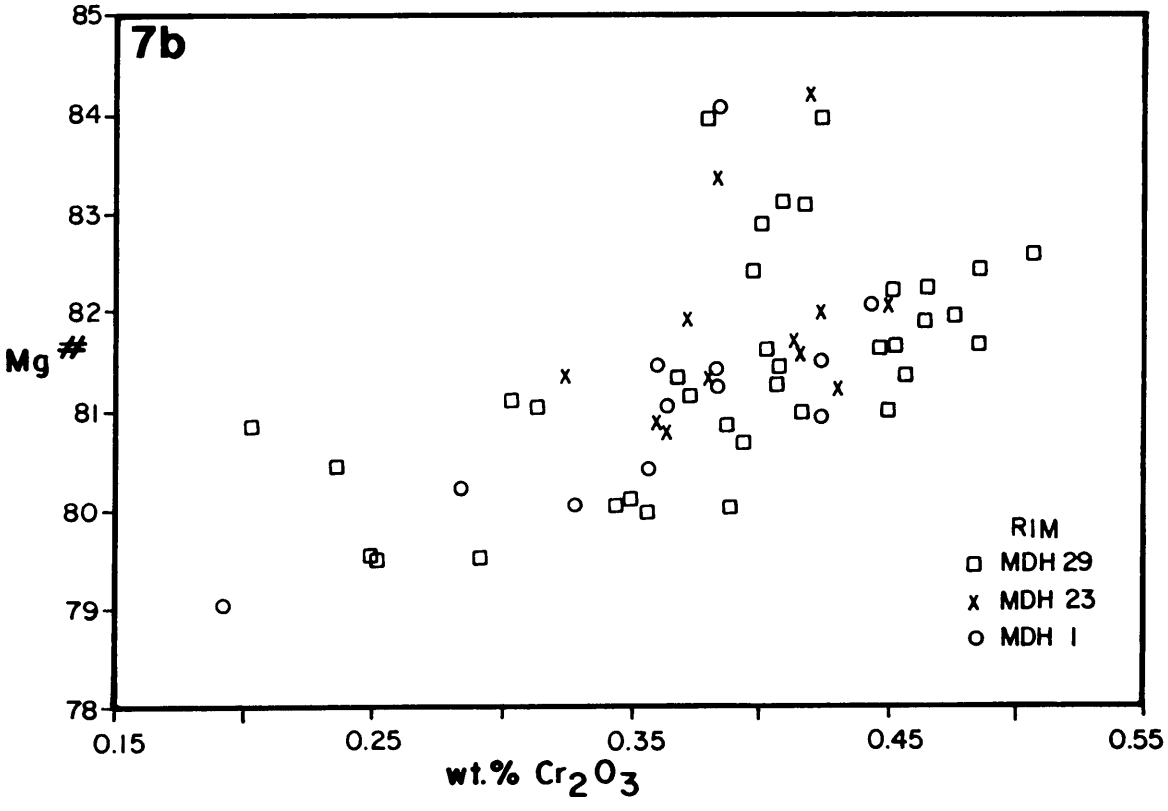

Figures V.7a and 7b: Mg# of orthopyroxene cores (7a) and rims (7b) versus chrome content (cores and rims) for the three boreholes. Each data point is the calculated average of 8-15 individual grains from the LG 7 - E/F interval. Pyroxenes with a Mg# higher than 82 are from chromite-rich samples.

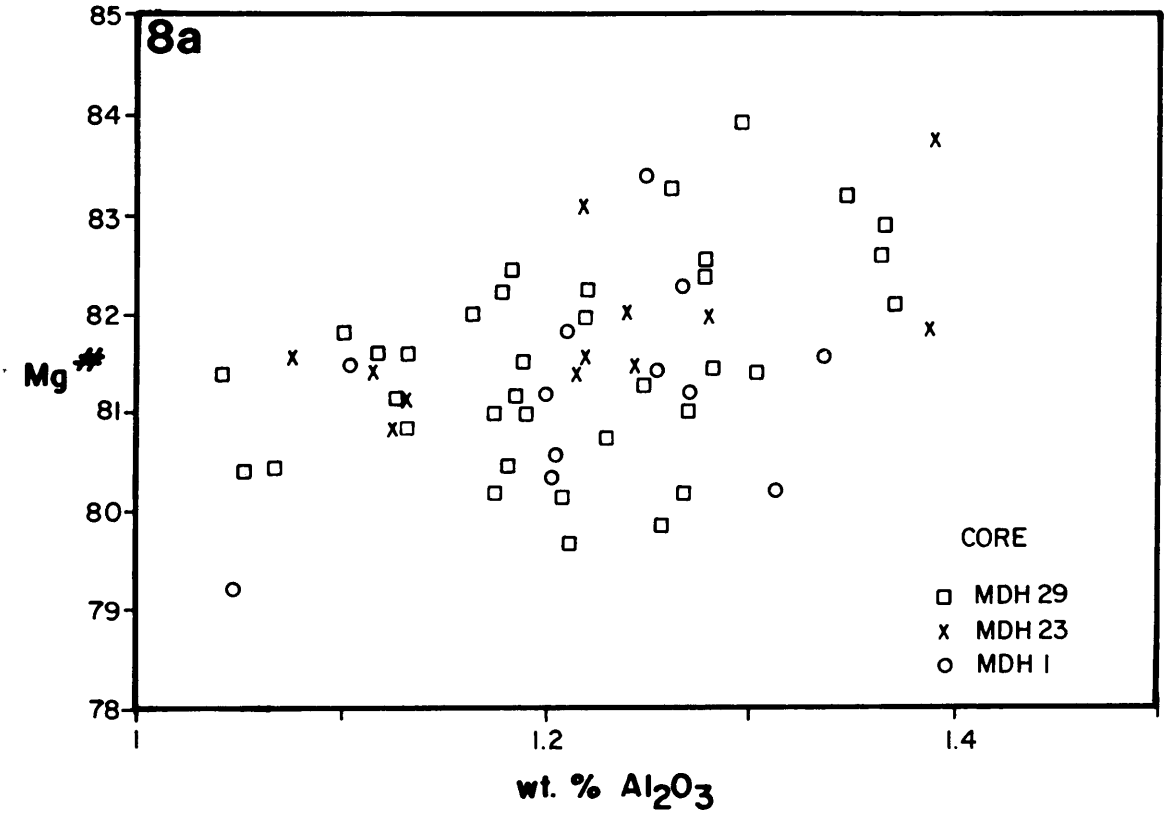

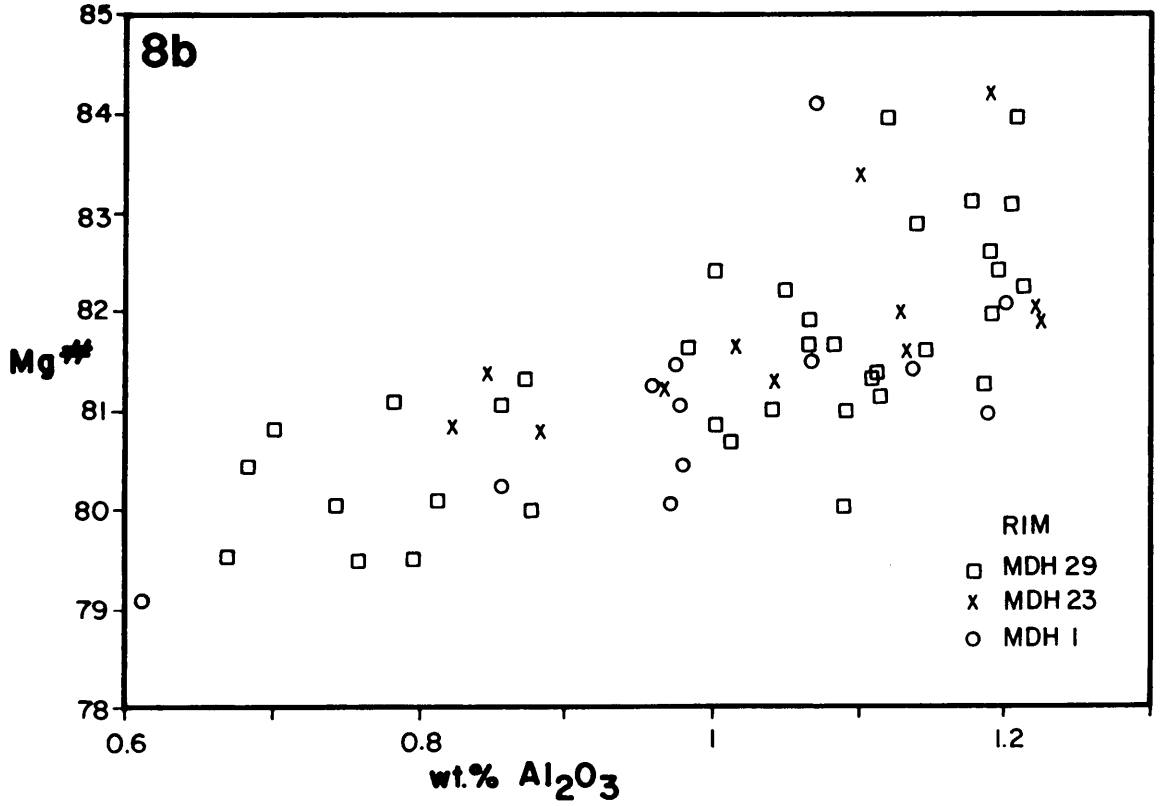

Figures V.8a and 8b: Mg# of orthopyroxene cores (8a) and rims (8b) versus aluminium content (cores and rims) for the three boreholes. Each data point is the calculated average of 8-15 individual grains from the LG 7-E/F interval. Pyroxenes with a Mg# higher than 82 are from chromite-rich samples.

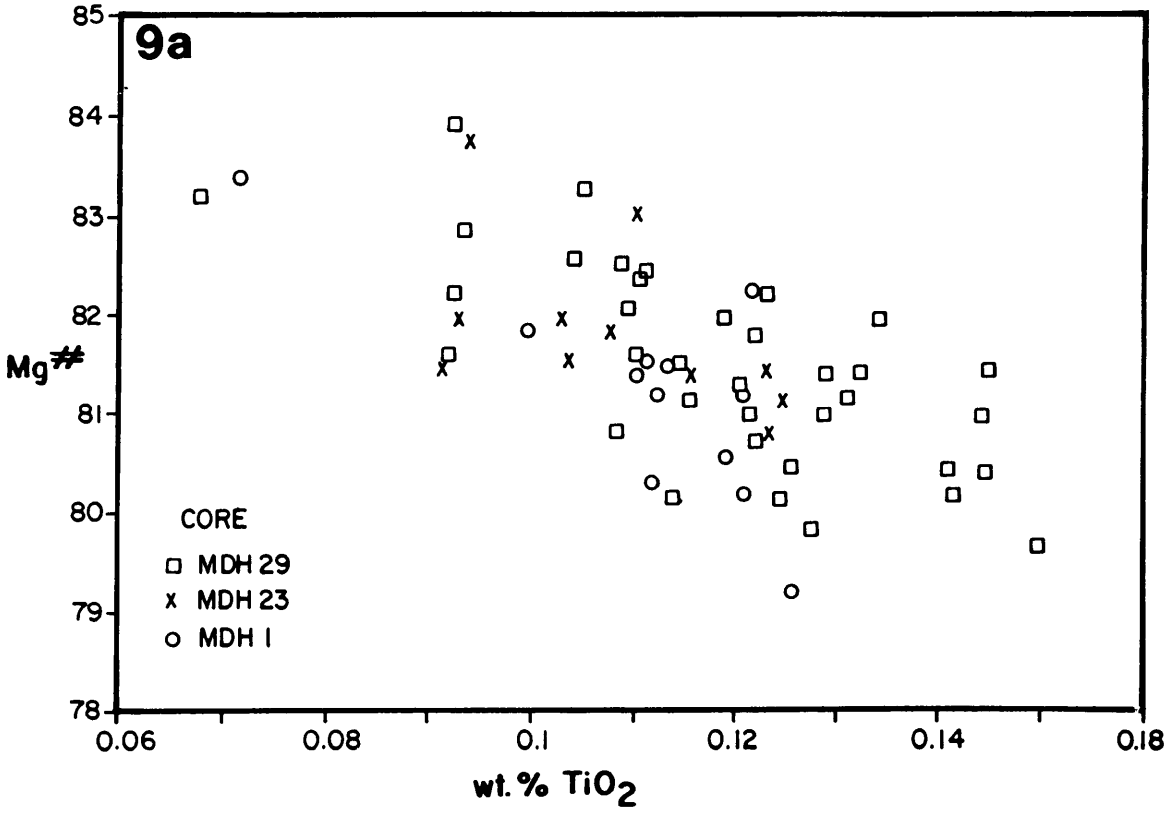

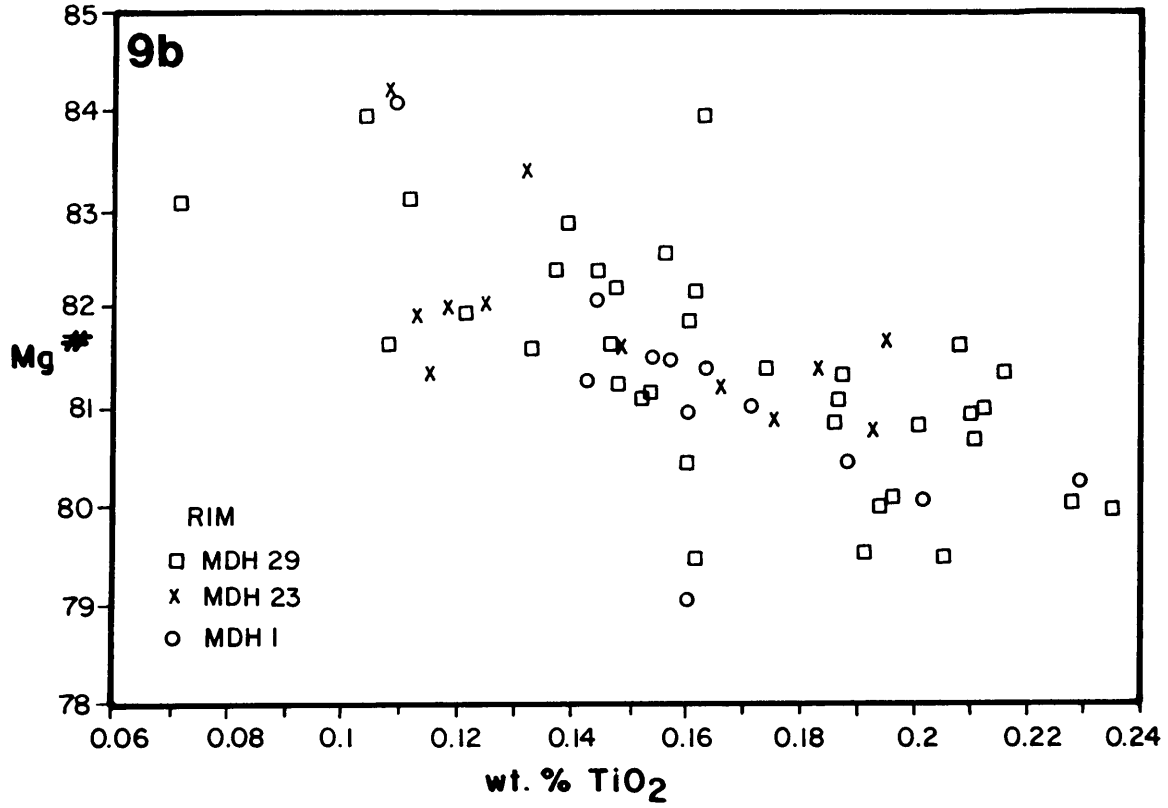

Figures V.9a and 9b: Mg# of orthopyroxene cores (9a) and rims (9b) versus titan content (cores and rims) for the three boreholes. Each data point is the calculated average of 8-15 individual grains from the LG 7 - E/F interval. Pyroxenes with a Mg# higher 82 are from chromite-rich samples.

in Al from LG 7 towards the top of the unit is found in all three drillcores and is graphically displayed for MDH 29 by an upwards increasing Al/Cr ratio (Folder 2 and Fig. VI.9)
The generally poor correlations between actual Mg# and both Al and Cr are most likely the result of the limited diffusional distances for Al and Cr in orthopyroxene (Chpt. III.5.3). Hence, as predominantly cores of large grains (> 1000 um) were analyzed, it is assumed that the scatter in Al and Cr reflects an incomplete re-equilibration process between pyroxene cores and surrounding fractionating liquid. The highly efficient Mg - Fe exchange between orthopyroxene and liquid, however, resulted in complete Mg# homogenization.
The good correlation between actual Mg# and Ti (Fig. V.9a) in orthopyroxene cores can be seen as further evidence that Ti has a slightly higher diffusion rate than Al or Cr (Chpt. III.5.3).

V.6. SUMMARY OF RESULTS DERIVED FROM MINERAL VARIATIONS

Detailed mineral-chemical investigations have shown that the feldspathic pyroxenites of the lower critical zone formed by an extremely complex interaction of cumulus and post-cumulus processes.
It is proposed that crystal settling/slumping into a hybrid liquid (Chpt. IX.1) led to the accumulation of a thick porous pile of orthopyroxenes. Solidification of interstitial liquid must have proceeded in such a manner that individual horizons crystallized while the residual melt in the pile immediately above became progressively more fractionated. This process has led to the formation of several crystallization fronts for the interstitial liquid.
Various stages of melt fractionation are indicated by a systematic and quasi-cyclic change in intercumulus mineral assemblages and their respective compositions. As a result of disequilibrium conditions, cumulus orthopyroxene reacted with surrounding liquid. Fractional crystallization of the fractionated intersititial liquid and simultaneous re-equilibration led to a complex diffusional controlled zoning pattern in pyroxene. Intercumulus plagioclase developed a normal magmatic zoning during primary growth.

Inter-grain variations of orthopyroxene show that the change in composition depends critically on the individual size of pyroxene, on the composition of the immediately surrounding phase and on the diffusion rate of a particular element.

The original Ca, Al, Cr and Ti concentrations seem to be preserved in the cores of orthopyroxenes which are large enough to prevent complete re-equilibration and grain homogenization. This is supported by the good agreement in Ca, Al, Cr and Ti abundances between the three boreholes for individual stratigraphic intervals. The data also indicate that orthopyroxene from below the LG 6 up to the E/F boundary shows no systematic primary variation in its Cr and Ti abundances.

The Mg#, however, due to the high diffusion rate for Fe and Mg, has invariably changed. Modification of Mg# took place during three distinct stages. It is proposed that re-equilibration with a hybrid liquid caused a shift (drop) in the Mg# of orthopyroxene (stage 1). Different shifts in the Mg# are possibly related to changes in the crystal/liquid ratio of descending plumes. A high crystal/liquid ratio is expected to cause a small decrease while a low crystal/liquid ratio will result in a higher shift. A decrease by at least 6 units can be assumed for the LG 6 - LG 7 interval whereas Mg# of pyroxene from the LG 7 - MG 1 presumably dropped by more than 3 units.

A further decrease in Mg# in orthopyroxene occurred during fractionation of interstitial liquid (stage 2). The extent of Mg- depletion during this stage is determined by the degree of trapped liquid fractionation.

A pronounced increase in Mg# in orthopyroxene occurs in chromite-bearing assemblages as a result of subliquidus/subsolidus re-equilibration with chromite (stage 3).

The "original" Mg# was recalculated by applying empirically derived correction factors. Recalculated values reveal several systematic changes in Mg# with stratigraphic height. The observed trends in Mg# are not reflected by changes in trace element concentrations and it seems likely that Mg# of orthopyroxene was modified by re-equilibration with a hybrid liquid as proposed in stage 1.

CHAPTER VI: MINERAL CHEMISTRY OF THE UPPER CRITICAL ZONE

VI.1. PLAGIOCLASE

Plagioclase occurs as a cumulus mineral throughout most of the upper critical zone and is an intercumulus constituent only in the feldspathic pyroxenites of the L unit, at the base of the G and J units, and in the upper part of the J unit (Folder 2). The core and rim data (mol % An) for each sample are the calculated averages of 10 - 15 core and an equal number of rim analyses. The total range in plagioclase composition within each sample is shown in Figure VI.1, which covers the variation at the transition of the lower to the upper critical zone from the LG 6 into the base of the J unit for each of the three investigated drillcores. The compositionally unusual F to J unit sequence of MDH 23 is discussed in Chapter XI.2.

Although plagioclase occurs as a cumulus phase, the total range in composition within samples from the base of the F unit up to a height of approximately 50 m (MDH 29) is comparable to the variation of intercumulus plagioclase of the lower critical zone. Plagioclase from the chromiferous anorthosites of the F unit are an exception, as they invariably show a smaller variation. The inter-grain variation in An content decreases markedly about halfway up the G unit and remains subsequently almost constant throughout the J, K and M units with an average range of about 5 mol % An.

A pronounced increase in the averaged An content from about 70 (MDH 29) and 65 (MDH 1) to about 75 is associated with the decrease in intra-grain variation in the G unit (Fig. VI.1). The lower average An contents up to the middle part of the G unit are most likely the result of trapped liquid fractionation. The frequent presence of mica, quartz and occassional K-feldspar is diagnostic of the F and lower G units and indicates trapping of moderate amounts of interstitial liquid (meso-cumulates). The degree of trapping appears to be intermediate between that of most lower critical zone samples and the remainder of the upper critical zone. The narrow range of maximum An values (72-78) throughout the F, G, H and J units also indicates that the observed lower average An contents up into the G unit are due to a mesocumulate character of these rocks.

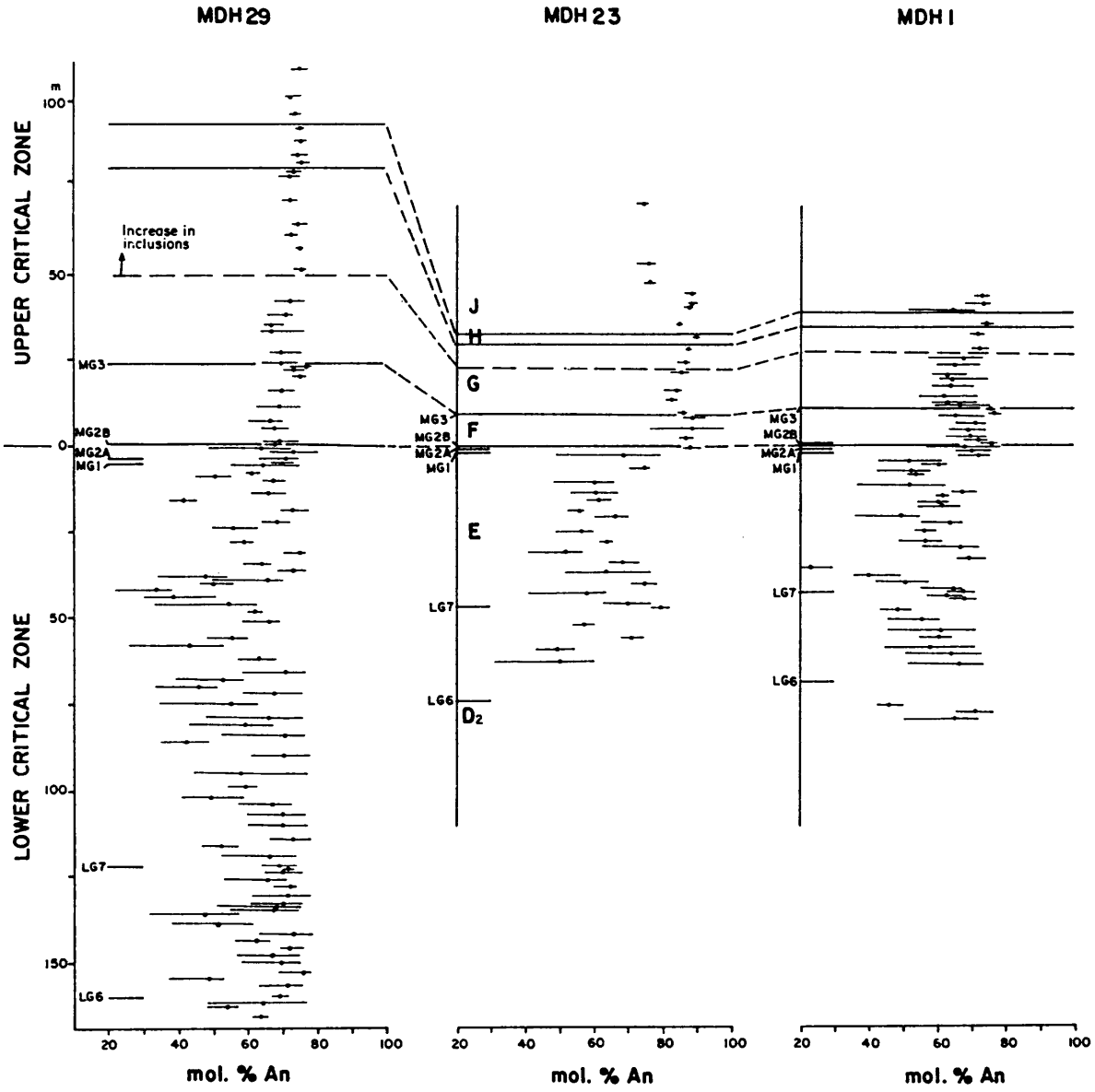

Figure VI.1: Stratigraphic variation of plagioclase (An %) for the three drillcores MDH 29, 23 and 1. The aberrant plagioclase composition from MDH 23 between the upper E and lower J units is discussed in Chapter X.1. Each data point is the calculated average of 8-15 individual grains. The arrow in the G unit indicates the re-appearance of abundant plagioclase inclusions in orthopyroxene. Inclusions first occur in the F unit.

Plagioclases from the feldspathic pyroxenites of the L unit (MDH 22, Fig. X.1) and of the basal (MDH 1 in Fig. VI.1) and upper (MDH 29) parts of the J unit (Folder 2) invariably have lower average An contents of about 65.

Plagioclases from norites show a slight decline in their average core composition from about 75 in the lower third of the J unit to about 72 in the upper J and K units (MDH 29, Folder 2). Throughout the L (MDH 22) and M (MDH 23) units cumulus plagioclase also shows very little variation with average core values ranging between 76 and 71 (Fig. X.1 and Folder 2). Lower values (+- 71) are found in the M unit at three stratigraphic horizons (Folder 2): the first decrease coincides with the appearance of cumulus clinopyroxene, the other two lows are found in very fine grained gabbronorites which characteristically contain abundant inverted pigeonite. The decrease in An content could be genetically linked to the appearence of clinopyroxene or clinopyroxene and inverted pigeonite. Morse (1979) has shown that crystallization of Ca-rich pyroxene from augite-bearing systems is the major cause of Ca depletion and that plagioclase accounts for only about one quarter of the total Ca depletion during fractional crystallization of both augite and plagioclase.

Throughout almost the entire M unit plagioclase rims have more calcic compositions than cores (Folder 2). Rims may be reverse zoned by as much as 4 mol % An. This feature appears to be due to the vermicular intergrowths of quartz and calcium-rich plagioclase. Such myrmekites occur randomly along plagioclase grain boundaries and comprise irregularly shaped areas up to several hundred microns wide (Plate 3.E). Maximum values of up to An 90 have been detected in individual myrmekites. Much attention was given during routine microprobe measurements to avoid myrmekitic areas. The analytical results, however, suggest that moderately affected areas do not necessarily display a characteristic myrmekitic texture.

The first pervasive and optically discernable occurrence of myrmekite is found in the K unit and is evidenced by the occasional reversed zoning within this unit. It is assumed that the apparent reversed zoning of plagioclase in other units is also related to the presence of myrmekitic rims although their mode of occurrence is less pronounced and the increase in An content relatively small.

Dymek and Schiffries (1987) have convincingly shown that myrmekitic and reversed compositional zonation similar to that described here resulted from an interaction between plagioclase crystals and a magmatically derived, high-temperature aqueous fluid.

VI.1.1. PLAGIOCLASE INCLUSIONS IN ORTHOPYROXENE - EVIDENCE FOR MAGMA MIXING ?

Although the presence of plagioclase inclusions in orthopyroxene is a common feature throughout almost the entire investigated part of the upper critical zone, the frequency and the size of inclusions change systematically within the F and G units. Inclusions increase in size and number from the base of the F unit to the top of the unit (MG 3), while orthopyroxene in the immediately overlying rocks of the G unit are almost free of inclusions (Plate 3.C-D). The frequency of inclusions increases markedly in the upper part of the G unit with a sudden increase at the horizon where the range in An content decreases (Fig. VI.1).

Similarly, orthopyroxenes in the feldspathic pyroxenite at the bottom of the J unit (MDH 1) are virtually free of inclusions, while orthopyroxenes in the remainder of the J unit have abundant inclusions. No obvious systematic variation in the frequency of inclusions was found within the remainder of the J unit. It should be mentioned that the described variations in the relative amount of inclusions are essentially qualitative estimates. The resolution of small scale variations would require a more quantitative determination.

Although orthopyroxenes in very plagioclase-rich horizons (top of F unit and H unit) invariably have abundant inclusions, the particular texture of these pyroxenes and the larger size of enclosed feldspar suggest that the latter crystallized in embayments (Plate 4.D). These feldspars are therefore not inclusions in the sense that individual early formed nuclei were enclosed by pyroxene crystallization.

To document possible chemical variations between enclosed plagioclase and non-enclosed "matrix" plagioclase, the composition of both types was analyzed in more than 70 samples (MDH 29) covering the F, G, H, J

and K units. Possible zoning has been investigated by analyzing 8 to 15 individual cores and margins of each plagioclase group. The individual analyses of feldspar cores and rims were then averaged for each group in every thin section. The rim composition of matrix plagioclase was determined on the side of contact with another plagioclase. Core compositions were determined in the geometrical centres of grains, while rims of enclosed plagioclase were analyzed at a minimum distance of about 20 um from the surrounding orthopyroxene.

Figure VI.2 shows the stratigraphic variation of feldspar composition (mol % 100*(Ca/(Ca+Na))) for cores of enclosed and matrix plagioclase. The broadly sympathetic behaviour shows that both grain types are closely genetically related. Both types of plagioclase have a similar range in calculated average An contents. This indicates that some plagioclase nucleated and became subsequently enclosed by pyroxene after the liquid had undergone some degree of fractionation. This feature is particularly obvious in the mesocumulates of the F and G units, where both feldspar types are characterized by lower average An contents. An alternative explanation whereby early formed high An nuclei re-equilibrated with a progressively more fractionated liquid prior to enclosure is precluded by the low interdiffusion rates of Ca, Al, Na and Si (e.g. Grove et al., 1984; Morse, 1984).

Compositional zoning of enclosed and matrix plagioclases is displayed in Figures VI.3a and VI.3b. The two plots clearly indicate that both types of plagioclase can be zoned normally or reversed. However, reversed zoning is more common in matrix plagioclase than in enclosed feldspar.

Figures VI.4a and VI.4b show that cores and rims of matrix plagioclase are commonly more calcic than those of enclosed feldspar. The same principal feature is expressed in Figure VI.5, which shows the compositional relationship between the two feldspar types against their stratigraphic position. There are neither marked correlations between the compositional inter-relationship of plagioclases and lithological changes nor with the above mentioned variations in the amount of enclosed feldspar.

The fact that cores of plagioclase outside pyroxene are on average more calcic than cores of enclosed plagioclases implies that the majority of enclosed feldspar represent relatively late formed nuclei.

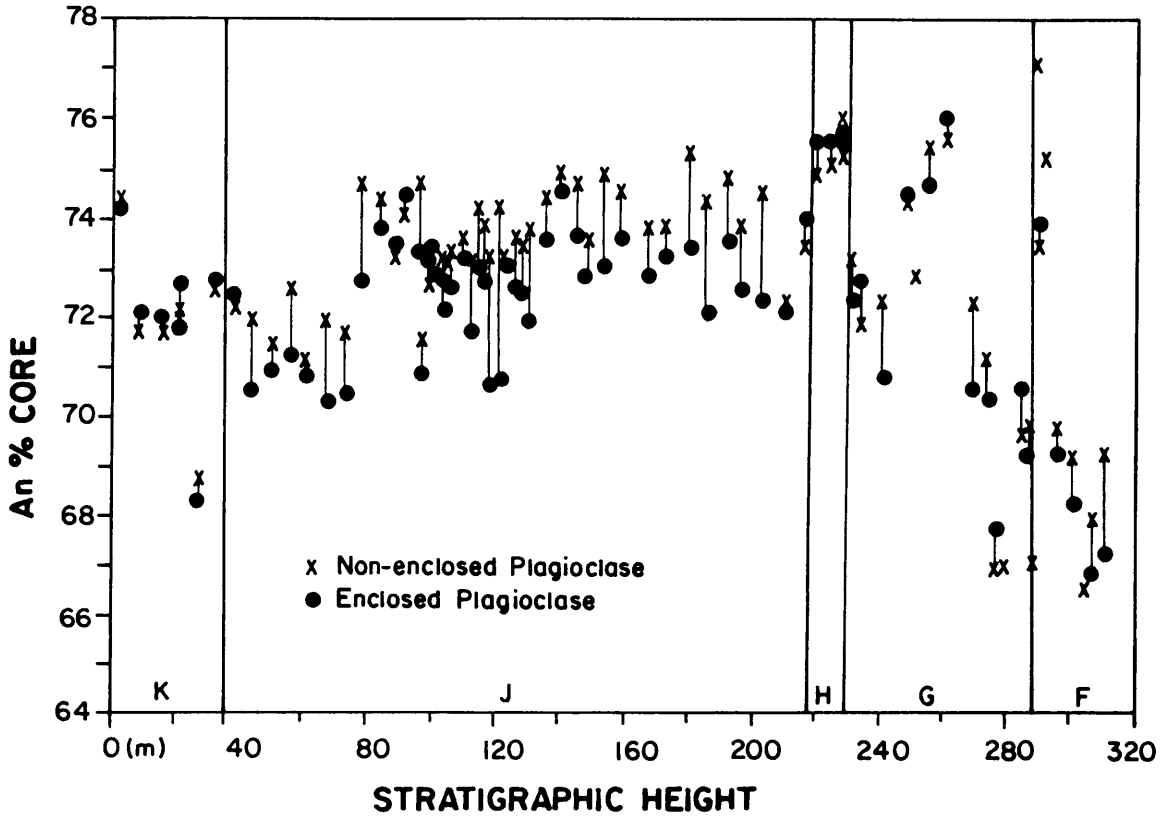

Figure VI.2: Comparison of enclosed and non-enclosed plagioclase composition within the F-K interval. Each data point is the calculated average of 8-15 individual grains.

One can therefore assume that plagioclase was initially the sole crystallizing phase and that early formed nuclei continued to grow. In contrast, later formed and therefore less calcic nuclei became enclosed after the onset of pyroxene crystallization. This process is consistent with experimental and theoretical investigations which show that crystallization is achieved through a series of nucleation steps followed by periods of crystal growth (e.g. Dowty, 1980; Brandeis et al., 1984). Periodic nucleation of new plagioclase crystals rather than continuous growth of initially formed nuclei must then be responsible for the observed range in core compositions between individual grains from one sample. The slow growth rate of plagioclase relative to orthopyroxene (Carmichael et al., 1974) caused the former to become enclosed by the much faster growing pyroxenes.

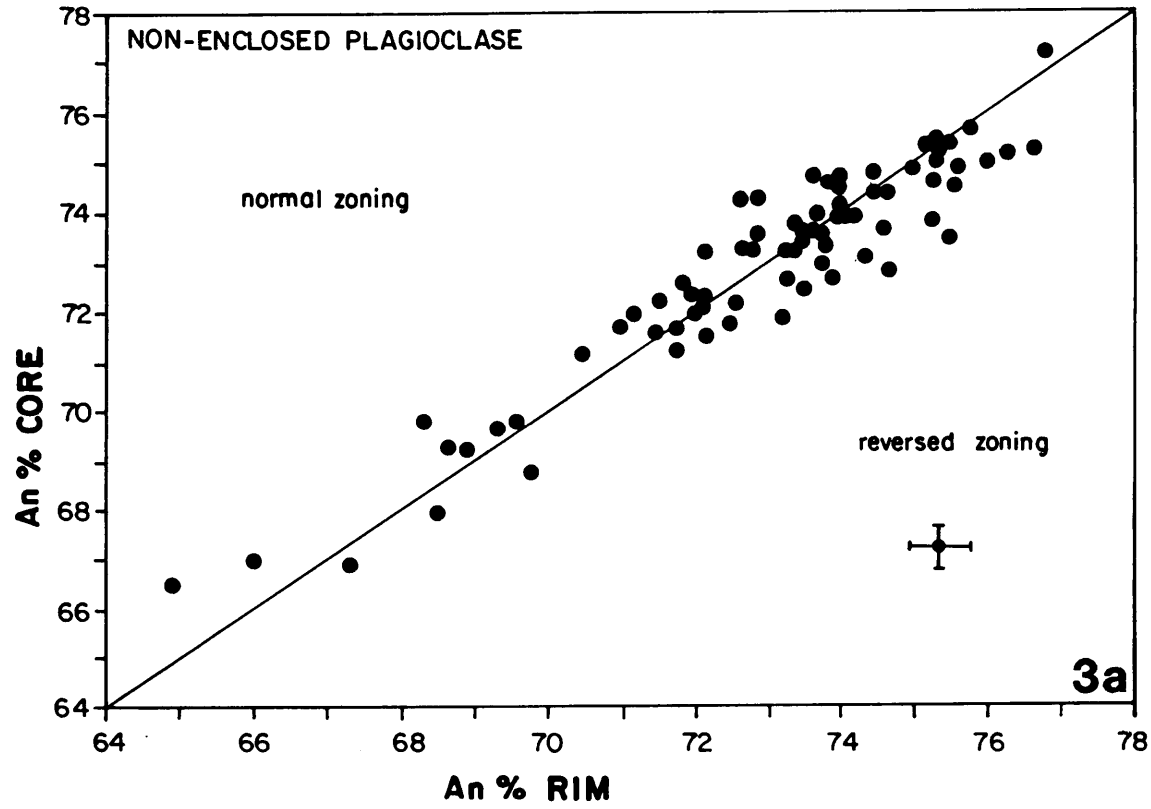

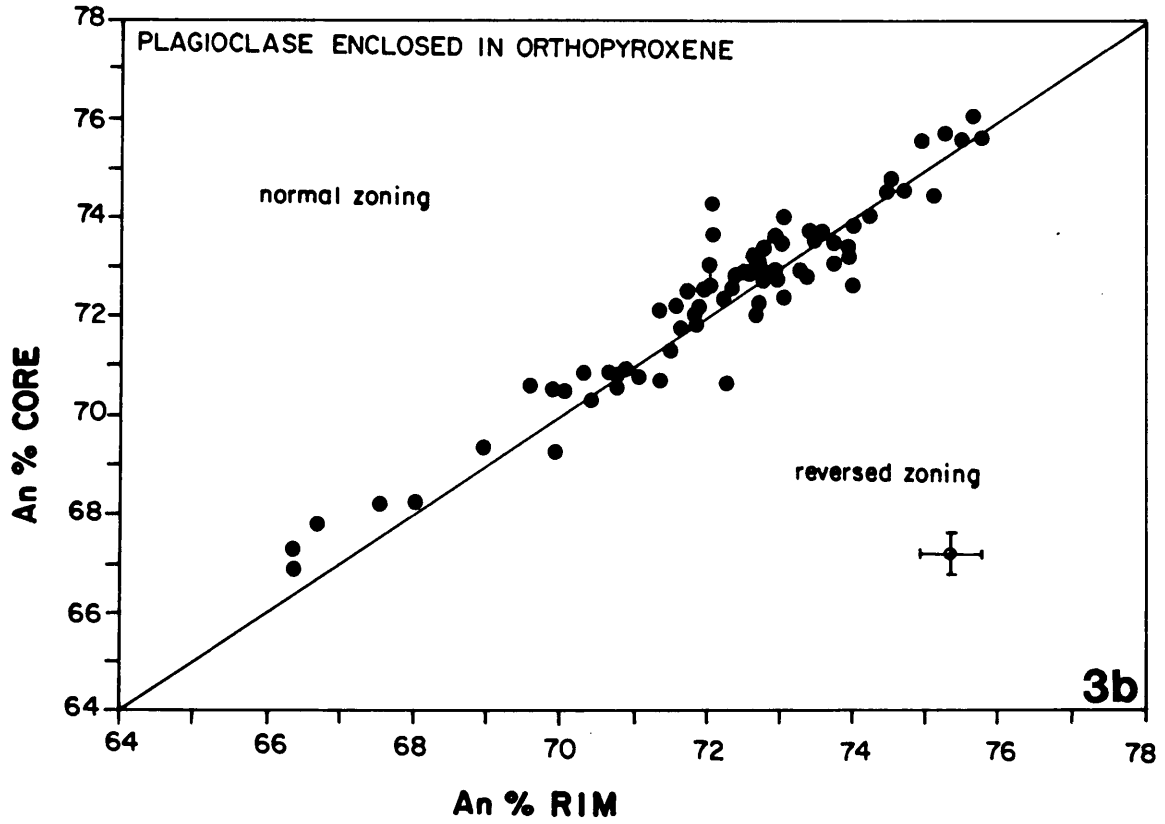

Figures VI.3a and 3b: Core composition of non-enclosed (3a) and enclosed (3b) plagioclase versus the particular rim composition. Each data point is the calculated average of 8-15 individual grains. Enclosed and non-enclosed plagioclase can be normal and reversed zoned. Reversed zoning is more common in non-enclosed plagioclase.

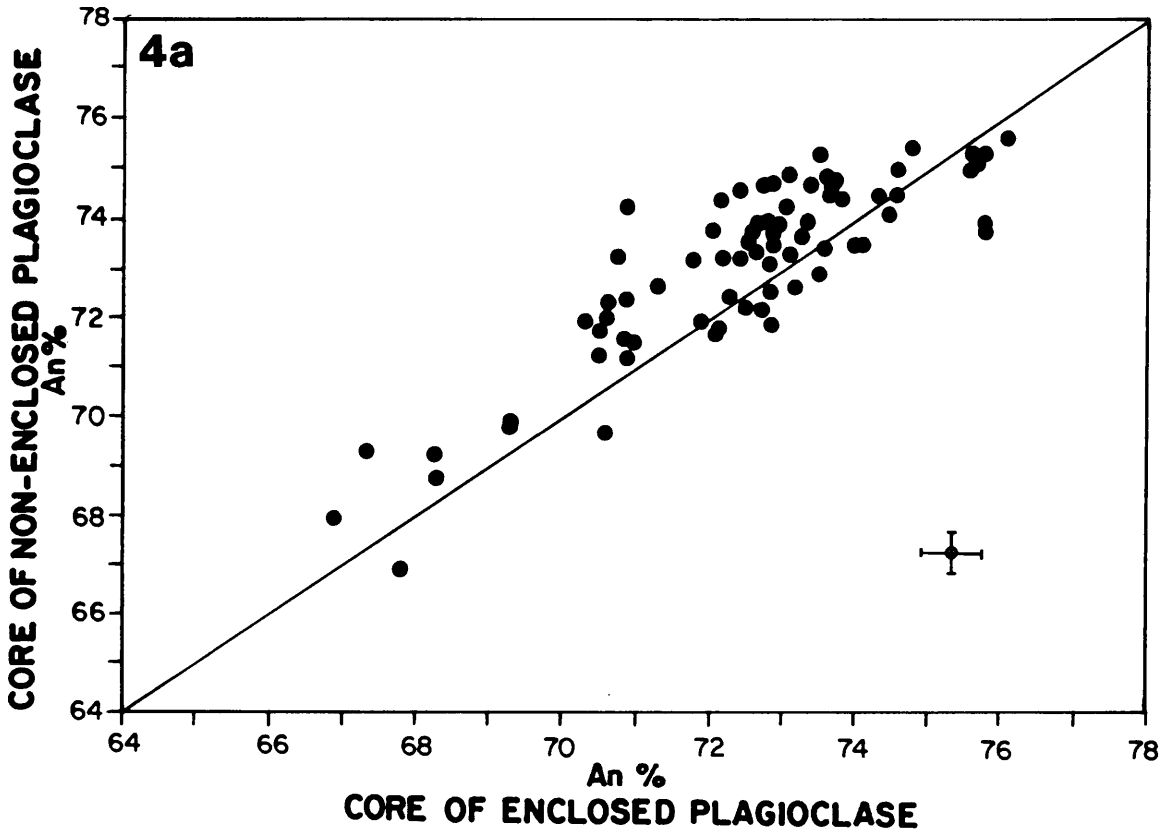

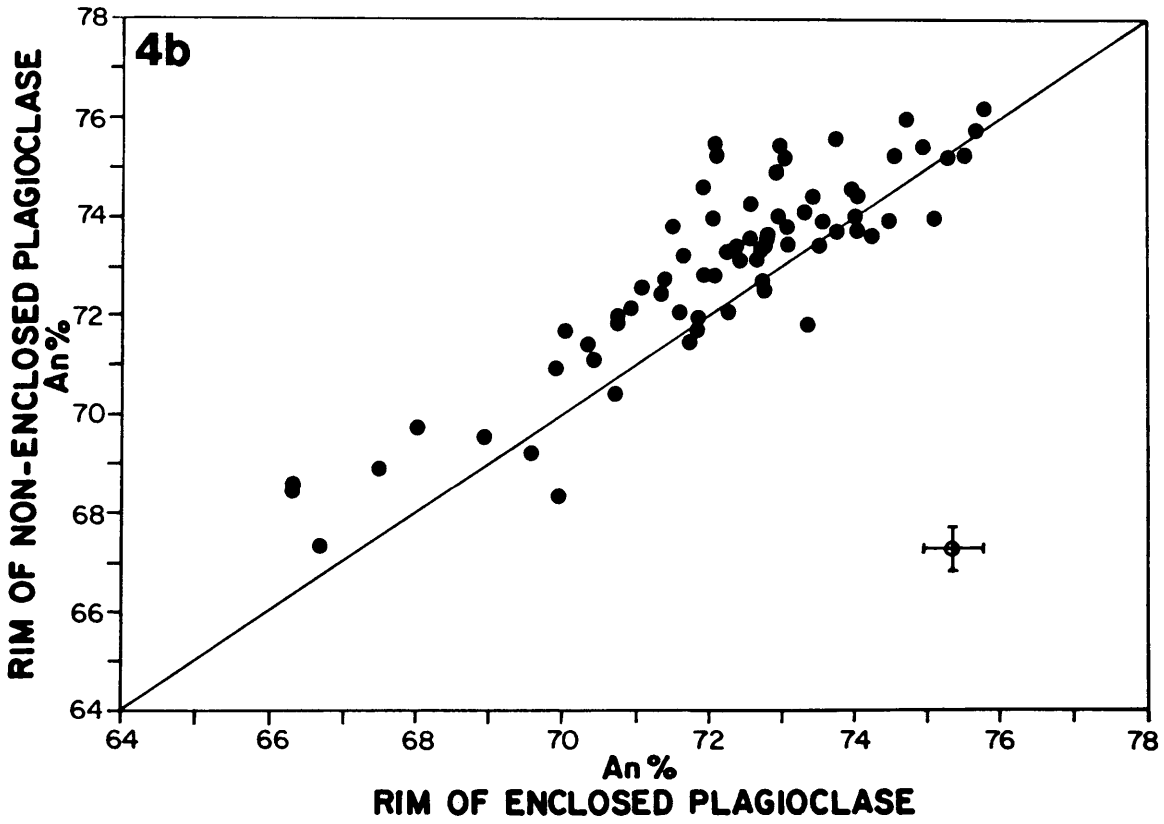

Figures VI.4a and 4b: Comparison of An content between cores (4a) and rims (4b) of non-enclosed and enclosed plagioclase. Each data point is the calculated average of 8-15 individual grains. Cores and rims of non-enclosed plagioclase appear to be more calcic than enclosed feldspar.

The evidence for plagioclase being a liquidus phase seems in conflict with the observed modal proportions of plagioclase and orthopyroxene in the F, G and J units. Experimental results (Sharpe and Irvine, 1983) have shown that only an almost pure B2 liquid (B1 < 10 %) has plagioclase on the liquidus. The eutectic ratio of such a liquid, however, cannot explain the melanorites of the F, G and J units which consist of more than 70 % pyroxenes. A hybrid liquid (B1/B2 mixture) on the other hand crystallizes mafic silicates before plagioclase begins to form.

One possible explanation for the early crystallization of plagioclase despite the large modal amount of pyroxenes is that at least some pyroxenes were added to the crystallizing system. Crystal settling or crystal/liquid slumping from a liquid layer some height above the crystallizing front could lead to hybridization of the bottom liquid. In response, plagioclase crystallization might temporarily cease while added pyroxenes undergo peritectic resorbtion. This process is consistent with the observed corrosional textures of some larger pyroxenes. The central parts of the latter are commonly free of small inclusions (Plate 4.E), although some grains contain plagioclase in embayments (Plate 4.D).

Similarly, Barnes and Naldrett (1986) have used the compositional discrepancy between enclosed plagioclase and non-enclosed "matrix" feldspar as evidence for mixing of magmas saturated in plagioclase and olivine respectively. In contrast to the case investigated here, however, both plagioclase types from the Stillwater Complex show a similar range of core compositions, while the rims of enclosed plagioclases were found to be on average more calcic than rims of outside plagioclase. Barnes and Naldrett attributed this feature to partial resorbtion and reaction of suspended plagioclase crystals. Subsequently the latter became enclosed and isolated from further reaction and melt fractionation.

Despite the different compositional behaviour of Bushveld and Stillwater plagioclases, the textural occurrence of enclosed feldspar in both cases appears to be closely related to the interaction of two physico-chemically distinct liquids. It is interesting to note that cumulus orthopyroxenes from the upper zone and from the middle portion of the main zone are devoid of plagioclase inclusions. However, more

detailed studies over larger stratigraphic portions will be necessary in order to evaluate the characteristic occurrence of feldspar inclusions as a potential indicator for magma mixing. Experimental work, whereby two chemically distinct melts are combined close to their respective liquidus temperatures, could also help to qualify various effects resulting from disequilibrium conditions.

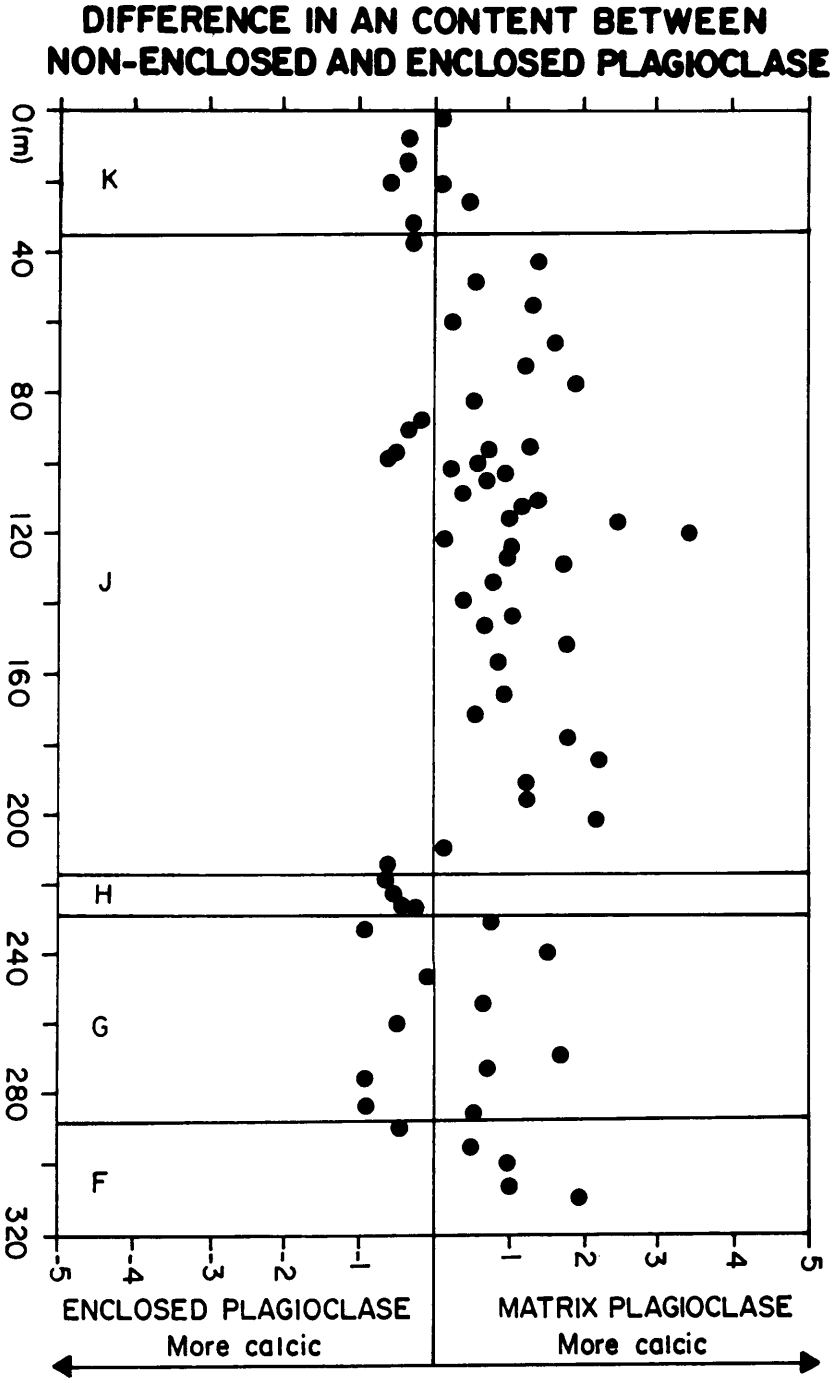

Figure VI.5: Difference in An content between cores of enclosed and non-enclosed plagioclase versus stratigraphic height. Each data point is the calculated average of 8-15 individual grains.

VI.2. ORTHOPYROXENE

Orthopyroxene is by far the most common pyroxene in the upper critical zone. Cumulus clinopyroxene first appears as an accessory mineral in a thin, lithologically distinct layer in the K unit (Chpt. II.4.5) and is subsequently present in varying amounts in the M unit (Folder 2). Cumulus clinopyroxene in the M unit exceeds the modal amount of orthopyroxene only in the very fine grained gabbronorite with an estimated maximum cpx:opx ratio of 2:1.

Clinopyroxene oikocrysts are present throughout the sequence investigated but their frequency decreases with stratigraphic height. Inverted pigeonite is the least common pyroxene and only occurs in a few lithologically distinct horizons in the K and M units. Orthopyroxene grains in the upper critical zone are commonly smaller (200 - 1500 um) than in the lower critical zone.

The orthopyroxene data presented in Folder 2 are averaged core and rim compositions. For each sample about 6 to 10 individual grains were analyzed in the centre and at the margin. The rim composition was determined at a minimum distance of about 20 um from the edge in contact with plagioclase.

VI.2.1. MG# OF ORTHOPYROXENE

Figure V.6 shows the change in orthopyroxene composition (Mg#) for the E to J interval for the three drillcores. Several features are noteworthy: Firstly, pyroxene from undisturbed (MDH 29 and MDH 1) upper critical zone rocks has a generally lower Mg# compared with lower critical zone pyroxene. Overall trends and absolute values within individual units are comparable between drillcores despite significant differences in thickness (the peculiar behaviour of MDH 23 is discussed in Chapter X.1).

Secondly, the lower/upper critical zone (E/F) boundary shows a systematic decrease in Mg# in both drillcores MDH 29 and MDH 1 which starts about 20 metres below the interface and continues to the top of the F unit.

Thirdly, the Mg# increases sharply across the F/G boundary but de-

creases subsequently towards the top of the G unit and into the H unit. The decrease in Mg# is, in both cases (E/F and G/H), accompanied by a general decrease in modal pyroxene. A tendency for a weak correlation between the modal amount and composition of pyroxene is found within and between individual units but not over the entire succession (Fig. VI.6). One can therefore assume that the observed differences in pyroxene composition between individual units (e.g. G and M) are primary features and not related to various mineral proportions, whereas compositional trends within individual units (e.g. F, G and H) which are correlatable with modal variations may reflect "secondary" features. The subliquidus shift in pyroxene composition according to various solid/liquid proportions was already addressed in Chapter V. It is proposed that individual units represent chemically distinct entities (liquid layers) which underwent similar internal processes. This is based entirely on the assumption that pyroxenes within an individual unit would have a constant composition given constant modal proportions.

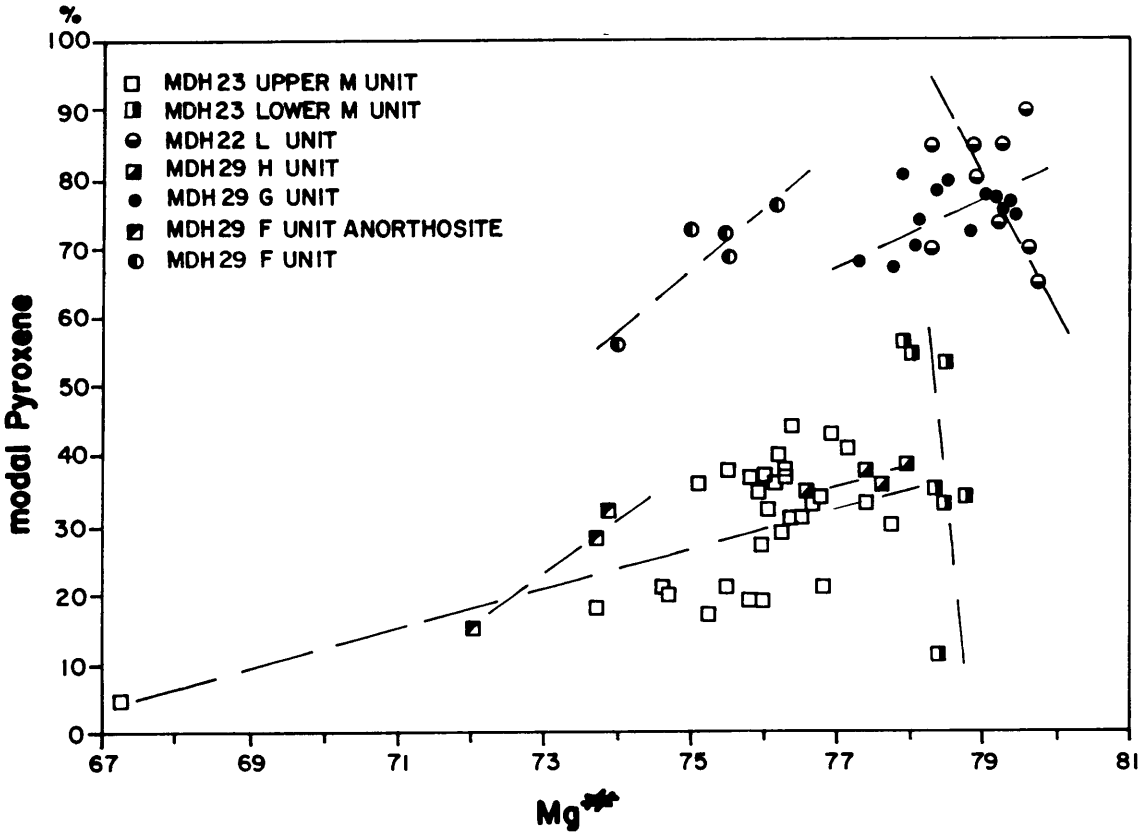

Figure VI.6: Modal amount of orthopyroxene versus Mg# of orthopyroxene for individual upper critical zone units. Pyroxene from F, G, H and upper M units shows a positive correlation between Mg# and modal amount, while pyroxene from the L and lower M units shows no or a slight antipathetic correlation.

Although melt fractionation within individual liquid layers can produce systematic changes in mineral chemistry, it must be questioned if fractional crystallization could lead to a systematic decrease in Mg# by more than 4 units (F unit) while the plagioclase composition remains almost constant. The An content in fact increases with stratigraphic height in the F unit.

The dependence of pyroxene composition (Mg#) on the modal amount is best illustrated in the upper M unit (Fig. VI.6) and in the lower portion of the J unit (Fig. VI.7a), where feldspar-rich layers invariably contain orthopyroxene with the lowest Mg#. In contrast, pyroxenes from the upper J - lower M interval (Fig. VI.6 and VI.7b) show no or even a negative correlation between Mg# and modal amount of pyroxene. The boundary between lower and upper J unit is taken at the stratigraphic level about two/third up the unit where the amount and the Mg# of pyroxene reach a relative maximum and subsequently decrease towards the top (Folder 2). Plagioclase, in contrast, shows a slight but systematic decrease in An content from the base to the top of the unit which is consistent with progressive melt fractionation.

The negative correlation between Mg# and the amount of pyroxene in the upper J and K units indicates that pyroxene composition is, unlike in other units, not a function of the modal proportions. A possible explanation for this discrepancy is that these orthopyroxenes are not preserved in their original chemical environment. This possibility is consistent with the macro-structural features such as fragmented layers, slumping structures (see Chap. II.4.4), which are unique to the upper J and K units. A mechanical re-working of partially consolidated material, which had already internaly re-equilibrated, seems a plausible mechanism to explain the unusual decoupling of pyroxene composition from their immediate surrounding mineralogy. The apparently antipathetic trend might be coincidental and simply due to an overlap of the normal trend and compositional features produced by a random re-arrangement of modal proportions. This seems to be confirmed by the observed fluctuations in modal proportions, and by the scatter in pyroxene composition (Mg#) which show no systematic trend throughout the upper J and K units. However, more closely-spaced sampling of this extremely heterogeneous portion would be necessary to evaluate the above mentioned features in more detail.

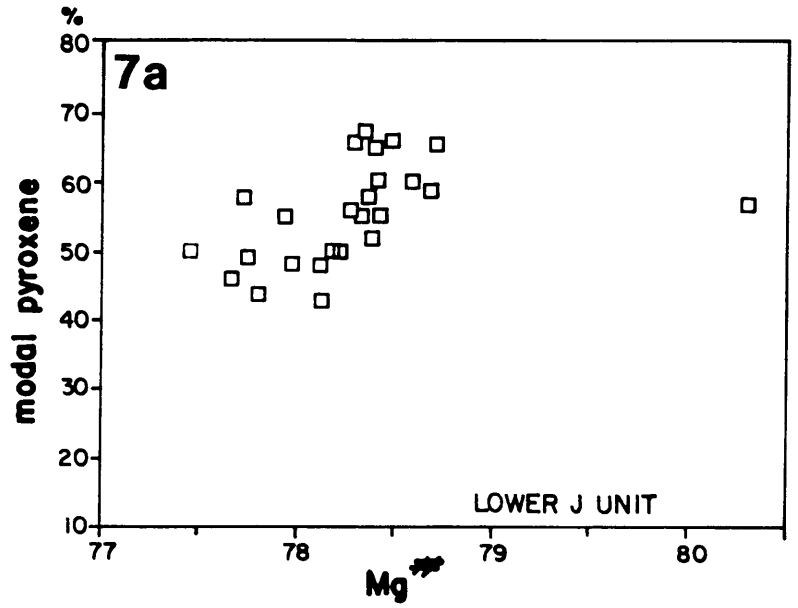

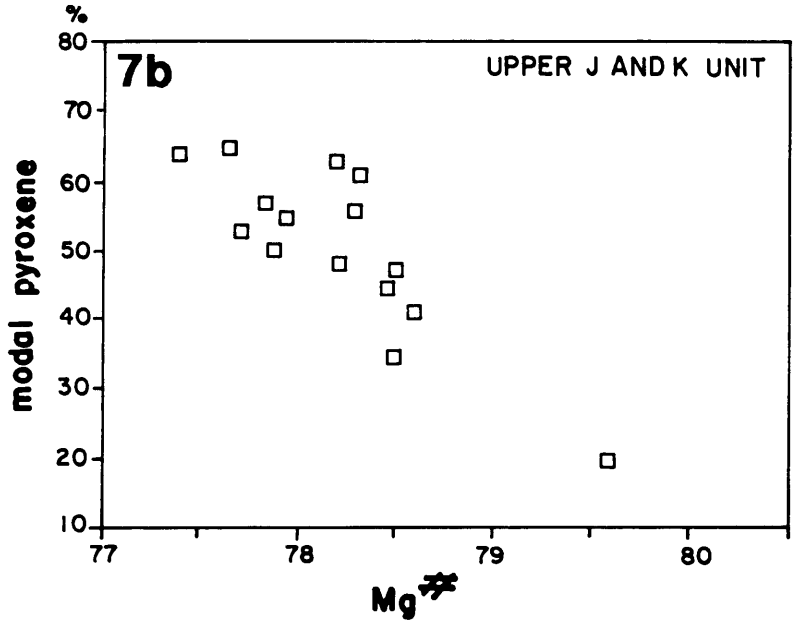

Figures VI.7a and 7b: Modal amount of orthopyroxene versus Mg# of orthopyroxene of the lower J unit (7a) and upper J and K units (7b). Pyroxene from the lower J unit shows a positive correlation between Mg# and modal amount, upper J and K unit pyroxenes display an antipathetic correlation.

The clinopyroxene-free, lower part of the M unit shows no evidence for physical disturbance. Pyroxenes display a systematic decrease in Mg# despite a considerable variation in modal proportions (Folder 2 and Fig. VI.6). The observed trend in Mg# records a transition from the underlying L unit to the upper M unit. It should be mentioned that the lower M unit is quite distinct, as it is, on bulk, more mafic than the remainder of the unit and that pyroxene has a higher Mg# (> 78) compared to pyroxene from the rest of the unit.
Pyroxene throughout the L unit (MDH 22, Fig. X.1) shows a narrow range in Mg# (78-80) but a significant variation in the modal amount (65-90 %). Values higher than 80 invariably occur in chromite-rich samples of the L unit and are explained by subliquidus Mg-Fe exchange between pyroxene and chromite.

VI.2.2. CHROMIUM IN ORTHOPYROXENE

The chrome content of pyroxene cores follows the trend shown by the Mg# fairly closely (Folder 2). The sympathetic behaviour of Cr and Mg# is well documented in the F, G, H and M units where all major variations in Mg# are mirrored by a corresponding change in Cr content. Figure VI.8 shows this relationship for the individual units.
It is of particular interest that pyroxenes from the upper M unit form a distinctive group which is relatively depleted in Cr compared to the underlying units. Pyroxenes from the lower part of the M unit appear to have a transitional composition. The general trend of decreasing Cr with a decrease in Mg# is however unchanged. It can therefore be assumed that pyroxenes from the upper M unit crystallized from a liquid which was relatively depleted in Cr. Within-unit variation in the Cr content of pyroxene is attributed to small-scale fluctuations in the initial crystal/liquid proportions, analogous to the change in Mg#. Melt fractionation is not a viable process to cause small-scale variations in the Cr content, because it could not explain nearly constant plagioclase composition. The relatively small stratigraphic distance over which the Cr content decreases in the M unit seems to indicate a mixing interface with a Cr-poor liquid rather than melt fractionation.

Rims of pyroxenes are invariably depleted in Cr relative to the grain centres. The decrease in Cr is generally small (< 0.05 wt % Cr_2O_3) compared to the extent of zoning in most pyroxenes from the lower critical zone. This feature is readily explained by the almost complete absence of phases which would indicate trapping and fractionation of interstitial melt. Except for the F, lower G and L units, rocks of the upper critical zone are proper adcumulates.

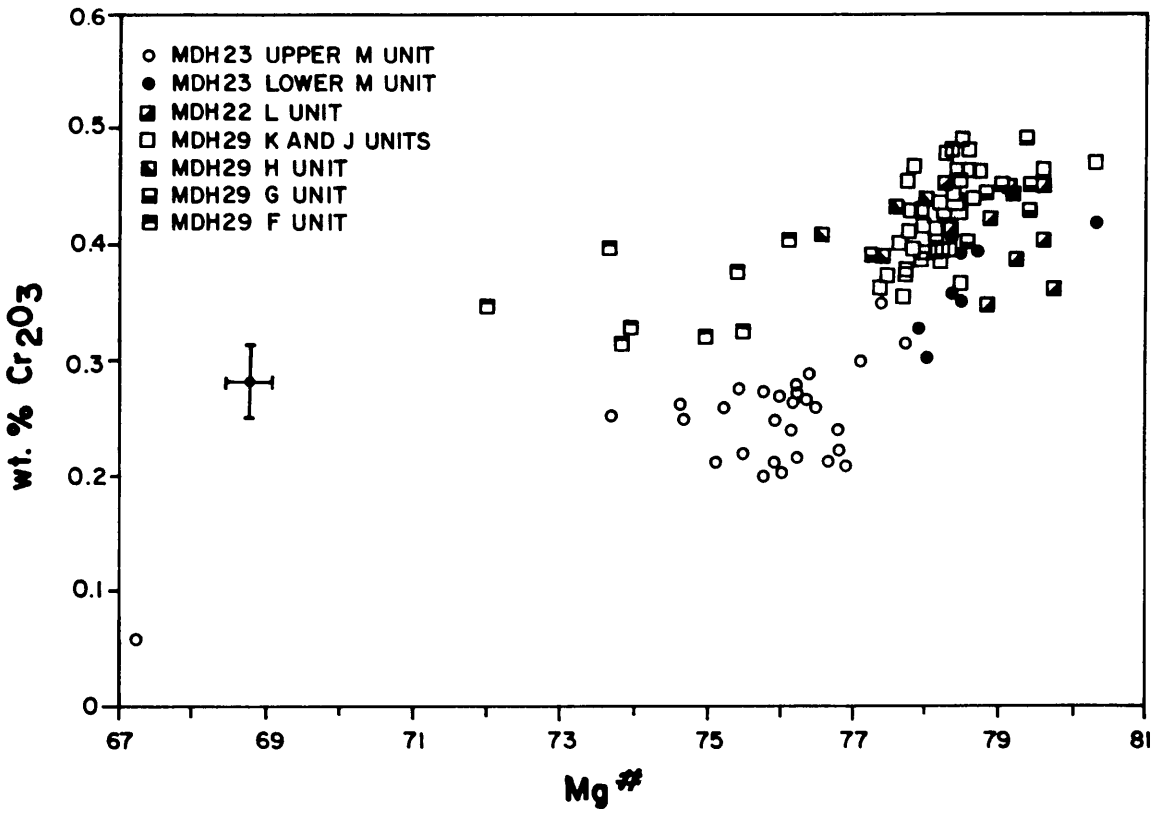

Figure VI.8: Cr abundance versus Mg# of orthopyroxene from the upper critical zone. Orthopyroxene from the upper M unit is depleted in Cr relative to orthopyroxene from the F - L interval. Pyroxene from both intervals (upper M and F - L) shows a positive correlation between Cr content and Mg#. Each data point is the calculated average composition of 8-15 individual grains.

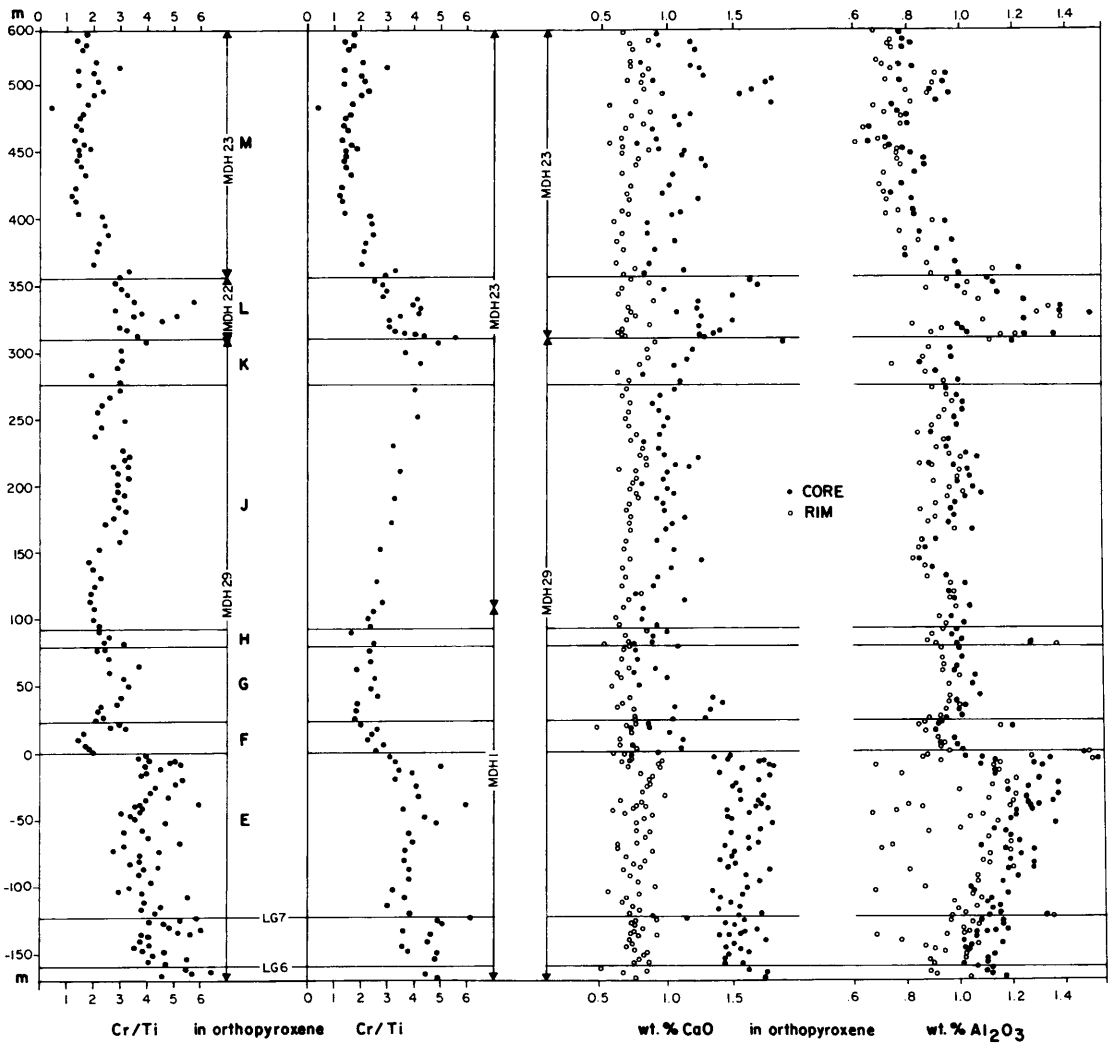

Figure VI.9: Compositional variation of orthopyroxene within the investigated interval. Cr/Ti ratios are presented for two composite sequences. Data from the M unit (MDH 23) are incorporated in both sequences in order to have continuous sections. Cr/Ti data within the first column are plotted at their real stratigraphic positions (as in Folder 2), while data of the second column (MDH 1 and 23) up to the base of the M unit were stretched to facilitate optical comparison. Each data point is the calculated average composition of 8-15 individual grains.

VI.2.3. ALUMINIUM IN ORTHOPYROXENE

The Al concentrations decrease markedly across the E/F boundary and subsequently stay low (< 1.1 wt % Al_2O_3) except for the L unit (Fig. VI.9). The lowest values are found in the upper M unit.

Figure VI.10 shows the systematic co-variation between Al and Cr and also defines two distinct compositional fields. The upper field with lower Al/Cr ratios (+- 2.4) covers the stratigraphic units F to L, while higher ratios (+- 3.3) dominate in the upper M unit. Pyroxenes from the lower M unit have ratios intermediate to the two groups. Data from chromite-rich samples (F and H units) were excluded as the Al/Cr ratio is expected to have changed during subliquidus re-equilibration with chromite (Chpt. V.4). The marked increase in Al in chromite-rich samples from the E, F and H units is depicted in Figure VI.9. Rims of pyroxenes in chromite-rich samples are commonly even more enriched in Al than cores.

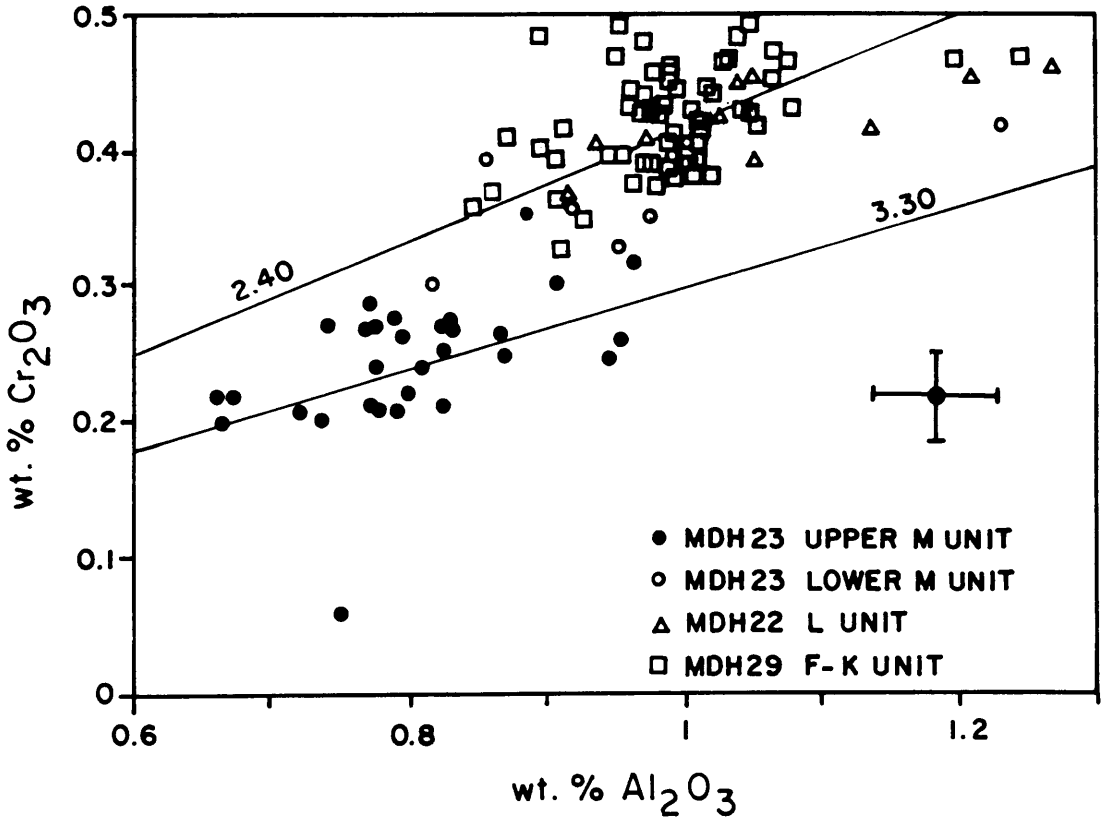

Figure VI.10: Cr abundance versus Al content in orthopyroxene from various units of the upper critical zone. Orthoyroxene from the F - L interval has a lower Al/Cr ratio than orthopyroxene from the upper M unit.

Pyroxenes from the upper M unit have generally lower Al and Cr concentrations compared to the underlying units. The simultaneous increase in the Al/Cr ratio is caused by the fact that pyroxenes are relatively more depleted in Cr than in Al.

Rims of pyroxene have generally slighly lower Al concentrations (Fig. VI.11). The degree of Al depletion is, similar to Cr, much less pronounced compared to pyroxenes from the lower critical zone.

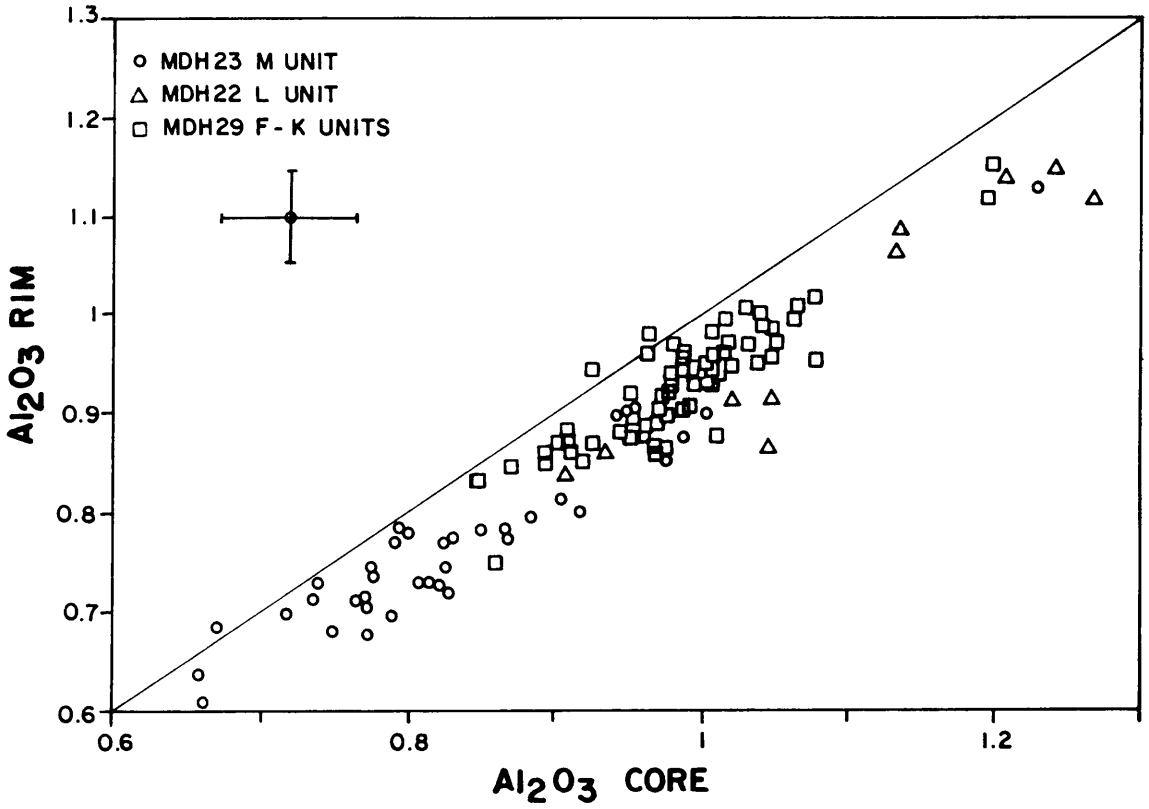

Figure VI.11: Al abundance of orthopyroxene cores versus rims. Orthopyroxene rims are generally depleted in Al independent of their stratigraphic position.

VI.2.4. TITANIUM IN ORTHOPYROXENE

The Ti content of pyroxene cores increases markedly across the lower - upper critical zone boundary. While lower critical zone pyroxenes contain between 0.05 and 0.15 wt % TiO_2, pyroxenes from the upper critical zone have, except for the L unit, generally between 0.15 and 0.20 wt % TiO_2 (Folder 2).

The relatively high Ti concentrations are also expressed by the presence of numerous orientated rutile needles. The absence of the latter in the outermost margins (30 - 50 um) is consistent with the lower Ti concentrations of rim analyses (Folder 2). It should be emphasized that the analyzed Ti concentrations reflect the pyroxene host composition, as indicated by the generally uniform Ti values within individual samples. Unusually high TiO_2 concentrations (> 0.5 wt %) as a result of rutile needles were sporadically encountered and were not included in the calculated average pyroxene compositions.

The change from low to high Ti pyroxenes at the E/F boundary is coupled with a marked decrease in the Cr/Ti ratio. This feature is depicted in Figure VI.9 for two different composite profiles. Both sections show relatively low ratios from the base of the F unit up into the lower portion of the J unit. Cr/Ti ratios then increase through the remainder of the J unit and reach a relative maximum in the pyroxene-rich L unit. A slight reversal is found near the top of the J unit. Intermediate values dominate in the lower M unit while very low values are present in the upper M unit. The overall trend shown by the Cr/Ti ratio can be broadly correlated with the change in the modal proportions (Folder 2). An increase in the Cr/Ti ratio coupled to an increase in modal orthopyroxene is particularly well displayed within the J and M units. Similarly, the highest overall ratios are found in the orthopyroxene-rich L unit, while minimum values characterize the leucocratic upper M unit.

The observed change in the Cr/Ti ratio with stratigraphic height appears to be controlled by the antipathetic behaviour of Cr and Ti. However, a broadly antipathetic relationship for the partition of the two elements into orthopyroxene is only indicated for the F - L interval (Fig. VI.12). Pyroxenes from the upper M unit show a vague sympathetic correlation for Cr and Ti, while pyroxenes from the lower M

unit are transitional (Fig. VI.12).

To the authors knowledge there are no published data on Ti concentrations in orthopyroxene covering the portion of the critical zone investigated here. However, pyroxene data from the Merensky and the Bastard cyclic units (Kruger, 1982) and from the lower layered series of the Jimberlana Intrusion (Campbell and Borley, 1974) show a similar, overall antipathetic behaviour for Cr and Ti. The peculiar behaviour of pyroxenes from the upper M unit is probably best explained by the assumption that these pyroxenes crystallized from a comparatively Cr-poor liquid which was added to the magma chamber. The transitional Cr and Ti concentrations of lower M unit pyroxenes could then record an interaction between fresh liquid and resident liquid.

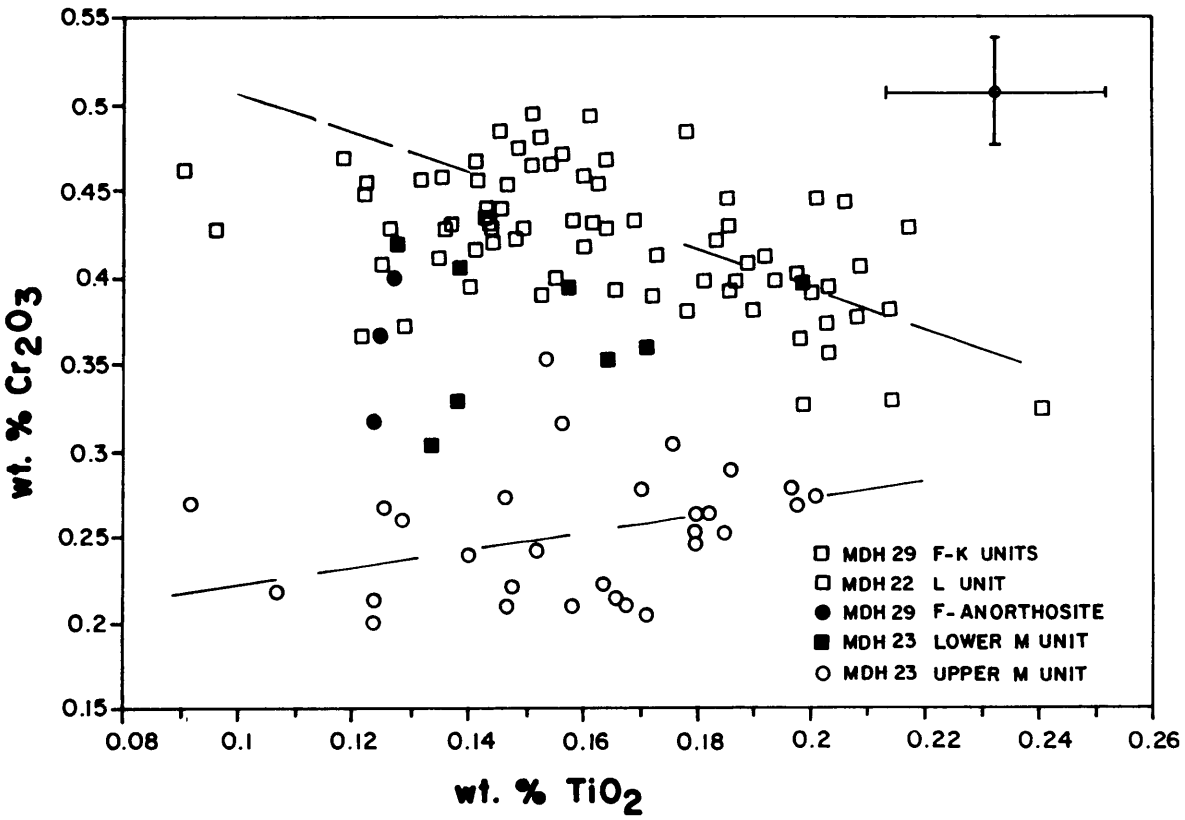

Figure VI.12: Cr abundance versus Ti content in orthopyroxene from various units of the upper critical zone. Orthopyroxene from the F - L interval shows an antipathetic relationship for Cr and Ti, while orthopyroxene from the upper M unit shows a slight positive correlation.

The drastic increase in Ti at the E/F boundary would suggest that upper critical zone orthopyroxenes either crystallized from, or re-equilibrated with a relatively Ti-rich liquid. Considering the generally low plagioclase content in the basal part of the upper critical zone (lower F and G units), it seems unlikely that crystallization of plagioclase caused a relative Ti increase in the melt prior to pyroxene formation, assuming that the crystallizing system remained chemically closed. The lower Al concentrations in upper critical zone pyroxene should rather reduce the entry of three or more valent cations (Cr and Ti), as their entry into octahedral sites relies on the charge-deficiency caused by substitution of Al into tetrahedral sites (Campbell and Borley, 1974). Cr concentrations on the other hand do not significantly decrease across the E/F boundary and are up to the M unit comparable to the lower critical zone.

The fact that rims of most pyroxenes are relatively depleted in Ti also indicates that the high Ti concentrations in the core are not due to subliquidus re-equilibration with evolved (Ti- enriched) liquid. Such a process has been proposed for lower critical zone pyroxenes to explain their Ti-enriched rims. Furthermore, the degree of interstitial melt fractionation in upper critical zone samples appears to be limited compared to most lower critical zone samples.

It is therefore concluded that the increase in Ti at the E/F boundary is a primary magmatic feature and that upper critical zone pyroxenes crystallized from a liquid which was comparatively Ti-rich.

VI.2.5. CALCIUM IN ORTHOPYROXENE

Ca, similar to Al, decreases markedly across the E/F contact. Lower critical zone pyroxenes contain on average about 1.6 wt % CaO, while pyroxenes from the upper critical zone have about 1.0 wt % CaO. Average values higher than 1.3 % are found in the lower G unit, in the L unit and near the top of the M unit (Fig. VI.9). The texture of those pyroxenes resembles that of lower critical zone pyroxenes which are characterized by their relative large size, by abundant clinopyroxene exsolution lamellae and the lack of feldspar inclusions. A further distinguishing feature of at least the lower G and L units is

that both are comparatively orthopyroxene-rich.

The generally low Ca concentrations in the upper critical zone can be explained by several processes. Ca depletion could either reflect a lower crystallization temperature, or that pyroxenes were able to exsolve a substantial amount of their augite component. Ca exsolution is indicated by numerous tiny patches of clinopyroxene commonly associated with enclosed plagioclase.

A considerable Ca depletion in the liquid due to early plagioclase crystallization is not likely considering the fact that the basal units of the upper critical zone are generally plagioclase-poor.

Subliquidus re-equilibration with surrounding liquid could also reduce an originally higher Ca content in pyroxene. The generally smaller grain size of upper critical zone orthopyroxenes suggests that, in contrast to the lower critical zone, even the central areas of grains became Ca depleted. The fact that grain margins are invariably depleted would favour a diffusion controlled post-cumulus depletion in Ca. The broadly positive correlation of the Ca content between cores and rims can also be explained in this way. However, due to the relative low diffusion rate of Ca in orthopyroxene at subliquidus temperatures (Chpt. III.5.3.1), no conclusive evidence for a change in magma composition or temperature can be drawn from the drop in the Ca content in orthopyroxene at the E/F boundary.

VI.3. CONCLUSIONS

Orthopyroxene shows a pronounced change in composition, texture and size across the E/F boundary. With the exception of the L unit, where pyroxenes show remarkable textural and chemical similarities with those from the lower critical zone, orthopyroxene from the upper critical zone appears to have formed under drastically changed conditions and from a chemically distinct melt. The latter is evidenced by a drop in the Mg#, Ca and Al and by an increase in Ti. Certain elements or element ratios show systematic trends in the upper critical zone which can frequently be related to simultaneous changes in modal proportions. Melt fractionation appears to be relatively unimportant in producing the observed mineral chemical variations. The overall compositional change in orthopyroxene from the lower J unit is in conflict with a liquid fractionation process and indicates a reversal towards a more primitive melt composition which seems to have produced the overlying pyroxenite- and chromite-rich L unit.
The indicated dependence of orthopyroxene composition on modal concentrations makes it difficult to define primary compositional differences between individual units. This is particularly problematic in the lower portion (F - H units) which shows abrupt lithological breaks followed by systematic and mostly gradual modal variations within individual units. On the other hand, certain distinct compositional changes of orthopyroxene with stratigraphic height cannot be explained by a simultaneous change in modal proportions. Orthopyroxenes from the upper M unit in particular form a chemically distinct group and presumably crystallized from an intermittent influx of a relatively Cr-poor liquid.

Plagioclase chemistry seems to be almost completely decoupled from pyroxene variation. The An content increases in the F, G and H units with stratigraphic height, while the Mg# of coexisting orthopyroxene decreases. In contrast, Mg# increases in the J unit whereas An decreases upwards. Plagioclase in the upper M unit has a relatively constant composition with a slight decline in An in samples containing inverted pigeonite. The Mg#, on the other hand, decreases markedly at three plagioclase-rich horizons and shows in general an antipathetic

correlation with the amount of plagioclase. The only stratigraphic portion where An and Mg# decrease simultaneously with stratigraphic height is the lower M unit. This unit possibly records the interaction of resident and newly emplaced liquid.

The overall variation in cumulus plagioclase above the F and G units in the upper critical zone is about 5 mol % An (70 - 75) with no systematic decrease over the entire investigated sequence. The range in Mg# of the orthopyroxene over the same stratigraphic interval is about 6 units (74 - 80; chromite-rich samples and intercumulus pyroxene excluded). Mg# shows no systematic decrease with stratigraphic height, but a sudden drop within the M unit. The studied portion of the upper critical zone is therefore not a progressive fractionation series. The observed decrease in An content within lithological units or parts of units (lower J and lower M units) indicates slight within-unit fractional crystallization. The latter can be seen as evidence for the former presence of liquid layers.

The presence of late-magmatic aqueous fluids is preserved in reversely zoned plagioclase rims which show a characteristic myrmekitic texture. These textural and chemical features first occur in the upper J and K units and persist throughout the M unit.

A comparison of plagioclase inclusions in orthopyroxene and non-enclosed plagioclase revealed that the latter are on average more calcic. This feature is attributed to the quasi-episodic nucleation of plagioclase which must have temporarily predated orthopyroxene crystallization. Tiny plagioclase inclusions in orthopyroxene occur almost throughout the upper critical zone. It is suggested that this characteristic feature is related to magma mixing or crystallization from a hybrid melt.

CHAPTER VII: WHOLE ROCK CHEMISTRY

VII.1. SAMPLING

A total of 223 whole rock analyses were carried out from drillcores MDH 29 (D_2-K units) and MDH 23 (L-M) using X-ray fluorescence analysis on pressed powder pellets. About 6 cm lengths of halved drillcore (+- 250 g) from the same samples from which thin sections were cut, were used for analysis. Sulphur concentrations were analyzed by infrared absorbtion spectroscopy. Reproducibilities and detection limits are presented in the Appendix.

VII.2. TRACE ELEMENT ABUNDANCE - INDICATIONS FOR PARENTAL MAGMA COMPOSITION

The dominant control on whole rock abundances of compatible trace elements (e.g. Cr, Ni, Sr) is the nature and proportion of the cumulus phases. Incompatible element (e.g. Zr, Y, Rb) abundance is indicative of trapped intercumulus liquid. This is best shown in the orthocumulates of the lower critical zone (E unit). Samples with strongly evolved intercumulus phases have high Zr (up to 68 ppm), Y (up to 12 ppm) and Rb (up to 30 ppm) concentrations, compared to typical background values of about 6 ppm Zr, 4 ppm Y and 1 ppm Rb in samples from e.g. the E unit with the least evolved intercumulus assemblage. The Zr/Y ratio increases from about 1 in "normal" samples to about 6 in samples with strongly evolved phases (Fig. VII.1). A ratio of 6 is comparable with the Zr/Y ratio of the B1 liquid (80 - 100 ppm Zr and 16 ppm Y; Sharpe, 1985). Using the mineral-liquid distribution coefficients given by Pearce and Norry (1979) the Zr/Y ratio for adcumulates derived from a B1 liquid can be calculated to be about 1. This ratio will stay almost constant during progressive fractionation provided orthopyroxene and subsequently orthopyroxene and plagioclase are the principal crystallizing minerals.

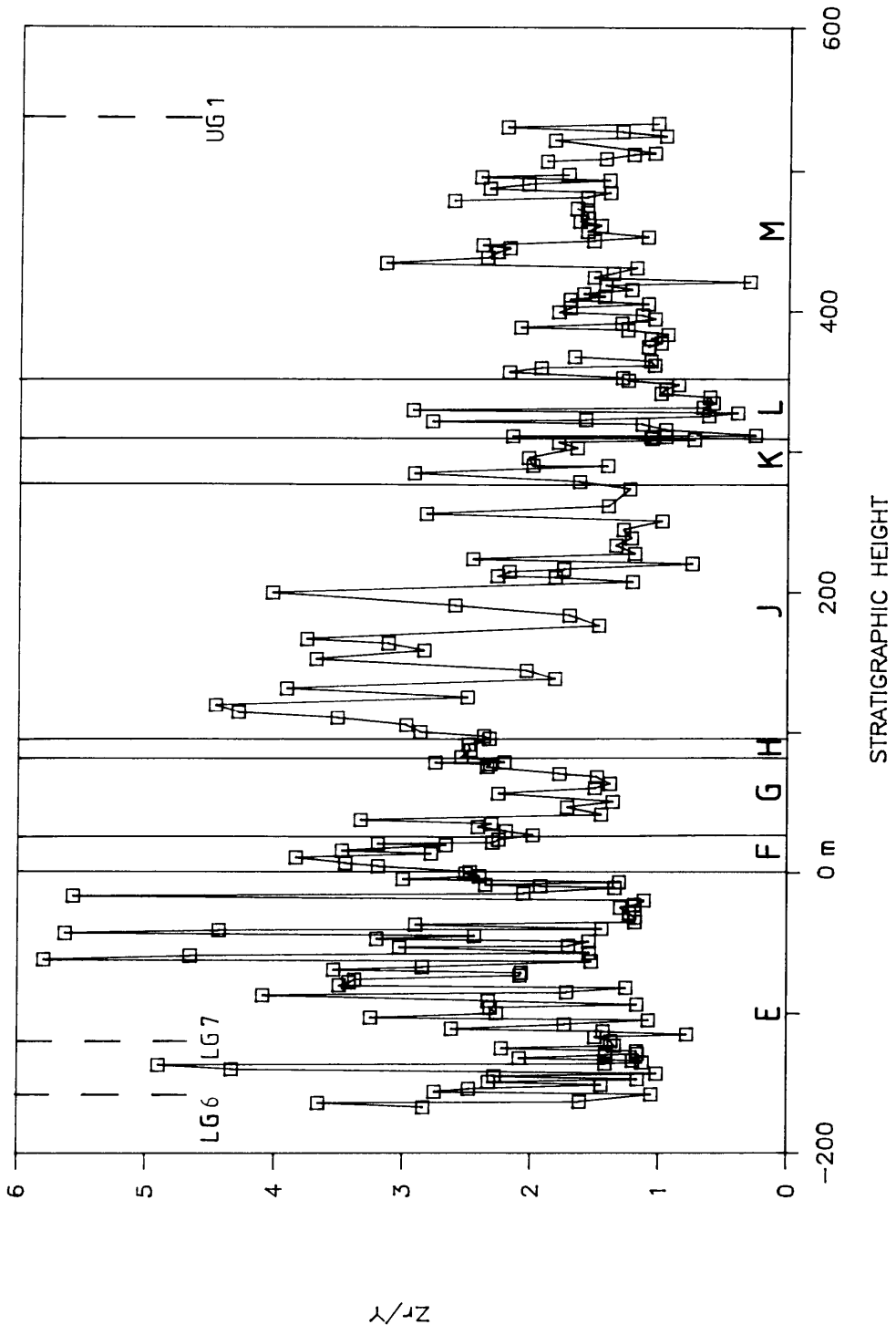

Figure VII.1: Whole rock Zr/Y ratio versus stratigraphic height. Samples with a low abundance (adcumulates) of fractionated interstitial phases (mainly phlogopite) have invariably low ratios (1 - 2). Zr/Y ratio of up to 6 occur in samples with a high proportion of evolved intercumulus minerals (orthocumulates).

An increase in the Zr/Y ratio to values above the ratio of proper adcumulates (+- 1), can be accomplished by trapping and fractionation of interstitial liquid, as the trapped B1 liquid has a Zr/Y ratio of about 6. The observed range in the Zr/Y ratio in the lower critical zone is attributed to various amounts of fractionated trapped liquid. Samples with high whole rock Zr and Y concentrations have commonly increased Zr/Y ratios and are characterized by the presence of phlogopite, loveringite, zircon (baddeleyite ?) and apatite. Whole rock Zr/Y ratio will slightly increase with the amount of phlogopite, as the latter is the only common silicate phase for which the distribution coefficient for Zr (+- 0.6) is higher than for Y (+- 0.03; Pearce and Norry, 1979). Phlogopite, however, cannot explain the high Zr concentrations (up to 68 ppm). High Zr values are due to the presence of loveringite (up to 500 um, Plate 2.H) and tiny grains (< 5 um) of zircon which have been identified in several samples.
A positive correlation between Rb and Zr is shown in Figure VII.2. Phlogopite is far more abundant than K-feldspar and one can assume that the analyzed Rb concentrations are mainly hosted by phlogopite. The presence of phlogopite can therefore be seen as evidence for trapped liquid, whereby the amount of phlogopite is proportional to the amount of trapped liquid. It is of significance that low Zr concentrations (< 5 ppm) are found in samples which contain no, or only traces of phlogopite, e.g. the middle portion of the G unit, the upper J unit, as well as the K, L and M units.

B1 and B2/B3 parental liquids differ substantially in their trace element abundances (see Harmer and Sharpe, 1985). Whole rock incompatible element concentrations (e.g. Ti, K, Rb, Zr and Y) should therefore provide a good indication from which liquid a particular lithological unit crystallized. A pre-requisite for this is that a sufficiently large amount of parental liquid became physically trapped. True adcumulates, like most rocks of the upper critical zone, are characterized by the almost complete absence of non-cumulus materials and provide, apart from trace element concentrations in cumulus minerals, little geochemical evidence about their liquid parentage.

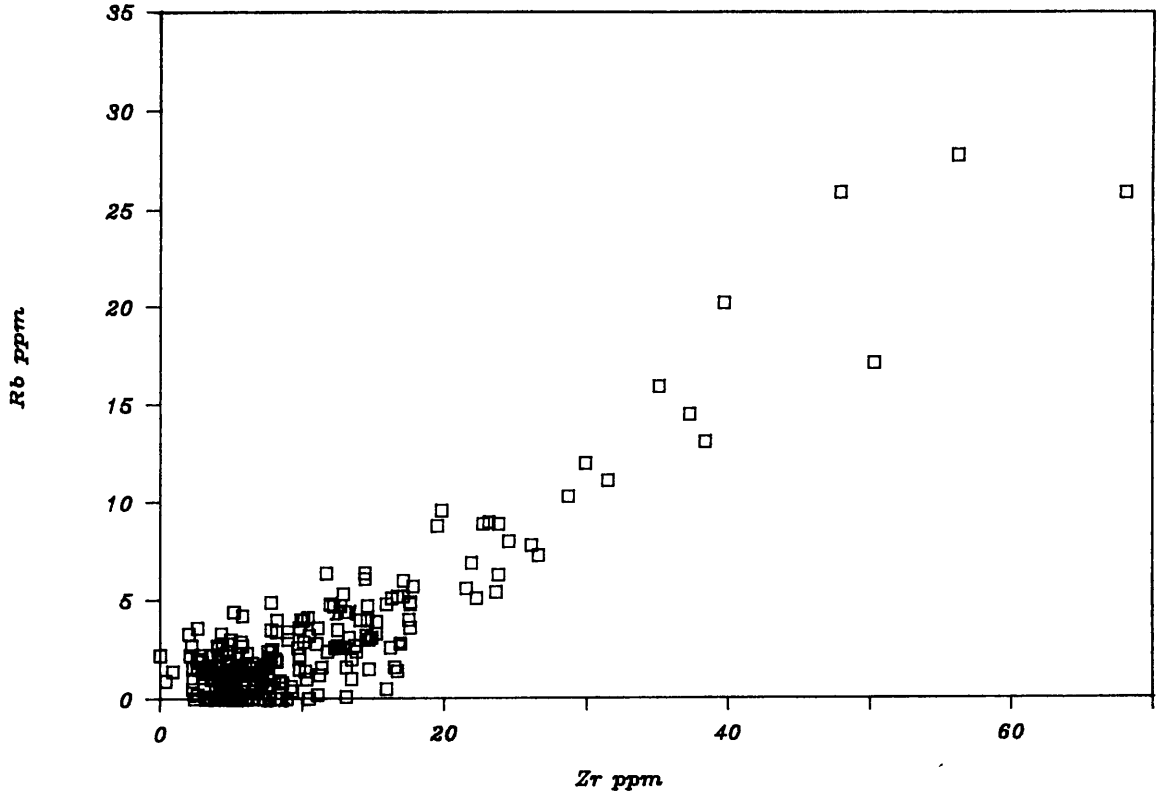

Figure VII.2: Plot of Rb versus Zr of whole-rock analyses from the investigated LG 6 - UG 1 sequence.

Figures VII.3a to VII.3g show the inter-relationship between various incompatible element concentrations from the E, F and G units. The respective concentrations for the proposed parental liquids (B1, B2 and B3) are shown in each diagram. Parental liquid concentrations represent the calculated averages of three analyses (CD-01, CO-017, CO-114) for B1, five analyses (CO-019, CO-066, CO-250, CO-252, CO-253) for B2 and four analyses (CO-045, CO-048, CO-052, CO-251) for B3 (data from Harmer and Sharpe, 1985). While all B2 and B3 analyses published by Harmer and Sharpe were averaged, only K- and Rb-rich analyses were chosen for the B1 composition to ensure a maximum range in incompatible element concentrations. The averaged concentrations for the E, F (excluding the anorthosite) and G units are plotted as well.

Figures VII.3a - 3b: Variation diagrams of incompatible element concentrations for cumulates of the E-G interval. Average compositions for the three units (E-G) are specially marked. The compositional field of cumulates is defined by the parental liquid compositions (after Harmer and Sharpe, 1985) and the hypothetical composition of a pure adcumulate (orthopyroxene or orthopyroxene and plagioclase). The grid within the compositional field shows liquid compositions (25 and 50 % B1 component) of possible B1/B2 hybrids and proportions (30, 50 and 70 %) of trapped liquid.

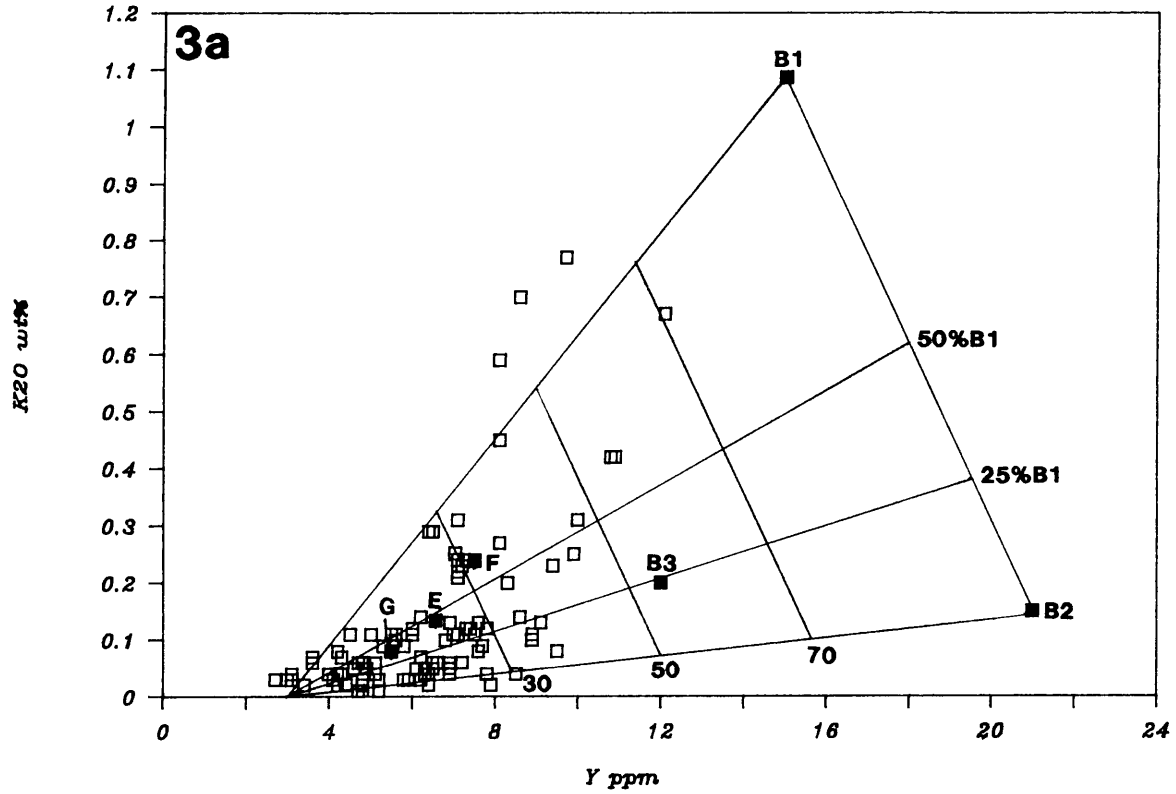

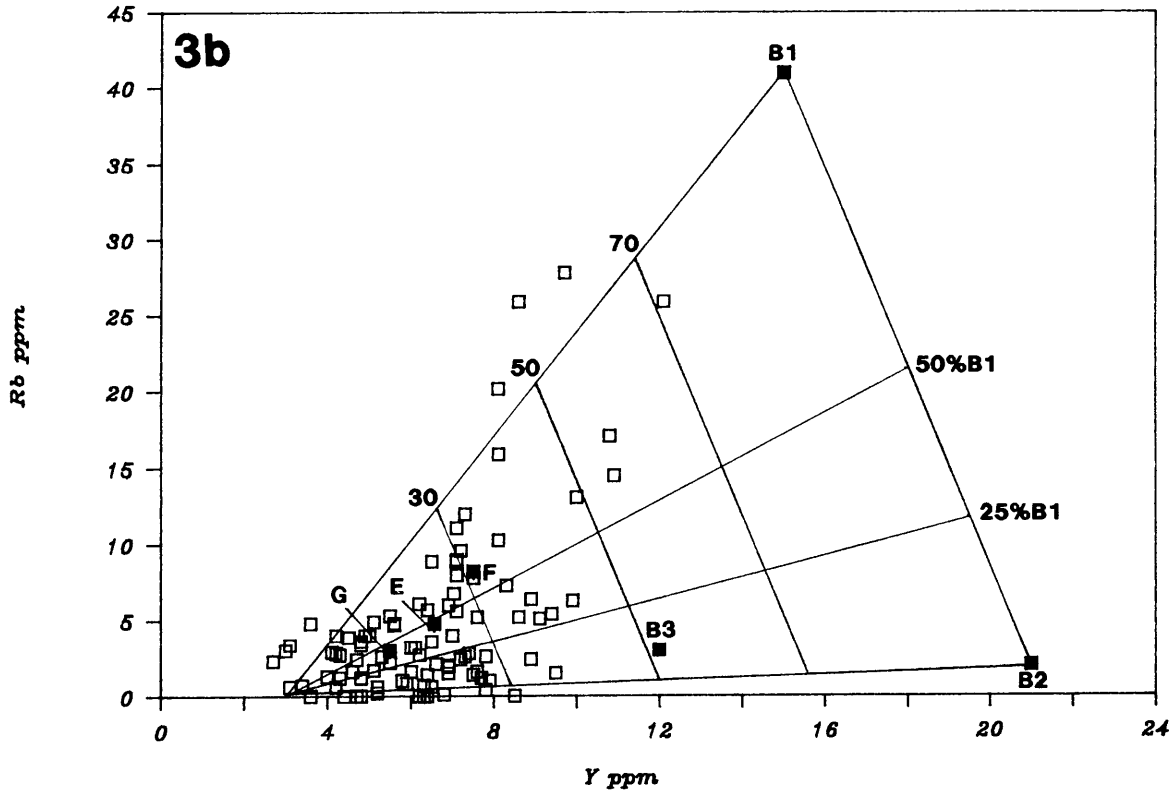

Figures VII.3c - 3d: Variation diagrams of incompatible element concentrations for the cumulates of the E-G interval. For further explanations see Figure VII.3a - 3b and text.

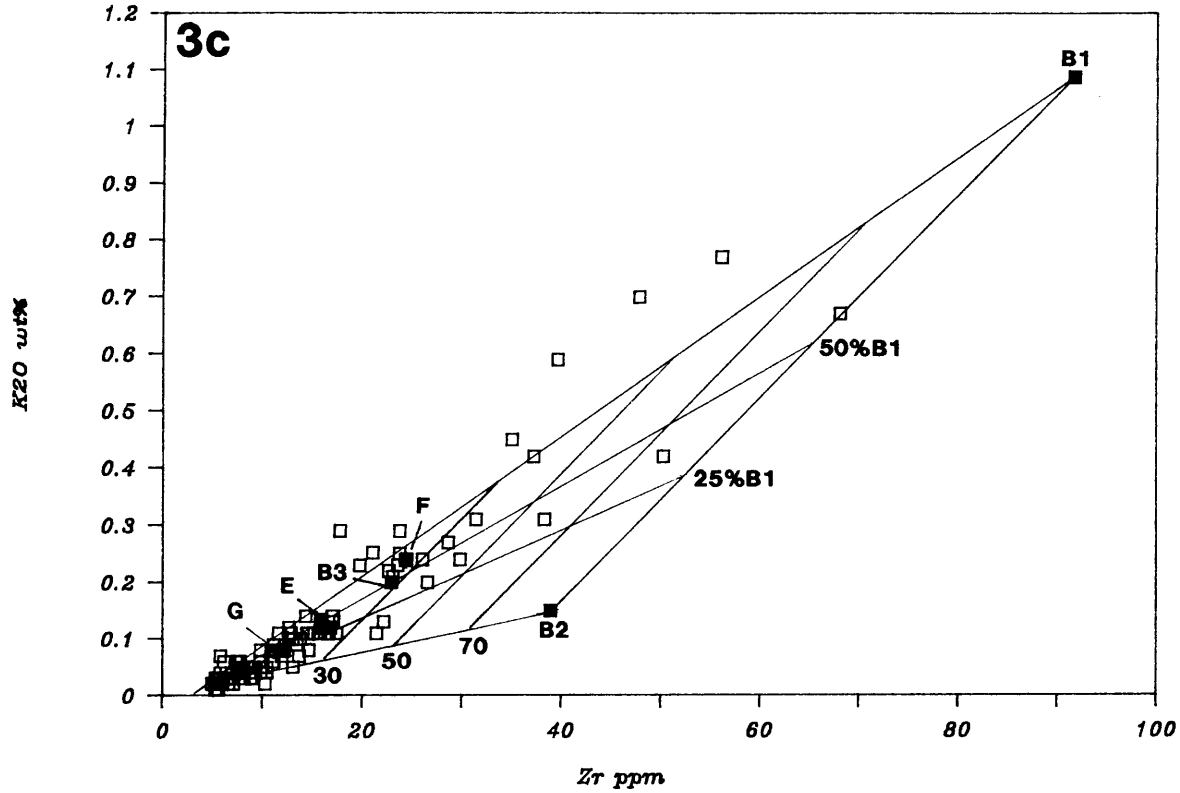

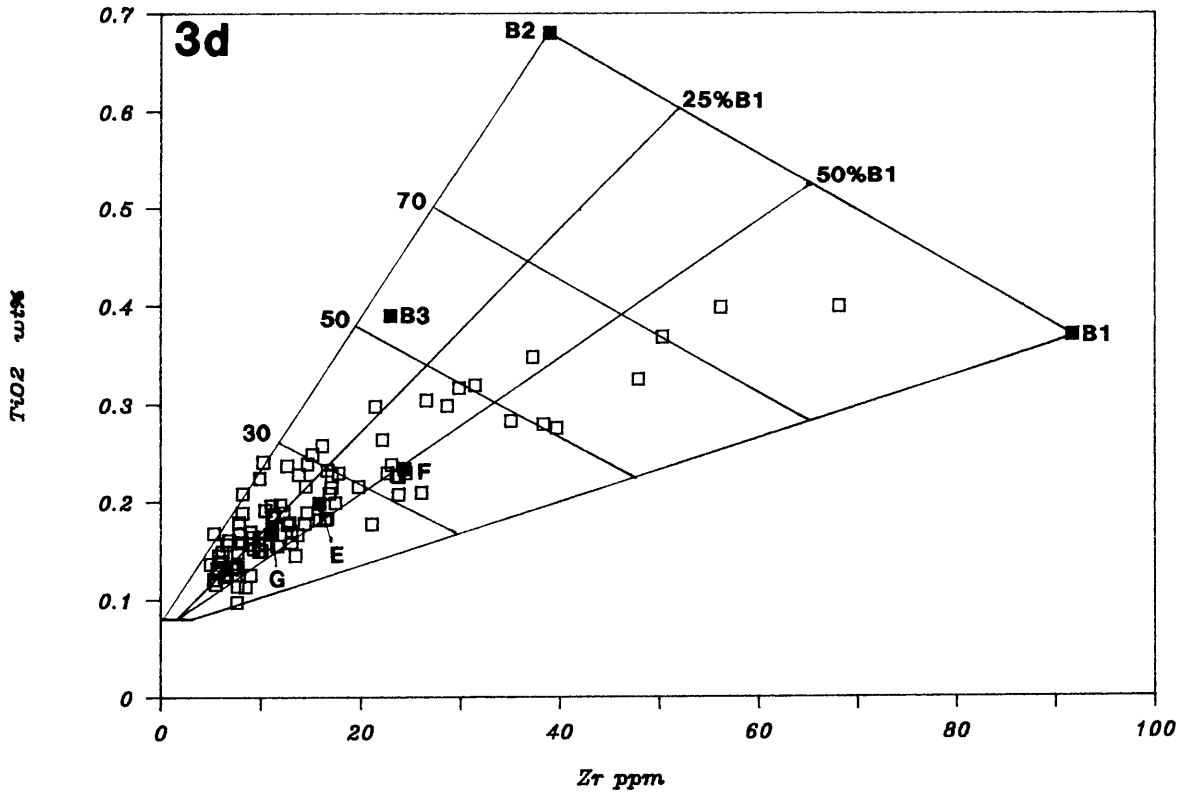

Figures VII.3e - 3f: Variation diagrams of incompatible element concentrations for the cumulates of the E-G interval. For further explanations see Figure VII.3a - 3b and text.

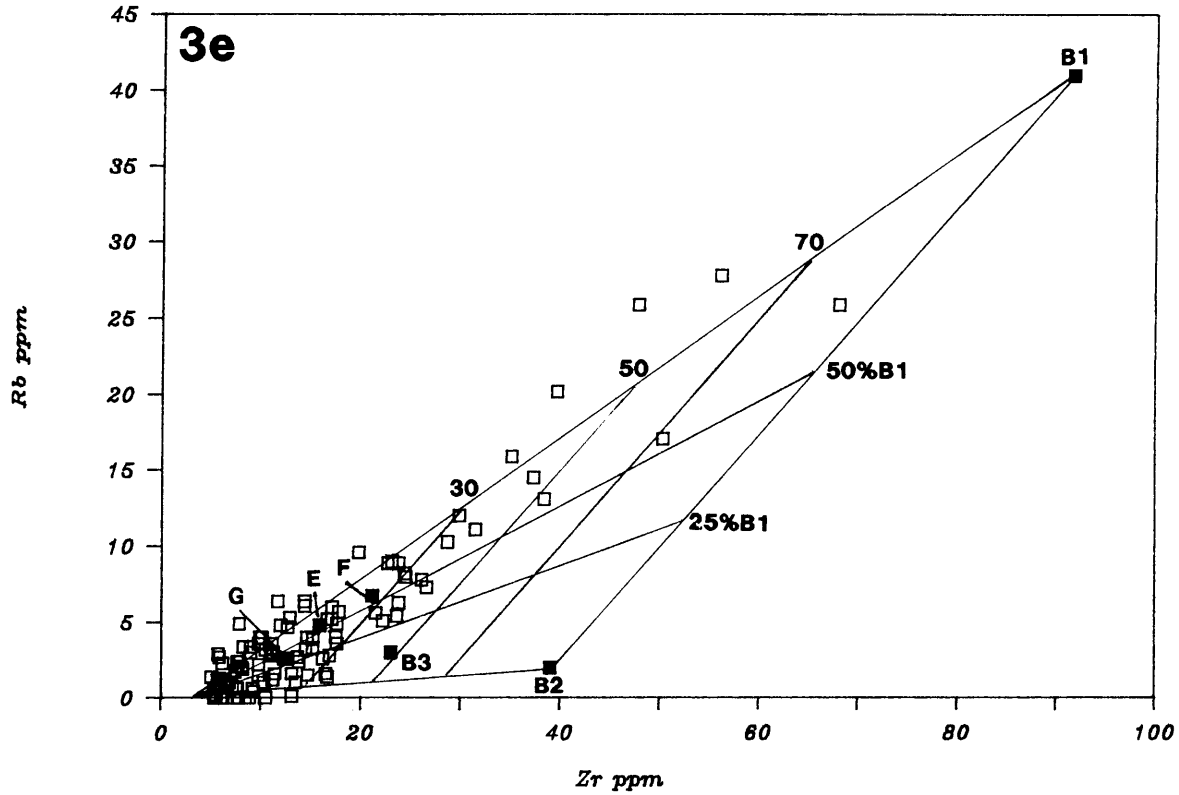

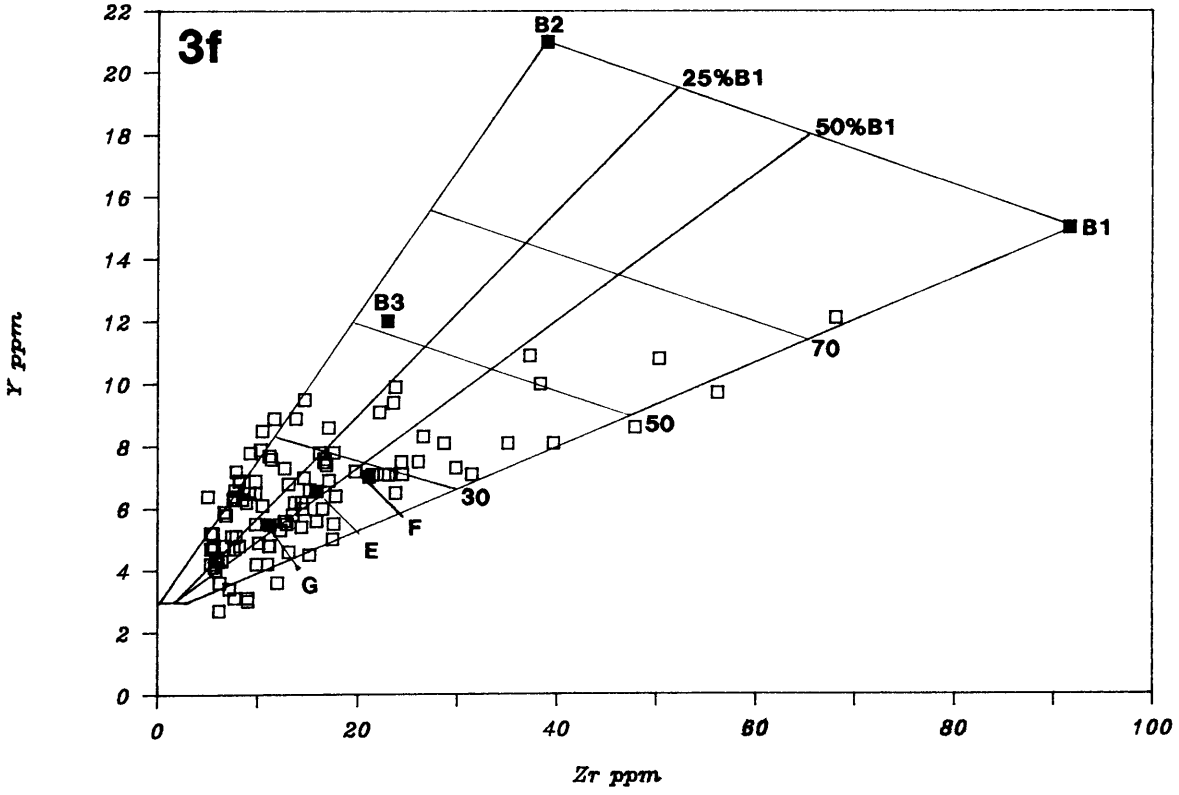

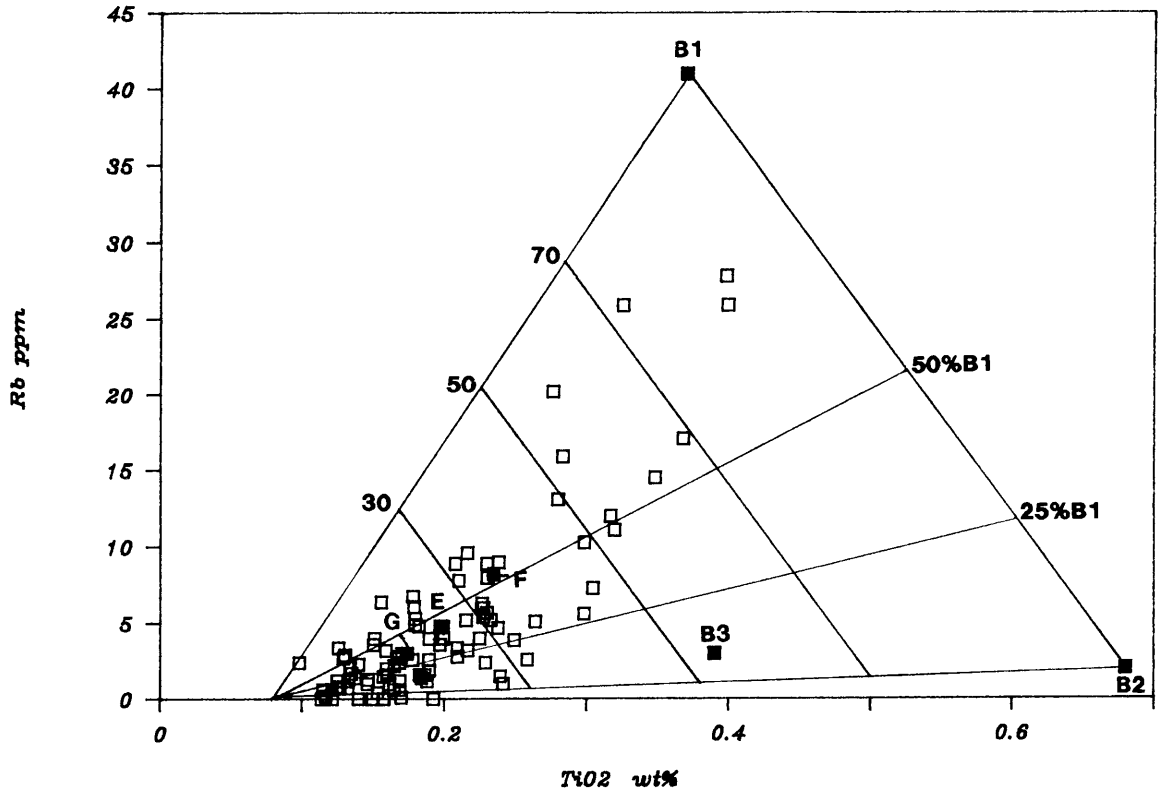

Figure VII.3g: Variation diagram of incompatible element concentrations for the cumulates of the E-G interval. For further explanations see Figure VII.3a - 3b and text.

The line between B1 and B2 represents a mixing line with the respective proportion of B1 and B2 (only a 25 % and a 50 % B1 component is shown). The numbers (30, 50 and 70 %) on the tie-lines from B1 and B2 towards the hypothetical adcumulate composition mark various proportions of trapped liquid. The adcumulate composition is not considered to plot at the origin for Ti, Zr and Y, as the respective B1 and B2 cumulates are expected to contain as much as 0.08 wt % TiO_2, 3 ppm Zr (only B1) and 3 ppm Y. These theoretical values are based on orthopyroxene-liquid partition coefficients (Pearce and Norry, 1979) for Y (+- 0.2) and Zr (+- 0.03) and on analyzed Ti concentrations in cumulus orthopyroxenes from the lower zone (Cameron, 1978).

Whole rock Ti concentrations have been recalculated to correct for the presence of modal chromite. For this purpose it was assumed that chromite contains on average 1.2 wt % TiO_2 and 45.0 wt % Cr_2O_3.

Three important features emerge from the diagrams: Firstly, whole rock trace element abundances generally lie within the range defined by parental liquids B1 and B2. The fact that several K- and Rb-rich samples plot outside the established range could possibly indicate that trapped liquid fractionation resulted in an increase in these elements relative to other incompatible elements (e.g. Zr and Y). The possibility that incompatible element-bearing phases (e.g. loveringite, zircon, phlogopite, K-feldspar) did not all crystallize simultaneously seems to be substantiated by petrographical evidence, e.g. loveringite which is commonly enclosed by phlogopite (Plate 2.H). Incompatible element ratios will only stay constant during fractionation if the particular elements are incorporated in the same mineral phase or if various incompatible-rich phases form more or less simultaneously.

Secondly, the majority of the analyzed samples cannot have been derived from just one parental liquid and must have formed from various mixtures (hybrid liquids) between B1 and B2 liquids. The averaged B1 component for the bulk E unit is 49 % (+- 5), for the F unit 59 % (+- 6) and for the G unit 34 % (+- 6). The composition of B3 liquid appears to be less suitable to explain the trace element abundance of the investigated lower critical zone samples. This is particularly obvious in Figure VII.3c (K_2O vs. Zr) where B3 lies within the compositional field of the cumulates. It must be mentioned however that those samples which are poor in incompatible elements could have formed from any of the proposed parental liquids.

Thirdly, the investigated samples contain various proportions of trapped liquid, consistent with the presence of intercumulus minerals. The bulk E unit contains an average 24 % (+- 2), the F unit 34 % (+- 2) and the G unit 19 % (+- 4).

VII.3. SULPHUR AND COPPER

Sulphur concentrations in the lower critical zone show a positive correlation with incompatible elements. High S values (up to 420 ppm) are generally found in samples with strongly evolved interstitial phases, while samples with low incompatible element abundances contain between 50 and 100 ppm S (Folder 2). The S content of the analyzed upper critical zone rocks (F, G, H and J units) is generally low with an average of about 50 ppm.

Copper shows a sympathetic behaviour with S except in those samples which contain the most evolved interstitial mineral assemblage. Cu concentrations in the latter are generally lower than in less fractionated samples (Fig. VII.4). The decoupling of Cu from S in strongly fractionated samples is graphically expressed in Folder 2 which shows a pronounced increase in the S/Cu ratio from average values of about 6 to values up to 82. The sample with the highest overall S content (420 ppm) has also the lowest overall Cu concentration (5 ppm). It is significant that anhydrite and pyrrhotite were found in two of the samples (353 29 and 372 29) rich in S and incompatible elements but relatively poor in Cu. It can therefore be assumed that the volatile content increased (as evidenced by anhydrite and phlogopite) during progressive fractionation to a critical level after which chalcopyrite was no longer stable. Carrol and Rutherford (1985) have shown experimentally that anhydrite can exist as a stable magmatic phase at 1025°C and 1 - 3 kbar, when the oxidation levels reach the upper limits of magnetite stability. More recently, Carrol and Rutherford (1988) showed that the change from sulphide dominant to sulphate dominant speciation occurs over the range of oxygen fugacity between the FMQ equilibrium and FMQ+2. Thus, interstitial melt must have been highly oxydized at the final stages for anhydrite to be a stable interstitial mineral.

An interesting feature is the sudden decrease in the S/Cu ratio across the lower/upper critical zone boundary (Folder 2 and Fig. VII.4). The analyzed samples from the upper critical zone have a S/Cu ratio of about 3 and are generally poorer in both S and Cu relative to rocks from the lower critical zone (chalcopyrite has a S/Cu ratio of about 1). The low S/Cu ratios in the upper critical zone presumably

originated from a different liquid which was enriched in Cu relative to S, thereby favouring chalcopyrite. Marginal rock analyses (Sharpe, 1982) show that a B3 liquid could be a possible source as the latter has a lower S/Cu ratio (S/Cu = 19, 74 ppm Cu) relative to B2 (S/Cu = 10 - 36, 10 - 59 ppm Cu) and B1 (S/Cu = 28, 65 ppm Cu).

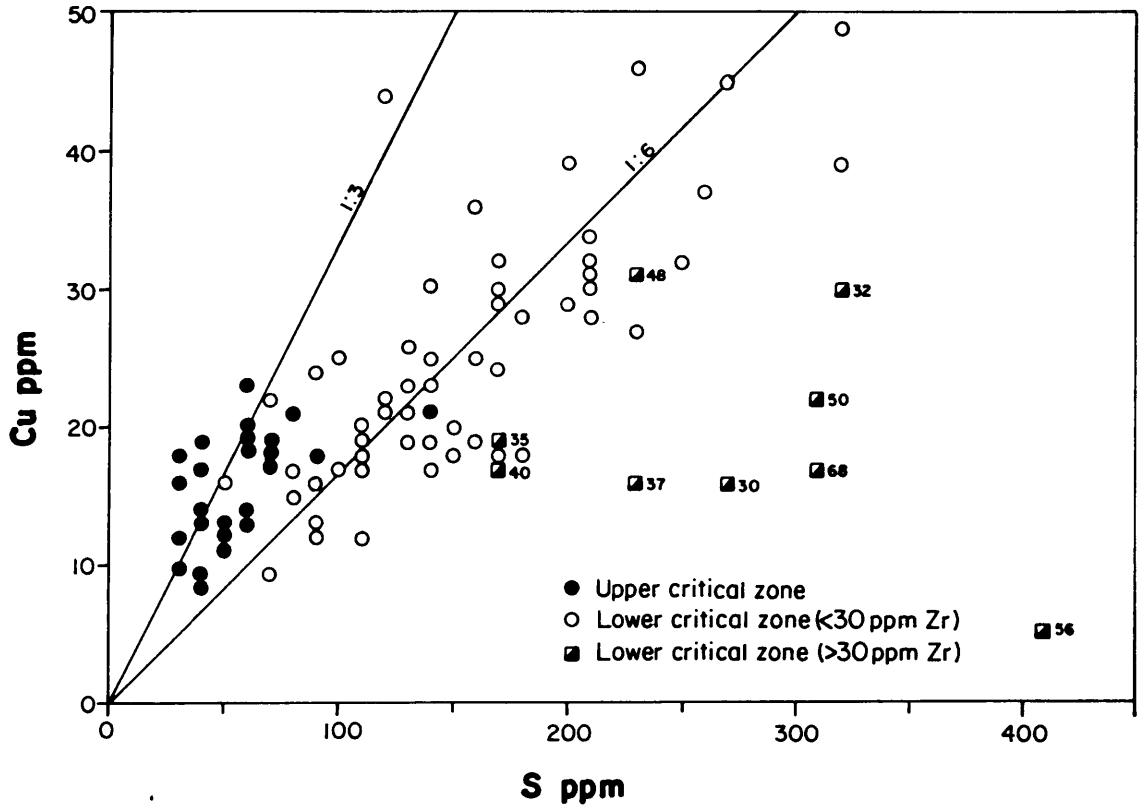

Figure VII.4: Plot of Copper versus Sulphur of samples from the lower-upper critical zone transition (E - J unit). Upper critical zone samples have generally a higher Cu/S ratio (+- 1:3) compared to samples from the lower critical zone (+- 1:6). Samples with strongly evolved interstitial phases (Zr-rich) are depleted in Cu relative to S. This feature is consistent with the presence of anhydrite in those samples.

VII.4. STRONTIUM

Sr concentrations in the analyzed samples vary between < 5 ppm in pyroxenite to about 480 ppm in anorthosite. The close relationship between the amount of plagioclase (expressed as whole rock MgO) and Sr abundance is displayed in Figure VII.5. The linear correlation indicates that plagioclase shows no systematic change in Sr content with stratigraphic height or lithology. This feature is based on the

assumption that Sr is predominantly present in plagioclase and that Sr concentrations in clinopyroxene are too low to cause a significant shift towards higher whole rock Sr abundances. Clinopyroxene from the critical zone have Sr contents of 20 - 50 ppm (pers. comm., Butcher, 1988). It must be mentioned that MgO concentrations were determined from powder briquettes, which might explain the observed scatter in Figure VII.5. Data from chromite rich samples (Cr > 40000 ppm) are excluded.

The relatively high Sr partition coefficient for plagioclase - liquid (> 2; Irving, 1978) should cause the residual liquid to become depleted in Sr when plagioclase is the dominant (> 50 %) crystallizing phase (Berlin and Henderson, 1968). The constant Sr content in plagioclase despite modal abundances in excess of 50 % (e.g. F, H and M units) would therefore indicate that melt fractionation was relatively unimportant during formation of the sequence investigated.

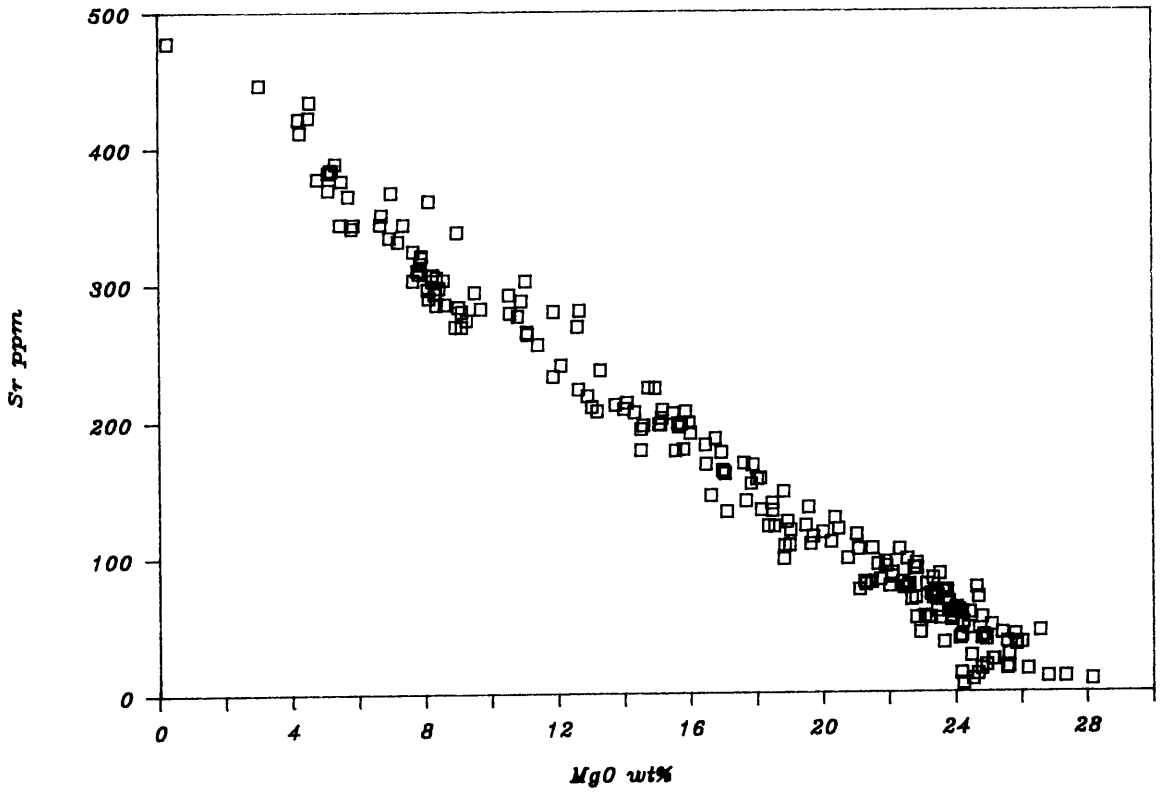

Figure VII.5: Plot of Sr versus Mg for the investigated sequence from the LG 6 - UG 1. Plagioclase (expressed as whole rock MgO) shows no systematic change in the Sr-abundance over the interval studied.

CHAPTER: VIII: STRONTIUM ISOTOPES

VIII.1. PREVIOUS SR ISOTOPE WORK ON THE BUSHVELD COMPLEX

The first comprehensive study on the Sr-isotope systematics of the Bushveld Complex was that by Hamilton in 1977. Based on whole rock samples he established an overall, but stepwise increase in the initial $^{87}Sr/^{86}Sr_o$ ratio (SrR_o) from the upper part of the lower zone to the top of the upper zone. This general trend was subsequently refined by other researchers in more detailed studies focussing on selected stratigraphic units. Kruger and Marsh (1982) identified a sharp increase in SrR_o at the level of the Merensky Reef in the western Bushveld. Sharpe (1985) established a similar trend across the Merensky Unit in the eastern Bushveld as well as a pronounced decrease in SrR_o across the Pyroxenite Marker. This decrease was subsequently also recognized by Kruger et al. (1986) in the western Bushveld.

In a recent compilation, Sharpe (1986) included previously unpublished Sr-isotope data of lower zone and critical zone cumulates. The data presented show a limited range in SrR_o with no systematic trend from the bottom of the lower zone up to the base of the upper critical zone. An abrupt increase in SrR_o occurs at the lower/upper critical zone boundary. This increase is followed by a brief reversal after which SrR_o increases through the remainder of the upper critical zone up to the Merensky Reef. A similar, rapid increase in SrR_o across the MG chromitite layers was found by Hatton et al. (1986), who investigated the lower/upper critical zone boundary in the western sector of the eastern compartment. Again, the sudden increase is followed by decreasing SrR_o values, which was attributed by the authors to a complex cyclic mixing event.

A detailed Sr-isotope study was recently presented by Kruger et al. (1987) from the upper zone in the western compartment. The fairly uniform SrR_o ratio throughout the upper zone, a confirmation of results from the eastern lobe (Sharpe, 1985, 1986), was used as evidence against magma addition and attributed to a thoroughly mixed magma chamber (Kruger et al., 1987).

Local increases in SrR_o in the cumulate sequence have been linked to influxes of high SrR_o magma (Kruger and Marsh, 1982; Sharpe, 1985). The former authors suggested that an initially sharp isotopic break was subsequently smoothed by infiltration of intercumulus liquid. The decrease in SrR_o at the level of the Pyroxenite Marker and across the E/F boundary has been interpreted as the result of a mixing process between a high SrR_o magma and an overlying layer with a relatively lower initial ratio (Sharpe, 1985; Kruger et al., 1986; Hatton et al., 1986).

VIII.2. SR-ISOTOPE SYSTEMATICS OF THE PROPOSED PARENTAL LIQUIDS

Based on a systematic Sr-isotope study of marginal rocks along the basal contact of the intrusion, Sharpe (1985) and Harmer and Sharpe (1985) identified two isotopically distinct groups (B1 and B2/B3). B1 has an average SrR_o of 0.7045 +- 9 while B2/B3 samples show a SrR_o of 0.7069 +- 5 (Harmer and Sharpe, 1985). These two magma series, viz. boninitic and tholeiitic, had been recognized from field observations and geochemical studies by various authors (e.g. Cawthorn et al., 1979; Davies et al., 1980; Sharpe, 1981; Cawthorn et al., 1981).
The inherent isotopic properties of the parental liquids were subsequently used as criteria to determine from which parental liquid or mixture of liquids the individual zones and units crystallized. This also led to the proposal of an additional B4 parental liquid (Sharpe, 1985), in order to explain the isotopic characteristics of the main zone cumulates, which have no known marginal zone equivalents.
Rare earth element analyses from marginal rocks (Harmer and Sharpe, 1985), adjacent to the upper critical zone and main zone supported the originally proposed subdivision (Sharpe, 1981) of these rocks into a B2 and B3 group, even though Sr-isotope data show complete overlap. Both liquids (B2 and B3) have the required chemical and isotopic properties to be parental to parts of the critical zone (Sharpe, 1985, 1986; Hatton, 1988).

VIII.3. SAMPLING

Plagioclase separates were chosen for this particular study for the following reasons: Firstly, the frequent occurrence of phlogopite and the generally low abundance of plagioclase in lower critical zone rocks result in high whole rock Rb/Sr ratios, which in turn increases the possible error in the recalculated initial $^{87}Sr/^{86}Sr$ ratio. In contrast, plagioclase has a very low Rb/Sr ratio.

Secondly, to investigate whether the textural transition from intercumulus to cumulus plagioclase is associated with a change in the isotopic ratio and/or Sr concentration. It has been shown that the proposed parental liquids differ substantially in their initial Sr concentrations (Sharpe, 1981), so that Sr abundance in plagioclase can therefore be expected to vary according to the Sr concentration of the particular liquid from which feldspar crystallized.

Finally, a comparison of isotopic data from plagioclase separates and whole rock samples should reveal whether the individual phases such as plagioclase, clinopyroxene and mica, which determine the isotopic signature, are in isotopic equilibrium. The textural evidence in the feldspathic pyroxenites of the lower critical zone (e.g. Chpt. II.3) suggests disequilibrium between cumulus phases and intercumulus melt. It should also be possible to monitor whether any migration of late stage interstitial melt has taken place. This, however, requires that the isotopic pattern of the liquid changed with progressive accumulation, as is expected in the case of progressive mixing between liquids with different isotopic signatures.

The samples analyzed cover the stratigraphic sequence from below the Steelpoort chromitite layer (LG 6) up to the footwall of the upper group chromitite layer 1 (UG 1). Samples from below the LG 6 up to the J unit were taken from the MDH 29 borehole, while the remaining samples from the K, L and M units were selected from MDH 23. Sample 465 23 from the F unit was also taken from borehole MDH 23, whilst sample 115 22 (K unit) is from MDH 22. Sample positions are marked in Folder 2. Sample number (e.g. 377 29) corresponds to the borehole depth (377 m) of the particular drillcore (MDH 29). Lateral correlation of boreholes is depicted in Figure II.4, and their exact geographic positions indicated on Folder 1.

Sampling was based on macroscopic changes in lithology and on previously determined variations in the mineral chemistry. The samples selected on this basis are therefore thought to cover the major lithological and chemical changes within the sequence studied. However, because plagioclase was not extracted from chromitite layers or chromite-rich rocks (chromite > 50 wt %), it cannot be excluded that the isotopic characteristics of the latter deviate from the trends observed for the silicate rocks. This possibility could be considered in future studies.

VIII.4. RESULTS

The initial $^{87}Sr/^{86}Sr$ ratios for the 39 "spiked" plagioclase separates (see Appendix A.IV) are plotted in Figure VIII.1 against their stratigraphic position. For clarity isotope data from whole rock and natural, "unspiked" plagioclase samples were excluded from the profile. The aberrant values from separates with unusually high Rb concentrations (see Chpt. X.2) and results from plagioclase which has abnormally high An contents (see Chpt. X.1) are marked by different symbols.

The investigated sequence shows an overall increase in SrR_o from about 0.7054 to 0.7062 with two distinct reversals. The first reversal is represented by a sharp decline across the F/G interface. If one includes the bottom most sample (high Rb) in the G unit, then the drop in SrR_o occurs over a vertical distance of less than 3 metres. A gradual mixing between two isotopically distinct liquids seems inappropriate to explain this sharp reversal. The F/G contact is marked by a change from chromiferous anorthosite to feldspathic pyroxenite/melanorite with a chromitite layer (MG 3) in between.

The H/J boundary can be taken as the approximate start of the second reversal. SrR_o values stay low (0.0758 - 0.7059) in the J, K, and L units and about 50 m into the M unit. The uniform isotopic behaviour within the J - M sequence is surprising, considering the wide range in lithology, covering norite, melanorite, chromiferous feldspathic pyroxenite and leuconorite (see Folder 2).

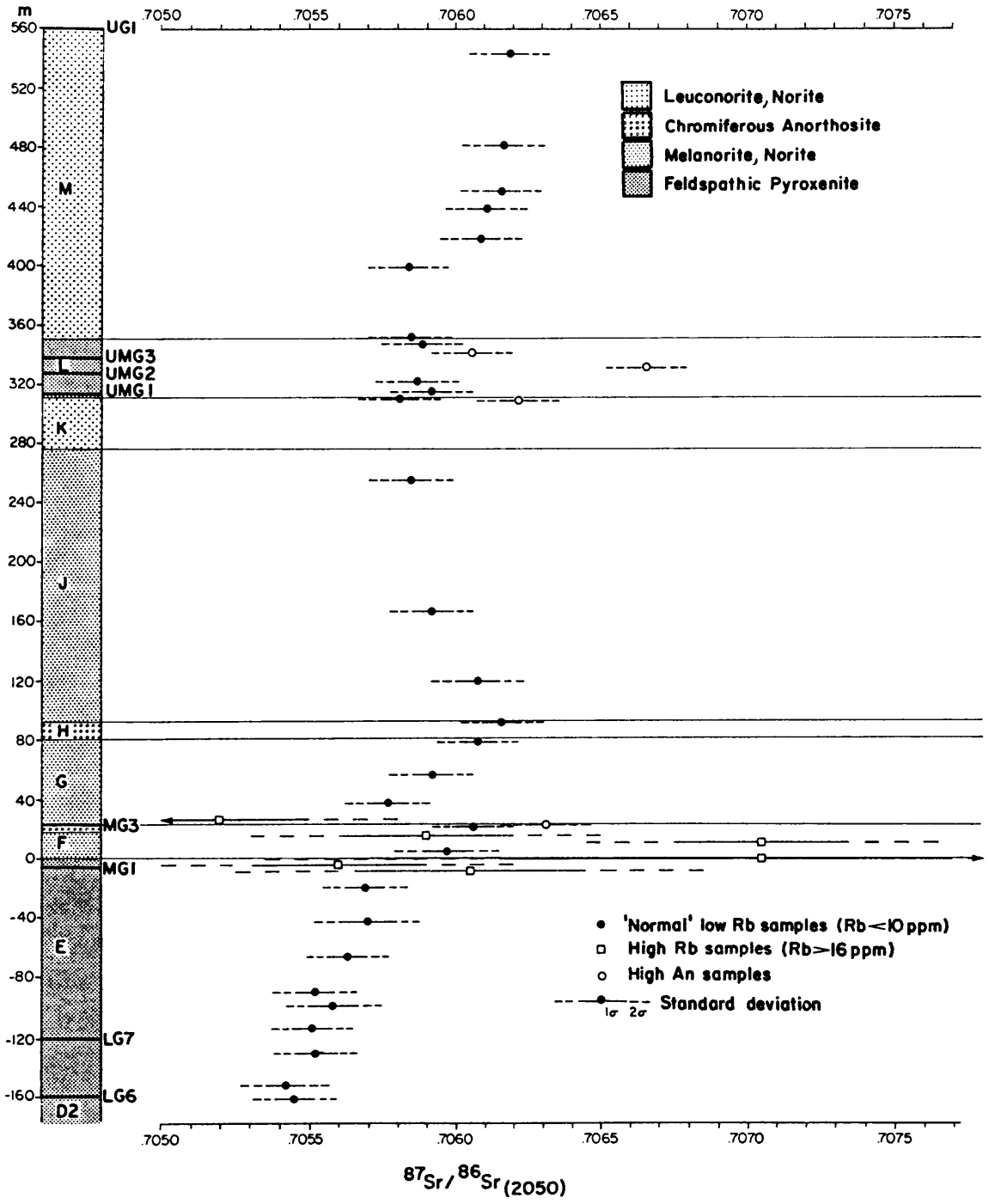

Figure VIII.1: $^{87}Sr/^{86}Sr$ at 2050 Ma of plagioclase separates against stratigraphic height for the LG 6 - UG 1 sequence. Datum marks the lower/upper critical zone boundary. Analytical results and sample numbers are presented in Table VIII.1

The L unit is of particular interest as it consists of an alternating succession of feldspathic pyroxenite (intercumulus plagioclase) with interlayered thin chromitites (UMG 1 - 3) and melanorite (cumulus plagioclase). The plagioclases extracted from the two lithologies are however isotopically identical. It can therefore be assumed that plagioclase from the J-M interval crystallized from one, isotopically homogeneous liquid. The variety of rock types within this sequence and in particular the stratigraphic order in which they occur, clearly contradicts the possibility that this succession formed from just one liquid undergoing progressive fractionation.

An overall increase in SrR_o with stratigraphic height is found from below the LG 6 (D_2 unit) up to the top of the F unit. However the limited number of usable data points close to the E/F boundary and the relative small variation in SrR_o between any two successive samples makes it difficult to determine whether the observed overall increase is gradual or marked by an abrupt increase across the lower/upper critical zone interface. The latter seems more plausible, considering the change in slope in the isotope profile.

The 4 lowest samples from the E unit were each taken within a distance of less than 10 metres below and above the LG 6 and the LG 7. No isotopic change was found across these prominent chromitite layers.

Two plagioclase separates (410 29 and 353 29) within the E unit were extracted from rocks with relatively evolved interstitial mineral composition (mol % An 55 and 35). Both separates are enriched in Rb and depleted in Sr relative to other plagioclase samples from the E unit which have higher average An contents (An 64 - 74). SrR_o ratios of the low An separates do not deviate from the established trend in the succession.

The steady increase in SrR_o from the base of the G unit into the H unit can be seen as a repetition of the isotopic trend in the D_2 - F succession. Both sequences (D_2-F and G-H) are marked by an overall increase in modal plagioclase with stratigraphic height, each topped by chromiferous anorthosite.

A similar correlation between the modal amount of plagioclase and SrR_o is found in the M unit where a marked increase in SrR_o occurs over a vertical distance of less than 20 metres. This increase also coincides stratigraphically with the first appearance of abundant cumulus clinopyroxene some 400 metres above the E/F boundary.

Finally, plagioclase shows no systematic change in Sr concentration with stratigraphic height (Table VIII.1). The apparently lower Sr abundances of certain lower critical zone separates are attributed to the presence of quartz in the analyzed separates, which reduces the overall Sr concentration in the sample (see Chap. X.2). It is therefore assumed that the reported differences in Sr concentration in the parental liquids (B1 and B2/B3, Sharpe, 1981) are due to the different modal amounts of plagioclase in the analyzed marginal rocks.

Table VIII.1: Rb, Sr and isotope data in relation to stratigraphic height. Sample name (e.g. ps 293 23) refers to the mode of sample (p = plagioclase, s = spiked, n = natural, wr = whole rock) and the drillcore depth of the particular borehole. Initial $^{87}Sr/^{86}Sr$ ratios (SrR_o) are given at the 1 sigma level. SrR_o is calculated at 2050 Ma (including a 2 sigma +- 25 Ma correction) using the ^{87}Rb decay constant of $1.42*10^{-11}$. Uncertainties in Rb and Sr concentrations ($^{87}Rb/^{86}Sr$) and in the $^{87}Sr/^{86}Sr_p$ ratio are presented in table A.4. Datum is taken at the base of the upper critical zone. Lithological units according to Cameron (1980, 1982).

Height above E/F	Sample	Unit	Rb ppm	Sr ppm	$^{87}Rb/^{86}Sr$	$^{87}Sr/^{86}Sr_p$	SrR_o (1 sigma)
533	ps 82 23	M	0.546	518.6	0.0031	0.706266 +- 16	0.70618 +- 7
533	pn 82 23	M	0.546	518.6	0.0031	0.706283 +- 16	0.70619 +- 7
481	ps 134 23	M	2.523	522.0	0.0140	0.706584 +- 17	0.70617 +- 7
450	ps 165 23	M	0.809	548.2	0.0043	0.706283 +- 12	0.70616 +- 7
438	ps 177 23	M	0.991	693.8	0.0041	0.706232 +- 9	0.70611 +- 7
418	ps 197 23	M	0.333	496.8	0.0019	0.706151 +- 12	0.70609 +- 7
399	ps 216 23	M	0.766	483.4	0.0046	0.705973 +- 13	0.70584 +- 7
352	ps 263 23	M	0.511	559.4	0.0026	0.705927 +- 10	0.70585 +- 7
347	ps 268 23	L	0.390	486.8	0.0023	0.705955 +- 10	0.70589 +- 7
341	ps 274 23	L	0.115	552.0	0.0006	0.706075 +- 10	0.70606 +- 7
331	ps 284 23	L	1.143	415.0	0.0080	0.706838 +- 11	0.70660 +- 7
322	ps 293 23	L	0.761	501.7	0.0044	0.705980 +- 11	0.70585 +- 7
322	pn 293 23	L	0.761	501.7	0.0044	0.706002 +- 10	0.70587 +- 7
315	ps 300 23	L	0.591	488.4	0.0035	0.706018 +- 15	0.70592 +- 7
310	ps 115 22	K	1.447	494.8	0.0085	0.706058 +- 14	0.70581 +- 7
309	ps 305 23	K	0.191	491.6	0.0011	0.706252 +- 13	0.70622 +- 7
255	ps 55 29	J	1.690	538.3	0.0091	0.706116 +- 12	0.70585 +- 7
166	ps 144 29	J	2.030	527.0	0.0111	0.706250 +- 10	0.70592 +- 7
121	ps 191 29	J	8.715	483.7	0.0522	0.707616 +- 14	0.70608 +- 8
93	ps 219 29	H	2.007	486.9	0.0119	0.706513 +- 16	0.70616 +- 7
80	ps 232 29	G	4.031	433.8	0.0269	0.706874 +- 12	0.70608 +- 7
58	ps 254 29	G	1.729	451.1	0.0111	0.706246 +- 12	0.70592 +- 7
37	ps 273 29	G	1.662	497.1	0.0097	0.706053 +- 26	0.70577 +- 7
26	ps 284 29	G	16.387	344.1	0.1378	0.709266 +- 14	0.70520 +- 34
22	ps 465 23	F	0.092	441.6	0.0006	0.706327 +- 18	0.70631 +- 7
21	ps 289 29	F	2.968	478.2	0.0180	0.706590 +- 15	0.70606 +- 7
15	ps 295 29	F	19.171	421.2	0.1317	0.709821 +- 16	0.70593 +- 33
10	ps 300 29	F	57.301	294.9	0.5630	0.723497 +- 18	0.70687 +- 33
10	ps 300 29	F	57.492	303.3	0.5493	0.723449 +- 27	0.70723 +- 32
10	wr 300 29	F	12.292	100.2	0.3552	0.717192 +- 19	0.70670 +- 29
4	ps 306 29	F	9.362	445.1	0.0608	0.707762 +- 32	0.70597 +- 9
-1	ps 311 29	E	54.101	356.8	0.4392	0.719886 +- 14	0.70691 +- 87
-1	pn 311 29	E	54.101	356.8	0.4392	0.720131 +- 16	0.70716 +- 87
-5	ps 315 29	E	18.984	382.8	0.1435	0.709796 +- 15	0.70556 +- 32
-9	ps 319 29	E	18.331	399.6	0.1328	0.709982 +- 12	0.70606 +- 33
-9	ps 319 29	E	18.889	375.5	0.1456	0.710259 +- 11	0.70596 +- 35
-20	ps 330 29	E	0.202	423.7	0.0014	0.705729 +- 14	0.70569 +- 7
-43	ps 353 29	E	7.544	204.6	0.1066	0.708912 +- 11	0.70576 +- 11
-43	ps 353 29	E	8.020	187.4	0.1238	0.709234 +- 11	0.70558 +- 12
-67	ps 377 29	E	2.890	466.1	0.0179	0.706163 +- 10	0.70563 +- 7
-67	ps 377 29	E	3.007	469.7	0.0185	0.706181 +- 12	0.70563 +- 7
-67	ps 377 29	E	2.763	452.9	0.0176	0.706149 +- 10	0.70563 +- 7
-91	ps 401 29	E	1.713	542.4	0.0091	0.705787 +- 24	0.70552 +- 7
-100	ps 410 29	E	9.314	416.1	0.0647	0.707488 +- 10	0.70558 +- 9
-100	wr 410 29	E	3.176	46.6	0.1975	0.711385 +- 32	0.70555 +- 17
-115	ps 425 29	E	1.009	442.9	0.0066	0.705705 +- 11	0.70551 +- 7
-132	ps 442 29	E	1.237	434.6	0.0083	0.705760 +- 13	0.70552 +- 7
-154	ps 464 29	E	0.814	493.3	0.0048	0.705560 +- 12	0.70542 +- 7
-154	wr 464 29	E	1.216	68.2	0.0518	0.707002 +- 14	0.70547 +- 8
-163	ps 473 29	D_2	2.306	430.4	0.0155	0.705907 +- 14	0.70545 +- 7

CHAPTER IX: DISCUSSION OF SR ISOTOPES AND PROPOSED MODEL FOR THE LG 6 - UG 1 SEQUENCE

IX.1. THE LOWER CRITICAL ZONE

IX.1.1. INTRODUCTION

Established thermal and density contrasts between the parental liquids (Sharpe et al., 1983; Sharpe and Irvine, 1983; Hatton, 1988), show that a B1 liquid with its higher liquidus temperature (1290°C) has a lower density than B2 and will therefore overlie the considerably cooler (1190°C) and denser B2 liquid in a stratified magma chamber. Thermal diffusion across the interface cannot cause the density relationship to reverse, because a superheated B2 liquid remains denser over the maximum possible thermal range of 1290 - 1190°C (Hatton, 1988). Simultaneous cooling of B1 liquid cannot reduce the density of B1 sufficiently (Hatton, 1988) to allow the liquids to become mechanically combined. A diffusive interface (see Irvine et al., 1983) can therefore be assumed for the two liquids. It should be noted that crystal fractionation in either of the liquids would increase the density contrast even further. Orthoyroxene crystallization in the B1 layer would lower the liquid density (e.g. Sparks and Huppert, 1984), whereas the density of B2 would increase as a result of predominant plagioclase fractionation (e.g. Sparks et al., 1980).

The observed increase in SrR_o in the lower critical zone (Fig. VIII.1) must therefore be caused by a mixing process different to the model proposed by Irvine et al. (1983) and Turner and Campbell (1986). These authors considered the case where a hot, less dense magma overlies initially a layer of cooler but denser magma. The proposed density difference in the system studied by these authors was however relatively small, so that heat transfer across the interface caused the lower layer to become less dense than the overlying liquid. This gravitationally unstable situation, described as a finger interface, allows the two liquids to become thoroughly mixed. A well mixed hybrid

liquid can however not explain the almost constant Cr and Ti concentrations of orthopyroxene in the D_2 and E units (Folder 2) which undoubtedly reflect a B1 parentage and which are comparable to Cr and Ti values of pyroxenes from the underlying 500 to 600 m thick feldspatic pyroxenites of the lower critical zone.
Furthermore, a B1/B2 hybrid crystallizes olivine prior to plagioclase (Chpt.V.2). Thus, a mixing process between the two liquids is required whereby the chemical properties of the B1 liquid remain almost unchanged during accumulation of the lower critical zone.

IX.1.2. CRYSTAL/LIQUID SLUMPING - TWO-PHASE CONVECTION

The observed variation in SrR_o in the studied section is interpreted as reflecting various mixing stages between the two isotopically distinct lineages (B1 and B2/B3). These liquids must have been present in the magma chamber during the formation of the LG 6 - UG 1 succession.
The model proposed here favors a process whereby thermally induced crystallization within the overlying B1 layer triggers the physical collapse and downfall of a crystal-laden portion of the B1 layer. Continuous heat loss to the underlying B2 layer and through the roof will cool the B1 layer resulting in pyroxene crystallization (Fig. IX.1a). Convective motion within the B1 layer will initially keep the crystals in suspension until sufficient growth enables them to overcome retention and to settle to the bottom of their layer (Weinstein et al., 1988) to form a cumulate enriched B1 boundary layer. This layer will become enriched in crystals until the bulk density exceeds that of of the underlying B2 liquid, leading to the descent of crystal-laden plumes (Fig. IX.1b and 1c). Down-spouting of an unstable boundary layer, due to conductive cooling, has been experimentally investigated by Jaupart et al. (1984), and a similar process was also proposed by Naldrett et al. (1986, 1987) as well as by Hatton (1988) as an important mechanism during the formation of the Merensky Reef.

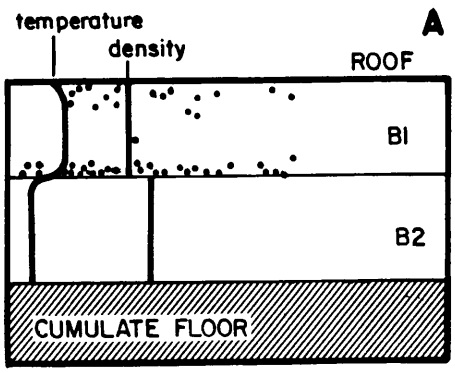

Hot and light B1 liquid overlies cool and dense B2 liquid. Thermal equilibration between layers results in orthopyroxene crystallization within the upper layer

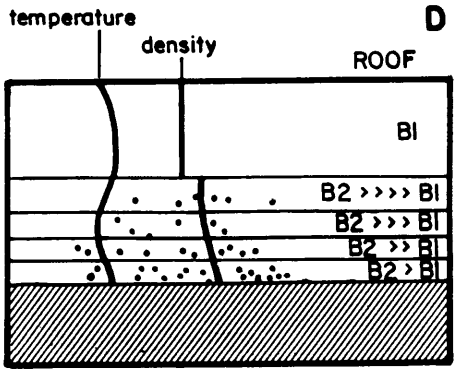

Repeated slumping and mixing results in the build-up of hybrid layers

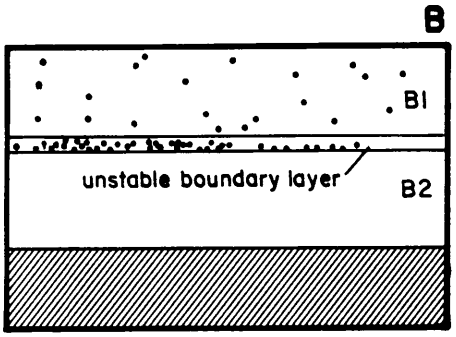

Orthopyroxenes settle within the upper layer and form a physically unstable boundary layer

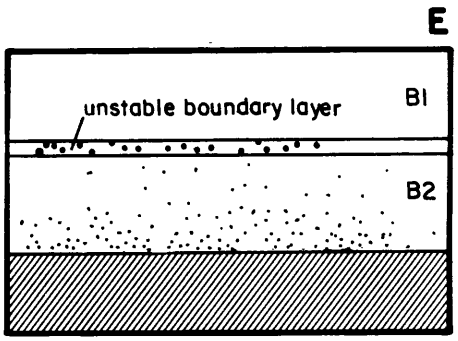

Chromite forms during each slumping event and remains temporarily in suspension

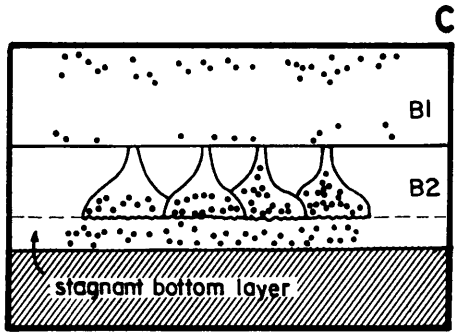

A crystal - bearing boundary layer with sufficiently high proportion of ortho-pyroxene collapses and plunges down. Plumes spread out above the stagnant bottom layer and suspended crystals settle to the floor

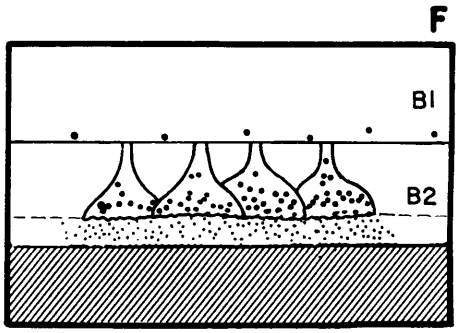

Descending plumes sweep suspended chromite crystals down

Figures IX.1a - 1f: Series of cartoons illustrating the principle set-up in the magma chamber (A), the formation of an unstable boundary layer (B), the descent of crystal-laden plumes (C), the development of hybrid layers (D), the presence of suspended chromite (E) and the sweeping down of chromite by succeeding crystal/liquid plumes (F).

The geological importance of this process as an agent of crystal transport was noted by Grout as early as 1918. Several authors (e.g. Hess, 1960, Raedeke and McCallum, 1984) have since examined the various effects caused by the density contrast of crystal-bearing liquid and surrounding liquid. The possible thermodynamic effects caused by the interaction of crystal-bearing plumes with surrounding liquid of contrasting physico-chemical properties have been previously re-examined by Morse (1986b).

To the authors knowledge no experiments have yet been carried out to study the proposed situation where a relatively cool and dense liquid is emplaced under a hotter and less dense liquid. However experiments with a simple one-liquid system (Jaupart et al., 1984; Jaupart and Brandeis, 1986) have shown that constant cooling at the top of a liquid generates cold plumes which subsequently move to the bottom. These plumes reflect the downward transport of a buoyantly unstable portion, and their physical presence and appearance provides an analogy to the proposed densitiy instabilities in the Bushveld magma chamber.

Probably the most important aspect of the process outlined above is that liquids of contrasting density and chemistry can become mechanically mixed simply due to the presence of "suspended" crystals. This process leaves the overlying liquid layer almost chemically unchanged, simultaneously the lower layer becomes more and more hybridised as plumes continue to descend. Detachment and down-spouting affects only a small portion of the upper layer, described as the unstable boundary layer, which then reforms until the next down-spouting event occurs (Brandeis and Jaupart, 1986). The particular chemical properties of the upper layer (B1) can therefore persist almost unchanged, although its total volume is gradually reduced by the intermittent breakdown of the boundary layer. At the same time the bottom liquid will change its chemical composition according to the proportions of added B1 material. It seems obvious that the amount of material added to the bottom layer is highest at an early stage when the temperature contrast at the B2/B1 interface is large. Hence, crystallization and detachment in the upper layer is initially fast and will gradually slow down as the two liquids approach thermal equilibrium. Hatton (1988) noted that a crystal content of less than

10 % in the B1 layer (at 1290°C) exceeds the density of the underlying B2/B3 liquid (at 1190°C). Thus, a relatively small amount of crystals in the boundary layer will cause a descent of plumes despite the initially large density contrast between the two liquids.
Jaupart et al. (1984) and Jaupart and Brandeis (1986) have shown in experiments that plumes descend to a stagnant bottom boundary layer at the floor of a magma chamber where they slow down and spread laterally (Fig. IX.1c). Final deposition of plume-crystals into the stagnant bottom layer will be controlled by the same parameters, such as crystal settling velocity, magmatic convective velocity etc., which govern the initial accumulation of crystals in the B1 boundary layer. Periodic release of crystals, accumulated above the stagnant bottom layer may well be responsible for small-scale modal layering or fluctuations in modal orthopyroxene, respectively. An in-depth discussion about the separation of crystals from a convecting magma is presented by Marsh and Maxey (1985) and Weinstein et al. (1988).
The relative proportion of B1 material added to the B2 liquid can be expected to increase from the top to the bottom (Fig. IX.1d), although some liquid in the descending plumes might become buoyant, either during descent or after deposition, as B1 liquid without crystals will have a lower density than the B2 liquid. Turbulent convection within the plumes and the temperature contrast between the liquids could trigger further crystal growth within the plumes.

IX.1.3. VISCOSITY EFFECTS AND CRYSTALLIZATION IN CRYSTAL/LIQUID PLUMES

Based on a series of aqueous solution experiments, Huppert and co-workers (1983, 1984) have documented the nucleation of crystals within plumes as they rise through a cooler and more viscous liquid. The experiments also showed that crystals kept on growing until they became detached from the plumes and settled individually or as chain-like aggregates to the floor. The most important result was that while plumes continued to rise very little mixing with surrounding liquid took place. This phenomenon was attributed by the authors entirely to the different viscosities of the two liquids. An analogy with the experimental results and the proposed descent of crystal-bearing

plumes is justified, considering that the viscosity of the crystal-liquid mixture will be much higher than that of the liquid through which it passes. One can therefore assume that descending crystal/liquid plumes undergo very little mixing with surrounding liquid prior to reaching the stagnant bottom layer.

The residual liquid, however, after it had undergone strong orthopyroxene fractionation within the plumes, is likely to mix with surrounding liquid. According to the modelled fractionation path of a B1 liquid (Barnes and Naldrett, 1986) cooling of B1 liquid to the temperature of B2 liquid (1190°C at liquidus) represents 15 - 20 % fractionation. The composition of the residual B1 liquid, which is effectively added and mixed, might therefore be close to the plagioclase - orthopyroxene cotectic (1180°C; Barnes and Naldrett, 1986). The exact degree of fractionation and hence the composition of the entrained plume liquid will depend on the temperature of the surrounding and probably superheated B2 liquid.

The ultimate fate of the "settled" crystals is complex and they may either grow or be resorbed depending on the specific composition of surrounding liquid which will be a hybrid. The relative proportion of B1 and B2 in the hybrid is expected to change with time and to vary within the hybrid layer.

IX.1.4. FORMATION OF THE D_2 AND E UNITS

It is proposed that periodic slumping of an unstable B1 boundary layer resulted in a series of hybrid layers which varied in composition according to the amount of added material. Each slumping event must be seen as a number of downward moving plumes, with individual plumes overlapping with plumes from the same cycle and possibly with plumes from previous ones. Although slumping might develop into a steady-state downward flow, the net-result will be that the bottom is relatively more enriched in the B1 component than the top. The amount of B1 liquid which is ultimately deposited at the stagnant bottom layer must be proportional to the amount of crystals carried within the plumes, as gravitational sinking is determined by the latter. The proportion of B1 liquid which is added and subsequently mixed with B2

should therefore increase downwards. A profile through the liquid layers would chemically resemble a mixing line between B1 and B2 with the proportion of B1 gradually decreasing upward (Fig. IX.1d).
The observed increase in SrR_o from the LG 6 to the top of the lower critical zone (E/F boundary) is interpreted as reflecting this chemical zoning, which was preserved during solidification. The overall increase in modal plagioclase (Folder 2) from LG 6 to the E/F boundary also points towards an upwards decrease in the B1 component.
The low Mg# (80-81) of orthopyroxene within the D_2 (LG 5 and LG 6) and lower E units (LG 7) relative to the underlying C and D_1 units (83-85; Cameron, 1980) and to pyroxene above the LG 7 (82-83) has been related to an intermittent influx of B2/B3 liquid (Chpt. V.5). Published whole rock Sr-isotope data (Sharpe, 1986) show, in fact, that samples from the base of the critical zone up to the LG 6 have slightly lower initial ratios (0.7053 +- 2; average of 7 samples) than rocks above the LG 6 (this study). The overall increase in SrR_o above the LG 6 would support addition of a liquid enriched in ^{87}Sr and subsequent mixing with resident liquid. However, the relatively wide spacing of Sharpe's samples (+- 30 m) and the scatter in SrR_o (0.7050 - 0.7057) within this 300 m thick sequence make it difficult to locate the exact stratigraphic position(s) of replenishment(s). Precise isotopic evidence for magma addition at this stratigraphic level (+- LG 5 - LG 6) would have to come from a future detailed study covering the succession below the LG 6.

IX.2. THE TRANSITION FROM THE LOWER TO THE UPPER CRITICAL ZONE

IX.2.1. GEOCHEMICAL AND LITHOLOGICAL FEATURES - A REVIEW

The sharp reversal in SrR_o at the F/G boundary, the subsequent increase through the G and H units and the following decrease through the J unit (Fig. VIII.1) are evidence for complex mixing events which interrupted the scenario outlined above. In order to reconstruct the number and sequence of possible events a brief summary of previously

proposed models is presented, highlighting the complex lithological features.

The rock sequence marking the transition from lower to upper critical zone has always been the subject of controversial discussions. The abrupt change in lithology, the sudden appearance of cumulus plagioclase, the local occurrence of erosional features and xenoliths and the close association with several chromitite layers have been explained by a variety of different hypotheses.

Schwellnus (1956) and Heckroodt (1959) concluded that anorthosite is intrusive into the chromitites and pyroxenite. Kuschke (1939) explained the anorthosites as an accumulation product of a magma from which pyroxene had already crystallized and settled. Cameron (1970, 1982) postulated a progressive shift in the liquid composition towards the spinel-pyroxene-plagioclase triple junction with a sudden shift into the plagioclase stability field. He related this sudden shift to either variations in total pressure or to magma movement in the chamber possibly caused by magma addition.

The associated chromitite layers have been related by Ulmer (1969) and by Cameron (1970) to changes in oxygen fugacity in the magma. Based on intrinsic oxygen fugacity measurements Flynn et al. (1978) concluded that near-solidus crystallization with minimal differentiation occurred between the F and L units.

In order to explain the chromiferous anorthosite/chromitite succession, Vermaak (1976) invoked magma turbulence by which plagioclase and chromite were winnowed into rhythmic isomodal layers. He pointed out that the chromite in the anorthositic environment actually "belongs" genetically in the chromitite layer and that plagioclase and chromite are products of two succeeding crystallization cycles.

Although many of the cited authors were more concerned with descriptive petrographic and chemical aspects, with little regard to their genesis, it is surprising that magma addition or at least severe magma movement has been invoked by the majority of workers to explain these "anomalous stratigraphic units" (Cameron, 1982).

Based on Sr-isotope data, Sharpe (1986) and Hatton et al. (1986) were eventually able to document an addition of high SrR_o magma at the transition of lower/upper critical zone. However, these authors did not relate their isotopic data to the variety of rock textures and

lithologies which occur within this sequence.
A comprehensive petrographic description of the units E - L is given by Cameron (1980, 1982) and in the previous Chapter II. The following summary lists diagnostic features in the studied area which are associated with the lower/upper critical zone boundary.

* Small inclusions (5-200 um) of plagioclase in orthopyroxene occur very sporadically from the MG 1 layer upwards and increase drastically in abundance at the E/F boundary (Plate 3.D).
* Cumulus plagioclase suddenly appears at the E/F boundary.
* The G unit starts with feldspathic pyroxenite where orthopyroxene is free of plagioclase inclusions (Plate 3.C).
* The amount of small cumulus orthopyroxene grains (< 1000 um) increases from the MG 1 layer upward.
* All rocks above the E/F boundary up to the M unit are fine to medium grained.
* The F and H units contain several chromiferous anorthosites, some of them capped by chromitite (Plate 1.E).
* At least two distinct chromitite layers are found less than 10 m below the E/F contact (Folder 2).
* Cumulus chromite above the E/F contact up to the K unit is almost exclusively restricted to the anorthositic layers.
* The degree of orthopyroxene resorption in the F unit increases with the modal amount of plagioclase (Plate 4.D). In the chromiferous anorthosites orthopyroxene usualy has a poikilitic, sponge-like texture (Plate 3.B).
* The transition from norite to anorthosite at the G/H boundary and within the F and H units is characterized by a sharp rise in modal plagioclase over a few centimetres.
* Anorthositic layers are characterized by gneissoid flow structures and the patchy occurrence of chromitite and orthopyroxene-rich fragments (Chpt. II.4).
* Orthopyroxene composition changes across the E/F boundary (Folder 2).

IX.2.2. MAGMA REPLENISHMENT - PHYSICO-CHEMICAL CONSIDERATIONS

From the petrographic and mineral-chemical evidence there is no doubt that magmatic conditions above the E/F contact changed drastically, resulting in a major break in the evolution of the critical zone. The most obvious petrological change is that plagioclase became a liquidus phase; sometimes the only liquidus phase. Experimentally determined phase relations (Sharpe and Irvine, 1983) have shown that neither a pure B1 nor a B1-B2 mixture has plagioclase as the sole liquidus phase. Only a B2 liquid with a B1 component of less than 10 % has only plagioclase on the liquidus for all studied T-fo_2 conditions, except for traces of chromite at QFM and NNO conditions (op. cit.). Thus, the anorthositic units F and H most likely formed from an undifferentiated and relatively pure B2/B3 liquid. The anorthosites in both units have, in fact, higher SrR_o values than the closely associated over- and underlying rocks (Fig. VIII.1).

Due to the high density of the B2 liquid (at 1190°C) one can expect an intermittent influx of B2 to spread on the floor of the chamber. A B3 liquid would only be denser relative to the liquid already occupying the chamber if the latter is a hybrid with a B1 component of more than 60 % (calculated after Bottinga et al., 1982, in Hatton, 1988). Considering the likely presence of "suspended" crystals, which increase the overall density in the resident melt, then the new liquid (B2 or B3) might be emplaced at some height above the floor, with the exact position depending on the amount of crystals carried within each individual liquid layer.

Emplacement of either B2 or B3 liquid will initially result in a sharp temperature gradient, because of a lower liquidus temperature of +- 1190°C of the B2 melt compared with the temperature of the hybrid in the magma chamber which is estimated to range between 1220 and 1260°C, depending on the relative proportions of B1 and B2. Finger mixing will take place between new liquid and the overlying, uplifted liquid (see Irvine et al., 1983). The mode of heat transfer at the bottom of the newly intruded liquid will depend on whether emplacement occurred at the immediate floor or some distance above. If the latter, a diffusive interface with very limited exchange of liquid can be expected (op. cit.), whereas conductive heat flow through the floor cumulates will

occur in the first case. No crystallization within the new liquid will occur during this stage, as the liquid is continuously superheated by the overlying B1/B2 hybrid.

Crystallization of the new liquid only commences after its temperature decreases sufficiently for nucleation of the liquidus phase. At this stage heat from the new liquid is lost to the underlying liquid and/or to the cumulate floor. The large volume of hot overlying liquid will keep the top of the new liquid superheated, whereas the underlying cumulate floor will eventually act as a heat-sink. The cumulate pile has a minimum thickness of several hundred meters and a shallow thermal gradient towards the underlying floor sediments is to be expected.

Conductive heat-loss to the underlying floor will thus result in a temperature gradient within the new liquid and hence in the build-up of stable density stratified liquid layers.

The time required for the new liquid to regain its liquidus temperature (liquid is initially heated by the hotter floor) must be proportional to the volume of added liquid. A large amount of cool B2/B3 liquid would reduce the temperature of the underlying cumulate pile relatively faster than a small volume, although the temperature of the liquid will initially increase. Cooling of B2/B3 to its liquidus temperature and hence the first stratigraphic appearance of plagioclase would therefore depend on the actual amount of added liquid. In the investigated drillcore MDH 29 cumulus plagioclase appears about 20 m above the pronounced increase in SrR_o.

XI.2.3. FORMATION OF THE F UNIT

Once the bottom of the new liquid has cooled to its respective liquidus temperature, as outlined above, crystallization begins. The formation of anorthosite (F unit) is then to be expected according to the established crystallization order for a B2/B3 liquid (Sharpe and Irvine, 1983).

Although slumping of B1 material will continue during emplacement of new liquid as well as afterwards, most of its petrological evidence might be obscured by the fact that a B2/B3 melt at its liquidus

temperature is pyroxene-undersaturated which would result in the refusion of pyroxene grains settling into this liquid. The pyroxene component might later crystallize as a postcumulus phase leading to an ophitic texture which is diagnostic for mottled anothosite. In order to explain the large variation of orthopyroxene textures in the F and H units, it is assumed that the relative amount of added pyroxene determines whether pyroxene has an eu- to subhedral, a corroded, or an ophitic sponge-like texture. Settling of only a small amount of pyroxene might result in almost complete resorption of this pyroxene, hence in a postcumulus pyroxene texture, whereas eu- to subhedral pyroxenes would indicate a large amount of added pyroxenes which simply displace the bottom liquid. This process could, in principle, explain the wide range of modal proportions and small-scale modal layering and the considerable change in the makeup of F and H units from place to place along strike.

It is essential for the proposed origin of anorthositic rocks that the B2/B3 liquid remained undersaturated in orthopyroxene. Once the liquid reached the cotectic, textural evidence for the addition of "plume-pyroxenes" has to be derived solely from modal proportions departing considerably from expected cotectic proportions. The sporadic occurrence of anorthositic horizons within the studied sequence above the E/F contact indicates that at least some layers of the B2/B3 liquid remained pyroxene undersaturated and that these layers crystallized without addition of orthopyroxene.

IX.2.4. FORMATION OF MIDDLE GROUP CHROMITITE LAYERS

In contrast to the likely resorption of orthopyroxene, reaction at the convolute boundary surfaces of descending B1 plumes and B2/B3 liquid should result in chromite crystallization, provided the temperature is at or below the liquidus (see Sharpe and Irvine, 1983). The initially random distribution of chromite along the numerous plume/surrounding liquid interfaces and the relative small particle size might result in the detachment of chromite from the descending plumes and in, at least temporarily, retention of chromite in the liquid (Fig. IX.1e). Weinstein et al. (1988) have shown that randomly nucleated particles take

an uncharacteristically long time to settle.

Seeing that chromitite layers in the upper critical zone are generally overlain by pyroxenite or melanorite, it is proposed that "suspended" chromite was finally swept down by a descending front of B1 plumes (Fig. IX.1f). The crystal-laden plumes are thought to act as a semi-permeable membrane filtering out "suspended" particles, while plumes passed through underlying liquid. The sudden drop in SrR_o above the MG 3 (F/G contact) associated with the re-appearence of feldspathic pyroxenite and melanorite would favour such a process. Differences in the thickness of individual chromitite layers might be a function of elapsed time between consecutive slumping events and the proportion of B1 and B2/B3 liquid involved in the mixing process.

The two chromitite layers (MG 1 and MG 2A) just below the F unit probably formed during an early stage of B2/B3 emplacement. The original isotopic properties of the samples hosting the two chromitite layers are uncertain because these samples (319 29, 315 29 and 311 29) were affected by a Rb-rich fluid/liquid (Chpt. X.2). However, a whole-rock sample from the immediate footwall of the MG1 shows a SrR_o of 0.70595 (Sharpe, 1986), indicating that the change towards higher SrR_o's took place prior to the formation of the middle group chromitite layers. The increase in SrR_o to values close to 0.706 can therefore be assumed to fall between sample 330 29 (0.7057) and the MG 1, which represents a maximum vertical distance of 14 m (Fig. VIII.1 and Folder 2). This stratigraphic interval is thought to mark the level at which the B2/B3 liquid was emplaced. It is of particular interest that the amount of cumulus chromite increases significantly about 10 m below the proposed lower level of B2/B3 intrusion and that chromite is an abundant phase up to the E/F boundary.

It is assumed that slumping of B1 material continued after the addition of fresh liquid, thereby forming the upper part of the lower critical zone. The two chromitite layers close to the top of this sequence could possibly indicate short periods during which slumping briefly ceased, to allow "suspended" chromite crystals either to settle on their own, or alternatively, to be swept down by the following slumping cycle.

IX.2.5. FORMATION OF THE G UNIT

The bottom part of the G unit is interpreted to have formed from collapsed B1 material, thereby interrupting the crystallization of anorthosite. It is also proposed that the chromitite layer (MG 3) which separates the F unit anorthosite and the G unit formed during this process, as outlined above.

The increase in SrR_o through the central and upper part of the G unit presumably resulted from a gradual vertical decrease in the amount of initially deposited and subsequently mixed B1 material. An upward decreasing addition of slumped material seems appropriate to explain the observed isotopic trend and the decrease in modal orthopyroxene with stratigraphic height in the G unit. The high SrR_o of the overlying H unit can then be seen as a logical progression of the trend established for the G unit.

IX.2.6. FORMATION OF THE H UNIT

The G/H contact is taken at the level where orthopyroxene becomes a postcumulus phase (Cameron, 1982), although cumulus orthopyroxene reappears at several horizons throughout the H unit. This petrologically rather intriguing feature of alternating intercumulus and cumulus pyroxene could be readily explained by small scale fluctuations in the amount of settled pyroxene, as already outlined for the F unit.

The chromiferous anorthosites and leuconorites of the H unit are thought to have formed by bottom growth from a relatively "uncontaminated" B2/B3 liquid, still undersaturated with respect to orthopyroxene. The occurrence of disseminated chromite and intercumulus orthopyroxene within the unit is explained by an "aftermath" situation where slumping and deposition of B1 material ceased temporarily and a relative stable situation was re-established, leaving the overlying liquid relatively enriched in suspended crystals. Remaining orthopyroxene and chromite crystals are believed to have settled subsequently to the slumping event which gave rise to the G unit. Descending chromite, as a stable phase, equilibrated with the bottom B2/B3 liquid, whereas orthopyroxene, depending on its local - cm scale

- abundance, dissolved and crystallized as an intercumulus phase.
The upper anorthosite of the H unit is occasionally capped by a thin chromitite layer (Chpt. II.4.3) in which case, and only in this case, the overlying J unit starts with a feldspathic pyroxenite instead of a norite. This rock sequence is in principle a repetition of the F/G sequence and would support the idea that chromite is only concentrated in appreciable amounts to form chromitite layers when a front of descending plumes carries a large enough number of pyroxene to filter out suspended chromite.

IX.2.7. FORMATION OF THE J UNIT

The gradual decrease in SrR_o through the J unit can be seen as a gradual decrease in a high SrR_o component (B2/B3). An increasing B1 contribution with stratigraphic height is indicated by the pronounced increase in modal orthopyroxene (see Cameron, 1982 and Chpt. VI.2), which becomes simultaneously more Cr- and Mg-rich. It is proposed that the isotopic and lithological properties of the J unit resulted from a mixing process between the emplaced B2/B3 liquid and the uplifted hybrid layers.
Based on experimental studies on double-diffusive convection (e.g. Linden, 1978), Irvine et al. (1983) argued that finger mixing along a liquid-liquid interface can lead to the development of several new convecting layers. The number of layers depends on the specific physico-chemical properties, such as temperature, density and viscosity of the two liquids. Each convecting layer is separated by a finger interface whereas the former contact between the two liquids becomes a diffusive interface (op. cit.). The development of multiple convecting layers might well explain the overall trend in the J unit.
The characteristic occurrence of abundant feldspar and chromitite patches in the upper J unit, together with the observed macro-slumping features (Chpt. II.4.4), indicate vigorous magma movement and at times chaotic accumulation. The presence of a thin layer of feldspathic pyroxenite with disseminated chromite can be seen as evidence that the formation of the J unit was, at least temporarily, accompanied by minor addition of B1 plumes. Despite the overall increase in modal

pyroxene with height, there is at least one major reversal about 2/3 up the J unit (Chpt. II.4.4) also indicating that the unit as a whole records a complex history. From the provided evidence it seems likely that the formation of the J unit was accompanied by a further influx of B2/B3 liquid. It is suggested that the lithologically and chemically distinct upper J unit formed during and after the emplacement of additional B2/B3 liquid. This further pulse of B2/B3 liquid was presumably emplaced some height above the crystallizing floor causing the observed physical disturbance within the crystal mush and temporarily preventing the descent of B1 plumes.

IX.2.8. FORMATION OF SMALL-SCALE LAYERING IN THE K UNIT

The distinctive microrhythmic layering at the top of the K unit gives the impression of an alternating crystallization from a plagioclase-dominant and a pyroxene-dominant liquid. Similar small-scale layering in the Stillwater Complex (Todd et al., 1982) has been interpreted by Irvine et al. (1983) as marking a former interface between two chemically distinct liquids (A and U liquids). It was further speculated that this liquid/liquid contact developed subsequently into a multi-interface with numerous diffusive boundaries separated by thin convecting layers (op. cit.).

To explain the alternating lithology by a series of pyroxene- and plagioclase dominant liquid layers would require that the two main liquid layers (B2/B3 and B1-rich hybrid) retained their individual chemical properties while building up a density-graded stack of liquid layers. Although such a situation could be accomplished under special circumstances (see Irvine et al., 1983), it would still leave a number of chemical and lithological features unexplained.

Firstly, the individual liquid layers (anorthositic and pyroxenitic) would certainly have different liquidus temperatures which would inhibit a continuous layer by layer crystallization without resulting in further mixing. The limited lateral persistence of the anorthositic and pyroxenitic micro-layers and their sometimes bifurcating and lenticular nature also seems to contradict their formation from a series of density stratified liquid layers.

Secondly, orthopyroxene shows disequilibrium features throughout the J and K units, indicating that the magma was constantly undersaturated in orthopyroxene.
Thirdly, plagioclase separates from feldspar-rich rocks of the K unit do not have an elevated SrR_o relative to the orthopyroxene-rich rocks of the L unit. The possibility that liquid layers equilibrate isotopically without changing their major element characteristics, can not be excluded but would need to be confirmed experimentally.
Although there is no doubt that the J and K units record a gradual transition from an anorthositic, high SrR_o liquid to a pyroxenitic, low SrR_o liquid, the proposed development of multiple convecting layers alone can not adequately explain the small-scale layering. It is therefore postulated that the upper K unit marks the onset of massive crystal/liquid slumping (L unit) initiated by the addition of a B2/B3 liquid to the magma chamber. The typical layering of the L unit footwall might then simply be due to initial fluctuations and a gradual build-up in the amount of descending pyroxenes.
Without any addition of plume-material, the predominantly B2/B3 hybrid liquid should crystallize predominantly plagioclase, because the liquid would have been held at its liquidus temperature.

IX.2.9. FORMATION OF THE L UNIT

The textural and chemical similarity between orthopyroxene from feldspathic pyroxenites in the L unit and those from pyroxene-rich parts in the K unit indicate a common source. Consequently the pyroxene-rich layers in the K unit can be regarded as the precursor of the thick pyroxenitic interval in the L unit, which in turn is attributed to a major collapse of B1 material in response to the further influx of B2/B3 liquid.
The occurrence of abundant chromite and thin chromitite layers within the feldspathic pyroxenites of the L unit is again explained by the interaction of descending B1 plumes with surrounding liquid.
The three melanorite intervals within the L unit which are characteristically chromite-free, possibly record stages where the amount of descending crystals was greatly reduced. Transition from

feldspathic pyroxenite to melanorite is gradual over about one metre and marked by a decrease in orthopyroxene. Simultaneously orthopyroxene loses its eu- to subhedral shape while feldspar becomes a cumulus phase. These features are consistent with the proposed concept whereby the pyroxene texture is determined by the amount of crystals deposited into an orthopyroxene-undersaturated bottom liquid. The fact that chromite occurs predominantly in the lower portion of pyroxene-rich intervals also favours cyclic slumping and mixing. The uniform SrR_o throughout the K and L units is interpreted to reflect the isotopic signature of the bottom liquid, to which various amounts of pyroxenes were added.

IX.2.10. FORMATION OF THE M UNIT

The L - M contact is a rapid (< 2 m) transition from feldspathic pyroxenite to norite. SrR_o of extracted plagioclase is however unchanged up to about 50 m from the base of the M unit. The distinct increase in SrR_o over a vertical distance of less than 20 m is followed by rather uniform values, similar to those from the anorthositic F and G units (Fig. VIII.1).

The M unit shows a repetitive (cyclic ?) variation in lithology (Folder 2 and Chpt. II.4.7). The seven analysed feldspar separates were selected from the three principle types of rocks i.e. gabbronorite, leuconorite-leucogabbronorite and very fine grained gabbronorite. No systematic correlation exists between the modal amount of plagioclase or the relative grain size of an individual sample and the isotopic ratio. However, the averaged lower part of the M unit ($SrR_o < 0.7059$) contains more pyroxene than the remainder of the unit ($SrR_o > 0.7061$), as well as higher whole-rock Cr abundance and higher Cr concentrations in the orthopyroxene, which increase from about 800 ppm in the upper part of the M unit to about 1500 ppm in the basal part (Folder 2).

A shift in magma composition during crystallization of the M unit is also recorded by the first appearance of cumulus clinopyroxene (Chpt. II.4.7), which coincides with the increase in SrR_o.

Prior to the M unit, clinopyroxene occurs exclusively as large eu- to subhedral oikocrysts, as anhedral intercumulus aggregates and as small

underlying rocks (10-28 wt % Al_2O_3; 15-2200 ppm Cr; Mg# 79.6-84.6; An 73-78).

The mineral, bulk-chemical and Sr-isotope data seem to support the field relations, which indicate that the very fine grained gabbronorites are an integral part of the M unit despite their unusually fine-grained texture and the abundant occurrence of inverted pigeonite and clinopyroxene. These features are possibly related to a periodic change in the magmatic system. It is speculated that either a drop in temperature or a slight shift in magma composition caused the liquid to crystallize plagioclase, pigeonite and clinopyroxene simultaneously. This is based on the assumption that plagioclase was the first crystallizing phase throughout the M unit, as evidenced by the either resorbed or intercumulus texture of orthopyroxene. It was already argued that the B2 liquid is constantly held near its liqidus temperature by the overlying hotter B1 liquid. It seems quite possible that, during a state of slow crystallization, sufficient heat is lost conductively through the underlying crystal pile to allow the temperature of the bottom liquid to reach the plg-opx-cpx cotectic at 1190°C (Sharpe and Irvine, 1983).

Seeing that the mineral assemblage of the gabbronorite (about 3:2:1 plg:cpx:opx) agrees well with the expected proportions of a tholeiitic (B2/B3) melt (op. cit.), it is concluded that fine grained gabbronorites in the M unit formed during a state of "supercooling", possibly caused by the slow crystallization of the underlying mottled gabbronorite, and that they are genuine cotectic cumulates of a B2/B3 liquid. The very fine grained texture must then be related to spontaneous and simultaneous nucleation of the three minerals from the supercooled liquid layer.

IX.3. SUMMARY

Sr-isotope data and lithological variations were synthesized into a model involving replenishment of the chamber by a B2/B3 liquid and the periodic collapse of crystal-bearing plumes from an overlying B1 liquid layer. The contrasting physico-chemical properties of a dense and cool B2/B3 liquid and a light and hot B1 liquid are suited to promote supercooling and hence crystallization in the B1 liquid, while the underlying B2/B3 liquid is initially superheated and therefore unable to crystallize. It is believed that the stratigraphic sequence up to the E/F boundary formed by continuous addition of crystal-liquid plumes into the superheated B2/B3 liquid, leading to the massive feldspathic pyroxenites of the lower critical zone. During this stage a downward increasing proportion of evolved B1 liquid, which formed as a result of continuous orthopyroxene crystallization within the plumes, was mixed with surrounding B2 liquid giving rise to a series of hybrid layers.

This scenario was interrupted by an intermittent influx of B2 or B3 liquid which spread out close to the bottom, thereby uplifting the resident B1-rich hybrid liquid layers. The various lithological units of the basal upper critical zone are explained by a combination of a crystallizing bottom liquid and the addition of plume-orthopyroxenes which settled into this liquid. Variations in the modal proportions are entirely attributed to different amounts of pyroxene added to a predominantly plagioclase crystallizing bottom liquid (B2/B3).

The re-appearance of feldspathic pyroxenites and chromitites in the L unit is attributed to a further influx of B2/B3 liquid which resulted in a major collapse of B1 material. Crystallization of the newly emplaced liquid without any major addition of B1 material gave subsequently rise to the leucocratic clinopyroxene-bearing rocks of the M unit.

The positive correlation between SrR_o and the modal amount of plagioclase (Fig. IX.2) indicates that variations in modal proportion are due to different degrees of hybridisation of two liquids and are not caused by changes of the intensive parameters in the magmatic system (e.g. temperature, pressure, fo_2) or the result of progressive fractionation or crystallization from one parental liquid around the

spinel-bronzite-plagioclase stability fields.

Formation of chromite is explained by the interaction of B1 derived plumes with surrounding B2/B3 liquid. Detachment of chromite from descending plumes could lead to a situation where the latter is temporarily retained within the liquid. Slow gravitative settling of suspended particles or forceful down-sweeping by succeeding plumes is thought to result in the formation of chromitite layers.

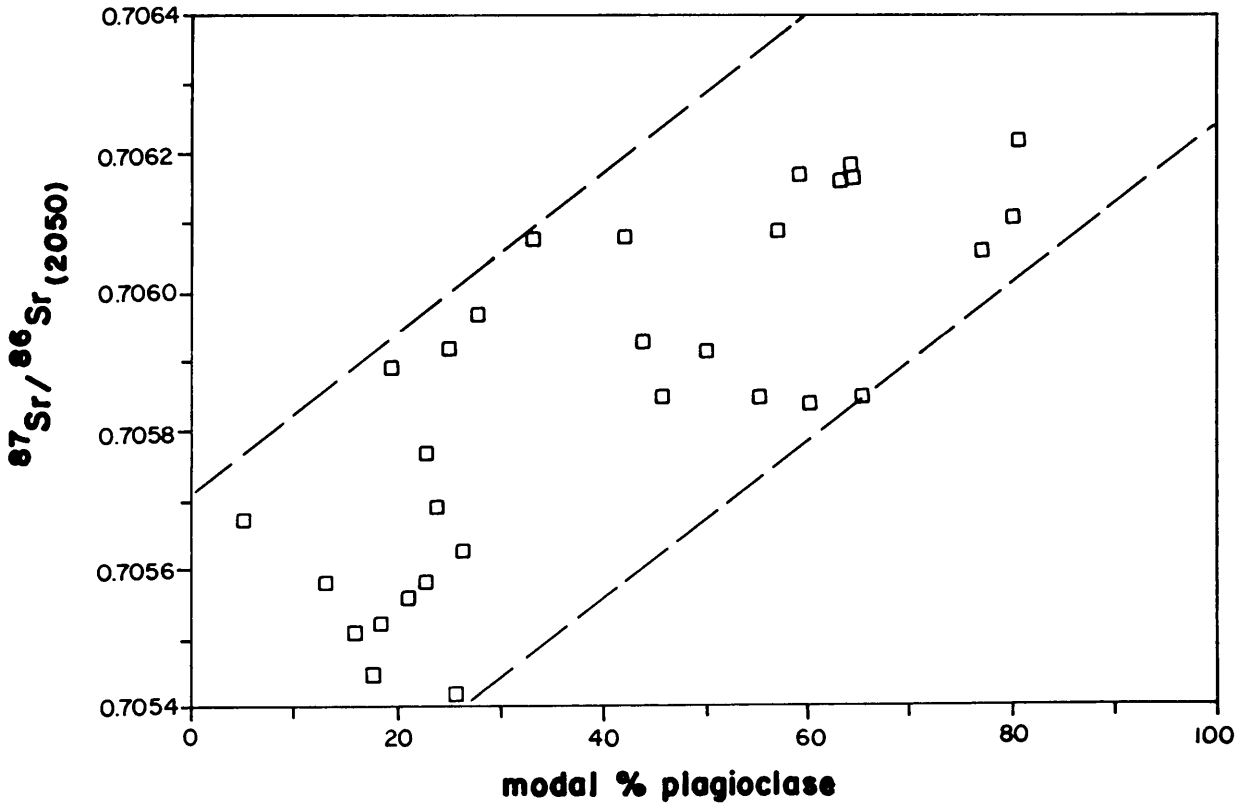

Figure IX.2: Initial $^{87}Sr/^{86}Sr$ ratio versus modal amount of plagioclase for each sample. Isotopic ratios were determined from plagioclase separates. Data from high An and high Rb plagioclase separates are excluded. Initial ratio shows a broad positive correlation with the amount of plagioclase. In other words, plagioclase from pyroxene-rich samples have a lower initial ratio than those from feldspar-rich rocks.

CHAPTER X: COMPOSITIONAL FEATURES AND SR ISOTOPE SYSTEMATICS OF CHEMICALLY ALTERED SEQUENCES

X.1. MINERAL-CHEMICAL FEATURES

Several geochemically anomalous layers have been intersected in boreholes MDH 29 and 23. The most obvious evidence for the interaction of pegmatitic fluids and presumably pre-existing cumulus minerals exists in drillcore MDH 23. Chemically altered rocks were intersected in this borehole within two stratigraphic intervals, viz. the upper E to lower J unit (Figs. V.6 and VI.1) and the upper K to lower M unit (Fig. X.1), each interval having a vertical thickness of about 50 metres. The K-M interval is erratically affected, while rocks of the E-J sequence appear to be uniformly altered. Coarse-grained pegmatitic textures are extremely rare and occur in less than 1 % of the chemically altered rocks. It must be stressed that the particular lithological properties (modal proportion) within and between individual units are not affected, despite the pronounced change in mineral chemistry. In other words all units are present in their characteristic mineralogical make-up.

For comparison both chemically affected intervals in MDH 23 have also been investigated from drillcores MDH 22 and MDH 1 which intersected chemically "normal" sequences. The composition of cumulus orthopyroxene and plagioclase as well as intercumulus plagioclase of the E unit deviates as follows from the normal, unaltered succession:

Plagioclase is invariably more calcic and cores of individual grains have an An content of up to 97. Their K content is accordingly low (< 0.05 wt % K_2O). The Fe content of plagioclase from the E-J interval is lower compared to the "normal" stratigraphic sequence in boreholes MDH 29 and MDH 1 (Table X.1). Plagioclase enclosed in orthopyroxene has a similar high An content as non-enclosed feldspar.

A comparison of normal and chemically altered plagioclase composition from the K-M interval is presented in Table X.1, whilst Figure X.1 shows the selective manner in which individual horizons are affected. Although plagioclase composition is increased by up to 20 An units in

individual samples, the bulk of the K-M interval is less affected than the E-J interval. Plagioclase in the K-M interval shows a relative moderated bulk increase in An content by about 7 An units relative to the increase in the E-J interval, where the shift in composition is more than 15 An units (Table X.1).

Orthopyroxene from the E-J interval are more magnesium-rich with a maximum Mg# of orthopyroxene from chromite-free rocks of about 84. Orthopyroxene is depleted in Ti and enriched in Cr and Al, while no change is found in the Ca content (Table. X.1).

The most orthopyroxene grains analyzed in the K-L succession appear not to have undergone a change in composition (Fig. X.1), despite the change in plagioclase composition.

To evaluate an increase in the Mg# of orthopyroxene in the L unit is difficult, as samples contain various amounts of chromite, which also results in an increase in Mg# (Chpt. V.4). Furthermore, plagioclase constitutes less than 10 modal % in the feldspathic pyroxenites of the L unit, which show a maximum shift in feldspar composition. The relatively small volume of plagioclase might thus explain the apparent discrepancy between orthopyroxene and plagioclase composition, assuming that the compositional shift in a particular mineral phase is controlled by the relative modal abundance of the mineral.

Plagioclase appears to be more sensitive to the effects of percolating fluids than orthopyroxene. The relative shift in composition is most likely the result of the specific properties and quantities of the fluid. A comparison of the E-J interval between the three boreholes (Fig. VI.1) clearly shows that the composition of individual plagioclase has shifted uniformly relative to the "normal" composition. The original cryptic variation within this stratigraphic interval is therefore preserved, as all samples seem to have shifted by the same margin. This is true whether plagioclase occurs in an almost pure anorthosite (top of F unit and H unit), in norite (J unit) or melanorite (G unit) or even in feldspathic pyroxenite (top of E unit). The fact that plagioclase rims are more calcic than their cores indicates that re-equilibration was not complete. The attained core composition can therefore not be regarded as an ultimate equilibrium composition.

Table X .1: Comparison of plagioclase and orthopyroxene compositions for "normal" and chemically altered rocks from two stratigraphic intervals (E - J units and K - M units).

Plagioclase from E - J interval	"normal"		altered
	MDH 29 (n = 33)	MDH 1 (n = 26)	MDH 23 (n = 15)
An %	71.6 +- 3.5	70.0 +- 4.5	87.0 +- 1.8
K_2O	0.22 +- 0.03	0.23 +- 0.05	0.03 +- 0.01
FeO	0.22 +- 0.04	0.21 +- 0.03	0.12 +- 0.03

Plagioclase from K - M interval	MDH 22 (n = 21)	MDH 23 (n = 22)
An %	69.9 +- 5.2	76.5 +- 5.6
K_2O	0.22 +- 0.09	0.13 +- 0.07
FeO	0.19 +- 0.05	0.18 +- 0.05

Orthopyroxene from E - J interval	"normal"		altered
	MDH 29 (n = 32)	MDH 1 (n = 25)	MDH 23 (n = 16)
Mg#	78.0 +- 2.0	78.0 +- 1.5	83.5 +- 2.3
Al_2O_3	1.03 +- 0.09	1.00 +- 0.08	1.43 +- 0.11
CaO	1.03 +- 0.26	1.10 +- 0.25	1.21 +- 0.30
Cr_2O_3	0.41 +- 0.05	0.39 +- 0.04	0.48 +- 0.05
TiO_2	0.17 +- 0.03	0.17 +- 0.02	0.08 +- 0.03

Orthopyroxene from K - M interval	MDH 22 (n = 21)	MDH 23 (n = 22)
Mg#	79.7 +- 2.2	79.7 +- 1.5
Al_2O_3	1.06 +- 0.12	1.20 +- 0.16
CaO	1.30 +- 0.28	1.23 +- 0.23
Cr_2O_3	0.42 +- 0.04	0.43 +- 0.03
TiO_2	0.12 +- 0.03	0.12 +- 0.02

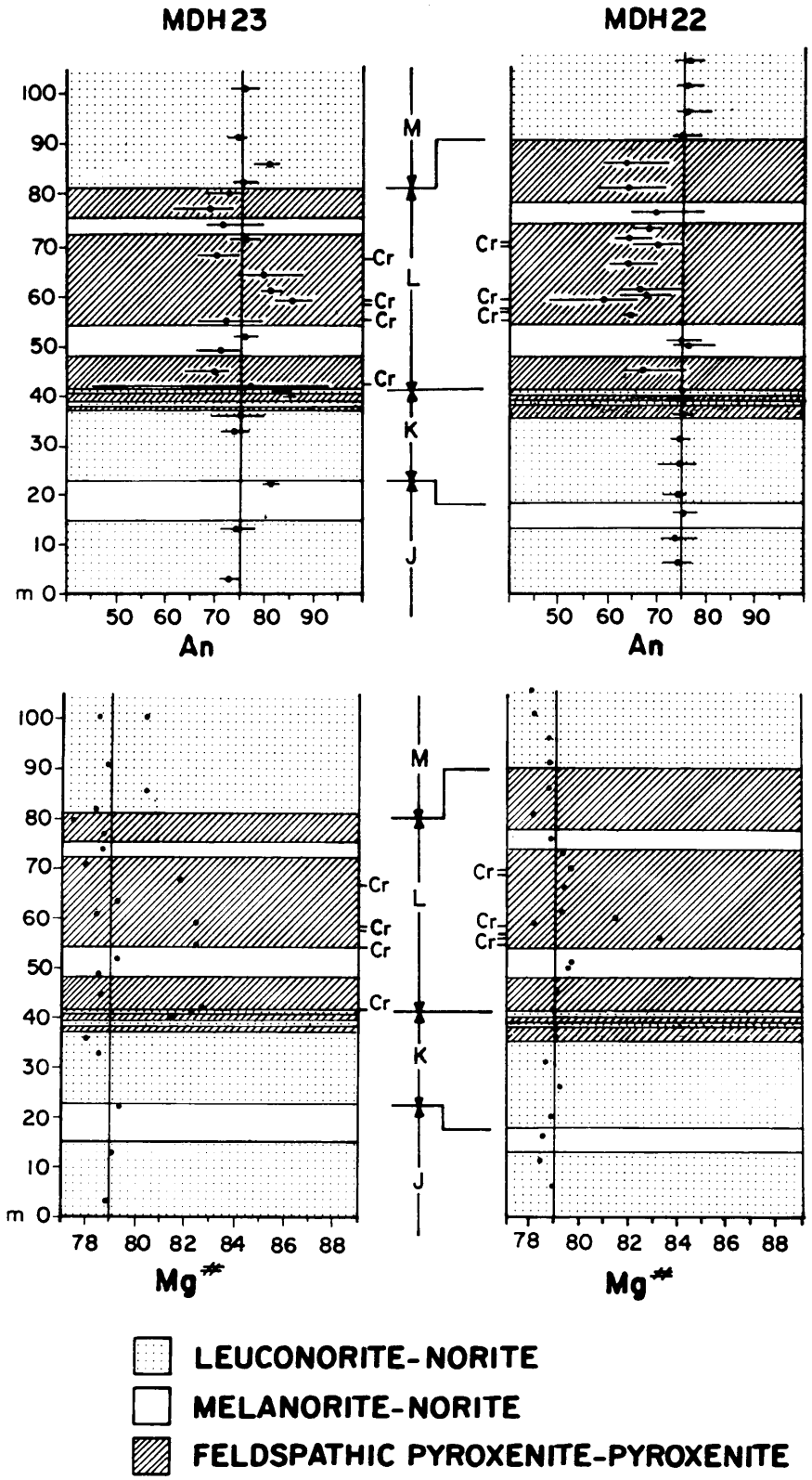

Figure X .1: Comparison of the chemically altered sequence in drill-core MDH 23 with a "normal" sequence from MDH 22. Plagioclase shows an increase in An content relative to feldspar from a normal sample. Orthopyroxene, in contrast, shows no compositional shift. High Mg# in the L unit invariably occur in orthopyroxene from chromite-rich samples.

The shift in orthopyroxene composition over the E-J interval is less uniform (Fig. V.6) compared to the change in plagioclase composition. Orthopyroxene from the middle portion of the G unit appears to be almost unaltered with respect to its Mg#. The degree of alteration is not related to modal variations. The decoupling of plagioclase and pyroxene compositions could possibly indicate that chemical alteration occurred as a series of individual events. Each phase might have selectively affected individual horizons and various phases in a different manner.

X.1.1. PROPOSED ORIGIN OF CHEMICALLY ALTERED SEQUENCES

Little doubt exists over the involvement of an aqueous fluid in order to explain the shift towards more calcic plagioclase compositions. Dymek and Schiffries (1987) have recently emphasized the effects of water on magmatic plagioclase. Based on the ternary system An-Ab-H_2O they illustrated that under isothermal conditions the composition of plagioclase becomes progressively more calcic as the water content of the magma increases. The simultaneous lowering of the plagioclase liquidus in response to an increase in water pressure is prompted by a more calcic plagioclase composition. Similarly, calcium-rich myrmekitic rims have been explained by corrosive interaction of early formed crystals with a high-temperature hydrous fluid (Chpt. VI.1). The relatively small volume of myrmekites can be attributed to the late stage of interaction between cumulates and aqueous fluids.
The observed shift towards more magnesium-rich pyroxene is explained by the same principle; the addition of water resulted in a pyroxene composition equivalent to a higher crystallization temperature. The dissociation of water in silicate melts as both molecular water and hydroxyl groups (Hamilton et al., 1964; Mysen et al., 1980; Stolper, 1982) will increase the f_{O_2} if P_{H_2O} is high (Burnham, 1979). Speidel and Osborn (1967) have shown that relative increases in f_{O_2} result in an enrichment in the magnesium component of pyroxene and olivine.
Kushiro (1969) showed for the forsterite-diopside-silica system that the stability field of forsterite increases with an increase in water pressure. The occasional presence of olivine in the anomalous E-J

interval, both interstitial as well as replacing orthopyroxene (Plate 4.F), could so be explained. The increase in the stability field of olivine under hydrous conditions has been seen as evidence for a lowered Si activity. A decrease in the Si activity seems to be consistent with the considerably higher Al and Cr concentrations in orthopyroxenes (Table X.1) from the E-J interval, as the substitution of Al^{3+} for tetrahedral Si^{4+} creates a charge balance that enables the entry of Cr^{3+} into octahedral sites. The relationship between decreasing Si activity and increasing Al^{3+} in pyroxene has been established amongst others by Carmichael et al. (1970) and Campbell and Borley (1974).

Based on petrological and mineral-chemical evidence, there seems to be good evidence that the observed mineral compositions originated from the addition of water to the crystallizing system. The relatively uniform plagioclase composition in the E-J interval, including that of the enclosed plagioclase, suggests that introduction of water took place at a relatively early stage during crystallization. The chemically anomalous E-J interval might therefore be the result of a locally water-enriched melt rather than a late replacement product (pegmatite) of an already semi-consolidated crystal mush.

A similar origin is proposed for the upper E - lower G interval intersected in drillcore MDH 29. Evidence for the introduction of a fluid phase is presented by the microscopic intergrowth and partial replacement of early formed plagioclase by highly evolved material. The intergrowth typically consists of K-feldspar, quartz, phlogopite and traces of sulphides (Plate 4.G). K-feldspar also occurs as thin rims around calcic cumulus plagioclase (An 70), which appear to be partially resorbed (Plate 4.H). The mode of occurrence of K-feldspar differs from that found in lower critical zone samples with a strongly evolved interstitial assemblage. In the latter, K-feldspar occurs as a separate interstitial phase which is invariably associated with sodic (An < 50) intercumulus plagioclase, quartz and phlogopite.

The presence of evolved phases in the E-G interval appears not to be related to in-situ fractionation of trapped liquid, but resulted from migration of late, fractionated fluids. The fact that at least some of these samples are enriched in ^{87}Sr (see Chpt. X.2) suggests a source

of possibly sedimentary origin. Higher ^{87}Sr concentrations were also found in several samples from borehole MDH 23 in the F unit and the K-M interval.

X.2. SR ISOTOPE SYSTEMATICS OF CHEMICALLY ALTERED SEQUENCES

X.2.1. SR ISOTOPES OF UNUSUALLY CALCIC (HIGH AN) PLAGIOCLASE SEPARATES

The aberrant high SrR_o values of 3 samples from the K and L units of borehole MDH 23 (Fig. VIII.1) are most probably caused by a secondary metasomatic process. Macroscopically, none of the 3 samples differ in texture from closely associated rocks. The plagioclase however, has a considerably higher An content when compared to rocks from stratigraphically comparable positions (Chpt. X.1). Included in this discussion is sample 465 from the F unit anorthosite of borehole MDH 23 (Fig. VIII.1), as it is also part of a sequence characterized by an anomalously high (An 89) An content (Chpt. X.1). It is of particular interest that rocks within the E-J sequence in borehole MDH 23 are occasionally very coarse grained, have a typical pegmatoidal texture and contain plagioclases with identically high An contents.

The generally extremely low Rb concentrations (0.09 - 0.19 ppm) found in the high An samples are consistent with the low abundance of other incompatible elements in these rocks, such as Na and K. The relatively "high" Rb concentration of 1.14 ppm in sample 284 23 from the L unit is most likely due to minor impurities, as this sample was separated from an almost pure pyroxenite (modal plag < 3 %).

The positive correlation between the relative shift towards higher An content and the increase in SrR_o (Fig. X.2) shows that the two features are genetically linked and indicates varying degrees of alteration. It is assumed that those plagioclase grains within a sequence of high An values which show no change in their An content relative to samples from a "normal" sequence (MDH 22), have not changed their original SrR_o ratios.

Plagioclase from sample 465 23 (F unit anorthosite) shows an increased An content of about 10 relative to plagioclase from the same lithological horizon in borehole MDH 1 (Fig. VI.1). An increase of 10 mol % An, according to Figure X.2, corresponds to an increase in SrR_o of about 0.0003. The original SrR_o of sample 465 23 is therefore estimated to be about 0.7060, which is identical with the value of sample 289 29 which is from a "normal" F unit anorthosite (Fig. VIII.1 and Table VIII.1).

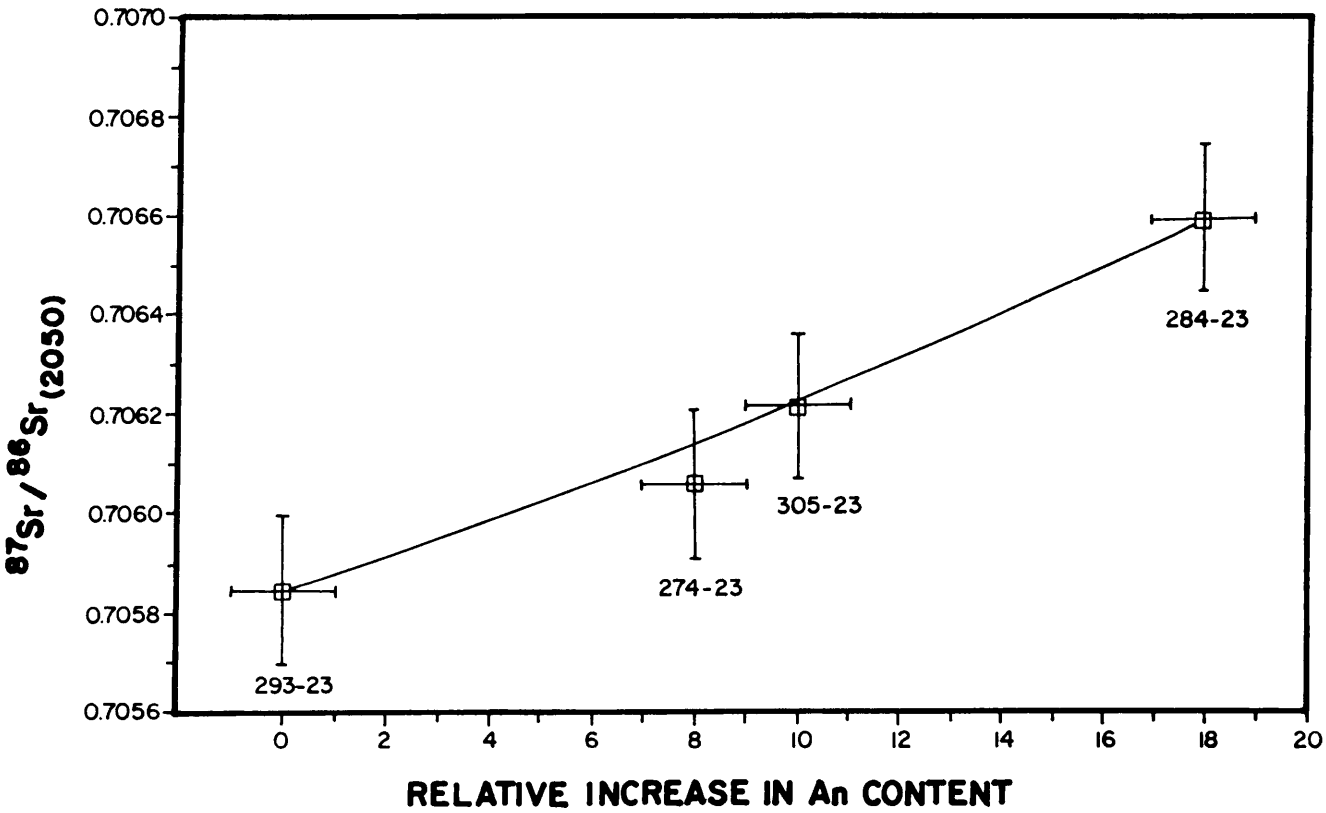

Figure X.2: Initial $^{87}Sr/^{86}Sr$ ratio versus shift (increase) in the An content relative to the An content of chemically unaltered plagioclase (293 23). The stratigraphic position of the samples is shown in Table VIII.1. Mixing line is calculated after Langmuir et al. (1978).

The limited range in An content in compositionally altered plagioclase suggests that plagioclase completely recrystallized during isotopical and chemical equilibration with the metasomatic fluids. However, the fact that plagioclase enclosed in orthopyroxene has equally high An values indicates an early interaction between these metasomatizing fluids and the crystallizing magma.

Similarly, Barton et al. (1986) related the unusually high SrR_o's of the Platreef to a local contamination by a melt derived from the underlying granite. The erratic and local occurrence of high An and high SrR_o plagioclase in the K-M interval indicate that migrating fluids affected the crystallizing pile selectively on a metre scale, which is also evident from plagioclase in MDH 23 which shows changes in An content and isotopic ratio over a vertical distance of less than 5 metres. To evaluate if other phases, such as clinopyroxene and mica, were affected as well would require further research.

The observed increase in SrR_o to values up to 0.7066 requires these fluids to be relatively enriched in ^{87}Sr. A genetic link with liquids parental to the layered sequence up to the L unit seems therefore unlikely. Clearly, the accumulation and subsequent post-cumulus processes of rocks with a relatively low SrR_o (< 0.7062) cannot lead to a late stage fluid/liquid with SrR_o's higher than the actual cumulate. It is therefore proposed that high SrR_o fluids were derived either directly from the sedimentary floor rocks or from sedimentary fragments incorporated in the magma. Hunter and Hamilton (1978) show that, at 2050 million years, the shales and limestones of the Transvaal Supergroup had initial ratios of 0.708 to 0.723. Degassing or assimilation of these sediments could explain the origin of a fluid phase and its isotopical signature.

X.2.2. SR ISOTOPES OF RB-RICH SEPARATES

Six plagioclase separates across the E-F-G interval in borehole MDH 29 have unusually high Rb concentrations (16-57 ppm Rb) and markedly lower Sr values (295-421 ppm Sr) relative to two separates within this 40 m thick succession which show "normal" Rb and Sr concentrations (Table VIII.1). One of these two samples (306 29: 9 ppm Rb; 445 ppm Sr) is from a melanorite from the lower part of the F unit; the other

one (289 29: 3 ppm Rb; 478 ppm Sr) was extracted from a chromiferous anorthosite with intercumulus orthopyroxene.

Unlike the aberrant plagioclase (high An and SrR_o) of the K-L-M interval, none of the high Rb plagioclase seem to have undergone a change in their major element concentrations. The analyzed An contents correspond well with published data (Cameron, 1982) and results from borehole MDH 1 covering the same stratigraphic sequence (Fig. VI.1). However, as none of the plagioclase in borehole MDH 1 was analysed for Sr and Rb it cannot be excluded that high Rb concentrations are inherent to this particular interval. The only whole-rock sample from the Rb-rich sequence in the studied borehole MDH 29 which was analysed for Sr-isotopes also revealed an elevated Rb concentration of 12 ppm. The only other known whole-rock sample from the same stratigraphic succession which was analysed for Rb and Sr has a Rb concentration of 1.6 ppm (Sharpe, unpublished data from MDH 22). It is therefore assumed that the high Rb values were caused by a secondary, late to post magmatic process.

The possibility that K-feldspar and hence Rb concentrated in the plagioclase separates seems likely, because accessory K-feldspar is present in small amounts (< 0.2 modal %) in three (319 29, 311 29 and 300 29) of the six analysed rock samples. However, K-feldspar enrichment during magnetic separation must have been relatively low as evidenced by moderate (8 ppm) Rb concentration in plagioclase separate 353 29, which was extracted from the sample with the highest modal K-feldspar abundance (1.2 %). The high modal amount of quartz (4.8 %) relative to plagioclase (2.8 %) in this particular sample (353 29) is expected to have a considerable diluting effect in the "plagioclase" separate. The actual Rb concentration of plagioclase from sample 353 29, which has an average An content of 35, is therefore not known. Considering the low An content of plagioclase, indicating severe melt fractionation, it seems reasonable to assume that all analysed Rb in plagioclase separate 353 29 is hosted by plagioclase and that no K-feldspar is present.

Thus, to explain the high Rb values in separates from relatively K-feldspar-poor samples on the one hand, and the low Rb values in separates from relatively K-feldspar-rich samples on the other hand, it is suggested that the particular mode of occurrence of K-feldspar

determines whether K-feldspar is present in a separate or not. In the case of sample 353 29, where K-feldspar occurs as an individual interstitial phase, the latter will not be present in the separate, while in the high Rb samples, where K-feldspar occurs as an intergrowth with plagioclase or as thin rims around plagioclase (Chpt. X.1.1 and Plate 4.G-H), K-feldspar will invariably be present in the separate.

Although the calculated SrR_o's of Rb-rich separates show an enormous range from 0.7052 to 0.7071, thereby effectively expanding the compositional field defined by "normal" samples, the SrR_o values do not depart from the established isotopic trend across the E-F-G interval. This means that up to the F/G boundary increasingly higher values predominate (0.7055-0.7071) whilst in the lowermost part of the G unit a drop to a SrR_o value of only 0.7052 is encountered (Fig. VIII.1).

Both the maximum (0.7071) and minimum value (0.7052) of Rb-rich separates fall within the SrR_o ranges of the proposed B2/B3 and B1 parental liquids (Harmer and Sharpe, 1985). The unusual mode of occurrence of K-feldspar in samples from Rb-rich separates, however, which partially replaces or surrounds early formed, calcic plagioclase, cannot be a primary magmatic feature.

No explanation other than a late-magmatic addition of a fluid enriched in incompatible elements seems acceptable. The isotopic properties of this fluid and the chemical process by which the cumulate rocks were selectively affected, are however uncertain. The inconsistent isotopic behaviour of Rb-rich samples is particularly intriguing and quite different to the trend observed in the metasomatically altered rocks of the K-L-M sequence which show a systematic increase in SrR_o.

It is important to note that the unusually high SrR_o values of samples from the Platreef are accompanied by high Rb contents (Barton et. al., 1986). A plagioclase separate from the Platreef contains a Rb content of 60.2 ppm (op. cit.) which is remarkably similar to the concentrations of 57.4 and 54.1 ppm found in the two separates 300 29 and 311 29 respectively, which have aberrant high initial $^{87}Sr/^{86}Sr$ ratios. The combination of high SrR_o and high Rb in these two samples is consistent with the proposed addition of a presumably sedimentary derived fluid. The shales and marls of the underlying Vermont and Nederhorst formations (see Button, 1976) are both rich in Rb and ^{87}Sr. As already discussed, degassing of the sedimentary floor itself or

assimilation of detached fragments can explain the generation of a fluid phase. The complex interaction of sedimentary xenoliths and Bushveld magma and the likely formation of large amounts of sedimentary derived fluids have been qualitatively documented by Wallmach (1988).

The contamination event itself seems to be unrelated to the crystallization of the E-G sequence as evidenced by the extremely heterogeneous occurrence of altered rocks. The two drastically altered samples (300 29 and 311 29) are separated by a horizon (306 29) which seems to be isotopically and chemically (Sr and Rb) unaffected, even though the three samples are only about 6 m apart.

The fact that four samples show no increase in their SrR_o's despite elevated Rb contents of 16.4 to 19.2 ppm could possibly indicate a percolating fluid selectively depleted in trace elements. Sr is more compatible in plagioclase than Rb (Iiyama, 1968; McKay and Weill, 1977), although K-feldspar is also a better solvent for Sr than for Rb (Long, 1978). Fractionation of such a fluid could therefore lead to an enrichment in Rb relative to Sr. The isotopic effect of a migrating fluid on the original isotopic ratios of the cumulates could therefore decrease as a function of Sr depletion within the fluid. The relatively low Sr concentrations in plagioclase from Rb-rich samples (Table VIII.1) seems to indicate that the fluid was relatively depleted in Sr compared to the already crystallized plagioclase. Sr depletion in plagioclase is more severe in the two separates 300 29 and 311 29 which show a drastic increase in SrRo and Rb. One could therefore assume that these samples reacted (re-equilibrated) either over a longer period and/or with a larger amount of fluid. The latter presumably had a low total Sr concentration but a high ^{87}Sr component and high Rb abundance.

It is quite feasible that percolating sediment-derived fluids change their particular chemical potential, presumably as a function of their temperature and volatile content, or simply by becoming gradually absorbed or mixed in with "autogenic" magmatically derived phases. The alternative possibility that the various types of underlying sediment generated chemically and isotopically different fluids awaits confirmation from future studies.

X.3. SUMMARY

Involvement of presumably sedimentary derived fluids seems to be the cause for a variety of textural and geochemical features in the cumulate sequence. It has been shown that an early addition of volatiles can lead to a change in melt parameters resulting in more primitive mineral compositions (Ca- and Mg-rich). A more evolved state of fluid composition can cause the partial replacement of cumulate minerals and the precipitation of highly fractionated phases. Although the two features, viz. calcic plagioclase and the presence of K-feldspar are chemically opposed, they are both caused by the addition and interaction of hydrous fluids.

In the field these features are extremely difficult to recognise due to the almost complete absence of pegmatitic textures. Migration and interaction of hydrous fluids might therefore be much more common in the cumulates than indicated by the relatively small volume of pegmatites and pegmatoidal layers.

The fact that chemically altered horizons are closely associated with chromite-rich intervals (F-G and K-L) could either be caused by the heterogeneous lithology of these sequences which might enhance selective trapping of migrating fluids, or by a locally increased amount of xenoliths which were subsequently partially or even completely assimilated by the Bushveld magma. The latter possibility seems likely as both horizons (F-G and K-L) coincide approximately with stratigraphic levels for which intermittent influxes of new liquid have been postulated (Sharpe, 1985 and Chpt. IX). It is quite possible that sedimentary fragments were rafted off during magma replenishment and were subsequently incorporated and devolatilized. Alternatively, intermittent injection of magma could have led to further tectonic deformation of floor rocks, whereby subjacent sedimentary horizons became exposed to higher temperature regimes. Slow degassing through the already consolidated cumulate pile and channelling of migrating fluids towards the crystallizing interface could set up pathways with a large but finite volatile supply. The relatively sharp lower and upper contacts of the altered E - J sequence would favour the former scenario.

CHAPTER XI: SUMMARY AND CONCLUSIONS

The transition from the lower to the upper critical zone and associated rocks (LG 6 - UG 1) has been investigated geochemically and petrographically. The main object was to identify and quantify physical and chemical processes within a crystallizing magma chamber and to relate the compositional and textural features of silicates to the various effects of these processes. The investigated sequence is explained by a scheme of stratified hybrid layers and a combination of crystal/liquid slumping and crystallization of the bottom liquid.

Intermittent magma influxes occurred prior to the formation of the LG 6, the F and the L units. It is proposed that the addition of relatively cool and dense tholeiitic liquid (B2/B3) initiated the collapse of orthopyroxene-bearing plumes from the overlying hot and less dense boninitic liquid (B1). The formation of chromite is attributed to a reaction process between the two chemically distinct liquids during the descent of crystal-laden boninitic plumes.

Whole rock incompatible trace element data confirm that B1 and B2 liquids are likely parental liquids to the lower critical zone. This is substantiated by isotope data which show that the initial $^{87}Sr/^{86}Sr$ ratios of cumulates of the D_2 and E units are within the expected range of B1/B2 mixtures. Systematic changes in the initial ratio in the upper critical zone are attributed to different amounts of B1 material mixed with the bottom liquid (B2/B3). Mixing occurred either by two-phase convection (crystal/liquid slumping) or by double-diffusive mixing between liquid layers.

Variations in mineral chemistry have been explained by changes in magma composition and by a series of postcumulus processes. Primary changes in orthopyroxene composition were found at the stratigraphic position of the LG 6 chromitite layer, across the lower/upper critical zone boundary and within the M unit. The observed changes in Mg# were attributed to magma addition and a subsequent change in melt composition. A change in liquid composition at the E/F boundary and within the M unit is also confirmed by significant changes in Cr and Ti concentrations in orthopyroxene.

Additional to primary variations, orthopyroxene compositions were substantially modified by reaction with surrounding hybrid liquid. Disequilibrium conditions between liquid and settled orthopyroxene increases with the degree of interstitial melt fractionation. This resulted in complex crystal zoning patterns. Orthopyroxene zoning developed according to the diffusion rates of individual elements. At magmatic temperatures Mg-Fe diffusion is by far the most rapid, followed by Ti which has a slightly higher diffusion rate than Cr and Al. Ca has the lowest diffusion rate.

The peculiar zoning pattern for Ti in orthopyroxene, characterized by an initial increase followed by a decrease, records a stepwise change in interstitial liquid composition due to the appearance of new mineral phases, such as clinopyroxene and phlogopite. Thus, re-equilibration between cumulus orthopyroxene and surrounding interstitial liquid must have proceeded until late in the magmatic history.

Subliquidus and subsolidus re-equilibration between orthopyroxene and chromite led to an increase in Mg* and Al in orthopyroxene. The shift in Mg* has been shown to be a function of the modal amount of chromite. A correction method has been developed with the aid of which the Mg* of orthopyroxene prior to the effects of trapped liquid and chromite can be calculated.

Plagioclase shows little compositional variation throughout the upper critical zone where it is a cumulus phase. The considerable range in An content in the feldspathic pyroxenites from the lower critical zone is attributed to interstitial liquid fractionation. It is believed that crystal/liquid slumping resulted in the build-up of a thick porous pile of orthopyroxene grains. Plagioclase crystallization from porous liquid proceeded in such a manner that individual layers crystallized while the residual melt in the pile immediately above became progressively more fractionated. This process resulted in the formation of several crystallization fronts. Extreme fractionation of trapped liquid is indicated in several layers. The latter contain a felsic intercumulus assemblage of quartz, phlogopite, sodic plagioclase and K-feldspar with accessory rutile, loveringite, apatite and anhydrite.

Clinopyroxene oikocrysts occur almost throughout the lower critical zone but are less abundant in the investigated portion of the upper

critical zone. The latter presumably formed at relatively low temperatures by partial replacement of plagioclase and orthopyroxene. Clinopyroxene oikocrysts characteristically enclose numerous corroded orthopyroxenes which are invariably compositionally changed due to two-pyroxene re-equilibration.

Abundant cumulus clinopyroxene first occurs in the M unit, although clinopyroxene is found in accessory amounts in a thin layer of the K unit. Its presence together with the occurrence of inverted pigeonite is seen as evidence for a change in magma composition in response to an intermittent influx of tholeiitic liquid (B3).

Orthopyroxene shows several textural changes associated with the first occurrence of cumulus plagioclase at the E/F boundary. Firstly, the grain size is markedly reduced in upper critical zone rocks. Secondly, orthopyroxene from the upper critical zone contains numerous tiny inclusions of plagioclase and has generally more evenly shaped crystal faces. A systematic transition towards anhedral (intercumulus) textures is found in the leucocratic F and H units and is associated with an increase in modal plagioclase. The latter is explained by the fact that orthopyroxene, added by crystal slumping, is not a stable liquidus phase in a relatively pure B2/B3 liquid. An intermittent influx of B2/B3 liquid at this stratigraphic level has already been documented.

The presence of plagioclase inclusions in orthopyroxene is explained similarly by the specific phase relations of orthopyroxene-undersaturated liquids (B2/B3) which crystallize plagioclase prior to pyroxene. However, hybridisation of B2/B3 liquid by B1 material (crystal and liquid) is indicated by the high modal amount of orthopyroxene which is typical for the G and J units of the basal upper critical zone.

The drillcores investigated show a systematic variation in the thickness of individual stratigraphic units. An increase in thickness is found along strike in a northerly direction and down-dip (east-west). A comparison with data from adjoining areas further north and south reveal a positive relationship between the floor morphology and the thickness of the layered sequence. It is believed that lithological units thin out above and marginal to anticlinal floor structures and thicken in trough-like synclinal areas. Mineral composition seems to be unaffected by changes in thickness of individual units.

The analyzed orthopyroxene and plagioclase are even comparable with the composition of those from the Jagdlust/Wintersveld area which is about 35 km to the north of the Maandagshoek area.

The occurrence of pegmatites appears to be structural controlled. The amount of ultramafic pipes and metasomatically altered rocks increases significantly near anticlinal structures. This feature is attributed to a change in the flow direction of late migrating fluids. It is believed that fluids followed the palaeotopography and were therefore forced upwards at anticlinal structures. Intermittent magma addition might be responsible for an increased fluid activity due to the incorporation and subsequent degassing of sedimentary fragments.

The chemical effects of an interaction of presumably hydrous fluids with partially crystallized material has been documented in detail. It is suggested that an early addition of a hydrous fluid to the crystallizing melt resulted in precipitation of high temperature plagioclase and orthopyroxene (and/or olivine) which are comparatively more calcic and more Mg-rich respectively. In contrast, late migration of an already chemically evolved fluid can lead to the partial replacement of early formed crystals and the precipitation of fractionated phases such as K-feldspar and quartz. Isotopic data suggest that hydrous fluids are at least partially sediment derived and not just the product of interstitial melt fractionation.

Finally, the stratigraphic units J and K seem to be properly developed only in the central sector of the eastern compartment and to be completely absent in the southern sector. The additional influx of tholeiitic liquid in the central sector, or vice versa a volumetrically more limited magma addition in the marginal areas, is believed to be responsible for the rather meagre development of middle group chromitite layers almost throughout the central sector. Middle group layers are well developed in the southern and western sector where J and K units are either missing or considerably reduced in thickness. The pyroxenitic L unit and the enclosed upper middle group chromitite layers of the central sector is believed to be the stratigraphic equivalent of the MG 4 chromitite and associated pyroxenites in the southern sector.

ACKNOWLEDGEMENTS

Many hours of discussions have been spent over the last three and a half years which helped to clarify my thoughts and to improve this thesis. My sincerest thanks go to my supervisors, Dr. Chris Hatton whose patient assistance and guidance were most inspiring and Prof. Gerhard von Gruenewaldt for his numerous valuable comments and suggestions during the more final stages of this project.
I am also indebted to Martin Sharpe, Steve Grimmer, Roland Merkle and David Twist for many discussions of Bushveld Complex problems. My fellow research students Thomas Wallmach, Jochen Schweitzer, Aki Wilhelm and Dirk Harney are thanked for their helpful comments.
Alan Butcher, Bruce Eglington and Jock Harmer introduced me to the special art of isotope analysis and contributed greatly to my knowledge of isotope geochemistry. Edward Retief is thanked for sharing his great knowledge of mineral separation.
I wish to thank Hanne Horsch for keeping the electron microprobe alive and well and for assisting me with the gathering and processing of probe data.
George Trojak at the Geological Survey of South Africa kindly carried out sulfur determinations.
Steve Gain from the South African Development Trust Corporation facilitated access to drillcore material, without which this work would not have been possible. Rand Mines and Samancor are thanked for allowing access to their mining property and for providing several drillcore logs.
Thanks are also due to Marina Potgieter who kindly drafted the diagrams and to Ludwig Jacobs for preparing the necessary thin sections.
A three and a half year post graduate grant from the C.S.I.R. provided financial support and I gratefully acknowledge their contribution as well as an additional six month bursary and other financial assistance that was made available from the University of Pretoria and the Institute for Geological Research on the Bushveld Complex, respectively.

REFERENCES

ADAMS, J.B., 1968. Differential solution of plagioclase in supercritical water. American Mineralogist, 53, 1603-13.

ANASTASIOU, P. and SEIFERT, F., 1972. Solid solubility of Al_2O_3 in enstatite at high temperatures and 1-5 kb water pressure. Contributions to Mineralogy and Petrology, 34, 272-87.

BARNES, S.J., 1986. The effect of trapped liquid crystallisation on cumulus mineral composition in layered intrusions. Contributions to Mineralogy and Petrology, 93, 524-31.

BARNES, S.J., 1986a. The distribution of chromium among orthopyroxene, spinel and silicate liquid at atmospheric pressure. Geochimica et Cosmochimica Acta, 50, 1889-1909.

BARNES, S.J. and NALDRETT, A.J., 1986. Geochemistry of the Stillwater Complex, Minneapolis adit area II. Silicate mineral chemistry and petrogenesis. Journal of Petrology, 27, 791-825.

BARTON, J.M., CAWTHORN, R.G. and WHITE, J., 1986. The role of contamination in the evolution of the Platreef of the Bushveld Complex. Economic Geology, 81, 1096-1104.

BARTON, M., VAREKAMP, J.C. and BERGEN, M.J. VAN, 1982. Complex zoning of clinopyroxenes in the lavas of Vulsini, Latium, Italy: Evidence for magma mixing. Journal of Volcanology and Geothermal Research, 14, 361-88.

BERLIN, B. and HENDERSON, C.M.B., 1968. A reinterpretation of Sr and Ca fractionation trends in plagioclase from basic rocks. Earth and Planetary Science Letters, 4, 79-83.

BERTRAND, P. and MERCIER J.-C. C., 1985. The mutual solubility of coexisting ortho- and clinopyroxene: toward an absolute geothermometer for the natural system? Earth and Planetary Science Letters, 76, 109-22.

BODINIER, J.-L., DUPUY, C., DOSTAL, J. and MERLET, C., 1987. Distribution of trace transition elements in olivine and pyroxenes from ultramafic xenoliths: Application of microprobe analysis. American Mineralogist, 72, 902-13.

BOTTINGA, Y., WEILL, D. and RICHET, P., 1982. Density calculations for silicate liquids. I. Revised method for aluminosilicate compositions. Geochimica et Cosmochimica Acta, 46, 909-19.

BOYD, G.M. and SCHAIRER, J.F., 1964. The system $MgSiO_3$-$CaMgSi_2O_6$. Journal of Petrology, 5, 275-309.

BRADY, J.B. and McCALLISTER, R.H., 1983. Diffusion data for clinopyroxenes from homogenization and self-diffusion experiments. American Mineralogist, 68, 95-105.

BRANDEIS, G. and JAUPART, C., 1986. On the interaction between convection and crystallization in cooling magma chambers. Earth and Planetary Science Letters, 77, 345-61.

BRANDEIS, G., JAUPART, C. and ALLEGRE, C.J., 1984. Nucleation, crystal growth and the thermal regime of cooling magmas. Journal of Geophysical Research, 89, 10161-77.

BURNHAM, C.W., 1979. The importance of volatile constituents. In: Yoder, H.S. (Editor), The evolution of the Igneous Rocks. Princeton, Princeton University Press, 439-82.

BUTTON, A., 1976. Stratigraphy and relations of the Bushveld floor in the eastern Transvaal. Transactions of the Geological Society of South Africa, 79, 3-12.

CAMERON, E.N., 1963. Structure and rock sequences of the Critical Zone of the Eastern Bushveld Complex. Mineralogical Society of

America, Special Paper, 1, 93-107.
CAMERON, E.N., 1964. Chrome deposits of the eastern part of the Bushveld Complex. In: Haughton, S.H., (Editor) The geology of some ore deposits in Southern Africa II. Geological Society of South Africa, Johannesburg, 131-168.
CAMERON, E.N., 1970. Composition of certain coexisting phases in the eastern part of the Bushveld Complex. Geological Society of South Africa, Special Paper 1, 46-58.
CAMERON, E.N., 1978. The Lower Zone of the Eastern Bushveld Complex in the Olifants River Trough. Journal of Petrology, 19, 437-62.
CAMERON, E.N., 1980. Evolution of the lower critical zone, central sector, Eastern Bushveld Complex, and its chromite deposits. Economic Geology, 75, 845-71.
CAMERON, E.N., 1982. The upper critical zone of the eastern Bushveld Complex - precursor of the Merensky Reef. Economic Geology, 7, 1307-27.
CAMERON, E.N. and DESBOROUGH, G.A., 1969. Occurrence and characteristics of chromite deposits - Eastern Bushveld Complex. Economic Geology Monograph 4, 23-40.
CAMERON, E.N. and EMERSON, E.D., 1959. The origin of certain chromite deposits of the eastern part of the Bushveld Complex. Economic Geology, 54, 1151-1213.
CAMPBELL, I.H., 1977. A study of macro-rhythmic layering and cumulate processes in the Jimberlana Intrusion, Western Australia. Part I: The upper layered series. Journal of Petrology, 18, 183-215.
CAMPBELL, I.H., 1987. Distribution of orthocumulate textures in the Jimberlana Intrusion. Journal of Petrology, 95, 35-54.
CAMPBELL, I.H. and BORLEY, G.D., 1974. The geochemistry of pyroxenes from the Lower Layered Series of the Jimberlana Intrusion, Western Australia. Contributions to Mineralogy and Petrology, 47, 281-97.
CARMICHAEL, I.S.E., NICHOLLS, J. and SMITH, A.L., 1970. Silica activity in igneous rocks. American Mineralogist, 55, 246-63.
CARMICHAEL, I.S.E., TURNER, F.J. and VERHOOGEN, J., 1974. Igneous Petrology. New York, McGraw-Hill, 740pp.
CARROL, M.R. and RUTHERFORD, M.J., 1985. Sulfide and Sulfate saturation in hydrous silicate melts. Journal of Geophysical Research, 90, Supplement, C601-C612.
CARROL, M.R. and RUTHERFORD, M.J., 1988. Sulfur speciation in hydrous experimental glasses of varying oxidation state: Results from measured wavelength shifts of sulfur X-rays. American Mineralogist, 73, 845-9.
CAWTHORN, R.G., BIGGAR, G.M., GRAHAM, A., FORD, C.E., SHARPE, M.R. and DAVIES, G., 1979. Experimental petrological data on the parental magmas to the Bushveld Complex. Institute for Geological Research on the Bushveld Complex, Univ. Pretoria, Research Report 18, 1-27.
CAWTHORN, R.G. and DAVIES, G., 1983. Experimental data at 3 kbars pressure on parental magma to the Bushveld Complex. Contributions to Mineralogy and Petrology, 83, 128-35.
CAWTHORN, R.G., DAVIES, G., CLUBLEY-ARMSTRONG, A. and McCARTHY, T.S., 1981. Sills associated with the Bushveld Complex, South Africa: An estimate of the parental magma composition. Lithos,14, 1-15.
CHEN, C.F. and TURNER, J.S., 1980. Crystallization in a double-diffusive system. Journal of Geophysical Research, 85, 2573-93.
COERTZE, F.J., 1958. Intrusive relationships and ore deposits in the western part of the Bushveld Igneous Complex. Transactions

of the Geological Society of South Africa, 61, 387-92.
COISH, R.A. and TAYLOR, L.A., 1979. The effects of cooling rate on texture and pyroxene chemistry in DSDP leg 34 basalt: A microprobe study. Earth and Planetary Science Letters, 42, 389-98.
COUSINS, C.A., 1959. The structure of the mafic portion of the Bushveld Igneous Complex. Transactions of the Geological Society of South Africa, 62, 179-89.
COUSINS, C.A., 1964. Additional notes on the chromite deposits of the eastern part of the Bushveld Complex. In: Haughton, S.H., (Editor) The Geology of some ore deposits in South Africa II, Geological Society of South Africa, Johannesburg, 169-182.
COUSINS, C.A. and FERINGA, G., 1964. The chromite deposits of the western belt of the Bushveld Complex. In: Haughton, S.H., (Editor) The Geology of some ore deposits in South Africa II, Geological Society of South Africa, Johannesburg, 183-202.
DAVIES, G., CAWTHORN, R.G., BARTON, J.M. and MORTON, M., 1980. Parental magma to the Bushveld Complex. Nature, 87, 33-5.
DOBOSI, G. and HORVATH, I., 1988. High- and low-pressure cognate clinopyroxenes from alkali lamprophyres of the Velence and Buda Mountains, Hungary. Neues Jahrbuch für Mineralogie, 158, 241-56.
DOWTY, E., 1980. Crystal growth and nucleation theory and the numerical simulation of igneous crystallization. In: Hargraves, R.B. (Editor) Physics of magmatic processes. Princeton, Princeton University Press, 419-85.
DYMEK, R. F. and SCHIFFRIES, C.M., 1987. Calcic myrmekite: Possible evidence for the involvement of water during the evolution of andesine anorthosite from St-Urbain, Quebec. Canadian Mineralogist, 25, 291-319.
EALES, H.V., MARSH, J.S., MITCHELL, A.A., KLERK, W.J. DE, KRUGER, F.J. and FIELD, M., 1986. Some geochemical constraints upon models for the crystallization of the upper critical zone - main zone interval, northwestern Bushveld Complex. Mineralogical Magazine, 50, 567-82.
EMSLIE, R.F., 1975. Pyroxene megacrysts from anorthositic rocks: New clues to the sources and evolution of the parent magmas. Canadian Mineralogist, 13, 138-45.
ERIKSSON, S.C., 1985. Oscillatory zoning in clinopyroxenes from the Guide Copper Mine, Phalaborwa, South Africa. American Mineralogist, 70, 74-79.
FERINGA, G., 1959. The geological succession in a portion of the north-western Bushveld (Union Section) and its interpretation. Transactions of the Geological Society of South Africa, 62, 219-38.
FLYNN, R.T., ULMER, G.C. and SUTPHEN, C.F., 1978. Petrogenesis of the Eastern Bushveld Complex: Crystallization of the Middle Critical Zone. Journal of Petrology, 19, 136-52.
GAIN, S.B., 1981. The cyclic units of the upper critical zone on Maandagshoek 254 KT, eastern Bushveld Complex. MSc thesis (unpubl.), Univ. Pretoria, 155pp.
GAIN, S.B., 1985. The geological setting of the platiniferous UG-2 chromitite layer on the farm Maandagshoek, eastern Bushveld Complex. Economic Geology, 80, 925-43.
GASPARIK, T., 1987. Orthopyroxene thermobarometry in simple and complex systems. Contributions to Mineralogy and Petrology, 96, 357-70.
GASPARIK, T. and NEWTON, R.C., 1984. The reversed alumina contents of

orthopyroxene in equilibrium with spinel and forsterite in the system MgO - Al_2O_3 - SiO_2. Contributions to Mineralogy and Petrology, 85, 186-96.

GREEN, D.H., 1963. Alumina content of enstatite in a Venezuelan high-temperature peridotite. Geological Society of America Bulletin, 74, 1397-1402.

GROUT, F.F., 1918. Two phase convection in igneous magmas. Journal of Geology, 26, 481-99.

GROVE, T.L., BAKER, M.B. and KINZLER, R.J., 1984. Coupled CaAl - NaSi diffusion in plagioclase feldspar: Experiments and applications to cooling rate speedometry. Geochimica et Cosmochimica Acta, 48, 2113-21.

GRUENEWALDT, G. VON, 1970. On the phase change orthopyroxene-pigeonite and the resulting textures in the Main and Upper Zones of the Bushveld Complex in the Eastern Transvaal. Geological Society of South Africa, Special Publication, 1, 67-73.

GRUENEWALDT, G. VON, 1971. A petrographical and mineralogical investigation of the rocks of the Bushveld Igneous Complex in the Tauteshoogte-Roossenekal area of the Eastern Transvaal. DSc thesis (unpubl.), Univ. Pretoria, 228pp.

HALL, A.L., 1932. The Bushveld Igneous Complex of the Central Transvaal. Geological Survey of South Africa Memoir, 28, 560pp.

HALL, A.L and HUMPHREY, W.A., 1908. On the occurrence of chromite deposits along the southern and eastern margins of the Bushveld Plutonic Complex. Transactions of the Geological Society of South Africa, 11, 69-77.

HAMILTON, P.J., 1977. Sr isotope and trace element studies of the Great Dyke and Bushveld mafic phase and their relationship to early proterozoic magma genesis in southern Africa. Journal of Petrology, 18, 24-52.

HAMILTON, D.L., BURNHAM, C.W. and OSBORN, E.F., 1964. The solubility of water and effects of oxygen fugacity and water content on crystallization in mafic magmas. Journal of Petrology,5, 21-39.

HARMER, R.E., 1985. Rb-Sr isotopic study of units of the Pinaars River Alkaline Complex, North of Pretoria, South Africa. Transactions of the Geological Society of South Africa, 88, 215-23.

HARMER, R.E. and SHARPE, M.R., 1985. Field relations and strontium isotope systematics of the marginal rocks of the eastern Bushveld Complex. Economic Geology, 80, 813-37.

HART, S.R, 1981. Diffusion compensation in natural silicates. Geochimica et Cosmochimica Acta, 45, 279-91.

HATTON, C.J., 1988. Densities and liquidus temperatures of Bushveld parental magmas as constraints on the formation of the Merensky Reef. Istitute for Geological Research on the Bushveld Complex, Univ. Pretoria, Research Report, 73, 22pp.

HATTON, C.J. and GRUNEWALDT, G. VON, 1987. The geological setting and petrogenesis of the Bushveld chromitite layers. in: Stowe, C.W., (Editor) Evolution of chromium ore fields. Van Nostrand Reinhold, New York, 109-43.

HATTON, C.J., HARMER, R.E. and SHARPE, M.R., 1986. The petrogenesis of the middle group of chromitite layers, Doornvlei, eastern Bushveld Complex. In: Gallagher, M.J., Ixer, R.A., Neary, C.R. and Prichard, H.M. (Editors) Metallogeny of basic and ultrabasic rocks. Institution of Mining and Metallurgy, London, 241-7.

HECKROODT, R.O., 1958. Die platinumdraende dunietpyp op Driekop, Oos-Transvaal, en die samestelling van olivien in die Bosveld-stollingskompleks. MSc thesis (unpubl.), Univ. Pretoria.

HENDERSON, J.A.L., 1898. Petrographical and geological investigations of certain Transvaal norites, gabbros and pyroxenites and other South African rocks. Dulau and Co., London, 56pp.
HENDERSON, P., 1970. The significance of the mesostasis of basic layered igneous rocks. Journal of Petrology, 11, 463-73.
HESS, H.H., 1960. Stillwater Igneous Complex, Montana. A quantitative mineralogical study. Memoirs of the Geological Society of America, 80, 230pp.
HOLOCOMBE, C.J., 1985. Paleoflow modeling for sedimentary orebodies. Economic Geology, 80, 172-79.
HUEBNER, A., 1872. Geognostische Skizzen aus Süd-Ost Afrika. Petermann's Mittheilungen, 422-431.
HUNTER, R.H., 1986. Textural equilibrium in layered igneous rocks. In: Parson, I., (Editor) Origins of igneous layering. NATO ASI Series C, 196, Reidel D., Dordrecht, 473-503.
HUNTER, D.R. and HAMILTON, P.J., 1978. The Bushveld Complex. In: Tarling, D.H., (Editor) Evolution of the earth's crust. London, Academic Press, 107-73.
HUPPERT, H.E. and SPARKS, R.S.J., 1980. The fluid dynamics of a basaltic magma chamber replenished by influx of hot, dense ultrabasic liquid. Contributions to Mineralogy and Petrology, 75, 279-90.
HUPPERT, H.E., SPARKS, R.S.J. and TURNER, J.S., 1983. Laboratory investigations of viscous effects in replenished magma chambers. Earth and Planetary Science Letters, 65, 377-81.
HUPPERT, H.E., SPARKS, R.S.J. and TURNER, J.S., 1984. Some effects of viscosity on the dynamics of replenished magma chambers. Journal of Geophysical Research, 89, B8, 6857-77.
HUPPERT, H.E. and TURNER, J.S., 1981. Double-diffusive convection. Journal of Fluid Mechanics, 106, 299-329.
IIYAMA, J.T., 1968. Etude expèrimentale de la distribution d'èlèments en traces entre deux feldspaths. Bulletin de la Sociètè Française de Minèralogie et Cristallographie, 91, 130-40.
IRVINE, T.N., 1967. Chromian spinel as a petrogenetic indicator. Part 2. Petrologic implications. Canadian Journal of Earth Sciences, 4, 71-103.
IRVINE, T.N., 1980a. Magmatic density currents and cumulus processes. American Journal of Science, 280-A, 1-58.
IRVINE, T.N., 1980b. Experimental modelling of convection in layered intrusions. Carnegie Institute Washington Year Book 79, 247-51.
IRVINE, T.N., 1980c. Magmatic infiltration metasomatism, double-diffusive fractional crystallization, and adcumulus growth in the Muscox Intrusion and other layered intrusions, in Hargraves, R.B., (Editor), Physics of magmatic processes. Princeton, Princeton Univ. Press, 325-83.
IRVINE, T.N., 1982. Terminology for layered intrusions. Journal of Petrology, 23, 127-62.
IRVINE, T.N., KEITH, D.W. and TODD, S.G., 1983. The J-M platinum-palladium reef of the Stillwater Complex, Montana II. Origin of double-diffusive convective magma mixing and implications for the Bushveld Complex. Economic Geology, 78, 1287-1334.
IRVINE, T.N. and SHARPE, M.R., 1986. Magma mixing and the origin of stratiform oxide ore zones in the Bushveld and Stillwater Complexes. In: Gallagher, M.J., Ixer, R.A., Neary, C.R. and Prichard, H.M., (Editors) Metallogeny of basic and ultrabasic rocks. Institution of Mining and Metallurgy, London, 183-98.
IRVING, A.J., 1978. A review of experimental studies of crystal/liquid

trace element partitioning. Geochimica et Cosmochimica Acta, 42, 743-70.

JACKSON, E.D., 1961. Primary textures and mineral associations in the ultramafic zone of the Stillwater Complex, Montana. U.S. Geological Survey Prof. Papers, 358, 106pp.

JACKSON, E.D., 1969. Chemical variation in coexisting chromite and olivine in the chromitite zones of the Stillwater Complex. In: Wilson, H.D.B, (Editor) Magmatic ore deposits. Economic Geology Publishing Company, Lancaster Press, Inc., Lancaster, Pa.

JACKSON, E.D., 1970. The cyclic unit in layered intrusions - a comparison of repetitive stratigraphy in the ultramafic parts of the Stillwater, Muscox, Great Dyke and Bushveld Complex. Geological Society of South Africa, Special Publication, 1, 391-424.

JAUPART, C. and BRANDEIS, G., 1986. The stagnant bottom layer of convecting magma chambers. Earth and Planetary Science Letters, 80, 183-99.

JAUPART, C., BRANDEIS, G. and ALLEGRE, C.J., 1984. Stagnant layer at the bottom of convecting magma chambers. Nature, 308, 535-38.

KAISER, H. and SPECKER, H., 1956. Bewertung und Vergleich von Analysenverfahren. Zeitschrift für Analytische Chemie, 149,44-66.

KENT, L.E., 1980. Sratigraphy of South Africa. South African Committee for Stratigraphy. Part I. Geological Survey of South Africa, Handbook 8, 690pp.

KIRKPATRICK, R.J., ROBINSON, G.R. and HAYS, J.F., 1976. Kinetics of crystal growth from silicate melts: Diopside and anorthite. Journal of Geophysical Research, 81, 5715-20.

KLERK, W.J. DE, 1982. The geology, geochemistry and silicate mineralogy of the upper critical zone of the north-western Bushveld Complex, at Rustenburg Platinum Mines, Union Section. MSc thesis (unpubl.), Rhodes Univ., Grahamstown, 204pp.

KONTAK, D.J., CLARK, A.H., FARRAR, E., PEARCE, T.H., STRONG, D.F. and BAADSGAARD, H., 1986. Pertogenesis of a neogene shoshonite suite, Cerro Moromoroni, Puno, southeastern Peru. Canadian Mineralogist, 24, 117-35.

KRETZ, R., 1982. Transfer and exchange equilibria in a portion of the pyroxene quadrilateral as deduced from natural and experimental data. Geochimica et Cosmochimica Acta, 46, 411-21.

KRUGER, F.J., 1982. The petrology of the Merensky Cyclic Unit and associated rocks and their significance in the evolution of the western Bushveld Complex. PhD thesis (unpubl.), Rhodes Univ.

KRUGER, F.J. and CAWTHORN, R.G., MEYER, P.S. and WALSH, K.L., 1986. Sr-isotopic, chemical and mineralogical variations across the Pyroxenite Marker and in the upper zone of the western Bushveld Complex. 21st Congress of the Geological Society of South Africa, Extended Abstracts, 609-12.

KRUGER, F.J. and MARSH, J.S., 1982. Significance of 87SR/86Sr ratios in the Merensky cyclic unit of the Bushveld Complex. Nature, 98, 53-55.

KRUGER, F.J., CAWTHORN, R.G. and WALSH, K.L., 1987. Strontium isotopic evidence against magma addition in the upper zone of the Bushveld Complex. Earth and Planetary Science Letters, 84, 51-8.

KUPFERBÜRGER, W., LOMBAARD, B.V., WASSERSTEIN, B. and SCHWELLNUS, C.M., 1937. The chromite deposits of the Bushveld Igneous Complex, Transvaal. Bulletin of the Geological Survey of South Africa, 10, 48pp.

KUSCHKE, G.S.J., 1939. The Critical Zone of the Bushveld Igneous

Complex, Lydenburg District. Transactions of the Geological Society of South Africa, 42, 57-81.
KUSHIRO, I., 1969. The system forsterite-diopside-silica with and without water at high pressures. American Journal of Science, 267-A, 269-94.
KUSHIRO, I., 1975. On the nature of silicate melt and its significance in magma genesis: regularities in the shift of the liquidus boundaries involving olivine, pyroxene and silica minerals. American Journal of Science, 275, 411-31.
LALLY, J.S., HEUER, A.H., NORD Jr. G.L. and CHRISTIE, J.M., 1975. Subsolidus reaction in lunar pyroxenes: An electron petrographic study. Contributions to Mineralogy and Petrology, 51, 263-81.
LANGMUIR, C.H., VOCKE, R.D.,Jr., HANSON, G.N. and HART, S.R., 1978. A general mixing equation with application to Icelandic basalts. Earth and Planetary Science Letters, 37, 380-92.
LEE, C.A., 1981. Post deposition structure in Bushveld Complex mafic sequences. Journal of the Geological Society of London, 138, 327-41.
LINDEN, P.F., 1978. The formation of banded salt finger structure. Journal of Geophysical Research, 83, 2902-12.
LINDSLEY, D.H., 1983. Pyroxene thermometry. American Mineralogist, 68, 477-93.
LINDSTROM, D.J., 1983. Kinetic effects on trace element partitioning. Geochimica et Cosmochimica Acta, 47, 617-22.
LOMBAARD, B.V., 1934. On the differentiation and relationships of the rocks of the Bushveld Complex. Transactions of the Geological Society of South Africa, 42, 5-52.
LONGHI, J., WALKER, D. and HAYS, J.F., 1976. Fe and Mg in plagioclase. Proceedings of the Lunar Science Conference 7th., 1281-1300.
LONG, P.E., 1978. Experimental determination of partition coefficients for Rb, Sr and Ba between alkali feldspar and silicate liquid. Geochimica et Cosmochimica Acta, 42, 833-46.
MAALØE, S. and HANSON, B., 1982. Olivine phenocrysts of Hawaiian olivine tholeiite and oceanite. Contributions to Mineralogy and Petrology, 81, 203-11.
MARSH, B.D. and MAXEY, M.R., 1985. On the distribution and separation of crystals in convecting magma. Journal of Volcanology and Geothermal Research, 24, 95-150.
McBIRNEY, A.R., 1980. Mixing and unmixing of magmas. Journal of Volcanological and Geothermal Research, 7, 357-71.
McKAY, G.A. and WEILL, D.F., 1976. KREEP petrogenesis revisited. Proceedings of the Lunar Science Conference 8th., 2339-55.
McKENZIE, D., 1984. The generation and compaction of partially molten rock. Journal of Petrology, 25, 713-65.
McDONALD, J.A., 1967. Evolution of part of the lower critical zone, farm Ruighoek, Western Bushveld. Journal of Petrology, 8, 165-209.
MERKLE, R.K.W., 1988. The effects of metasomatising fluids on the PGE-content of the UG-1 chromitite layer. In: Prichard, H.M., Potts, P.J., Bowles, J.F.W. and Cribb, S.J. (Editors) Geo-Platinum 87, Elsevier Science Publishers Ltd, London and New York, 359-60.
MINERALS BUREAU OF SOUTH AFRICA, 1986. South Africa's Mineral Industry.
MOLENGRAAFF, G.A.F., 1901. Gèologie de la Republique Sud Africaine du Transvaal. Bulletin de la Sociètè Gèologique de France, Serie 4, 1, 13-92.
MOLYNEUX, T.G. 1974. A geological investigation of the Bushveld Com-

plex in Sekhukhuneland and part of the Steelpoort valley. Transactions of the Geolocical Society of South Africa, 77, 329- 38.

MOLYNEUX, T.G. and KLINKERT, P.S., 1978. A structural interpretation of part of the eastern mafic lobe of the Bushveld complex and its surroundings. Transactions of the Geological Society of South Africa, 81, 359-68.

MOORE, A., 1968. Rutile exsolution in orthopyroxene. Contributions to Mineralogy and Petrology, 17, 233-36.

MORSE, S.A., 1979. Influence of augite on plagioclase fractionation. Journal of Geology, 87, 202-208.

MORSE, S.A., 1984. Cation diffusion in plagioclase feldspar. Science, 225, 504-5.

MORSE, S.A., 1986a. Convection in aid of adcumulus growth. Journal of Petrology, 27, 1183-1214.

MORSE, S.A., 1986b. Thermal structure of crystallizing magma with two-phase convection. Geological Magazine, 123, 205-14.

MYSEN, B.O, VIRGO, D., HARRISON, W.J. and SCARFE, C.M., 1980. Solubility mechanisms of H_2O in silicate melts at high pressures and temperatures: A Raman spectroscopy study. American Mineralogist, 65, 900-14.

NABELEK, P.I. and LANGMUIR, C.H., 1986. The significance of unusual zoning in olivines from FAMOUS area basalt 527-1-1. Contributions to Mineralogy and Petrology, 93, 1-8.

NABELEK, P.I., LINDSLEY, D.H. and BOHLEN, S.R., 1987. Experimental examination of two-pyroxene graphical thermometers using natural pyroxenes with application to metaigneous pyroxenes from the Adirondack Mountains, New York. Contributions to Mineralogy and Petrology, 97, 66-71.

NALDRETT, A.J., CAMERON, G., GRUENEWALDT, G. VON and SHARPE, M.R., 1987. The formation of stratiform Platinum-Group element deposits in layered intrusions. In: Parsons, I. (Editor) Origin of igneous layering. NATO ASI Series C, 196, Reidel, D. Dordrecht, 313-97.

NALDRETT, A.J., GASPARRINI, E.C., BARNES, S.J., GRUENEWALDT, G. VON and SHARPE, M.R., 1986. The upper critical zone of the Bushveld Complex and the origin of Merensky-type ores. Economic Geology, 81, 1105-17.

NALDRETT, A.J. and GRUENEWALDT, G. VON, 1988. The upper critical zone of the Bushveld Complex and the origin of Merensky-type ores - A reply. Economic Geology, 83, 1085-91.

OBATA, M., 1976. The solubility of Al_2O_3 in orthopyroxenes in spinel and plagioclase peridotites and spinel pyroxenite. American Mineralogist, 61, 804-16.

O'HARA, M.J., 1977. Geochemical evolution during fractional crystallization of a periodically refilled magma chamber. Nature, 266, 503-07.

PEARCE, T.H., 1985. The analysis of zoning in magmatic crystals with emphasis on olivine. Contributions to Mineralogy and Petrology, 86, 149-54.

PEARCE, J.A. and NORRY, M.J., 1979. Petrogenetic implications of Ti, Zr, Y and Nb variation in volcanic rocks. Contributions to Mineralogy and Petrology, 69, 33-47.

PETERSEN, J.S., 1986. Solidification contraction: Another approach to cumulus processes and the origin of igneous layering. In: Parsons, I., (Editor) Origins of igneous layering. NATO ASI Series C, 196, Reidel, D., Dordrecht, 505-26.

RAEDEKE, L.D. and McCALLUM, I.S., 1984. Investigations of the Stillwater Complex: II. Petrology and petrogenesis of the Ultramafic Series. Journal of Petrology, 25, 395-420.

REICHHARDT, F.J., 1984. Geologische Kartierung, tektonische und petrographische Bearbeitung der Haupt- und Oberen Zone des östlichen Bushveld Complex, südlich Roossenekal, eastern Transvaal. MSc thesis (unpubl.), Univ. München, 151pp.

REUNING, E., 1928. Verbansverhältnisse und Chemismus der Gesteine des "Bushveld Igneous Complex" und das Problem seiner Entstehung. Neues Jahrbuch für Mineralogie, 57A, 631-664.

RICHTER, F.M. and McKENZIE, D., 1984. Dynamical models for melt segregation from a deformable matrix. Journal of Geology,92, 729-40.

RIETMEIJER, F.J.M., 1983. Inter-diffusion coefficients parallel to the c - axis in iron-rich clinopyroxenes calculated from microstructures. Contributions to Mineralogy and Petrology, 83, 169-176.

ROEDER, P.L. and CAMPBELL, I.H., 1985. The effect of postcumulus reactions on composition of chrome-spinels from the Jimberlana Intrusion. Journal of Petrology, 26, 763-86.

SAMPSON, E., 1932. Magmatic chromite deposits in Southern Africa. Economic Geology, 27, 113-44.

SAXENA, S.K., 1976. Two-pyroxene geothermometer: A model with an approximate solution. American Mineralogist, 61, 643-52.

SCHWELLNUS, J.S.I., 1956. The basal portion of the Bushveld Igneous Complex and the adjoining metamorphosed sediments in the north-eastern Transvaal. DSc thesis (unpubl.), Univ. Pretoria 207pp.

SCHWELLNUS, J.S.I., ENGELBRECHT, L.N.J., COERTZE, F.J., RUSSEL, M.D., MALHERBE, S.J., ROOYEN, D.P. VAN and COOKE, R., 1962. The geology of the Olifants River area, Transvaal. Explan. Sheets 2429B (Chuniespoort) and 2430A (Wolkberg), Geological Survey of South Africa, 87.

SHARPE, M.R., 1981. The chronology of magma influxes to the eastern compartment of the Bushveld Complex as exemplified by its marginal border groups. Journal of the Geological Society of London, 138, 307-26.

SHARPE, M.R., 1982. Noble metals in the marginal rocks of the Bushveld Complex. Economic Geology, 77, 1286-95.

SHARPE, M.R., 1985. Strontium isotope evidence for preserved density stratification in the main zone of the Bushveld Complex, South Africa. Nature, 316, 119-26.

SHARPE, M.R., 1986. REE and isotopic evidence for multiple parental magmas to the Bushveld Complex. Institute for Geological Research on the Bushveld Complex, Univ. Pretoria, Annual Report, 1985/1986, 51-62.

SHARPE, M.R. and CHADWICK, B., 1982. Structures in Transvaal Sequence rocks within and adjacent to the eastern Bushveld Complex. Transactions of the Geological Society of South Africa, 85, 29-41.

SHARPE, M.R. and IRVINE, T.N., 1983. Melting relations of two Bushveld chilled margin rocks and implications for the origin of chromite. Carnegie Institute Year Book, 82, 295-300.

SHARPE, M.R., IRVINE, T.N., MYSEN, B.O. and HAZEN, R.M., 1983. Density and viscosity characteristics of melts of Bushveld chilled margin rocks. Carnegie Inst. Washington Year Book, 82, 300-05.

SHATSKY, V.S., STENINA, N.G., PAVLYUCHENKO, V.S. and USOVA, L.V., 1986. Genetic significance of exsolution structures in eclogite type rocks. In: Minceva-Stefanova, J. (Editor) Morphology and

phase equilibria of minerals. Proceedings of the 13th meeting of the International Mineralogical Association, Varna, 1982. Bulgarian Academy of Sciences, Sofia, 365-76.

SHIRLEY, D.N., 1986. Compaction of igneous cumulates. Journal of Geology, 94, 795-809.

SKINNER, B.J., 1966. Thermal Expansion. In: Clark Jr., S.P. (Editor) Handbook of physical constants. Geological Society of America, Memoir, 97, 75-96.

SMITH, J.V., 1983. Some chemical properties of feldspar. In: Ribbe, P.H. (Editor) Reviews in mineralogy, vol. 2, second edition: Feldspar Mineralogy. Mineralogical Society of America, 281-96.

SPARKS, R.S.J. and HUPPERT, H.E., 1984. Density changes during the fractional crystallization of basaltic magmas: Implications for the evolution of layered intrusions. Contributions to Mineralogy and Petrology, 85, 300-09.

SPARKS, R.S.J., MEYER, P. and SIGURDSON, H., 1980. Density variation amongst mid-ocean ridge basalts: Implications for magma mixing and the scarcity of primitive lavas. Earth and Planetary Science Letters, 46, 419-30.

SPARKS, R.S.J., HUPPERT, H.E., KERR, R.G., McKENZIE, D.P. and TAIT, S.R., 1985. Postcumulus processes in layered intrusions. Geological Magazine, 122, 555-68.

SPEIDEL, D.H. and OSBORN, E.F., 1967. Element distribution among co-existing phases in the system MgO-FeO-Fe_2O_3-SiO_2 as a function of temperature and oxygen fugacity. American Mineralogist, 52, 1139-52.

STOLPER, E., 1982. Water in silicate glasses: An infrared spectroscopic study. Contributions to Mineralogy and Petrology, 81, 1-17.

STRECKEISEN, A., 1976. To each plutonic rock its proper name. Earth Science Review, 12, 1-33.

TAIT, S.R., HUPPERT, H.E. and SPARKS, R.S.J., 1984. The role of compositional convection in the formation of adcumulate rocks. Lithos, 17, 139-46.

TANKARD, A.J., JACKSON, M.P.A., ERIKSSON, K.A., HOBDAY, D.K., HUNTER, D.R. and MINTER, W.E.L., 1982. Crustal Evolution of South Africa. Springer Verlag New York, New York, 523pp.

TODD, S.G., KEITH, D.W., SCHISSEL, D.J., LeROY, L.L., MANN, E.L. and IRVINE, T.N., 1982. The J-M platinum-palladium reef of the Stillwater Complex, Montana: I. Stratigraphy and petrology. Economic Geology, 77, 1454-80.

TSUCHIYAMA, A., 1985. Partial melting kinetics of plagioclase-diopside pairs. Contribution to Mineralogy and Petrology, 91, 12-23.

TURNER, J.S., 1973. Buoyancy effects in fluids: Cambridge, Cambridge Univ. Press, 367pp.

TURNER, J.S., 1978. Double-diffusive intrusions into a density gradient. Journal of Geophysical Research, 83, 2887-2901.

TURNER, J.S., 1980. A fluid dynamical model of differentiation and layering in magma chambers. Nature, 285, 213-215.

TURNER, J.S. and CAMPBELL, I.H., 1986. Convection and mixing in magma chambers. Earth Science Reviews, 23, 255-352.

TURNER, J.S. and GUSTAFSON, L.B., 1978. The flow of hot saline solutions from vents in the sea floor - some implications for exhalative massive sulfides and other ore deposits. Economic Geology, 73, 1082-1100.

TURNER, J.S. and GUSTAFSON, L.B., 1981. Fluid motions and compositional gradients produced by crystallization or melting at vertical boundaries. Journal of Volcanological and

Geothermal Research, 11, 93-125.
ULMER, G.C., 1969. Experimental investigations of chromite spinels. Economic Geology Monography 4, 114-31.
VERMAAK, C.F., 1976. The Merensky Reef - thoughts on its environment and genesis. Economic Geology, 71, 1270-98.
VILJOEN, M.J. and SCOON, R.N., 1985. The distribution and main geologic features of discordant bodies of iron-rich ultramafic pegmatite in the Bushveld Complex. Economic Geology, 80, 1109-1128.
VILLIERS, J.S. DE, 1968. A contribution to the geology of chromitite seams occurring in the southern sector of the eastern part of the Bushveld Complex. Transactions of the Geological Society of South Africa, 71, 203-8.
VIRGO, D. and HAFNER, S., 1970. Fe^{2+} - Mg order-disorder in natural orthopyroxenes. American Mineralogist, 55, 201-23.
WADSWORTH, W.J., 1985. Terminology of postcumulus processes and products in the Rhum layered intrusion. Geological Magazine, 122, 549-54.
WAGER, L.R. and BROWN, G.M., 1967. Layered igneous rocks. Oliver and Boyd, Edinburgh and London, 588pp.
WAGNER, P.A., 1923. The chromite of the Bushveld Complex. South African Journal of Science, 20, 223-35.
WAGNER, P.A., 1929. The Platinum deposits and mines of South Africa. Oliver and Boyd, Edinburgh and London.
WALLMACH, T., 1988. The petrogenesis of high grade contact metamorphic mineral assemblages in calc-silicate xenoliths, eastern Bushveld Complex, South Africa. DSc thesis (unpubl.), Univ. Pretoria, 200pp.
WALT, C.F.J. VAN DER, 1941, Chrome ores of the Western Bushveld Complex. Transactions of the Geological Society of South Africa, 44, 79-112.
WEINSTEIN, S.A., YUEN, D.A. and OLSON, P.L., 1988. Evolution of crystal-settling in magma-chamber convection. Earth and Planetary Science Letters, 87, 237-48.
WET, J.F. DE, 1952. Chromite investigations - Part III: Variations in the composition of the pure chromite mineral from the Eastern Chrome Belt, Lydenburg District. Journal of the Chemical, Metallurgical and Mining Society of South Africa, 52, 143-55.
WILLEMSE, J., 1959. The "floor" of the Bushveld Igneous Complex and its relationship, with special reference to the Eastern Transvaal. Proceedings of the Geological Society of South Africa, 62, xxi-lxxx.
WILLEMSE, J., 1969. The geology of the Bushveld Igneous Complex, the largest repository of magmatic ore deposits in the world. Economic Geology, Monogr. 4, 1-22.
WILSON, A.H., 1982. The geology of the Great "Dyke", Zimbabwe: The ultramafic rocks. Journal of Petrology, 23, 240-292.
WOOD, B.J. and BANNO, S., 1973. Garnet-orthopyroxene and orthopyroxene-clinopyroxene relationships in simple and complex systems. Contributions to Mineralogy and Petrology, 42, 109-24.
YORK, D., 1969. Least-squares fitting of a straight line with correlated errors. Earth and Planetary Science Letters, 5, 320-24.

APPENDIX

A.I: ELECTRON MICROPROBE ANALYSES

Table A.1: Analytical parameters and statistical errors calculated from 90 duplicate analyses carried out on two orthopyroxene grains. All analyses were performed with a JEOL 733 electron microprobe at 20 kV and 20 nA. The beam diameter was fixed at 10 um. Major and trace element concentrations were determined using the K_a -lines. Counting time for each element was 20 seconds on the peak and 10 seconds for background.

ELEMENT	CRYSTAL	STANDARD	LLD*	RANGE**	AVG**	STD***	C#
Si	TAP	quartz	nd	53.47-55.33	54.70	0.274	0.501
Al	TAP	Al_2O_3	nd	0.69- 1.11	0.91	0.047	5.165
Mg	TAP	MgO	nd	27.11-28.80	28.01	0.151	0.539
Ti	PET	TiO_2	450	0.13- 0.94	0.23	0.019	8.284
Ca	PET	wollastonite	590	0.62- 2.20	1.03	0.039	3.812
Fe	LIF	nat. Fe_2O_3	nd	13.96-16.47	15.16	0.275	1.812
Mn	LIF	MnO	270	0.22- 0.34	0.28	0.033	12.052
Cr	LIF	Cr_2O_3	370	0.29- 0.55	0.38	0.035	9.349
Na	TAP	omphacite	240	0.00- 0.05	0.02	0.013	75.870
Ni	LIF	NiO	300	0.03- 0.07	0.05	0.009	19.164
Mg#	100*(Mg/(Mg+Fe))			75.03-78.10	76.71	0.297	0.388

Table A.2: Analytical parameters and statistical errors calculated from 45 duplicate anlyses carried out on several plagioclase grains. All analyses were performed with a JEOL 733 electron microprobe at 15 kV and 20 nA. The beam diameter was fixed at 10 um. Major and trace element concentrations were detremined using the K_a -lines. Counting time for each element was 20 seconds on the peak and 10 seconds for background.

ELEMENT	CRYSTAL	STANDARD	LLD*	RANGE**	AVG**	STD***	C#
Si	TAP	quartz	nd	47.69-50.62	49.53	0.217	0.437
Na	TAP	albite	150	2.21- 3.12	2.86	0.067	2.336
Ca	PET	wollastonite	320	13.96-16.02	14.84	0.203	1.371
Fe	LIF	nat. Fe_2O_3	400	0.18- 0.33	0.25	0.039	15.356
Al	TAP	Al_2O_3	nd	31.29-33.11	31.85	0.144	0.452
K	PET	sanidine	330	0.11- 0.22	0.17	0.029	12.192
An %	100*(Ca/(Ca+Na))			71.35-79.59	73.48	0.434	0.586

nd = not determined
* = lower limit of detection in ppm (3 sigma)
** = compositional range and average in oxide wt %
*** = standard deviation (1 sigma) calculated after Kaiser and Specker (1956)
# = relative standard deviation in %

A.II: X-RAY FLUORESCENCE SPECTROMETRY

An ARL 8420 X-ray fluorescence spectrometer was used for the determination of major and trace elements. Analyses were performed on pressed powder pellets. All analyses carried out using a Rhodium tube energised at 50 kV and 50 mA with the Vacuum ON.
Running conditions and instrumental settings are listed in Table A.3 together with the detection limits (ppm) of trace elements.

Table A.3: Instrumental setting for major and trace element analyses.

Element	Line	Crystal	Counter	Count Time	Detection Limit
Si	Ka	PET	FC*	20 sec	-
Ti	Ka	LiF 200	FC	20 "	-
Al	Ka	PET	FC	20 "	-
Fe	Ka	LiF 200	FC	10 "	-
Mn	Ka	LiF 200	FC	10 "	-
Mg	Ka	AX06	FC	10 "	-
Ca	Ka	LiF 200	FC	20 "	-
Na	Ka	AX06	FC	10 "	-
K	Ka	LiF 200	FC	15 "	-
P	Ka	Ge 111	FC	20 "	-
Zn	Ka	LiF 200	SC+	100 "	4
Cu	Ka	LiF 200	SC	100 "	5
Ni	Ka	LiF 200	FC	100 "	4
Co	Ka	LiF 200	FC	100 "	5
Ga	Ka	LiF 200	SC	100 "	5
Zr	Ka	LiF 220	SC	100 "	3
Y	Ka	LiF 220	SC	100 "	3
Sr	Ka	LiF 220	SC	100 "	2
Rb	Ka	LiF 220	SC	100 "	2
Pb	Lb	LiF 200	SC	100 "	5
Cr	Ka	LiF 220	FC	100 "	12
V	Ka	LiF 220	FC	100 "	10
Ba	La	LiF 200	FC	100 "	15
Sc	Ka	LiF 200	FC	100 "	8

* = Flow counter
\+ = Scintillometer

A.III: SULPHUR DETERMINATION

Sulphur determination for 105 samples were carried out at the Geological Survey in Pretoria using a LECO CS244 infrared absorption spectrometer with a HF100 induction furnace in an oxygen stream at 1200 - 1400°C.
Detection limit for S is 6 ppm (6 sigma). Reproducibility for a S concentration of 16 ppm and 330 ppm are 2 ppm and 16 ppm respectively.

A.IV: ANALYTICAL PROCEDURES OF SR-ISOTOPES

Sample preparation and analytical processing were carried out exclusively at the C.S.I.R in Pretoria. Halved drill cores (+- 300 g) were split into small chips after the sample surface had been abraded with a diamond saw. At this stage about 50 g were separated for whole-rock Sr isotope analyses. The remaining material was then put through a gyrol-crusher, followed by 3-4 runs through a roller-crusher. The material was sieved after each run and the remaining fraction (> 250 um) reprocessed. The final product (< 250 um) was then sieved into four size fractions: > 150 um, 150 - 100 um, 100 - 75 um and < 75 um (Careful and extensive sieving was necessary at this stage to optimize magnetic separation).
The 150-100 um fraction proved to be the best size range for magnetic separation, as the individual grain particles were still large enough to ensure even separation, but too small for composite grains to be present. Plagioclase separation was done with a Frantz magnetic separator in 6 consecutive runs. Both the voltage and crossways tilting angle were gradually changed from 0.7 A and 15° to 1.5 A and 0.5°, while the slope angle was fixed at 9°. The impure fractions were regularly discarded.
The final separate (0.5-1.0 g) of samples containing plagioclase as the sole leucocratic mineral had a visually estimated purity of more than 99 % plagioclase. A few separates contained additional quartz and K-feldspar. Quartz in particular remained in the final non-magnetic fraction and its presence was qualitatively confirmed by means of XRD. The possible presence of K-feldspar, although not detected by XRD in a separate from a K-feldspar-rich rock (1.2 modal %), is discussed in Chapter X.2.2.
Each separate was screened under a binocular microscope and remaining mafic minerals were picked out to maximize the final purity. Samples were afterwards washed with analytical grade acetone and dried under an infra-red lamp.
Whole rock samples were powdered for 7 minutes in a tungsten carbide swingmill. Approximately 0.2 g of either powdered whole rock sample or crystalline plagioclase separates were chemically processed according to the techniques outlined by Harmer (1985). Rubidium and strontium concentrations were analyzed by isotope dilution (ID) mass spectrometry. Isotopic determination was done from spiked aliquots (subscript "s" = spiked in Table VIII.1) and from unspiked aliquots (subscript "n" = natural). Rubidium concentrations were determined on a VG Instruments MM 30 mass spectrometer, whereas strontium concentrations and Sr-isotopic ratios were determined on a VG 354 automatic spectrometer fitted with a five collector array.

Uncertainties in $^{87}Sr/^{86}Sr_p$ were determined for 2 spiked duplicates (high Rb samples) and 1 spiked triplicate (Tab. A.4). A constant error of 0.01 % for $^{87}Sr/^{86}Sr_p$ was used for calculating the initial $^{87}Sr/^{86}Sr_o$ ratios (SrR_o) of Rb-poor samples (ppm Rb < 10). SrR_o's of Rb-rich samples (ppm Rb > 16) were recalculated with an error for $^{87}Sr/^{86}Sr_p$ of 0.03 %, except for sample ps 300 29 for which an error of 0.01 % was used based on an individual determination (Tab. A.4).

Based on replicate analyses (Tab. A.4) a 2.6 % error was used for Rb - poor samples for the $^{87}Rb/^{86}Sr$ ratio. An error of 6.5 % was used for high Rb samples, except for sample ps 300 29 (1.8 %). Initial $^{87}Sr/^{86}Sr_o$ ratios are calculated at 2050 Ma (including a 2 sigma +-25 Ma correction) using the ^{87}Rb decay constant of $1.42*10^{-11}$ yr^{-1}. The total error (1 sigma) is based on analytical errors in Rb and Sr concentrations and on the $^{87}Sr/^{86}Sr_p$ ratio and was calculated with the isotope regression package developed by the C.S.I.R., following the equations of York (1969).
A total of 7 measurements on the NBS SRM 987 standard gave a mean of 0.71029 +- 3 (1 sigma) during the period the samples were run. All present-day ratios have been normalized to 0.71024 for this standard.

Table A.4: Uncertainties in $^{87}Rb/^{86}Sr$ and $^{87}Sr/^{86}Sr_p$ as determined from replicate analyses. The individual errors used for calculating the initial $^{87}Sr/^{86}Sr$ ratio is discussed in the text.

Sample	$^{87}Rb/^{86}Sr$ (% error)	$^{87}Sr/^{86}Sr_p$ (% error)	Remarks
ps 377 29 (tripl.)	2.6 %	0.002 %	Rb-poor sample (3 ppm)
ps 300 29 (dupl.)	1.8 %	0.005 %	Rb-rich sample (57 ppm)
ps 319 29 (dupl.)	6.5 %	0.027 %	Rb-rich sample (18 ppm)

Excluding replicate analyses, a total of 39 spiked plagioclase separates, 3 natural plagioclase separates, 3 spiked and 3 natural whole-rock samples were analyzed.
While two of the high Rb separates (ps 319 29 and ps 300 29) are duplicate analyses, separate 311 29 was run as a spiked and as a natural sample. In addition a whole-rock powder of sample wr 300 29 was analysed as well. Results (SrR_o) were identical within analytical uncertainty (1 sigma), independent of the mode of reproduction (duplicates, spiked/unspiked, separate/whole-rock). The aberrant SrR_o's of high Rb samples therefore seem to be "real" values and not just the result of an increasing error associated with the recalculation of Rb-rich samples.
The milled material (< 250 um) of one sample (ps 353 29) was split prior to magnetic separation; the recalculated SrR_o's of the duplicates are indistinguishable at 1 sigma.
Initial ratios of replicate analyses are plotted as the calculated averages. Where initial $^{87}Sr/^{86}Sr$ ratios have been determined for a spiked and a natural sample, only the value of the latter is shown in Figure VIII.1. The results of all the investigated samples are listed in Table VIII.1 according to their stratigraphic position.

MINERAL ANALYSES

Orthopyroxene and plagioclase analyses of the boreholes MDH 1, 22, 23 and 29 are listed according to borehole heights. The stratigraphic unit is given for each sample. Analyses are the calculated averages for grain cores and rims. The number of individual analyses are given for each sample. Only analyses with totals between 98.5 and 101.0 were considered.

Typical standard deviations (1 sigma) of the within-sample variations and the range of the calculated means of the particular samples are presented in the following table. Standard deviations were determined for cumulus and intercumulus plagioclase and for orthopyroxene from the J, K, L and M units. Standard deviations of within-sample variation of cumulus plagioclase and orthopyroxene are close to the analytical precisions (table A.1 and A.2). The latter are presented for comparison.

CUMULUS PLAGIOCLASE

	wt% range	std range	x	n	analytical precision
SiO_2	49.22 - 50.49	0.22 - 0.76	0.40	21	0.22
Al_2O_3	31.62 - 32.24	0.10 - 0.42	0.23	21	0.14
FeO	0.23 - 0.33	0.03 - 0.04	0.03	21	0.04
CaO	14.75 - 15.11	0.17 - 0.38	0.28	21	0.20
Na_2O	2.78 - 3.04	0.07 - 0.16	0.10	21	0.07
K_2O	0.15 - 0.26	0.01 - 0.04	0.02	21	0.03
An%	73.05 - 74.96	0.39 - 1.36	0.72	21	0.43

INTERCUMULUS PLAGIOCLASE

	wt% range	std range	x	n	analytical precision
SiO_2	49.73 - 53.28	0.30 - 1.41	0.77	24	0.22
Al_2O_3	29.85 - 31.95	0.18 - 0.86	0.57	24	0.14
FeO	0.06 - 0.22	0.01 - 0.04	0.03	24	0.04
CaO	12.49 - 15.16	0.18 - 1.11	0.58	24	0.20
Na_2O	2.82 - 4.35	0.09 - 0.61	0.31	24	0.07
K_2O	0.07 - 0.43	0.01 - 0.09	0.04	24	0.03
An%	61.41 - 74.84	0.70 - 5.39	2.73	24	0.43

ORTHOPYROXENE

	wt% range	std range	x	n	analytical precision
SiO_2	53.99 - 55.75	0.11 - 0.79	0.32	26	0.27
TiO_2	0.06 - 0.22	0.00 - 0.04	0.02	26	0.02
Al_2O_3	0.89 - 1.31	0.04 - 0.11	0.06	26	0.05
FeO	7.89 - 14.47	0.13 - 0.63	0.29	26	0.28
MnO	0.18 - 0.26	0.01 - 0.03	0.02	26	0.03
MgO	27.81 - 32.21	0.14 - 0.50	0.29	26	0.15
CaO	0.61 - 1.98	0.12 - 0.67	0.39	26	0.04
Cr_2O_3	0.35 - 0.48	0.01 - 0.04	0.03	26	0.04
Mg#	77.70 - 87.91	0.06 - 0.73	0.30	26	0.30

An% : 100 mol% Ca/(Ca + Na)
Mg# : 100 mol% Mg/(Mg + Fe)

n : number of samples in average, each sample including 8 - 12 analyses.

MDH 1 ORTHOPYROXENE ANALYSES

UNIT - STRATIGRAPHIC HEIGHT - CORE/RIM - NUMBER OF ANALYSES

U	SH	C/R	N	SiO_2	Al_2O_3	MgO	TiO_2	CaO	FeO	MnO	Cr_2O_3	TOTAL	Mg#
J	216.0	C	06	54.57	1.00	28.18	0.14	0.69	14.70	0.27	0.36	99.90	77.4
J	218.0	C	06	54.43	0.95	27.97	0.17	1.06	14.59	0.24	0.39	99.80	77.4
J	220.0	C	07	54.52	1.06	27.49	0.17	1.56	14.79	0.25	0.40	100.24	76.8
H	221.0	C	05	53.99	0.81	26.61	0.17	0.72	16.67	0.33	0.28	99.58	74.0
H	224.0	C	05	54.30	0.98	28.08	0.16	0.98	14.25	0.23	0.39	99.37	77.8
G	227.0	C	06	54.21	1.03	28.18	0.19	1.01	14.03	0.25	0.43	99.33	78.2
G	231.0	C	07	54.46	1.05	28.36	0.17	0.75	14.18	0.24	0.41	99.62	78.1
G	234.0	C	05	54.11	0.99	28.20	0.19	1.09	14.04	0.23	0.33	99.18	78.2
G	236.0	C	06	54.33	1.05	28.30	0.15	1.18	13.95	0.24	0.38	99.58	78.3
G	239.0	C	17	54.56	0.99	28.74	0.16	0.98	14.17	0.25	0.38	100.23	78.3
G	240.0	C	08	55.04	0.94	28.35	0.15	1.33	14.29	0.28	0.39	100.76	78.0
G	242.0	C	13	54.69	0.89	28.58	0.19	1.16	14.06	0.26	0.35	100.17	78.4
G	245.0	C	09	54.58	0.96	28.24	0.20	1.35	13.92	0.28	0.36	99.89	78.3
G	247.0	C	14	54.90	1.00	28.67	0.19	1.08	13.85	0.26	0.34	100.30	78.7
G	248.0	C	07	54.58	0.99	28.55	0.18	1.24	14.59	0.27	0.37	100.77	77.7
F	250.0	C	09	54.45	1.03	27.74	0.14	0.83	14.71	0.29	0.37	99.56	77.1
F	251.0	C	15	54.45	0.92	27.23	0.20	1.11	15.10	0.29	0.32	99.62	76.3
F	253.0	C	11	54.30	1.01	27.51	0.17	1.03	14.89	0.28	0.40	99.57	76.7
F	255.0	C	07	54.34	0.99	28.38	0.17	1.10	14.51	0.30	0.38	100.15	77.7
F	257.0	C	06	54.01	1.08	27.86	0.14	0.94	14.20	0.26	0.42	98.91	77.8
F	258.0	C	10	54.63	1.01	28.03	0.16	1.04	13.48	0.25	0.41	99.01	78.8
E	260.0	C	16	54.51	1.03	28.53	0.15	1.25	13.15	0.24	0.47	99.33	79.5
E	261.0	C	14	54.52	1.14	29.02	0.14	1.50	11.89	0.25	0.45	98.92	81.3
E	262.0	C	13	54.89	1.21	29.37	0.10	1.71	11.70	0.22	0.48	99.68	81.7
E	264.0	C	09	54.90	1.12	28.65	0.14	1.57	12.89	0.22	0.46	99.95	79.9
E	265.0	C	07	55.20	1.23	28.88	0.12	1.66	12.68	0.21	0.47	100.44	80.2
E	267.0	C	12	55.22	1.10	29.23	0.13	1.36	12.15	0.20	0.41	99.79	81.1
E	268.0	C	06	55.09	1.21	28.87	0.11	1.62	12.18	0.20	0.44	99.72	80.9
E	271.0	C	07	54.92	1.25	29.35	0.11	1.50	11.94	0.23	0.46	99.77	81.4
E	273.0	C	06	55.52	1.16	29.54	0.07	1.62	10.49	0.17	0.43	99.00	83.4
E	274.0	C	06	55.21	1.10	29.06	0.11	1.54	11.77	0.23	0.41	99.43	81.5
E	276.0	C	06	54.99	1.33	28.71	0.11	1.95	11.58	0.18	0.49	99.34	81.6
E	277.0	C	07	55.02	1.21	28.92	0.10	1.94	11.45	0.21	0.48	99.33	81.8
E	280.0	C	09	54.76	1.20	28.32	0.11	1.97	12.34	0.20	0.43	99.33	80.4
E	282.0	C	05	54.75	1.27	28.62	0.12	1.72	11.82	0.20	0.47	98.97	81.2
E	284.0	C	10	54.78	1.20	29.10	0.12	1.39	12.53	0.23	0.43	99.78	80.6
E	287.0	C	06	54.49	1.31	28.69	0.12	1.84	12.64	0.19	0.44	99.73	80.2
E	289.0	C	15	54.63	1.20	29.39	0.11	1.35	12.12	0.22	0.42	99.46	81.2
E	292.0	C	09	54.96	1.27	29.85	0.12	1.47	11.46	0.25	0.46	99.84	82.3
E	295.0	C	10	54.82	1.05	28.33	0.12	1.55	13.25	0.24	0.38	99.74	79.2
E	297.0	C	06	54.80	1.25	28.07	0.11	1.46	13.53	0.20	0.41	99.83	78.7
E	299.0	C	06	54.38	1.16	28.15	0.13	1.54	13.45	0.20	0.38	99.38	78.9
E	301.0	C	06	54.40	1.20	28.42	0.11	1.57	13.14	0.24	0.42	99.49	79.4
E	302.0	C	05	55.92	1.23	31.72	0.08	1.40	8.50	0.17	0.46	99.48	86.9
E	303.0	C	08	55.45	1.17	29.44	0.09	1.56	11.66	0.23	0.46	100.06	81.8
E	304.0	C	07	54.80	1.15	28.40	0.10	1.63	12.32	0.23	0.50	99.13	80.4
E	307.0	C	11	55.09	1.09	28.51	0.12	1.51	12.75	0.22	0.43	99.72	80.0
E	310.0	C	08	54.83	1.13	28.73	0.11	1.63	12.94	0.23	0.49	100.10	79.8
E	313.0	C	07	55.20	1.17	28.51	0.10	1.56	12.59	0.21	0.45	99.80	80.1
E	315.0	C	08	55.08	1.06	28.54	0.12	1.51	12.71	0.17	0.43	99.61	80.0
E	318.0	C	06	55.29	1.10	29.22	0.12	1.46	12.76	0.22	0.45	100.62	80.3
E	320.0	C	12	54.77	1.18	29.11	0.10	1.72	12.15	0.26	0.50	99.79	81.0
E	323.0	C	12	55.01	1.16	29.32	0.10	1.41	12.03	0.21	0.48	99.71	81.3
D	335.0	C	07	55.59	1.10	29.59	0.10	1.45	12.02	0.21	0.46	100.53	81.4
D	337.0	C	08	55.91	1.15	30.24	0.10	1.53	10.83	0.20	0.47	100.42	83.3
D	339.0	C	09	54.89	1.13	29.84	0.10	1.59	11.39	0.24	0.51	99.69	82.4
J	216.0	R	06	54.43	1.00	28.20	0.15	0.65	14.72	0.28	0.35	99.77	77.4
J	218.0	R	06	54.36	0.88	28.24	0.17	0.69	14.89	0.27	0.36	99.86	77.2
J	220.0	R	08	54.55	0.90	27.93	0.19	0.87	15.16	0.26	0.27	100.14	76.7
H	221.0	R	04	53.97	0.76	26.79	0.16	0.61	16.47	0.33	0.25	99.35	74.4
H	224.0	R	06	54.23	0.89	28.20	0.16	0.70	14.45	0.22	0.34	99.18	77.7
G	227.0	R	05	54.28	0.99	28.27	0.19	0.70	14.28	0.27	0.41	99.39	77.9
G	231.0	R	07	54.47	0.92	28.40	0.16	0.62	14.22	0.25	0.37	99.41	78.1
G	234.0	R	04	53.98	0.85	28.23	0.18	0.65	14.30	0.22	0.31	98.72	77.9
G	236.0	R	06	54.13	0.96	28.54	0.16	0.68	14.19	0.24	0.37	99.27	78.2
G	239.0	R	16	54.62	0.92	28.95	0.15	0.69	14.24	0.25	0.33	100.15	78.4

MDH 1 ORTHOPYROXENE ANALYSES - continued -

U	SH	C/R	N	SiO_2	Al_2O_3	MgO	TiO_2	CaO	FeO	MnO	Cr_2O_3	TOTAL	Mg#
G	240.0	R	10	55.12	0.82	28.74	0.13	0.70	14.52	0.27	0.31	100.61	77.9
G	242.0	R	13	54.76	0.84	28.93	0.18	0.63	14.25	0.28	0.32	100.19	78.4
G	245.0	R	08	54.59	0.90	28.65	0.17	0.79	14.02	0.26	0.29	99.66	78.5
G	247.0	R	15	54.72	0.86	29.05	0.17	0.75	13.97	0.27	0.29	100.08	78.8
G	248.0	R	07	54.49	0.91	28.92	0.17	0.69	14.85	0.29	0.31	100.62	77.6
F	250.0	R	08	54.37	0.94	27.80	0.15	0.60	14.87	0.28	0.31	99.32	76.9
F	251.0	R	16	54.44	0.85	27.29	0.19	0.75	15.22	0.28	0.29	99.31	76.2
F	253.0	R	11	54.42	0.90	27.62	0.16	0.72	14.94	0.27	0.35	99.38	76.7
F	255.0	R	10	54.26	0.92	28.68	0.15	0.69	14.67	0.30	0.33	100.01	77.7
F	257.0	R	06	54.09	0.91	27.97	0.14	0.65	14.32	0.26	0.38	98.71	77.7
F	258.0	R	10	54.63	0.92	28.23	0.16	0.68	13.55	0.26	0.37	98.80	78.8
E	260.0	R	16	54.48	0.92	28.89	0.17	0.84	13.17	0.25	0.43	99.14	79.6
E	261.0	R	12	54.73	1.00	29.72	0.14	0.66	12.16	0.25	0.42	99.08	81.3
E	262.0	R	10	55.09	1.09	30.15	0.09	0.68	12.01	0.23	0.43	99.77	81.7
E	264.0	R	10	54.75	0.97	29.40	0.19	0.73	13.29	0.22	0.37	99.93	79.8
E	265.0	R	07	55.15	1.14	29.61	0.15	0.78	13.16	0.20	0.42	100.60	80.0
E	267.0	R	12	55.36	0.89	29.83	0.15	0.86	12.13	0.19	0.37	99.79	81.4
E	268.0	R	06	54.98	0.94	29.53	0.15	0.82	12.30	0.22	0.36	99.30	81.1
E	271.0	R	06	55.32	0.97	30.20	0.15	0.73	12.23	0.23	0.36	100.19	81.5
E	273.0	R	05	55.80	1.07	30.37	0.11	0.89	10.25	0.19	0.38	99.06	84.1
E	274.0	R	07	55.09	0.96	29.50	0.14	0.83	12.11	0.23	0.38	99.25	81.3
E	276.0	R	06	55.13	1.14	29.61	0.16	0.73	12.05	0.22	0.38	99.43	81.4
E	277.0	R	06	55.23	1.07	29.54	0.16	0.80	11.95	0.22	0.42	99.38	81.5
E	280.0	R	09	54.82	0.86	29.26	0.23	0.89	12.82	0.23	0.28	99.39	80.3
E	282.0	R	05	54.72	1.19	29.31	0.16	0.53	12.28	0.21	0.42	98.82	81.0
E	284.0	R	10	54.80	0.98	29.45	0.19	0.70	12.77	0.24	0.36	99.48	80.4
E	287.0	R	06	54.77	0.97	29.23	0.20	0.87	12.97	0.19	0.33	99.54	80.1
E	289.0	R	15	54.70	0.98	29.74	0.17	0.72	12.40	0.23	0.36	99.30	81.1
E	292.0	R	09	54.79	1.20	30.18	0.14	0.73	11.74	0.25	0.44	99.47	82.1
E	295.0	R	11	55.15	0.56	28.93	0.16	0.60	13.66	0.28	0.19	99.54	79.1
E	297.0	R	07	55.01	0.66	28.65	0.20	0.70	14.27	0.22	0.22	99.92	78.2
E	299.0	R	06	54.66	0.93	28.66	0.24	0.87	13.57	0.21	0.33	99.46	79.0
E	301.0	R	06	54.39	1.02	28.71	0.18	0.83	13.42	0.24	0.38	99.17	79.2
E	302.0	R	04	55.99	1.14	32.71	0.08	0.70	8.03	0.14	0.44	99.23	87.9
E	303.0	R	09	55.64	0.90	30.16	0.11	0.72	11.58	0.23	0.35	99.69	82.3
E	304.0	R	07	54.73	0.95	29.18	0.09	0.76	12.60	0.23	0.42	98.97	80.5
E	307.0	R	08	55.29	0.78	29.10	0.17	0.75	12.97	0.24	0.29	99.59	80.0
E	310.0	R	06	54.83	0.88	29.07	0.19	1.03	13.17	0.23	0.42	99.83	79.7
E	313.0	R	07	55.23	0.93	28.85	0.15	0.72	13.16	0.23	0.35	99.63	79.6
E	315.0	R	08	55.25	0.94	29.01	0.16	0.85	12.98	0.19	0.40	99.77	79.9
E	318.0	R	06	55.12	0.96	29.64	0.18	0.73	12.93	0.21	0.40	100.18	80.3
E	320.0	R	10	54.64	1.11	29.64	0.12	0.78	12.47	0.26	0.48	99.50	80.9
E	323.0	R	12	54.97	1.01	29.72	0.12	0.82	12.32	0.21	0.44	99.60	81.1
D	335.0	R	07	55.75	0.76	30.10	0.14	0.71	12.22	0.21	0.30	100.19	81.5
D	337.0	R	08	55.93	0.98	30.78	0.12	0.80	10.83	0.20	0.38	100.03	83.5
D	339.0	R	10	54.95	0.97	30.48	0.11	0.78	11.60	0.24	0.44	99.57	82.4

MDH 22 ORTHOPYROXENE ANALYSES

UNIT - STRATIGRAPHIC HEIGHT - CORE/RIM - NUMBER OF ANALYSES

U	SH	C/R	N	SiO_2	TiO_2	Al_2O_3	FeO	MnO	MgO	CaO	Cr_2O_3	Total	Mg#
M	50.0	C	07	55.02	0.20	0.92	14.47	0.25	28.27	1.06	0.40	100.59	77.7
M	55.0	C	07	54.98	0.22	0.98	14.22	0.24	28.63	1.07	0.41	100.76	78.2
M	60.0	C	07	54.37	0.19	0.99	13.97	0.24	28.90	1.36	0.39	100.42	78.7
M	65.0	C	14	54.61	0.20	0.97	13.88	0.24	28.98	1.11	0.38	100.36	78.8
L	70.0	C	07	54.38	0.13	0.97	13.50	0.25	28.25	1.60	0.41	99.49	78.9
L	75.0	C	07	54.06	0.14	1.13	13.93	0.25	28.16	1.26	0.42	99.36	78.3
L	80.0	C	06	54.58	0.11	1.14	13.46	0.23	28.17	1.27	0.35	99.32	78.9
L	85.0	C	06	54.31	0.13	1.21	13.05	0.24	28.58	1.00	0.46	98.98	79.6
L	86.0	C	07	55.71	0.06	1.24	7.89	0.19	32.21	1.66	0.46	99.42	87.9
L	90.0	C	07	53.99	0.14	1.05	13.26	0.25	28.40	1.41	0.39	98.88	79.3
L	95.0	C	07	54.26	0.12	1.04	13.28	0.23	28.36	1.18	0.45	98.91	79.2
L	96.0	C	07	55.11	0.09	1.27	12.06	0.25	28.90	1.98	0.46	100.12	81.0
L	97.0	C	07	54.65	0.14	1.05	13.75	0.26	27.81	1.46	0.46	99.57	78.3
L	100.0	C	07	55.75	0.10	1.31	10.61	0.18	30.16	1.61	0.43	100.14	83.5
L	105.0	C	07	54.95	0.12	0.91	13.00	0.23	28.70	1.37	0.37	99.64	79.7
L	106.0	C	07	55.07	0.12	0.94	13.07	0.22	28.65	1.17	0.41	99.65	79.6
L	111.0	C	07	54.44	0.13	1.02	13.51	0.21	28.37	1.17	0.43	99.27	78.9
K	115.0	C	19	54.68	0.12	1.02	13.60	0.25	28.59	0.94	0.48	99.69	78.9
K	120.0	C	07	54.88	0.12	1.11	13.22	0.22	28.02	1.74	0.47	99.78	79.1
K	125.0	C	07	55.01	0.11	0.93	13.75	0.26	28.40	1.12	0.43	100.01	78.6
K	130.0	C	06	54.82	0.09	1.01	13.54	0.24	28.71	1.02	0.45	99.89	79.1
K	135.0	C	07	55.14	0.11	0.89	13.95	0.25	28.84	0.84	0.40	100.40	78.7
J	140.0	C	07	54.88	0.13	0.99	14.02	0.24	28.69	1.09	0.43	100.46	78.5
J	145.0	C	07	55.20	0.16	0.94	14.24	0.23	28.58	0.94	0.40	100.69	78.2
J	150.0	C	07	55.19	0.15	0.95	13.78	0.22	28.85	0.90	0.40	100.43	78.9
M	50.0	R	07	54.88	0.20	0.90	14.63	0.26	28.42	0.73	0.37	100.38	77.6
M	55.0	R	06	54.96	0.20	0.94	14.50	0.25	28.91	0.64	0.35	100.75	78.1
M	60.0	R	07	54.68	0.21	1.02	14.30	0.27	29.25	0.72	0.37	100.81	78.5
M	65.0	R	13	54.65	0.18	0.93	14.09	0.23	29.22	0.66	0.36	100.32	78.7
L	70.0	R	06	54.30	0.16	0.86	14.00	0.25	28.74	0.83	0.39	99.52	78.5
L	75.0	R	07	53.99	0.13	1.06	14.15	0.26	28.31	0.81	0.40	99.11	78.1
L	80.0	R	07	54.55	0.11	1.08	13.66	0.25	28.29	0.81	0.31	99.06	78.7
L	85.0	R	07	54.17	0.13	1.14	13.15	0.24	28.77	0.78	0.42	98.81	79.6
L	86.0	R	07	55.96	0.06	1.15	7.26	0.17	33.54	0.84	0.42	99.41	89.2
L	90.0	R	06	54.01	0.15	0.91	13.43	0.24	28.72	0.85	0.38	98.69	79.2
L	95.0	R	06	54.68	0.12	0.95	13.20	0.24	28.45	0.84	0.42	98.89	79.4
L	96.0	R	07	54.92	0.10	1.12	11.87	0.25	29.76	0.97	0.43	99.42	81.7
L	97.0	R	07	54.79	0.17	0.87	14.20	0.26	28.25	0.89	0.38	99.81	78.0
L	100.0	R	07	55.84	0.11	1.24	10.02	0.16	31.00	1.08	0.39	99.84	84.6
L	105.0	R	07	55.00	0.12	0.84	13.25	0.23	29.18	0.68	0.32	99.62	79.7
L	106.0	R	07	55.35	0.12	0.86	13.26	0.23	29.07	0.60	0.37	99.87	79.6
L	111.0	R	06	54.66	0.15	0.91	13.48	0.21	28.56	0.83	0.40	99.22	79.1
K	115.0	R	18	54.85	0.11	0.92	13.65	0.25	28.90	0.67	0.43	99.77	79.1
K	120.0	R	07	54.96	0.12	0.97	13.46	0.21	28.61	0.94	0.43	99.70	79.1
K	125.0	R	06	55.12	0.11	0.85	14.00	0.27	28.73	0.73	0.41	100.22	78.5
K	130.0	R	07	55.05	0.10	0.93	13.46	0.24	28.90	0.74	0.44	99.86	79.3
K	135.0	R	07	54.96	0.09	0.79	13.85	0.24	28.89	0.80	0.36	99.97	78.8
J	140.0	R	07	54.84	0.13	0.93	14.05	0.26	28.94	0.69	0.40	100.23	78.6
J	145.0	R	07	55.06	0.16	0.86	14.05	0.22	28.74	0.78	0.38	100.25	78.5
J	150.0	R	07	55.15	0.15	0.88	13.81	0.22	29.00	0.69	0.38	100.27	78.9

MDH 23 ORTHOPYROXENE ANALYSES

UNIT - STRATIGRAPHIC HEIGHT - CORE/RIM - NUMBER OF ANALYSES

U	SH	C/R	N	SiO_2	TiO_2	Al_2O_3	FeO	MnO	MgO	CaO	Cr_2O_3	Total	Mg#
M	82.0	C	09	54.22	0.12	0.77	15.96	0.32	27.02	0.91	0.21	99.53	75.1
M	88.0	C	06	54.39	0.15	0.78	15.45	0.27	27.41	1.17	0.21	99.83	76.0
M	91.0	C	05	54.31	0.14	0.81	14.98	0.29	26.85	1.81	0.24	99.43	76.2
M	94.0	C	10	54.68	0.15	0.78	14.97	0.31	27.77	1.20	0.24	100.11	76.8
M	104.0	C	05	54.38	0.11	0.67	15.31	0.34	27.60	0.79	0.22	99.41	76.3
M	107.0	C	05	54.61	0.09	0.77	15.39	0.31	27.38	1.17	0.27	100.00	76.0
M	109.0	C	09	54.10	0.20	0.82	15.47	0.30	27.21	1.24	0.27	99.62	75.8
M	114.0	C	06	54.30	0.13	0.95	15.81	0.27	26.97	1.27	0.26	99.96	75.3
M	118.0	C	10	54.59	0.13	0.77	15.23	0.32	27.62	0.89	0.27	99.81	76.4
M	120.0	C	06	54.33	0.18	0.94	15.28	0.27	27.10	1.74	0.25	100.10	76.0
M	125.0	C	10	54.30	0.10	0.80	14.30	0.20	27.60	1.60	0.30	99.70	77.4
M	128.0	C	06	54.40	0.16	0.96	14.26	0.30	27.91	1.54	0.32	99.85	77.7
M	134.0	C	10	54.18	0.18	0.91	14.48	0.30	27.40	1.88	0.30	99.63	77.1
M	137.0	C	04	53.74	0.15	0.75	21.01	0.41	24.20	0.60	0.06	100.92	67.2
M	142.0	C	06	54.67	0.19	0.77	15.23	0.27	27.61	1.17	0.29	100.20	76.4
M	145.0	C	10	54.56	0.18	0.80	15.15	0.28	27.68	1.06	0.26	99.96	76.5
M	151.0	C	06	54.42	0.16	0.80	14.91	0.29	27.72	1.09	0.22	99.61	76.8
M	154.0	C	10	54.23	0.15	0.66	15.67	0.34	27.08	0.89	0.22	99.23	75.5
M	162.0	C	06	53.97	0.16	0.72	15.64	0.28	27.66	0.91	0.21	99.55	75.9
M	165.0	C	10	54.69	0.12	0.66	15.69	0.37	27.57	0.77	0.20	100.07	75.8
M	168.0	C	06	54.45	0.15	0.74	15.24	0.24	27.44	0.93	0.27	99.45	76.3
M	170.0	C	06	54.24	0.20	0.79	15.71	0.28	27.14	1.13	0.28	99.76	75.5
M	173.0	C	06	53.95	0.18	0.82	16.64	0.30	26.18	1.12	0.25	99.44	73.7
M	177.0	C	10	53.74	0.19	0.87	16.09	0.32	26.65	1.25	0.25	99.35	74.7
M	181.0	C	05	54.24	0.18	0.87	15.94	0.30	26.32	1.49	0.26	99.61	74.6
M	188.0	C	08	54.52	0.17	0.83	15.36	0.40	27.63	1.04	0.28	100.23	76.2
M	197.0	C	10	54.49	0.17	0.79	14.79	0.32	27.65	1.01	0.21	99.43	76.9
M	203.0	C	06	54.36	0.17	0.74	15.29	0.29	27.25	0.96	0.20	99.26	76.1
M	207.0	C	08	54.44	0.17	0.82	14.83	0.31	27.33	1.25	0.21	99.37	76.7
M	216.0	C	10	54.44	0.20	0.83	15.23	0.30	27.36	1.10	0.27	99.73	76.2
M	218.0	C	06	54.78	0.13	0.82	14.22	0.30	28.32	1.03	0.30	99.91	78.0
M	224.0	C	09	54.60	0.14	0.95	14.09	0.29	27.91	0.85	0.33	99.15	77.9
M	232.0	C	10	54.89	0.16	0.85	13.95	0.29	28.54	0.85	0.40	99.92	78.5
M	238.0	C	09	54.75	0.16	0.98	13.73	0.27	28.09	1.06	0.35	99.39	78.5
M	244.0	C	10	54.51	0.17	0.92	13.92	0.28	28.36	0.90	0.36	99.42	78.4
M	254.0	C	10	54.58	0.20	0.99	13.85	0.28	28.77	0.86	0.40	99.92	78.7
M	259.0	C	06	54.74	0.13	1.23	12.72	0.23	29.18	1.13	0.42	99.78	80.4
M	263.0	C	05	54.67	0.14	1.00	13.87	0.25	28.14	0.82	0.41	99.29	78.3
L	265.0	C	08	53.83	0.15	1.11	14.15	0.27	27.15	1.62	0.39	98.67	77.4
L	268.0	C	06	54.11	0.16	1.13	13.58	0.26	28.03	1.69	0.45	99.41	78.6
L	271.0	C	12	54.53	0.12	1.00	13.76	0.23	28.28	0.98	0.37	99.27	78.6
L	274.0	C	06	54.25	0.15	1.15	13.84	0.26	27.44	1.50	0.41	98.99	78.0
L	277.0	C	06	55.06	0.11	1.25	12.44	0.25	29.34	1.23	0.44	100.12	80.8
L	281.0	C	09	54.77	0.11	1.39	13.34	0.29	28.45	1.22	0.43	100.00	79.2
L	284.0	C	12	54.11	0.10	1.39	13.52	0.26	28.15	1.07	0.41	99.00	78.8
L	286.0	C	06	55.26	0.10	1.50	11.70	0.21	29.88	1.26	0.41	100.32	82.0
L	290.0	C	06	54.70	0.13	1.25	11.48	0.24	29.19	1.59	0.44	99.02	81.9
L	293.0	C	06	54.82	0.14	1.00	13.37	0.27	28.56	1.24	0.43	99.83	79.2
L	296.0	C	06	54.34	0.14	1.02	13.49	0.23	28.71	1.40	0.44	99.77	79.1
L	300.0	C	10	54.41	0.15	1.03	13.70	0.28	28.21	1.35	0.49	99.61	78.6
L	303.0	C	08	55.24	0.11	1.36	11.44	0.26	30.35	1.23	0.40	100.38	82.5
K	304.4	C	06	54.24	0.10	1.26	13.03	0.26	28.88	0.91	0.42	99.10	79.8
K	304.5	C	06	54.27	0.10	1.24	12.15	0.26	29.46	1.25	0.42	99.14	81.2
K	304.9	C	10	54.80	0.08	1.42	11.54	0.25	29.72	1.28	0.43	99.52	82.1
K	305.0	C	10	54.61	0.09	1.43	12.07	0.24	29.48	1.22	0.43	99.58	81.3
K	309.0	C	06	54.66	0.13	1.00	14.09	0.24	27.74	0.96	0.46	99.28	77.8
K	312.0	C	16	54.48	0.11	1.07	13.91	0.26	28.32	1.08	0.48	99.71	78.4
J	323.0	C	09	54.46	0.11	1.13	13.46	0.28	28.70	0.95	0.43	99.50	79.2
J	332.0	C	10	54.42	0.13	0.97	13.67	0.28	28.58	0.93	0.52	99.49	78.8
J	342.0	C	10	54.40	0.13	1.04	13.95	0.33	28.78	0.80	0.44	99.86	78.6
J	353.0	C	10	54.42	0.15	0.94	13.99	0.26	28.62	0.72	0.48	99.57	78.5
J	363.0	C	10	54.16	0.14	1.03	13.91	0.27	28.23	0.92	0.49	99.15	78.4
J	373.0	C	09	54.65	0.15	1.07	13.47	0.30	28.49	0.88	0.49	99.49	79.0
J	382.0	C	07	54.76	0.15	1.09	13.70	0.27	28.51	0.90	0.47	99.85	78.8
J	392.0	C	09	54.53	0.18	1.07	13.63	0.28	28.13	0.80	0.48	99.10	78.6
J	404.0	C	09	54.37	0.17	0.95	13.87	0.28	28.34	0.86	0.45	99.29	78.5

MDH 23 ORTHOPYROXENE ANALYSES - continued -

U	SH	C/R	N	SiO_2	TiO_2	Al_2O_3	FeO	MnO	MgO	CaO	Cr_2O_3	Total	Mg#
J	412.0	C	08	54.58	0.15	0.92	13.74	0.26	28.29	0.94	0.42	99.28	78.6
J	427.0	C	09	54.53	0.13	1.01	13.73	0.26	28.16	1.04	0.51	99.37	78.5
J	430.0	C	06	55.03	0.07	1.51	10.76	0.21	30.38	0.83	0.49	99.29	83.4
J	433.0	C	06	54.93	0.07	1.53	11.10	0.20	29.67	1.37	0.49	99.35	82.7
J	434.0	C	10	54.89	0.05	1.35	10.97	0.23	30.07	0.92	0.54	99.01	83.0
J	439.0	C	06	54.75	0.09	1.60	10.39	0.21	29.96	1.50	0.51	99.02	83.7
H	442.0	C	06	55.51	0.04	1.58	8.43	0.21	32.28	0.87	0.54	99.47	87.2
G	446.0	C	09	54.77	0.06	1.53	10.44	0.22	30.47	1.36	0.57	99.42	83.9
G	450.0	C	06	54.78	0.09	1.38	12.02	0.24	29.77	1.00	0.45	99.73	81.5
G	453.0	C	06	54.87	0.10	1.38	13.14	0.24	28.38	1.33	0.44	99.89	79.4
G	458.0	C	09	54.51	0.10	1.27	12.42	0.27	29.02	1.14	0.45	99.16	80.6
G	461.0	C	06	55.14	0.06	1.42	11.24	0.24	29.77	1.45	0.46	99.79	82.5
G	465.4	C	06	54.78	0.07	1.43	10.53	0.24	29.61	1.78	0.41	98.84	83.4
F	465.6	C	10	56.13	0.08	1.26	6.87	0.17	33.67	0.60	0.38	99.16	89.7
F	469.0	C	09	54.71	0.08	1.39	10.73	0.25	30.23	1.29	0.46	99.14	83.4
F	472.0	C	10	55.49	0.11	1.32	10.56	0.24	30.54	1.16	0.50	99.93	83.8
E	475.0	C	04	54.88	0.07	1.60	9.90	0.22	30.08	1.58	0.53	98.86	84.4
E	477.0	C	09	55.07	0.10	1.40	11.08	0.24	29.48	1.20	0.46	99.02	82.6
E	481.0	C	10	55.14	0.11	1.39	11.59	0.25	29.28	1.57	0.45	99.77	81.8
E	485.0	C	09	54.57	0.10	1.28	11.33	0.26	28.94	1.75	0.49	98.71	82.0
E	488.0	C	10	55.38	0.09	1.39	10.68	0.26	30.87	1.33	0.49	100.49	83.7
E	490.0	C	06	54.95	0.11	1.22	10.83	0.25	29.77	1.52	0.43	99.08	83.1
E	493.0	C	08	54.36	0.12	1.22	11.77	0.22	28.92	1.76	0.47	98.86	81.4
E	495.0	C	06	54.63	0.09	1.24	11.94	0.22	29.44	1.35	0.45	99.35	81.5
E	499.0	C	09	55.11	0.12	1.13	12.19	0.26	28.80	1.53	0.45	99.59	80.8
E	502.0	C	10	55.12	0.12	1.13	12.08	0.23	29.11	1.66	0.47	99.94	81.1
E	505.0	C	10	54.54	0.16	1.08	11.79	0.21	29.21	1.59	0.43	99.01	81.5
E	508.0	C	10	54.86	0.09	1.24	11.57	0.24	29.57	1.50	0.45	99.52	82.0
E	511.0	C	09	55.08	0.12	1.11	11.86	0.23	29.13	1.68	0.46	99.67	81.4
E	514.0	C	06	54.93	0.10	1.22	11.77	0.19	29.20	1.52	0.44	99.37	81.6
E	517.0	C	10	55.00	0.16	1.05	12.90	0.25	29.27	1.51	0.41	100.55	80.2
E	520.0	C	10	54.94	0.10	1.01	12.37	0.26	28.73	1.45	0.49	99.34	80.5
E	521.0	C	09	55.24	0.08	1.33	8.65	0.19	30.95	1.70	0.50	98.64	86.4
E	523.0	C	10	54.82	0.09	1.36	11.55	0.25	29.59	1.22	0.45	99.34	82.0
E	526.0	C	10	54.86	0.12	1.19	12.18	0.24	29.44	1.35	0.50	99.88	81.2
E	530.0	C	10	55.00	0.09	1.13	12.15	0.25	29.36	1.51	0.51	100.00	81.2
E	533.0	C	08	54.96	0.15	1.08	12.55	0.24	29.37	1.36	0.44	100.15	80.7
E	537.0	C	10	54.38	0.10	1.06	12.46	0.27	28.41	1.60	0.49	98.78	80.3
M	82.0	R	10	54.16	0.12	0.68	16.01	0.32	27.14	0.67	0.20	99.30	75.1
M	88.0	R	06	54.23	0.14	0.74	15.52	0.26	27.51	0.85	0.21	99.46	76.0
M	91.0	R	05	54.34	0.14	0.73	15.46	0.27	27.29	0.72	0.20	99.15	75.9
M	94.0	R	10	54.70	0.15	0.74	15.20	0.33	27.99	0.74	0.23	100.08	76.7
M	104.0	R	04	54.31	0.12	0.69	15.37	0.38	27.55	0.73	0.21	99.34	76.2
M	107.0	R	05	54.54	0.09	0.71	15.51	0.31	27.67	0.73	0.26	99.83	76.1
M	109.0	R	10	54.04	0.19	0.74	15.57	0.31	27.44	0.86	0.25	99.40	75.9
M	114.0	R	06	54.14	0.12	0.91	16.56	0.29	27.03	0.82	0.26	100.13	74.4
M	118.0	R	10	54.48	0.12	0.72	15.26	0.32	27.69	0.70	0.27	99.55	76.4
M	120.0	R	06	54.39	0.19	0.90	15.73	0.26	27.49	0.81	0.25	100.02	75.7
M	125.0	R	08	54.39	0.17	0.80	14.66	0.28	28.09	0.83	0.32	99.54	77.4
M	128.0	R	06	54.38	0.18	0.88	14.43	0.30	28.14	0.96	0.30	99.56	77.7
M	134.0	R	10	54.15	0.18	0.82	14.96	0.29	27.92	0.77	0.28	99.36	76.9
M	137.0	R	03	53.51	0.15	0.68	21.80	0.41	24.02	0.58	0.05	101.19	66.3
M	142.0	R	06	54.77	0.18	0.72	15.27	0.28	27.88	0.87	0.28	100.23	76.5
M	145.0	R	10	54.59	0.18	0.79	15.18	0.30	27.87	0.73	0.23	99.86	76.6
M	151.0	R	06	54.25	0.15	0.78	15.07	0.28	27.61	0.83	0.22	99.18	76.6
M	154.0	R	10	54.24	0.15	0.64	15.64	0.35	27.18	0.69	0.20	99.09	75.6
M	162.0	R	06	53.95	0.15	0.70	15.62	0.27	27.81	0.66	0.21	99.37	76.0
M	165.0	R	10	54.66	0.12	0.61	15.65	0.37	27.77	0.57	0.20	99.95	76.0
M	168.0	R	06	54.53	0.13	0.73	15.33	0.25	27.56	0.67	0.24	99.43	76.2
M	170.0	R	06	54.20	0.18	0.77	15.81	0.28	27.29	0.86	0.25	99.65	75.5
M	173.0	R	06	53.81	0.18	0.77	17.07	0.33	26.43	0.66	0.22	99.47	73.4
M	177.0	R	10	53.56	0.21	0.77	16.47	0.33	26.64	0.79	0.22	99.00	74.3
M	181.0	R	05	54.20	0.16	0.78	16.38	0.32	26.68	0.76	0.22	99.51	74.4
M	188.0	R	07	54.39	0.18	0.72	15.45	0.33	27.82	0.66	0.25	99.80	76.3
M	197.0	R	10	54.45	0.17	0.70	14.93	0.32	27.85	0.72	0.21	99.35	76.9
M	203.0	R	06	54.44	0.17	0.72	15.26	0.29	27.33	0.70	0.21	99.11	76.2
M	207.0	R	07	54.64	0.18	0.73	14.99	0.33	27.68	0.71	0.19	99.46	76.7
M	216.0	R	09	54.40	0.18	0.78	15.26	0.31	27.51	0.67	0.25	99.37	76.3

MDH 23 ORTHOPYROXENE ANALYSES - continued -

U	SH	C/R	N	SiO_2	TiO_2	Al_2O_3	FeO	MnO	MgO	CaO	Cr_2O_3	Total	Mg#
M	218.0	R	06	54.91	0.15	0.73	14.15	0.29	28.27	0.71	0.26	99.47	78.1
M	224.0	R	10	54.67	0.13	0.90	14.14	0.28	28.20	0.60	0.31	99.23	78.1
M	232.0	R	10	54.72	0.15	0.78	13.91	0.30	28.58	0.66	0.38	99.48	78.6
M	238.0	R	09	54.78	0.15	0.85	13.98	0.25	28.42	0.62	0.33	99.37	78.4
M	244.0	R	10	54.44	0.18	0.80	13.90	0.28	28.43	0.67	0.35	99.06	78.5
M	254.0	R	10	54.70	0.18	0.88	13.88	0.27	28.90	0.62	0.36	99.79	78.8
M	259.0	R	06	54.65	0.12	1.13	12.95	0.24	29.17	0.76	0.40	99.43	80.1
M	263.0	R	05	54.62	0.12	0.90	13.91	0.26	28.09	0.67	0.36	98.93	78.3
L	265.0	R	10	54.60	0.15	0.96	14.39	0.27	27.50	0.73	0.36	98.95	77.3
L	268.0	R	06	54.21	0.14	1.04	13.83	0.27	28.47	0.86	0.41	99.25	78.6
L	271.0	R	12	54.52	0.13	0.88	13.94	0.22	28.57	0.66	0.34	99.26	78.5
L	274.0	R	06	54.32	0.14	1.03	14.02	0.27	27.96	0.64	0.36	98.75	78.0
L	277.0	R	06	55.28	0.10	1.08	11.34	0.22	30.17	0.90	0.36	99.45	82.6
L	281.0	R	10	54.69	0.10	1.34	13.45	0.29	28.81	0.71	0.41	99.78	79.3
L	284.0	R	11	54.18	0.10	1.30	13.77	0.26	28.40	0.73	0.40	99.13	78.6
L	286.0	R	06	55.33	0.10	1.39	11.68	0.20	30.09	0.74	0.38	99.91	82.0
L	290.0	R	06	54.85	0.11	1.10	11.17	0.23	30.30	0.75	0.37	98.89	82.9
L	293.0	R	06	54.91	0.13	0.83	13.47	0.27	28.96	0.70	0.39	99.66	79.3
L	296.0	R	06	54.06	0.14	0.94	13.83	0.24	29.03	0.88	0.44	99.56	78.9
L	300.0	R	10	54.54	0.13	0.90	13.88	0.28	28.79	0.66	0.42	99.61	78.7
L	303.0	R	08	55.43	0.08	1.22	11.50	0.24	30.80	0.64	0.34	100.26	82.7
K	304.4	R	06	54.36	0.11	1.16	13.08	0.24	28.98	0.66	0.40	98.98	79.8
K	304.5	R	06	54.67	0.08	1.05	12.14	0.24	29.63	0.66	0.37	98.83	81.3
K	304.9	R	10	54.83	0.06	1.27	11.51	0.27	30.17	0.84	0.40	99.35	82.4
K	305.0	R	10	54.61	0.09	1.26	11.98	0.23	29.72	0.81	0.38	99.08	81.6
K	309.0	R	06	54.61	0.12	0.86	14.02	0.25	28.00	0.87	0.40	99.13	78.1
K	312.0	R	16	54.56	0.12	0.88	13.96	0.27	28.54	0.67	0.45	99.45	78.5
J	323.0	R	09	54.70	0.09	0.98	13.47	0.26	29.02	0.57	0.41	99.51	79.3
J	332.0	R	10	54.49	0.13	0.94	13.70	0.26	28.89	0.66	0.48	99.56	79.0
J	342.0	R	10	54.56	0.12	0.95	13.90	0.29	28.90	0.60	0.42	99.73	78.8
J	353.0	R	10	54.62	0.15	0.97	14.32	0.28	28.79	0.65	0.46	100.24	78.2
J	363.0	R	10	54.15	0.14	0.90	13.88	0.27	28.52	0.67	0.45	98.96	78.6
J	373.0	R	10	54.78	0.15	1.00	13.57	0.29	28.77	0.63	0.45	99.64	79.1
J	382.0	R	07	54.83	0.15	0.98	13.54	0.26	28.78	0.64	0.43	99.63	79.1
J	392.0	R	09	54.69	0.17	0.95	13.59	0.28	28.36	0.64	0.44	99.13	78.8
J	404.0	R	08	54.32	0.17	0.89	13.87	0.28	28.42	0.64	0.43	99.03	78.5
J	412.0	R	08	54.43	0.14	0.85	13.73	0.25	28.44	0.70	0.39	98.94	78.7
J	427.0	R	08	54.80	0.12	0.88	13.89	0.25	28.38	0.69	0.45	99.47	78.5
J	430.0	R	06	54.95	0.06	1.35	10.74	0.22	30.46	0.58	0.46	98.83	83.5
J	433.0	R	06	54.88	0.07	1.44	11.27	0.22	29.94	1.16	0.47	99.44	82.6
J	434.0	R	10	55.01	0.05	1.21	11.09	0.24	30.26	0.70	0.48	99.05	82.9
J	439.0	R	06	55.13	0.10	1.41	10.78	0.21	30.58	0.86	0.40	99.47	83.5
H	442.0	R	06	55.46	0.05	1.42	8.41	0.21	32.47	0.72	0.48	99.23	87.3
G	446.0	R	09	54.71	0.06	1.46	10.50	0.22	30.85	0.77	0.51	99.08	84.0
G	450.0	R	05	54.88	0.08	1.32	12.09	0.24	29.93	0.78	0.44	99.75	81.5
G	453.0	R	06	54.85	0.11	1.30	13.41	0.23	28.66	0.80	0.40	99.76	79.2
G	458.0	R	09	54.56	0.10	1.16	12.48	0.28	29.18	0.95	0.43	99.12	80.6
G	461.0	R	05	55.15	0.07	1.27	11.48	0.23	30.32	0.69	0.41	99.62	82.5
G	465.4	R	06	54.82	0.06	1.42	10.87	0.24	30.41	0.75	0.33	98.89	83.3
F	465.6	R	09	56.40	0.09	1.22	6.47	0.15	34.18	0.46	0.50	99.48	90.4
F	469.0	R	09	54.95	0.09	1.16	10.80	0.25	30.62	0.67	0.40	98.95	83.5
F	472.0	R	10	55.63	0.10	1.21	10.62	0.25	30.95	0.74	0.48	99.96	83.9
E	475.0	R	04	54.88	0.09	1.50	10.55	0.22	30.34	0.89	0.39	98.84	83.7
E	477.0	R	08	55.24	0.10	1.23	11.10	0.22	29.92	0.73	0.36	98.91	82.8
E	481.0	R	10	55.31	0.11	1.22	11.72	0.26	29.76	0.83	0.37	99.59	81.9
E	485.0	R	08	54.72	0.12	1.13	11.62	0.26	29.67	0.87	0.42	98.81	82.0
E	488.0	R	10	55.09	0.11	1.19	10.47	0.25	31.30	0.77	0.42	99.59	84.2
E	490.0	R	06	55.11	0.13	1.10	10.84	0.22	30.51	0.75	0.38	99.05	83.4
E	493.0	R	08	54.71	0.20	1.01	11.90	0.24	29.74	0.92	0.41	99.13	81.7
E	495.0	R	06	54.69	0.15	1.13	11.92	0.23	29.71	0.71	0.42	98.96	81.6
E	499.0	R	07	55.41	0.18	0.82	12.54	0.26	29.72	0.71	0.36	100.00	80.9
E	502.0	R	09	55.30	0.19	0.88	12.68	0.25	29.90	0.66	0.36	100.22	80.8
E	505.0	R	10	54.69	0.18	0.85	12.30	0.22	30.16	0.54	0.32	99.26	81.4
E	508.0	R	10	55.11	0.12	1.22	11.76	0.24	30.14	0.83	0.45	99.88	82.0
E	511.0	R	08	55.27	0.17	0.97	12.23	0.25	29.68	0.87	0.43	99.86	81.2
E	514.0	R	06	54.93	0.12	1.04	12.13	0.21	29.68	0.73	0.38	99.22	81.3
E	517.0	R	10	55.05	0.19	0.91	12.96	0.25	29.81	0.91	0.37	100.46	80.4
E	520.0	R	10	55.18	0.11	0.94	12.61	0.25	29.31	0.82	0.44	99.67	80.6

MDH 23 ORTHOPYROXENE ANALYSES - continued -

U	SH	C/R	N	SiO_2	TiO_2	Al_2O_3	FeO	MnO	MgO	CaO	Cr_2O_3	Total	Mg#
E	521.0	R	08	55.50	0.09	1.27	8.16	0.18	32.11	0.84	0.43	98.58	87.5
E	523.0	R	10	54.95	0.08	1.40	11.61	0.25	30.19	0.69	0.42	99.58	82.3
E	526.0	R	10	55.11	0.12	1.04	12.32	0.25	30.01	0.76	0.45	100.07	81.3
E	530.0	R	09	55.10	0.11	1.01	12.34	0.26	29.87	0.79	0.48	99.97	81.2
E	533.0	R	08	55.12	0.14	0.88	12.78	0.26	29.63	0.74	0.33	99.88	80.5
E	537.0	R	09	54.57	0.15	0.88	12.76	0.28	28.99	0.90	0.40	98.93	80.2

MDH 29 ORTHOPYROXENE ANALYSES

UNIT - STRATIGRAPHIC HEIGHT - CORE/RIM - NUMBER OF ANALYSES

U	SH	C/R	N	SiO_2	TiO_2	Al_2O_3	FeO	MnO	MgO	CaO	Cr_2O_3	Total	Mg#
K	2.0	C	07	55.16	0.12	1.20	12.88	0.25	28.18	1.86	0.47	100.12	79.6
K	8.0	C	07	54.76	0.14	0.97	14.17	0.25	27.97	1.19	0.43	99.88	77.9
K	15.0	C	14	55.28	0.14	0.97	14.07	0.27	28.32	1.14	0.44	100.64	78.2
K	20.4	C	07	55.40	0.13	0.86	14.06	0.27	28.76	1.05	0.37	100.90	78.5
K	26.0	C	07	55.03	0.20	0.91	14.61	0.25	28.04	0.82	0.36	100.22	77.4
K	32.0	C	07	55.04	0.15	0.99	13.84	0.25	28.49	1.10	0.46	100.32	78.6
J	37.0	C	05	54.83	0.16	0.95	14.42	0.29	28.40	1.06	0.47	100.58	77.8
J	43.0	C	07	55.30	0.16	0.99	14.15	0.29	28.62	0.95	0.40	100.86	78.3
J	49.0	C	07	54.98	0.18	1.01	14.22	0.28	28.17	0.89	0.42	100.15	77.9
J	55.0	C	07	54.76	0.18	1.01	14.56	0.22	28.47	0.94	0.38	100.51	77.7
J	60.0	C	07	55.43	0.14	0.98	14.06	0.29	28.47	1.01	0.43	100.82	78.3
J	66.0	C	07	54.59	0.17	0.99	14.27	0.26	28.68	0.97	0.39	100.31	78.2
J	72.0	C	07	54.75	0.20	0.89	14.57	0.28	28.37	0.94	0.40	100.39	77.6
J	77.0	C	07	55.02	0.16	0.96	14.19	0.24	28.98	0.83	0.43	100.80	78.5
J	83.0	C	07	54.89	0.16	0.95	14.03	0.26	28.74	0.94	0.49	100.48	78.5
J	88.0	C	07	54.95	0.14	1.03	14.22	0.23	28.88	0.98	0.47	100.90	78.4
J	90.0	C	12	55.31	0.15	1.07	12.85	0.24	29.38	1.24	0.47	100.71	80.3
J	95.0	C	07	55.32	0.18	0.89	13.95	0.26	28.73	1.06	0.48	100.88	78.6
J	96.0	C	10	54.19	0.14	0.98	14.23	0.28	27.91	1.17	0.46	99.35	77.8
J	100.0	C	07	54.81	0.16	1.03	14.13	0.23	28.78	1.00	0.47	100.60	78.4
J	105.0	C	07	54.50	0.15	1.04	14.19	0.26	28.78	0.98	0.48	100.38	78.3
J	109.0	C	07	54.87	0.16	0.99	14.01	0.26	28.63	0.81	0.46	100.19	78.5
J	113.0	C	14	55.20	0.15	1.05	14.13	0.28	28.59	0.99	0.42	100.79	78.3
J	117.0	C	07	55.08	0.15	1.08	13.74	0.24	28.49	1.05	0.47	100.29	78.7
J	120.0	C	07	55.18	0.16	1.02	14.02	0.26	28.53	0.93	0.43	100.53	78.4
J	125.0	C	07	54.98	0.15	0.98	14.12	0.22	28.75	0.98	0.43	100.59	78.4
J	129.0	C	07	54.91	0.15	0.97	14.14	0.27	28.56	0.99	0.48	100.47	78.3
J	134.0	C	06	54.26	0.16	0.98	13.92	0.23	28.21	1.14	0.43	99.33	78.3
J	139.0	C	07	54.67	0.19	0.96	13.99	0.27	28.45	1.04	0.44	100.02	78.4
J	144.0	C	07	55.06	0.14	1.05	14.12	0.27	28.43	0.99	0.43	100.47	78.2
J	152.0	C	07	54.86	0.14	0.91	14.11	0.25	28.26	0.92	0.42	99.86	78.1
J	158.0	C	07	54.62	0.19	0.87	14.25	0.24	28.52	1.05	0.41	100.15	78.1
J	166.0	C	07	54.75	0.20	0.85	14.41	0.25	28.11	1.26	0.36	100.18	77.7
J	172.0	C	07	54.57	0.20	0.90	14.30	0.28	28.38	1.03	0.39	100.07	78.0
J	179.0	C	07	55.01	0.18	0.95	14.29	0.27	28.71	0.93	0.40	100.74	78.2
J	185.0	C	14	54.91	0.19	1.02	14.36	0.26	28.13	0.90	0.38	100.15	77.7
J	191.0	C	06	55.12	0.21	0.96	14.65	0.23	28.67	0.77	0.38	100.98	77.7
J	196.0	C	07	54.73	0.20	0.98	14.63	0.22	28.20	1.13	0.37	100.47	77.5
J	202.0	C	10	55.16	0.22	1.04	14.51	0.19	28.52	0.82	0.43	100.88	77.8
J	210.0	C	09	54.30	0.20	0.97	14.48	0.19	28.68	0.81	0.39	100.03	77.9
J	215.0	C	09	55.08	0.21	1.02	13.75	0.19	28.44	0.92	0.44	100.05	78.7
H	219.0	C	08	54.83	0.19	0.99	14.81	0.21	27.69	1.00	0.41	100.12	76.9
H	223.0	C	09	54.87	0.17	0.97	14.21	0.20	28.37	0.89	0.43	100.11	78.1
H	227.0	C	08	55.25	0.17	1.01	13.38	0.24	28.96	0.89	0.39	100.29	79.4
H	229.0	C	06	55.26	0.14	1.27	11.76	0.23	30.16	0.75	0.44	100.00	82.1
G	231.0	C	14	54.95	0.17	0.99	14.30	0.26	28.04	1.09	0.41	100.21	77.8
G	233.0	C	06	54.31	0.19	1.00	14.51	0.27	27.77	0.76	0.39	99.20	77.3
G	240.0	C	16	55.42	0.16	1.01	14.28	0.26	28.58	0.78	0.42	100.91	78.1
G	247.0	C	09	55.42	0.12	0.99	13.76	0.21	28.77	0.92	0.45	100.65	78.9
G	250.0	C	06	54.71	0.15	0.98	14.15	0.23	28.41	0.76	0.39	99.80	78.2
G	254.0	C	10	55.54	0.15	1.06	13.40	0.22	28.96	1.00	0.45	100.79	79.4
G	260.0	C	09	55.40	0.15	1.05	13.52	0.21	29.16	0.79	0.49	100.77	79.4
G	269.0	C	07	55.31	0.14	1.08	13.26	0.15	28.73	1.34	0.43	100.44	79.4
G	273.0	C	07	55.23	0.16	0.99	13.37	0.22	28.35	1.42	0.45	100.19	79.1
G	276.0	C	10	55.56	0.20	1.02	13.55	0.20	28.87	1.06	0.45	100.90	79.2
G	278.0	C	06	54.43	0.19	1.00	13.70	0.23	28.08	1.32	0.40	99.35	78.5
G	284.0	C	10	54.88	0.19	1.01	13.97	0.19	28.43	1.29	0.43	100.38	78.4
G	286.0	C	06	54.85	0.19	0.95	14.31	0.26	28.22	1.05	0.40	100.22	77.9
F	288.0	C	16	53.95	0.12	0.93	17.28	0.27	25.93	0.85	0.37	99.70	72.8
F	289.0	C	05	54.62	0.12	0.92	15.33	0.27	27.40	0.86	0.32	99.84	76.1
F	291.0	C	06	54.20	0.13	1.20	13.28	0.24	29.05	0.73	0.40	99.23	79.6
F	295.0	C	05	54.50	0.21	0.91	16.59	0.29	26.59	1.02	0.33	100.44	74.1
F	300.0	C	13	54.67	0.24	0.98	16.15	0.30	27.24	1.12	0.32	101.01	75.0
F	304.0	C	06	54.13	0.20	0.93	15.56	0.25	27.20	0.74	0.33	99.33	75.7
F	306.0	C	10	54.68	0.21	0.99	15.95	0.29	27.47	1.11	0.38	101.09	75.4
F	310.0	C	06	55.04	0.21	1.01	15.45	0.28	27.66	0.93	0.41	100.98	76.1

MDH 29 ORTHOPYROXENE ANALYSES - continued -

U	SH	C/R	N	SiO_2	TiO_2	Al_2O_3	FeO	MnO	MgO	CaO	Cr_2O_3	Total	Mg#
E	311.5	C	06	55.74	0.10	1.47	8.91	0.18	32.82	0.73	0.44	100.38	86.8
E	311.8	C	10	54.40	0.13	1.02	13.97	0.27	27.85	1.47	0.50	99.60	78.0
E	313.0	C	08	55.18	0.13	1.09	14.11	0.26	27.89	1.35	0.47	100.48	77.9
E	315.0	C	06	55.67	0.11	1.34	11.26	0.22	30.44	1.45	0.46	100.95	82.8
E	316.8	C	05	55.11	0.10	1.52	8.76	0.12	31.57	1.72	0.49	99.39	86.5
E	317.0	C	08	54.61	0.09	1.13	13.00	0.25	28.29	1.70	0.45	99.51	79.5
E	319.1	C	10	55.23	0.10	1.28	11.19	0.16	29.80	1.77	0.52	100.04	82.6
E	319.8	C	10	54.81	0.12	1.08	13.17	0.18	28.86	1.80	0.48	100.52	79.6
E	321.0	C	09	55.01	0.11	1.26	12.57	0.23	28.63	1.56	0.47	99.85	80.2
E	325.0	C	10	56.01	0.11	1.13	11.95	0.17	29.74	1.39	0.44	100.93	81.6
E	327.0	C	09	55.49	0.12	1.13	11.98	0.23	28.92	1.77	0.43	100.07	81.2
E	330.0	C	09	55.60	0.09	1.30	10.39	0.17	30.42	1.69	0.49	100.15	83.9
E	333.0	C	10	55.39	0.09	1.37	11.12	0.15	30.21	1.51	0.47	100.32	82.9
E	335.0	C	10	55.98	0.11	1.26	10.88	0.16	30.38	1.49	0.45	100.70	83.3
E	339.0	C	10	55.66	0.11	1.18	11.44	0.16	30.16	1.54	0.46	100.70	82.5
E	342.0	C	07	55.56	0.11	1.37	11.61	0.18	29.85	1.72	0.52	100.93	82.1
E	345.0	C	09	55.09	0.12	1.25	11.94	0.21	29.14	1.55	0.47	99.78	81.3
E	347.0	C	10	55.74	0.07	1.35	10.94	0.16	30.37	1.69	0.49	100.80	83.2
E	349.0	C	14	55.06	0.13	1.26	12.63	0.23	28.94	1.70	0.47	100.42	80.3
E	350.0	C	09	55.21	0.13	1.30	11.89	0.23	29.24	1.66	0.46	100.12	81.4
E	351.0	C	11	55.42	0.12	1.27	12.18	0.16	29.17	1.76	0.46	100.54	81.0
E	353.0	C	08	55.16	0.11	1.27	13.24	0.17	28.89	1.45	0.42	100.62	79.6
E	355.0	C	07	55.01	0.15	1.21	13.02	0.26	28.64	1.62	0.44	100.35	79.7
E	357.0	C	09	54.92	0.12	1.21	12.56	0.26	29.12	1.46	0.42	100.07	80.5
E	359.0	C	09	55.10	0.13	1.19	12.11	0.20	29.29	1.48	0.45	99.94	81.2
E	362.0	C	10	55.16	0.10	1.36	11.24	0.18	29.90	1.79	0.49	100.23	82.6
E	367.0	C	17	54.97	0.11	1.13	12.26	0.23	29.01	1.70	0.41	99.82	80.8
E	369.0	C	09	55.22	0.14	1.17	12.65	0.21	28.73	1.49	0.44	100.07	80.2
E	373.0	C	10	55.32	0.11	1.19	12.04	0.19	29.80	1.61	0.46	100.73	81.5
E	377.0	C	09	55.61	0.09	1.22	11.45	0.18	29.77	1.69	0.49	100.49	82.3
E	379.0	C	08	54.88	0.14	1.07	12.53	0.20	28.92	1.43	0.44	99.60	80.4
E	381.0	C	07	55.19	0.14	1.17	12.00	0.22	28.68	1.62	0.38	99.41	81.0
E	383.0	C	09	55.64	0.11	1.28	11.42	0.20	29.95	1.51	0.49	100.59	82.4
E	386.0	C	07	54.80	0.12	1.23	12.44	0.23	29.26	1.49	0.45	100.01	80.8
E	390.0	C	07	54.83	0.13	1.19	12.31	0.23	29.40	1.39	0.47	99.95	81.0
E	392.0	C	08	54.55	0.14	1.28	11.77	0.23	29.02	1.51	0.48	98.98	81.5
E	395.0	C	09	55.99	0.11	1.28	11.38	0.17	30.19	1.46	0.48	101.05	82.5
E	397.0	C	09	55.11	0.13	1.18	12.34	0.22	28.49	1.76	0.48	99.71	80.5
E	401.0	C	08	55.78	0.13	1.22	11.72	0.16	29.90	1.49	0.49	100.90	82.0
E	406.0	C	16	55.34	0.12	1.16	11.53	0.20	29.47	1.69	0.49	100.01	82.0
E	410.0	C	08	55.05	0.13	1.04	11.85	0.26	29.12	1.60	0.44	99.49	81.4
E	413.0	C	09	55.60	0.14	1.05	12.49	0.22	28.78	1.34	0.41	100.05	80.4
E	415.0	C	05	54.91	0.12	1.18	11.21	0.23	29.07	1.57	0.47	98.75	82.2
E	418.0	C	10	55.35	0.09	1.12	11.82	0.21	29.42	1.40	0.50	99.92	81.6
E	421.0	C	06	54.70	0.12	1.10	11.65	0.20	29.39	1.48	0.47	99.13	81.8
E	425.0	C	08	54.38	0.12	1.15	12.08	0.23	29.04	1.55	0.53	99.07	81.1
E	427.0	C	05	54.62	0.12	1.12	12.87	0.22	28.94	1.38	0.46	99.72	80.0
E	430.0	C	09	54.41	0.12	1.15	12.46	0.25	28.59	1.70	0.52	99.20	80.4
E	433.3	C	10	55.30	0.09	1.11	12.17	0.27	29.17	1.53	0.51	100.14	81.0
E	433.8	C	09	55.63	0.09	1.32	8.65	0.19	31.62	1.15	0.47	99.13	86.7
E	435.0	C	08	54.54	0.12	1.08	12.37	0.27	28.64	1.58	0.46	99.05	80.5
E	437.0	C	08	55.32	0.11	1.16	12.50	0.21	28.89	1.44	0.52	100.15	80.5
E	439.0	C	06	54.93	0.11	1.16	12.23	0.21	28.78	1.50	0.50	99.41	80.8
E	442.0	C	10	54.70	0.08	1.18	11.82	0.26	28.99	1.67	0.48	99.18	81.4
E	444.0	C	10	54.64	0.10	1.13	12.46	0.27	28.60	1.57	0.49	99.24	80.4
E	445.0	C	10	54.80	0.09	1.10	12.59	0.24	28.52	1.55	0.49	99.39	80.2
E	446.0	C	09	55.04	0.13	1.06	12.90	0.27	28.63	1.47	0.47	99.97	79.8
E	447.0	C	07	54.62	0.12	1.06	13.41	0.27	28.15	1.39	0.47	99.49	78.9
E	450.0	C	10	55.04	0.12	1.01	13.00	0.26	28.22	1.75	0.44	99.83	79.5
E	453.0	C	10	55.04	0.12	1.16	12.23	0.27	28.92	1.50	0.48	99.71	80.8
E	455.0	C	16	55.34	0.13	1.04	12.84	0.27	28.74	1.44	0.45	100.26	80.0
E	457.0	C	10	54.67	0.12	1.02	12.79	0.25	28.70	1.54	0.47	99.28	80.0
E	459.0	C	18	54.92	0.11	1.03	12.50	0.26	28.88	1.61	0.50	99.80	80.5
E	461.0	C	10	54.88	0.11	1.13	12.44	0.27	29.11	1.45	0.47	99.87	80.7
E	464.0	C	09	54.83	0.09	1.10	12.27	0.26	29.05	1.43	0.48	99.51	80.9
E	466.0	C	05	54.77	0.11	1.10	12.32	0.25	28.47	1.57	0.45	99.03	80.5
E	468.0	C	10	55.13	0.10	1.01	11.26	0.26	29.63	1.43	0.48	99.29	82.4
D	471.0	C	06	56.78	0.09	1.11	6.25	0.15	34.48	0.53	0.49	99.88	90.8

MDH 29 ORTHOPYROXENE ANALYSES - continued -

U	SH	C/R	N	SiO_2	TiO_2	Al_2O_3	FeO	MnO	MgO	CaO	Cr_2O_3	Total	Mg#
D	473.0	C	10	55.34	0.07	1.10	11.62	0.26	29.41	1.61	0.48	99.89	81.9
D	474.0	C	09	55.06	0.09	1.12	11.70	0.25	29.38	1.75	0.52	99.86	81.7
D	477.0	C	14	54.42	0.10	1.17	11.65	0.24	29.08	1.74	0.47	98.87	81.7
K	2.0	R	06	54.74	0.11	1.12	13.24	0.26	29.01	0.91	0.40	99.78	79.6
K	8.0	R	07	54.85	0.14	0.89	14.29	0.26	28.15	0.85	0.39	99.82	77.8
K	15.0	R	14	55.34	0.14	0.87	14.17	0.29	28.42	0.86	0.41	100.51	78.2
K	20.4	R	07	55.38	0.12	0.75	14.19	0.27	28.93	0.80	0.33	100.77	78.4
K	26.0	R	07	55.20	0.19	0.88	14.81	0.25	28.19	0.63	0.34	100.50	77.3
K	32.0	R	07	55.20	0.14	0.95	14.08	0.23	28.54	0.72	0.41	100.27	78.3
J	37.0	R	05	54.88	0.15	0.90	14.62	0.28	28.56	0.70	0.44	100.53	77.7
J	43.0	R	06	55.31	0.15	0.96	14.36	0.28	28.86	0.67	0.40	100.98	78.2
J	49.0	R	07	55.14	0.18	0.98	14.22	0.29	28.38	0.73	0.41	100.33	78.1
J	55.0	R	07	54.77	0.17	0.95	14.66	0.23	28.60	0.71	0.37	100.46	77.7
J	60.0	R	07	55.52	0.14	0.93	14.23	0.26	28.71	0.69	0.41	100.88	78.3
J	66.0	R	07	54.36	0.17	0.90	14.44	0.26	28.80	0.71	0.38	100.02	78.1
J	72.0	R	07	54.98	0.19	0.85	14.48	0.27	28.39	0.77	0.39	100.32	77.8
J	77.0	R	07	54.86	0.17	0.96	14.31	0.26	28.99	0.73	0.41	100.69	78.3
J	83.0	R	07	54.75	0.15	0.92	14.19	0.26	28.81	0.82	0.46	100.35	78.4
J	88.0	R	07	55.10	0.14	0.97	14.31	0.24	28.80	0.80	0.46	100.80	78.2
J	90.0	R	12	55.53	0.15	1.01	12.90	0.23	29.64	0.84	0.45	100.73	80.4
J	95.0	R	07	55.46	0.17	0.86	13.96	0.27	28.91	0.85	0.47	100.94	78.7
J	96.0	R	09	54.41	0.13	0.90	14.36	0.28	28.18	0.64	0.44	99.34	77.8
J	100.0	R	06	54.96	0.16	1.01	14.04	0.23	29.02	0.77	0.46	100.65	78.7
J	105.0	R	07	54.91	0.15	1.00	14.21	0.24	28.99	0.77	0.47	100.73	78.4
J	109.0	R	07	55.30	0.15	0.91	13.94	0.25	28.76	0.75	0.45	100.50	78.6
J	113.0	R	13	55.06	0.15	0.97	14.38	0.27	28.64	0.72	0.38	100.57	78.0
J	117.0	R	07	55.09	0.14	1.02	13.74	0.26	28.59	0.77	0.44	100.04	78.8
J	120.0	R	07	55.30	0.15	0.96	14.25	0.25	28.62	0.79	0.40	100.72	78.2
J	125.0	R	06	54.95	0.15	0.92	14.15	0.24	28.92	0.72	0.40	100.45	78.5
J	129.0	R	07	54.80	0.14	0.86	14.15	0.28	28.77	0.70	0.45	100.16	78.4
J	134.0	R	06	54.13	0.15	0.92	14.03	0.23	28.46	0.73	0.39	99.05	78.4
J	139.0	R	07	55.01	0.18	0.89	14.16	0.27	28.76	0.71	0.42	100.40	78.4
J	144.0	R	07	54.92	0.14	0.99	14.06	0.27	28.54	0.73	0.42	100.07	78.4
J	152.0	R	07	54.85	0.14	0.86	14.41	0.25	28.44	0.69	0.42	100.05	77.9
J	158.0	R	07	54.84	0.20	0.85	14.52	0.23	28.81	0.68	0.37	100.49	78.0
J	166.0	R	07	54.67	0.21	0.83	14.65	0.28	28.50	0.73	0.35	100.20	77.6
J	172.0	R	07	54.83	0.19	0.87	14.63	0.28	28.64	0.67	0.39	100.50	77.7
J	179.0	R	06	55.12	0.18	0.88	14.32	0.28	28.79	0.69	0.38	100.62	78.2
J	185.0	R	14	55.10	0.18	0.97	14.38	0.26	28.31	0.67	0.36	100.23	77.8
J	191.0	R	07	55.11	0.18	0.98	14.55	0.25	28.67	0.81	0.36	100.91	77.9
J	196.0	R	07	54.51	0.21	0.97	14.74	0.22	28.42	0.72	0.37	100.15	77.5
J	202.0	R	07	55.33	0.17	0.99	14.54	0.18	28.69	0.67	0.38	100.96	77.9
J	210.0	R	09	54.70	0.14	0.92	14.39	0.19	28.92	0.62	0.34	100.21	78.2
J	215.0	R	09	55.01	0.19	0.95	14.00	0.19	28.45	0.64	0.40	99.82	78.4
H	219.0	R	10	54.54	0.18	0.94	14.85	0.22	27.51	0.85	0.38	99.48	76.8
H	223.0	R	10	55.15	0.15	0.90	13.98	0.20	28.60	0.69	0.40	100.08	78.5
H	227.0	R	10	55.66	0.15	0.88	13.05	0.21	29.63	0.71	0.33	100.61	80.2
H	229.0	R	06	55.24	0.15	1.37	11.66	0.19	30.60	0.53	0.40	100.15	82.4
G	231.0	R	14	55.18	0.17	0.91	14.30	0.26	28.27	0.71	0.36	100.16	77.9
G	233.0	R	06	54.19	0.17	0.93	14.49	0.26	27.85	0.68	0.39	98.95	77.4
G	240.0	R	12	55.31	0.14	0.94	14.00	0.26	28.59	0.66	0.40	100.32	78.5
G	247.0	R	09	55.14	0.12	0.94	13.73	0.21	28.74	0.72	0.44	100.04	78.9
G	250.0	R	06	54.82	0.15	0.94	14.40	0.23	28.59	0.63	0.36	100.12	78.0
G	254.0	R	10	55.60	0.13	1.00	13.12	0.23	29.21	0.66	0.42	100.36	79.9
G	260.0	R	10	55.54	0.14	0.96	13.22	0.22	29.26	0.59	0.43	100.36	79.8
G	269.0	R	07	55.40	0.15	0.96	13.61	0.16	29.16	0.72	0.36	100.51	79.3
G	273.0	R	07	54.96	0.17	0.96	13.60	0.21	28.73	0.67	0.42	99.72	79.0
G	276.0	R	09	55.50	0.18	1.00	13.66	0.19	29.08	0.64	0.42	100.68	79.2
G	278.0	R	05	54.49	0.18	0.95	13.91	0.22	28.47	0.76	0.37	99.36	78.5
G	284.0	R	10	55.01	0.17	0.93	14.05	0.19	28.72	0.75	0.39	100.21	78.5
G	286.0	R	05	54.93	0.19	0.88	14.37	0.27	28.29	0.75	0.36	100.04	77.8
F	288.0	R	04	54.18	0.11	0.87	17.25	0.27	26.20	0.77	0.34	100.00	73.0
F	289.0	R	04	54.55	0.12	0.85	15.28	0.28	27.58	0.72	0.26	99.63	76.3
F	291.0	R	05	54.65	0.12	1.15	12.68	0.25	29.71	0.47	0.33	99.36	80.7
F	295.0	R	05	54.41	0.18	0.87	16.74	0.29	26.74	0.73	0.27	100.24	74.0
F	300.0	R	14	54.56	0.19	0.92	16.28	0.30	27.54	0.65	0.29	100.72	75.1
F	304.0	R	06	53.91	0.17	0.94	15.66	0.26	26.96	0.65	0.33	98.88	75.4
F	306.0	R	15	54.82	0.16	0.93	15.94	0.29	27.74	0.77	0.34	100.99	75.6

MDH 29 ORTHOPYROXENE ANALYSES - continued -

U	SH	C/R	N	SiO_2	TiO_2	Al_2O_3	FeO	MnO	MgO	CaO	Cr_2O_3	Total	Mg#
F	310.0	R	06	55.19	0.18	0.96	15.34	0.31	27.71	0.60	0.38	100.66	76.3
E	311.5	R	06	55.76	0.11	1.49	8.77	0.19	32.71	0.68	0.49	100.20	86.9
E	311.8	R	10	54.75	0.17	0.88	14.24	0.27	28.36	0.86	0.42	99.95	78.0
E	313.0	R	09	55.19	0.17	0.86	14.30	0.26	28.11	0.73	0.38	99.99	77.8
E	315.0	R	04	55.57	0.12	1.17	11.23	0.22	30.95	0.72	0.38	100.36	83.1
E	316.8	R	15	55.55	0.10	1.50	7.91	0.10	33.29	0.67	0.47	99.59	88.2
E	317.0	R	08	54.77	0.17	0.93	13.13	0.26	28.65	0.96	0.40	99.25	79.5
E	319.1	R	10	55.38	0.13	1.15	10.95	0.14	30.56	0.93	0.43	99.67	83.3
E	319.8	R	09	54.91	0.18	0.68	13.53	0.21	29.87	0.70	0.31	100.41	79.7
E	321.0	R	10	55.16	0.15	1.13	12.81	0.23	29.09	0.94	0.45	99.97	80.2
E	325.0	R	10	55.84	0.13	1.14	12.07	0.17	30.03	0.80	0.40	100.59	81.6
E	327.0	R	09	55.60	0.15	0.78	12.30	0.23	29.62	0.89	0.30	99.88	81.1
E	330.0	R	10	55.65	0.10	1.21	10.59	0.15	31.11	0.87	0.42	100.10	84.0
E	333.0	R	10	55.65	0.11	1.18	11.15	0.16	30.83	0.87	0.41	100.36	83.1
E	335.0	R	09	56.10	0.16	1.12	10.58	0.15	31.08	0.84	0.38	100.41	84.0
E	339.0	R	10	55.66	0.14	1.00	11.65	0.17	30.60	0.80	0.40	100.43	82.4
E	342.0	R	07	55.53	0.15	1.21	11.68	0.18	30.38	0.98	0.47	100.58	82.3
E	345.0	R	08	55.25	0.15	1.11	12.34	0.20	29.83	0.65	0.37	99.91	81.2
E	347.0	R	10	55.90	0.07	1.20	11.22	0.17	30.90	0.81	0.42	100.70	83.1
E	349.0	R	14	55.38	0.21	0.80	13.03	0.25	29.24	0.77	0.29	99.97	79.5
E	350.0	R	09	55.53	0.15	1.19	12.20	0.24	29.70	0.84	0.41	100.25	81.3
E	351.0	R	09	55.63	0.19	0.86	12.45	0.17	29.89	0.75	0.31	100.25	81.1
E	353.0	R	08	55.59	0.16	0.76	13.53	0.20	29.32	0.59	0.25	100.52	79.4
E	355.0	R	08	55.54	0.19	0.67	13.40	0.26	29.21	0.68	0.25	100.20	79.5
E	357.0	R	09	54.94	0.19	1.09	12.68	0.27	29.10	0.89	0.39	99.55	80.4
E	359.0	R	09	55.17	0.21	1.04	12.40	0.20	29.66	0.82	0.42	99.91	81.0
E	362.0	R	10	55.06	0.14	1.14	11.28	0.19	30.67	0.77	0.40	99.65	82.9
E	367.0	R	17	55.09	0.19	1.00	12.51	0.23	29.63	0.77	0.39	99.81	80.9
E	369.0	R	09	55.46	0.24	0.88	12.99	0.22	29.10	0.87	0.36	100.11	80.0
E	373.0	R	10	55.50	0.17	1.11	12.29	0.19	30.18	0.84	0.41	100.69	81.4
E	377.0	R	08	55.42	0.12	1.19	11.83	0.20	30.20	0.77	0.48	100.21	82.0
E	379.0	R	07	55.06	0.23	0.74	12.98	0.20	29.23	0.63	0.34	99.42	80.1
E	381.0	R	07	55.53	0.20	0.70	12.44	0.23	29.43	0.63	0.20	99.36	80.8
E	383.0	R	07	55.62	0.16	1.19	11.36	0.21	30.23	0.89	0.51	100.17	82.6
E	386.0	R	07	54.91	0.21	1.01	12.76	0.22	29.92	0.69	0.39	100.12	80.7
E	390.0	R	06	55.04	0.21	1.09	12.35	0.23	29.57	0.83	0.45	99.77	81.0
E	392.0	R	08	54.73	0.22	1.11	12.07	0.23	29.57	0.75	0.46	99.14	81.4
E	395.0	R	07	55.93	0.14	1.20	11.70	0.16	30.77	0.80	0.49	101.19	82.4
E	397.0	R	08	55.16	0.20	0.81	12.88	0.25	29.10	0.67	0.35	99.42	80.1
E	401.0	R	08	55.57	0.21	1.07	12.11	0.17	30.26	0.72	0.45	100.55	81.7
E	406.0	R	17	55.44	0.16	1.07	11.86	0.20	30.15	0.78	0.46	100.12	81.9
E	410.0	R	08	55.19	0.19	0.87	12.14	0.25	29.67	0.91	0.37	99.60	81.3
E	413.0	R	08	55.99	0.16	0.68	12.68	0.22	29.24	0.56	0.24	99.77	80.4
E	415.0	R	05	55.04	0.16	1.05	11.46	0.23	29.70	0.79	0.45	98.88	82.2
E	418.0	R	10	55.17	0.11	1.08	11.94	0.21	29.87	0.69	0.49	99.56	81.7
E	421.0	R	05	54.78	0.15	0.98	12.00	0.21	29.97	0.66	0.45	99.20	81.7
E	425.0	R	07	54.35	0.13	1.06	12.31	0.24	29.53	0.74	0.49	98.85	81.1
E	427.0	R	05	54.41	0.15	0.99	12.85	0.24	29.11	0.79	0.41	98.95	80.2
E	430.0	R	09	54.65	0.14	1.02	12.84	0.26	29.24	0.71	0.48	99.34	80.2
E	433.3	R	10	55.61	0.10	0.97	12.00	0.26	29.74	0.82	0.44	99.94	81.5
E	433.8	R	10	55.91	0.08	1.35	7.96	0.18	32.39	0.82	0.48	99.18	87.9
E	435.0	R	09	54.82	0.13	0.96	12.50	0.26	29.26	0.76	0.43	99.12	80.7
E	437.0	R	08	55.37	0.13	1.04	12.80	0.23	29.37	0.74	0.48	100.16	80.4
E	439.0	R	05	55.20	0.12	1.07	12.52	0.22	29.38	0.75	0.48	99.73	80.7
E	442.0	R	10	55.05	0.10	1.01	12.00	0.26	29.69	0.82	0.43	99.36	81.5
E	444.0	R	10	54.90	0.10	1.03	12.61	0.26	29.20	0.75	0.44	99.28	80.5
E	445.0	R	10	54.84	0.10	1.01	12.86	0.25	29.08	0.73	0.44	99.33	80.1
E	446.0	R	09	55.19	0.16	0.95	13.02	0.27	29.17	0.92	0.42	100.10	80.0
E	447.0	R	08	54.57	0.16	0.68	13.65	0.27	28.58	0.78	0.30	98.98	79.2
E	450.0	R	10	55.22	0.17	0.77	13.33	0.28	28.85	0.72	0.34	99.66	79.4
E	453.0	R	10	55.12	0.13	1.07	12.44	0.27	29.42	0.73	0.47	99.65	80.8
E	455.0	R	19	55.20	0.18	0.87	12.96	0.27	29.17	0.70	0.38	99.72	80.1
E	457.0	R	07	54.89	0.18	0.90	13.19	0.26	29.06	0.75	0.42	99.65	79.7
E	459.0	R	18	55.07	0.17	0.94	12.78	0.27	29.27	0.84	0.47	99.79	80.3
E	461.0	R	08	55.12	0.14	1.02	12.70	0.25	29.42	0.82	0.43	99.90	80.5
E	464.0	R	09	54.96	0.12	1.02	12.41	0.26	29.46	0.79	0.44	99.45	80.9
E	466.0	R	05	54.87	0.16	0.89	12.45	0.26	29.02	0.87	0.33	98.85	80.6

MDH 29 ORTHOPYROXENE ANALYSES - continued -

U	SH	C/R	N	SiO_2	TiO_2	Al_2O_3	FeO	MnO	MgO	CaO	Cr_2O_3	Total	Mg#
E	468.0	R	08	55.37	0.12	0.90	11.24	0.26	30.16	0.75	0.44	99.24	82.7
D	471.0	R	04	56.88	0.10	1.06	6.24	0.13	34.55	0.52	0.46	99.92	90.8
D	473.0	R	09	55.35	0.11	0.89	11.89	0.26	29.81	0.85	0.40	99.55	81.7
D	474.0	R	09	55.34	0.14	0.91	12.12	0.27	30.25	0.67	0.41	100.10	81.7
D	477.0	R	12	54.61	0.12	1.04	11.91	0.25	29.82	0.75	0.42	98.91	81.7

MDH 1 PLAGIOCLASE ANALYSES

UNIT - STRATIGRAPHIC HEIGHT - CORE/RIM - NUMBER OF ANALYSES

U	SH	C/R	N	SiO_2	Al_2O_3	FeO	CaO	Na_2O	K_2O	Total	An%
J	216.0	C	09	48.87	32.13	0.24	14.75	2.93	0.21	99.13	73.5
J	218.0	C	09	49.89	31.85	0.19	14.91	2.87	0.20	99.91	74.1
J	220.0	C	10	52.04	30.65	0.20	12.99	3.81	0.22	99.90	65.3
H	221.0	C	10	49.70	32.07	0.19	15.21	2.55	0.20	99.93	76.7
H	224.0	C	10	50.05	31.85	0.23	14.94	2.81	0.22	100.10	74.6
G	227.0	C	08	50.45	32.72	0.22	14.44	3.07	0.23	101.13	72.3
G	231.0	C	09	49.58	32.58	0.22	14.70	3.03	0.19	100.30	72.9
G	234.0	C	10	51.26	31.06	0.19	13.77	3.51	0.22	100.00	68.5
G	236.0	C	07	51.27	30.33	0.19	13.08	3.83	0.26	98.96	65.4
G	239.0	C	08	52.18	30.26	0.21	12.56	3.97	0.27	99.45	63.6
G	240.0	C	08	51.61	29.88	0.20	12.91	3.84	0.29	98.72	65.0
G	242.0	C	10	51.57	30.19	0.19	13.07	3.95	0.31	99.28	64.6
G	245.0	C	08	52.34	29.60	0.23	12.45	4.16	0.32	99.09	62.3
G	247.0	C	09	51.78	30.10	0.19	12.83	4.03	0.30	99.22	63.8
G	248.0	C	15	51.33	30.52	0.22	13.42	3.63	0.28	99.41	67.1
F	248.7	C	08	48.56	32.29	0.18	15.26	2.63	0.21	99.13	76.2
F	250.0	C	10	48.49	32.52	0.31	15.44	2.53	0.16	99.46	77.1
F	251.0	C	09	51.31	30.65	0.22	13.33	3.81	0.26	99.58	65.9
F	253.0	C	08	49.28	31.72	0.22	14.51	3.19	0.20	99.12	71.5
F	255.0	C	10	49.99	31.56	0.21	13.79	3.37	0.26	99.18	69.3
F	257.0	C	10	49.98	31.55	0.20	14.13	3.30	0.25	99.41	70.3
F	258.0	C	08	49.41	31.46	0.21	14.50	3.04	0.19	98.81	72.5
F	259.0	C	10	48.56	32.45	0.25	15.37	2.62	0.15	99.41	76.4
E	260.0	C	10	50.33	31.45	0.16	13.69	3.48	0.24	99.35	68.5
E	261.0	C	07	49.66	31.66	0.14	14.30	3.27	0.21	99.23	70.7
E	262.0	C	10	49.34	32.12	0.19	14.85	3.04	0.14	99.67	73.0
E	264.0	C	10	54.34	28.89	0.15	10.72	5.41	0.19	99.70	52.3
E	265.0	C	10	52.32	30.10	0.16	12.41	4.38	0.25	99.61	61.0
E	267.0	C	07	54.06	28.53	0.13	10.73	5.25	0.24	98.94	53.0
E	268.0	C	10	54.21	28.92	0.11	11.04	5.17	0.24	99.68	54.2
E	271.0	C	10	54.52	28.28	0.13	10.59	5.30	0.28	99.10	52.5
E	273.0	C	08	50.55	31.34	0.15	13.26	3.53	0.13	98.97	67.5
E	274.0	C	10	52.16	30.18	0.15	12.56	4.20	0.24	99.47	62.3
E	276.0	C	09	52.24	30.27	0.13	12.44	4.34	0.23	99.65	61.3
E	277.0	C	10	52.02	30.49	0.16	12.42	4.21	0.21	99.51	62.0
E	280.0	C	09	55.18	28.49	0.08	10.18	5.69	0.25	99.86	49.7
E	282.0	C	09	51.34	30.71	0.14	12.91	3.99	0.21	99.30	64.1
E	284.0	C	10	53.81	29.62	0.11	11.39	4.84	0.25	100.02	56.5
E	287.0	C	10	53.43	30.02	0.13	11.73	4.81	0.26	100.38	57.4
E	289.0	C	08	50.34	31.12	0.16	13.56	3.65	0.19	99.00	67.3
E	292.0	C	09	50.10	31.68	0.17	13.87	3.33	0.17	99.33	69.7
E	295.0	C	08	62.13	23.65	0.09	4.50	8.46	0.29	99.12	22.7
E	297.0	C	08	57.27	26.74	0.09	8.16	6.74	0.28	99.29	40.1
E	299.0	C	07	55.17	28.36	0.06	10.41	5.51	0.32	99.83	51.1
E	301.0	C	08	51.38	30.58	0.17	13.31	3.95	0.22	99.61	65.1
E	302.0	C	09	51.28	31.39	0.19	13.90	3.62	0.05	100.42	68.0
E	303.0	C	10	52.37	30.25	0.21	12.94	4.14	0.20	100.12	63.3
E	304.0	C	07	50.00	31.30	0.13	13.79	3.53	0.20	98.95	68.3
E	307.0	C	10	54.87	28.25	0.12	9.85	5.77	0.29	99.15	48.6
E	310.0	C	09	53.68	29.06	0.11	11.32	4.92	0.32	99.40	56.0
E	313.0	C	10	51.99	30.37	0.16	12.66	4.39	0.24	99.80	61.5
E	315.0	C	10	52.35	29.81	0.12	12.36	4.40	0.21	99.26	60.8
E	318.0	C	10	53.09	29.68	0.11	11.95	4.73	0.29	99.85	58.2
E	320.0	C	10	51.82	30.74	0.12	13.34	4.03	0.23	100.29	64.6
E	323.0	C	10	51.51	31.12	0.16	13.73	3.74	0.19	100.45	67.0
D	335.0	C	08	56.78	27.77	0.07	9.63	6.14	0.27	100.66	46.4
D	337.0	C	10	50.30	32.20	0.19	14.58	3.25	0.17	100.69	71.3
D	339.0	C	10	51.75	31.33	0.13	13.56	3.90	0.19	100.85	65.8
J	216.0	R	09	48.14	32.55	0.22	15.14	2.66	0.18	98.89	75.9
J	218.0	R	10	49.33	32.17	0.17	15.36	2.69	0.17	99.89	76.0
J	220.0	R	10	52.90	29.94	0.25	12.42	4.25	0.24	100.00	61.8
H	221.0	R	07	49.40	32.32	0.18	15.42	2.48	0.18	99.98	77.5
H	224.0	R	10	49.55	32.19	0.25	15.22	2.62	0.19	100.01	76.2
G	227.0	R	08	50.70	32.57	0.26	14.14	3.24	0.25	101.15	70.7
G	231.0	R	09	49.59	32.69	0.23	14.55	3.11	0.20	100.35	72.1
G	234.0	R	10	51.73	30.79	0.19	13.23	3.77	0.22	99.94	66.0

MDH 1 PLAGIOCLASE ANALYSES - continued -

U	SH	C/R	N	SiO_2	Al_2O_3	FeO	CaO	Na_2O	K_2O	Total	An%
G	236.0	R	09	51.64	30.24	0.22	12.76	3.99	0.25	99.10	63.9
G	239.0	R	08	52.86	29.84	0.25	11.86	4.32	0.28	99.41	60.3
G	240.0	R	08	53.08	29.25	0.22	11.83	4.38	0.35	99.11	59.9
G	242.0	R	10	52.63	29.30	0.20	12.11	4.53	0.36	99.12	59.6
G	245.0	R	08	53.42	28.91	0.23	11.77	4.52	0.36	99.21	59.0
G	247.0	R	09	52.44	29.87	0.27	12.23	4.31	0.33	99.44	61.1
G	248.0	R	15	52.13	30.08	0.24	12.81	3.98	0.29	99.54	64.0
F	248.7	R	09	48.34	32.59	0.16	15.52	2.52	0.18	99.32	77.3
F	250.0	R	09	48.30	32.79	0.29	15.47	2.41	0.15	99.41	78.0
F	251.0	R	09	51.43	30.54	0.21	13.11	3.98	0.25	99.51	64.5
F	253.0	R	10	50.24	31.20	0.22	13.69	3.62	0.24	99.21	67.7
F	255.0	R	09	50.35	31.31	0.23	13.49	3.62	0.26	99.26	67.3
F	257.0	R	10	50.75	31.16	0.23	13.48	3.63	0.29	99.55	67.2
F	258.0	R	10	50.45	30.94	0.28	13.66	3.53	0.23	99.10	68.1
F	259.0	R	09	47.81	32.78	0.25	15.52	2.41	0.13	98.89	78.1
E	260.0	R	08	51.70	30.71	0.18	12.68	4.08	0.32	99.67	63.2
E	261.0	R	06	50.91	30.90	0.18	12.85	3.90	0.21	98.96	64.5
E	262.0	R	08	49.69	32.00	0.25	14.20	3.22	0.15	99.51	70.9
E	264.0	R	10	55.48	28.18	0.22	9.72	5.99	0.18	99.76	47.3
E	265.0	R	09	53.45	29.46	0.22	11.49	4.92	0.28	99.81	56.3
E	267.0	R	10	54.29	28.51	0.17	10.55	5.43	0.22	99.18	51.8
E	268.0	R	10	54.87	28.67	0.17	10.73	5.51	0.23	100.16	51.8
E	271.0	R	08	55.10	28.16	0.20	10.14	5.52	0.24	99.36	50.4
E	273.0	R	07	50.24	31.45	0.24	13.43	3.52	0.10	98.99	67.8
E	274.0	R	10	52.77	29.98	0.20	11.96	4.47	0.25	99.63	59.7
E	276.0	R	08	55.10	28.46	0.16	10.40	5.66	0.30	100.07	50.4
E	277.0	R	10	53.40	29.73	0.26	11.46	4.85	0.23	99.93	56.6
E	280.0	R	09	56.69	27.54	0.14	9.04	6.45	0.29	100.16	43.6
E	282.0	R	10	52.69	29.99	0.19	11.73	4.63	0.25	99.48	58.4
E	284.0	R	10	55.93	28.43	0.17	9.81	5.70	0.31	100.34	48.7
E	287.0	R	10	55.31	28.62	0.19	10.13	5.70	0.34	100.30	49.6
E	289.0	R	07	52.88	29.39	0.19	11.48	4.84	0.26	99.04	56.8
E	292.0	R	10	50.89	31.43	0.22	13.22	3.69	0.18	99.64	66.4
E	295.0	R	10	62.60	23.46	0.16	4.34	8.69	0.27	99.51	21.6
E	297.0	R	09	58.60	25.77	0.17	7.12	7.40	0.31	99.37	34.7
E	299.0	R	09	56.88	27.58	0.14	9.05	6.37	0.35	100.36	44.0
E	301.0	R	09	53.11	29.44	0.22	11.76	4.78	0.27	99.58	57.6
E	302.0	R	09	50.55	31.88	0.22	14.41	3.30	0.04	100.41	70.7
E	303.0	R	10	52.88	29.80	0.27	12.43	4.41	0.21	100.01	60.9
E	304.0	R	09	49.57	31.79	0.25	14.11	3.24	0.17	99.13	70.6
E	307.0	R	08	55.30	27.97	0.18	9.56	5.99	0.26	99.26	46.9
E	310.0	R	11	55.12	28.19	0.18	10.34	5.53	0.36	99.72	50.8
E	313.0	R	09	54.43	28.95	0.21	10.80	5.46	0.28	100.13	52.2
E	315.0	R	09	54.25	28.61	0.21	10.77	5.29	0.27	99.41	53.0
E	318.0	R	09	54.97	28.68	0.22	10.68	5.47	0.35	100.38	51.9
E	320.0	R	10	53.76	29.47	0.19	11.63	4.93	0.30	100.28	56.6
E	323.0	R	09	51.97	30.47	0.25	13.09	4.11	0.20	100.09	63.8
D	335.0	R	08	57.98	26.98	0.15	8.55	6.64	0.27	100.57	41.6
D	337.0	R	09	49.34	32.76	0.30	15.12	2.93	0.13	100.57	74.1
D	339.0	R	10	53.23	30.28	0.23	12.32	4.61	0.23	100.91	59.6

MDH 22 PLAGIOCLASE ANALYSES

UNIT - STRATIGRAPHIC HEIGHT - CORE/RIM - NUMBER OF ANALYSES

U	SH	C/R	N	SiO_2	Al_2O_3	FeO	CaO	Na_2O	K_2O	Total	An%
M	50.0	C	10	49.50	31.99	0.23	15.03	2.78	0.22	99.75	75.0
M	55.0	C	10	50.08	32.24	0.33	15.10	2.81	0.19	100.76	74.8
M	60.0	C	10	49.76	31.94	0.33	14.86	2.82	0.22	99.92	74.5
M	65.0	C	09	49.78	31.73	0.27	14.91	2.88	0.21	99.79	74.1
L	70.0	C	10	52.46	30.30	0.16	13.19	3.84	0.35	100.31	65.5
L	75.0	C	10	51.69	30.69	0.06	13.27	3.68	0.21	99.60	66.7
L	80.0	C	10	51.17	30.86	0.12	13.98	3.55	0.23	99.91	68.6
L	85.0	C	10	52.38	30.64	0.18	13.26	3.92	0.21	100.58	65.2
L	86.0	C	10	51.13	31.48	0.13	14.03	3.47	0.07	100.30	69.1
L	90.0	C	10	51.97	30.61	0.17	13.11	3.80	0.43	100.09	65.6
L	95.0	C	09	51.70	31.07	0.21	13.65	3.52	0.35	100.50	68.2
L	96.0	C	10	51.25	31.14	0.11	13.93	3.47	0.22	100.13	68.9
L	97.0	C	10	53.28	29.85	0.17	12.49	4.35	0.33	100.46	61.4
L	100.0	C	10	52.14	30.52	0.13	12.98	3.97	0.14	99.87	64.4
L	105.0	C	10	50.39	31.80	0.22	14.77	3.01	0.20	100.38	73.1
L	106.0	C	09	49.73	31.77	0.21	15.16	2.82	0.17	99.87	74.8
L	111.0	C	10	51.32	31.24	0.15	13.83	3.39	0.29	100.23	69.3
K	115.0	C	10	50.34	31.95	0.17	14.91	3.01	0.18	100.56	73.3
K	120.0	C	10	49.71	31.98	0.24	15.04	2.85	0.15	99.97	74.5
K	125.0	C	10	50.51	31.76	0.23	14.84	2.91	0.18	100.43	73.8
K	130.0	C	10	50.22	31.85	0.25	15.11	3.00	0.17	100.88	73.6
K	135.0	C	10	50.49	31.77	0.28	14.87	3.04	0.18	100.63	73.0
J	140.0	C	10	49.22	31.98	0.24	14.90	2.79	0.23	99.37	74.7
J	145.0	C	09	50.20	31.80	0.25	14.75	2.95	0.26	100.23	73.4
J	150.0	C	10	50.18	31.62	0.26	14.75	2.86	0.26	99.93	74.0
M	50.0	R	08	49.23	32.32	0.22	15.24	2.72	0.20	99.92	75.6
M	55.0	R	08	49.46	32.54	0.31	15.27	2.61	0.18	100.38	76.4
M	60.0	R	07	49.52	32.23	0.29	15.17	2.73	0.19	100.13	75.4
M	65.0	R	10	49.36	32.08	0.28	15.11	2.73	0.19	99.75	75.4
L	70.0	R	10	53.47	29.59	0.24	12.26	4.31	0.38	100.24	61.1
L	75.0	R	10	52.94	29.88	0.14	12.22	4.24	0.27	99.68	61.5
L	80.0	R	10	51.19	30.84	0.12	13.94	3.64	0.22	99.96	68.0
L	85.0	R	10	53.02	30.28	0.25	12.70	4.24	0.24	100.72	62.4
L	86.0	R	10	50.56	31.92	0.16	14.44	3.26	0.07	100.40	71.0
L	90.0	R	10	52.91	30.07	0.22	12.43	4.20	0.43	100.26	62.1
L	95.0	R	10	52.70	30.29	0.25	12.74	3.91	0.43	100.33	64.3
L	96.0	R	10	51.98	30.69	0.16	13.43	3.75	0.24	100.25	66.5
L	97.0	R	10	54.37	29.14	0.24	11.68	4.84	0.39	100.65	57.2
L	100.0	R	10	52.09	30.59	0.19	13.04	3.96	0.13	99.98	64.6
L	105.0	R	10	49.55	32.34	0.19	15.39	2.68	0.17	100.31	76.1
L	106.0	R	08	49.24	32.13	0.19	15.45	2.63	0.17	99.81	76.5
L	111.0	R	09	52.55	30.43	0.23	12.88	3.87	0.39	100.36	64.8
K	115.0	R	08	49.84	32.11	0.19	15.11	2.85	0.16	100.26	74.6
K	120.0	R	09	49.60	32.13	0.21	15.12	2.79	0.15	99.99	75.0
K	125.0	R	09	50.51	31.80	0.21	14.87	2.95	0.19	100.54	73.6
K	130.0	R	08	50.21	32.04	0.23	15.15	2.95	0.15	100.72	74.0
K	135.0	R	09	49.93	32.12	0.25	14.68	2.87	0.16	100.01	73.9
J	140.0	R	08	48.81	32.24	0.23	15.14	2.70	0.22	99.34	75.7
J	145.0	R	06	50.44	31.76	0.24	14.59	2.97	0.30	100.30	73.1
J	150.0	R	09	50.21	31.60	0.22	14.73	2.91	0.26	99.93	73.7

MDH 23 PLAGIOCLASE ANALYSES

UNIT - STRATIGRAPHIC HEIGHT - CORE/RIM - NUMBER OF ANALYSES

U	SH	C/R	N	SiO_2	Al_2O_3	FeO	CaO	Na_2O	K_2O	Total	An%
M	82.0	C	09	50.78	31.45	0.24	14.58	3.05	0.19	100.28	72.5
M	88.0	C	19	50.74	31.58	0.29	14.63	2.86	0.20	100.30	73.9
M	91.0	C	10	50.41	31.47	0.27	14.49	3.14	0.22	100.01	71.8
M	94.0	C	10	50.20	32.13	0.28	14.72	3.16	0.17	100.65	72.0
M	104.0	C	10	51.09	31.62	0.25	14.61	3.24	0.16	100.96	71.4
M	107.0	C	10	51.16	31.37	0.23	14.11	3.21	0.18	100.25	70.9
M	109.0	C	10	50.01	31.90	0.32	14.89	2.82	0.16	100.11	74.5
M	114.0	C	10	50.01	31.95	0.31	15.07	2.87	0.14	100.35	74.4
M	118.0	C	10	50.38	31.95	0.24	14.96	2.87	0.19	100.58	74.2
M	120.0	C	10	50.04	31.72	0.36	15.03	2.83	0.21	100.19	74.6
M	125.0	C	10	50.07	31.93	0.25	14.77	2.94	0.19	100.14	73.6
M	128.0	C	09	49.94	31.78	0.28	15.18	2.87	0.22	100.27	74.5
M	134.0	C	10	49.75	31.54	0.30	14.91	2.92	0.21	99.62	73.9
M	137.0	C	10	50.28	31.84	0.46	15.02	2.76	0.19	100.56	75.0
M	142.0	C	10	50.25	31.86	0.29	15.08	2.79	0.21	100.48	74.9
M	145.0	C	09	49.67	31.88	0.27	14.98	2.88	0.23	99.90	74.2
M	151.0	C	09	50.65	31.64	0.30	14.83	2.90	0.18	100.50	73.8
M	154.0	C	10	50.62	31.26	0.28	14.24	3.25	0.21	99.85	70.8
M	162.0	C	10	50.77	31.41	0.26	14.37	3.17	0.18	100.17	71.4
M	165.0	C	09	50.50	31.84	0.22	14.90	3.12	0.17	100.76	72.5
M	168.0	C	10	50.85	31.22	0.22	14.56	3.12	0.17	100.14	72.1
M	170.0	C	09	50.04	32.03	0.24	14.39	2.85	0.18	99.74	73.6
M	173.0	C	09	50.25	31.40	0.25	14.78	2.77	0.18	99.63	74.7
M	177.0	C	10	50.12	31.98	0.31	15.08	2.95	0.19	100.64	73.8
M	181.0	C	09	50.58	31.85	0.22	14.88	2.86	0.16	100.55	74.2
M	188.0	C	09	50.00	32.21	0.26	14.86	2.94	0.14	100.41	73.6
M	197.0	C	10	50.56	31.97	0.22	14.73	3.14	0.16	100.79	72.2
M	203.0	C	10	51.15	31.52	0.21	14.47	3.13	0.17	100.66	71.8
M	207.0	C	10	51.04	31.78	0.26	14.34	3.27	0.19	100.88	70.8
M	216.0	C	08	50.59	31.80	0.26	14.62	3.28	0.17	100.72	71.1
M	218.0	C	09	51.06	31.71	0.24	14.56	3.16	0.19	100.93	71.8
M	224.0	C	10	49.85	32.00	0.19	14.85	3.11	0.14	100.13	72.5
M	232.0	C	09	50.03	32.47	0.21	14.85	2.95	0.19	100.70	73.5
M	238.0	C	10	48.82	32.77	0.22	15.80	2.53	0.11	100.25	77.6
M	244.0	C	09	49.73	32.71	0.25	15.35	2.81	0.11	100.96	75.1
M	254.0	C	09	49.61	32.05	0.23	15.15	2.86	0.16	100.06	74.6
M	259.0	C	09	48.58	33.23	0.23	15.73	2.17	0.11	100.06	80.0
M	263.0	C	10	50.10	32.41	0.18	14.89	2.94	0.16	100.67	73.7
L	265.0	C	09	50.83	31.82	0.13	14.44	3.13	0.16	100.51	71.8
L	268.0	C	10	51.60	31.46	0.14	14.10	3.35	0.19	100.84	70.0
L	271.0	C	09	51.10	31.55	0.14	14.44	3.40	0.22	100.85	70.1
L	274.0	C	09	48.80	32.95	0.15	15.78	2.63	0.12	100.43	76.8
L	277.0	C	10	51.29	31.53	0.13	14.01	3.59	0.11	100.66	68.3
L	281.0	C	06	47.90	32.50	0.20	16.30	2.19	0.05	99.14	80.4
L	284.0	C	10	48.11	33.55	0.20	16.54	2.07	0.04	100.50	81.5
L	286.0	C	05	46.91	34.54	0.35	17.46	1.62	0.03	100.91	85.6
L	290.0	C	10	51.29	31.51	0.14	14.31	3.38	0.19	100.80	70.1
L	293.0	C	09	49.76	32.16	0.12	15.26	2.79	0.17	100.27	75.2
L	296.0	C	06	49.10	31.99	0.16	14.54	3.16	0.22	99.18	71.7
L	300.0	C	09	51.05	31.10	0.15	13.63	3.47	0.27	99.66	68.5
L	303.0	C	11	48.37	33.42	0.16	16.01	2.46	0.02	100.43	78.3
K	304.4	C	10	47.51	33.91	0.21	16.77	1.92	0.09	100.41	82.9
K	304.5	C	09	47.99	33.80	0.20	16.83	1.97	0.07	100.86	82.5
K	304.9	C	09	47.16	33.88	0.20	16.60	1.91	0.06	99.81	82.7
K	305.0	C	10	46.91	34.58	0.23	17.29	1.64	0.09	100.74	85.4
K	309.0	C	10	49.96	32.20	0.20	14.98	2.98	0.19	100.51	73.6
K	312.0	C	10	50.65	32.08	0.19	14.77	3.04	0.18	100.90	72.8
J	323.0	C	10	48.08	33.51	0.22	16.32	2.15	0.08	100.36	80.7
J	332.0	C	09	50.45	32.02	0.20	14.95	3.08	0.22	100.92	72.8
J	342.0	C	10	50.38	31.74	0.21	14.88	3.16	0.24	100.61	72.2
J	353.0	C	10	49.01	32.23	0.22	15.25	2.95	0.16	99.82	74.1
J	363.0	C	09	50.05	32.06	0.19	14.74	3.07	0.22	100.33	72.6
J	373.0	C	10	49.51	32.30	0.19	15.00	2.99	0.18	100.17	73.5
J	382.0	C	10	49.56	32.11	0.23	14.85	2.94	0.12	99.82	73.6
J	392.0	C	10	49.77	32.07	0.21	14.66	2.94	0.23	99.88	73.4
J	404.0	C	10	49.29	32.41	0.21	15.11	2.76	0.11	99.89	75.1

MDH 23 PLAGIOCLASE ANALYSES - continued -

U	SH	C/R	N	SiO_2	Al_2O_3	FeO	CaO	Na_2O	K_2O	Total	An%
J	421.0	C	14	48.71	32.49	0.19	15.56	2.67	0.11	99.73	76.3
J	427.0	C	07	49.40	32.24	0.14	15.80	2.64	0.13	100.35	76.8
J	430.0	C	09	45.15	34.39	0.13	18.18	1.23	0.04	99.13	89.1
J	433.0	C	11	45.87	35.07	0.09	18.10	1.26	0.04	100.44	88.8
J	434.0	C	08	45.72	35.25	0.12	17.93	1.36	0.05	100.42	87.9
J	439.0	C	09	46.37	34.64	0.10	17.30	1.66	0.03	100.11	85.2
H	442.0	C	10	45.31	34.92	0.13	18.19	1.11	0.02	99.68	90.1
G	446.0	C	06	46.23	34.22	0.08	18.11	1.37	0.04	100.05	87.9
G	450.0	C	08	46.01	34.09	0.10	17.71	1.39	0.02	99.32	87.5
G	453.0	C	10	46.68	34.21	0.13	17.64	1.56	0.03	100.25	86.2
G	458.0	C	10	46.93	33.60	0.13	17.31	1.73	0.03	99.73	84.7
G	461.0	C	10	47.32	33.91	0.09	16.90	1.90	0.04	100.15	83.1
G	465.4	C	09	46.41	33.77	0.16	17.05	1.48	0.02	98.90	86.4
F	465.6	C	10	45.78	34.51	0.12	18.23	1.23	0.02	99.90	89.1
F	469.0	C	09	45.54	34.34	0.19	18.08	1.25	0.03	99.42	88.9
F	472.0	C	10	46.24	34.57	0.15	17.88	1.46	0.04	100.35	87.1
E	475.0	C	09	45.63	34.16	0.09	17.94	1.34	0.00	99.16	88.1
E	477.0	C	10	50.64	31.18	0.15	14.01	3.42	0.07	99.49	69.3
E	481.0	C	14	48.81	33.28	0.18	15.52	2.84	0.08	100.70	75.1
E	485.0	C	10	53.77	29.32	0.12	12.23	4.41	0.28	100.13	60.5
E	488.0	C	09	52.53	30.93	0.15	12.67	4.53	0.15	100.96	60.7
E	490.0	C	09	52.32	30.07	0.14	12.43	4.25	0.14	99.35	61.8
E	493.0	C	06	53.95	28.31	0.14	11.37	4.89	0.19	98.86	56.2
E	495.0	C	09	51.62	30.78	0.20	13.33	3.68	0.20	99.81	66.7
E	499.0	C	09	53.60	30.30	0.11	11.91	4.97	0.24	101.12	57.0
E	502.0	C	09	52.13	29.63	0.15	13.03	4.00	0.24	99.17	64.3
E	505.0	C	09	54.39	28.84	0.14	10.53	5.34	0.30	99.53	52.2
E	508.0	C	10	50.33	32.09	0.20	13.51	3.41	0.21	99.76	68.6
E	511.0	C	10	52.16	29.70	0.14	12.89	4.02	0.23	99.15	63.9
E	514.0	C	10	49.55	32.32	0.17	15.20	2.74	0.18	100.16	75.4
E	517.0	C	09	53.64	29.66	0.16	11.86	4.62	0.27	100.20	58.7
E	520.0	C	10	50.76	30.93	0.19	13.82	3.28	0.22	99.20	70.0
E	521.0	C	06	48.15	32.70	0.27	16.18	2.31	0.01	99.62	79.5
E	526.0	C	07	53.38	30.27	0.23	11.38	4.64	0.31	100.20	57.6
E	530.0	C	10	50.55	31.00	0.21	14.35	3.22	0.21	99.55	71.1
E	533.0	C	08	55.30	28.96	0.13	10.20	5.65	0.31	100.54	49.9
E	537.0	C	10	55.45	27.55	0.15	10.42	5.62	0.27	99.46	50.6
M	82.0	R	09	50.63	31.71	0.26	14.82	2.97	0.18	100.57	73.4
M	88.0	R	16	50.81	31.45	0.28	14.57	3.00	0.20	100.31	72.8
M	91.0	R	08	50.42	31.35	0.25	14.36	3.25	0.23	99.87	70.9
M	94.0	R	08	50.30	32.02	0.27	14.49	3.25	0.18	100.50	71.2
M	104.0	R	10	50.73	31.73	0.22	14.75	3.13	0.16	100.71	72.3
M	107.0	R	10	50.75	31.57	0.21	14.27	3.07	0.17	100.04	72.0
M	109.0	R	08	49.76	31.99	0.28	15.07	2.75	0.15	100.00	75.1
M	114.0	R	08	49.61	32.13	0.28	15.32	2.74	0.13	100.20	75.6
M	118.0	R	08	49.73	32.41	0.26	15.27	2.71	0.16	100.54	75.7
M	120.0	R	08	49.65	31.94	0.31	15.14	2.78	0.18	100.00	75.0
M	125.0	R	08	49.42	32.41	0.22	15.21	2.69	0.15	100.09	75.8
M	128.0	R	09	50.03	32.03	0.24	15.19	2.88	0.21	100.58	74.5
M	134.0	R	09	49.23	32.05	0.31	15.09	2.78	0.20	99.66	75.0
M	137.0	R	09	49.60	32.44	0.41	15.45	2.51	0.16	100.56	77.3
M	142.0	R	09	49.82	32.19	0.26	15.24	2.71	0.19	100.41	75.6
M	145.0	R	09	49.44	32.03	0.28	14.98	2.91	0.20	99.82	74.0
M	151.0	R	08	50.34	31.82	0.28	15.04	2.77	0.17	100.42	75.0
M	154.0	R	10	50.49	31.55	0.27	14.43	3.14	0.21	100.09	71.7
M	162.0	R	09	50.41	31.60	0.24	14.76	3.02	0.17	100.19	73.0
M	165.0	R	09	50.43	31.90	0.22	14.88	3.08	0.17	100.67	72.8
M	168.0	R	08	50.18	31.24	0.20	14.87	2.98	0.15	99.62	73.4
M	170.0	R	09	49.46	32.51	0.21	14.93	2.62	0.14	99.87	75.9
M	173.0	R	07	49.37	32.05	0.25	15.59	2.41	0.14	99.80	78.2
M	177.0	R	09	49.58	32.51	0.29	15.51	2.71	0.15	100.76	76.0
M	181.0	R	07	49.63	32.41	0.19	15.43	2.59	0.12	100.37	76.7
M	188.0	R	07	49.44	32.73	0.28	15.30	2.72	0.11	100.57	75.7
M	197.0	R	09	50.07	32.36	0.19	15.08	2.96	0.14	100.81	73.8
M	203.0	R	10	50.64	31.97	0.17	15.01	2.89	0.16	100.84	74.1
M	207.0	R	09	49.98	32.53	0.27	15.04	2.95	0.15	100.91	73.8
M	216.0	R	08	49.67	32.48	0.26	15.13	2.88	0.14	100.57	74.4
M	218.0	R	09	50.23	32.18	0.20	14.79	2.90	0.17	100.48	73.8

MDH 23 PLAGIOCLASE ANALYSES - continued -

U	SH	C/R	N	SiO_2	Al_2O_3	FeO	CaO	Na_2O	K_2O	Total	An%
M	224.0	R	10	49.32	32.51	0.23	15.14	2.91	0.12	100.22	74.2
M	232.0	R	08	49.60	32.90	0.24	15.16	2.81	0.15	100.87	74.9
M	238.0	R	09	48.07	33.24	0.21	16.24	2.26	0.09	100.10	79.9
M	244.0	R	09	49.06	33.16	0.25	15.64	2.57	0.11	100.79	77.1
M	254.0	R	10	49.52	32.39	0.27	15.08	2.75	0.15	100.16	75.2
M	259.0	R	08	48.52	33.38	0.20	16.07	2.02	0.10	100.31	81.5
M	263.0	R	07	49.22	33.00	0.21	15.54	2.63	0.12	100.73	76.5
L	265.0	R	09	49.87	32.49	0.21	14.87	2.85	0.15	100.44	74.2
L	268.0	R	09	52.13	31.20	0.24	13.60	3.58	0.19	100.94	67.7
L	271.0	R	08	50.11	32.28	0.21	14.89	2.99	0.16	100.65	73.3
L	274.0	R	07	48.59	33.19	0.23	15.96	2.55	0.10	100.62	77.6
L	277.0	R	10	50.06	32.47	0.19	15.10	3.07	0.06	100.96	73.1
L	281.0	R	07	48.10	32.44	0.22	16.11	2.34	0.06	99.26	79.2
L	284.0	R	10	47.93	33.51	0.25	16.57	2.05	0.04	100.35	81.7
L	286.0	R	08	46.42	34.98	0.36	17.73	1.45	0.02	100.97	87.1
L	290.0	R	09	49.83	32.53	0.22	15.34	2.79	0.13	100.84	75.2
L	293.0	R	09	48.87	32.59	0.14	15.62	2.53	0.15	99.90	77.3
L	296.0	R	06	49.14	31.96	0.19	14.26	3.35	0.24	99.13	70.2
L	300.0	R	09	50.70	31.47	0.19	13.85	3.30	0.22	99.73	69.9
L	303.0	R	21	48.40	32.95	0.24	15.77	2.59	0.02	99.97	77.1
K	304.4	R	10	47.25	34.20	0.27	16.90	1.80	0.08	100.51	83.9
K	304.5	R	10	48.06	33.72	0.27	16.68	2.09	0.05	100.88	81.5
K	304.9	R	09	46.65	34.16	0.25	16.98	1.86	0.05	99.96	83.4
K	305.0	R	10	46.96	34.56	0.24	17.29	1.67	0.07	100.80	85.2
K	309.0	R	10	49.20	32.74	0.21	15.75	2.61	0.14	100.65	76.9
K	312.0	R	10	50.12	32.07	0.25	14.86	2.98	0.18	100.45	73.4
J	323.0	R	09	47.79	33.87	0.24	16.51	2.06	0.08	100.55	81.6
J	332.0	R	08	49.47	32.45	0.25	15.41	2.79	0.19	100.57	75.3
J	342.0	R	10	49.84	32.15	0.23	15.12	2.97	0.21	100.51	73.8
J	353.0	R	09	49.16	32.78	0.26	15.78	2.74	0.14	100.86	76.1
J	363.0	R	09	49.45	32.71	0.21	15.35	2.75	0.17	100.63	75.5
J	373.0	R	10	49.02	32.72	0.25	15.29	2.78	0.17	100.22	75.3
J	382.0	R	10	49.18	32.58	0.25	15.09	2.72	0.10	99.92	75.4
J	392.0	R	09	49.30	32.55	0.19	15.23	2.76	0.20	100.23	75.3
J	404.0	R	10	48.82	32.87	0.24	15.20	2.58	0.09	99.81	76.5
J	421.0	R	15	48.59	32.77	0.20	15.75	2.55	0.11	99.96	77.3
J	427.0	R	07	48.85	32.62	0.19	16.01	2.45	0.12	100.24	78.3
J	430.0	R	08	45.04	34.72	0.15	18.31	1.13	0.03	99.38	90.0
J	433.0	R	09	45.35	35.08	0.12	18.61	1.04	0.03	100.23	90.8
J	434.0	R	08	45.44	35.85	0.16	17.87	1.29	0.03	100.64	88.4
J	439.0	R	08	45.86	34.86	0.16	17.38	1.52	0.03	99.80	86.4
H	442.0	R	10	44.79	35.22	0.10	18.43	0.92	0.01	99.47	91.7
G	446.0	R	06	46.14	34.32	0.13	17.73	1.32	0.04	99.68	88.1
G	450.0	R	08	45.74	34.33	0.20	17.78	1.30	0.01	99.37	88.3
G	453.0	R	10	46.18	34.65	0.18	17.98	1.34	0.03	100.36	88.1
G	458.0	R	07	46.62	33.71	0.21	17.50	1.62	0.03	99.69	85.6
G	461.0	R	09	46.79	34.01	0.15	17.20	1.73	0.03	99.91	84.6
G	465.4	R	07	45.71	34.19	0.21	17.62	1.21	0.02	98.97	89.0
F	465.6	R	10	45.63	34.60	0.14	18.27	1.20	0.02	99.86	89.4
F	469.0	R	08	45.51	34.51	0.22	18.26	1.18	0.03	99.71	89.6
F	472.0	R	09	46.06	34.98	0.21	17.85	1.42	0.03	100.54	87.4
E	475.0	R	06	44.45	34.71	0.13	18.71	0.95	0.01	98.96	91.6
E	477.0	R	09	50.87	31.01	0.18	13.75	3.60	0.06	99.49	67.8
E	481.0	R	13	48.38	33.43	0.23	15.58	2.71	0.07	100.41	76.1
E	485.0	R	09	54.30	29.02	0.19	11.64	4.71	0.26	100.12	57.8
E	488.0	R	07	52.66	30.92	0.21	12.53	4.59	0.15	101.06	60.1
E	490.0	R	10	52.31	30.29	0.22	12.53	4.22	0.12	99.68	62.1
E	493.0	R	10	54.69	27.92	0.20	10.75	5.22	0.20	98.97	53.2
E	495.0	R	10	54.04	29.16	0.25	11.41	4.65	0.32	99.82	57.5
E	499.0	R	05	55.19	29.18	0.17	10.66	5.81	0.24	101.26	50.3
E	502.0	R	10	54.18	28.44	0.23	11.30	4.90	0.30	99.35	56.0
E	505.0	R	09	54.88	28.66	0.22	10.06	5.63	0.32	99.76	49.7
E	508.0	R	08	50.59	31.85	0.24	13.06	3.57	0.23	99.53	66.9
E	511.0	R	10	54.91	27.81	0.19	10.78	5.15	0.36	99.20	53.6
E	514.0	R	10	50.15	31.91	0.26	14.70	2.99	0.19	100.20	73.1
E	517.0	R	08	54.85	28.83	0.23	10.59	5.36	0.28	100.14	52.2
E	520.0	R	08	50.48	31.26	0.27	14.32	3.16	0.18	99.68	71.4
E	521.0	R	09	48.08	32.82	0.30	16.14	2.27	0.00	99.61	79.7

MDH 23 PLAGIOCLASE ANALYSES - continued -

U	SH	C/R	N	SiO_2	Al_2O_3	FeO	CaO	Na_2O	K_2O	Total	An%
E	526.0	R	10	53.49	30.29	0.28	11.13	4.69	0.30	100.18	56.8
E	530.0	R	08	51.37	30.65	0.29	13.78	3.47	0.23	99.79	68.7
E	533.0	R	10	56.47	28.30	0.18	9.21	6.21	0.31	100.69	45.0
E	537.0	R	10	56.16	27.29	0.23	9.90	5.89	0.27	99.75	48.2

MDH 29 PLAGIOCLASE ANALYSES

UNIT - STRATIGRAPHIC HEIGHT - CORE/RIM - FREE/ENCLOSED IN OPX - NUMBER OF ANALYSES

U	SH	C/R	N	F/E	SiO_2	Al_2O_3	FeO	CaO	Na_2O	K_2O	Total	An%
K	2.0	C	08	F	50.01	32.16	0.21	15.14	2.87	0.17	100.56	74.5
K	8.0	C	13	F	50.04	31.13	0.24	14.50	3.15	0.24	99.30	71.8
K	15.0	C	12	F	50.89	31.22	0.26	14.76	3.22	0.23	100.58	71.7
K	20.4	C	10	F	50.39	31.36	0.25	14.79	3.15	0.17	100.11	72.2
K	20.5	C	13	F	50.67	31.15	0.20	14.76	3.18	0.20	100.16	71.9
K	26.0	C	13	F	51.38	30.51	0.25	13.90	3.49	0.31	99.84	68.8
K	32.0	C	12	F	50.33	30.89	0.27	14.83	3.10	0.21	99.63	72.6
J	37.0	C	13	F	50.75	31.22	0.31	14.40	3.06	0.27	100.01	72.2
J	43.0	C	08	F	50.72	31.83	0.25	14.75	3.17	0.25	100.97	72.0
J	49.0	C	09	F	50.76	31.37	0.26	14.58	3.21	0.24	100.42	71.5
J	55.0	C	09	F	50.41	31.30	0.23	14.65	3.05	0.26	99.90	72.6
J	60.0	C	14	F	50.87	31.31	0.25	14.12	3.16	0.25	99.96	71.2
J	66.0	C	10	F	50.85	31.23	0.29	14.72	3.17	0.28	100.54	72.0
J	72.0	C	09	F	50.71	31.42	0.26	14.64	3.19	0.28	100.50	71.7
J	77.0	C	10	F	50.49	31.66	0.25	15.07	2.82	0.22	100.51	74.7
J	83.0	C	09	F	50.53	31.79	0.24	14.96	2.85	0.23	100.60	74.4
J	88.0	C	08	F	50.40	31.47	0.29	14.75	2.95	0.24	100.10	73.4
J	90.0	C	09	F	50.25	31.72	0.25	15.03	2.90	0.22	100.37	74.1
J	95.0	C	08	F	49.73	32.23	0.25	15.16	2.84	0.21	100.42	74.7
J	96.0	C	09	F	50.72	30.78	0.28	14.41	3.16	0.29	99.64	71.6
J	98.0	C	08	F	50.44	32.00	0.25	14.42	3.00	0.22	100.33	72.6
J	99.0	C	09	F	50.58	31.99	0.28	14.76	3.03	0.22	100.86	72.9
J	100.0	C	10	F	50.43	32.19	0.24	14.80	2.95	0.20	100.81	73.5
J	102.0	C	15	F	50.39	31.99	0.25	14.60	2.97	0.22	100.42	73.1
J	103.0	C	09	F	50.22	31.79	0.29	14.62	2.96	0.22	100.10	73.2
J	105.0	C	07	F	50.59	32.26	0.28	14.74	2.96	0.20	101.03	73.3
J	109.0	C	14	F	49.52	31.64	0.27	14.65	2.90	0.23	99.21	73.6
J	111.0	C	10	F	50.02	31.74	0.29	14.82	3.00	0.25	100.12	73.2
J	113.0	C	14	F	49.89	32.00	0.25	15.12	2.90	0.21	100.37	74.2
J	115.0	C	16	F	49.94	31.88	0.27	14.88	2.91	0.24	100.12	73.9
J	117.0	C	06	F	50.30	31.87	0.27	14.99	3.03	0.23	100.69	73.2
J	120.0	C	11	F	50.21	31.68	0.27	14.98	2.87	0.21	100.22	74.3
J	122.0	C	14	F	50.07	31.98	0.25	14.68	2.96	0.24	100.18	73.3
J	125.0	C	13	F	50.08	31.64	0.27	15.02	2.97	0.22	100.20	73.6
J	127.0	C	12	F	50.26	32.03	0.24	15.00	2.98	0.25	100.76	73.6
J	129.0	C	14	F	50.12	32.04	0.24	14.86	2.92	0.23	100.41	73.8
J	134.0	C	09	F	49.63	31.24	0.24	14.87	2.82	0.24	99.04	74.4
J	139.0	C	10	F	49.72	31.19	0.25	15.06	2.78	0.22	99.22	75.0
J	144.0	C	09	F	49.99	31.51	0.26	15.11	2.82	0.21	99.90	74.8
J	147.0	C	06	F	49.58	32.18	0.26	14.88	2.95	0.22	100.07	73.6
J	152.0	C	10	F	50.10	31.69	0.30	15.04	2.79	0.23	100.15	74.9
J	158.0	C	08	F	50.07	31.64	0.24	15.22	2.87	0.22	100.26	74.6
J	166.0	C	10	F	50.15	31.35	0.25	14.96	2.92	0.23	99.86	73.9
J	172.0	C	08	F	50.28	31.71	0.25	14.88	2.90	0.23	100.25	73.9
J	179.0	C	08	F	50.24	32.06	0.28	15.56	2.82	0.20	101.16	75.3
J	185.0	C	10	F	50.41	31.48	0.25	15.07	2.87	0.20	100.28	74.4
J	191.0	C	09	F	50.24	31.89	0.25	15.38	2.86	0.20	100.82	74.8
J	196.0	C	14	F	50.18	31.76	0.24	15.15	2.95	0.23	100.51	73.9
J	202.0	C	08	F	50.38	31.97	0.21	15.24	2.87	0.23	100.90	74.6
J	210.0	C	09	F	50.91	31.53	0.20	14.65	3.08	0.21	100.58	72.4
J	215.0	C	08	F	50.35	31.94	0.21	15.21	3.03	0.23	100.97	73.5
H	219.0	C	12	F	49.65	31.96	0.19	15.14	2.80	0.21	99.95	74.9
H	223.0	C	10	F	49.54	31.69	0.23	14.90	2.73	0.21	99.30	75.1
H	227.0	C	12	F	49.95	32.24	0.20	15.01	2.70	0.22	100.32	75.4
H	229.0	C	10	F	49.30	32.22	0.20	15.06	2.73	0.19	99.70	75.3
G	231.0	C	10	F	49.94	31.07	0.19	14.86	3.01	0.20	99.27	73.2
G	233.0	C	10	F	50.16	31.28	0.18	14.27	3.08	0.24	99.21	71.9
G	240.0	C	14	F	50.90	31.24	0.21	14.42	3.04	0.25	100.06	72.4
G	247.0	C	09	F	50.10	31.62	0.24	15.10	2.86	0.22	100.14	74.5
G	250.0	C	10	F	49.69	31.79	0.27	14.65	3.02	0.21	99.63	72.8
G	254.0	C	12	F	49.89	32.01	0.24	15.39	2.77	0.22	100.52	75.4
G	260.0	C	09	F	49.82	31.72	0.27	15.26	2.72	0.23	100.02	75.6
G	269.0	C	14	F	50.86	31.50	0.21	14.71	3.11	0.24	100.63	72.3
G	273.0	C	06	F	50.12	31.60	0.28	14.19	3.17	0.21	99.57	71.2
G	276.0	C	09	F	52.17	29.91	0.19	13.54	3.70	0.30	99.81	66.9
G	278.0	C	08	F	51.56	30.35	0.16	13.24	3.61	0.27	99.19	67.0

MDH 29 PLAGIOCLASE ANALYSES - continued -

U	SH	C/R	N	F/E	SiO_2	Al_2O_3	FeO	CaO	Na_2O	K_2O	Total	An%
G	284.0	C	08	F	51.45	30.92	0.21	14.10	3.39	0.25	100.32	69.7
G	286.0	C	18	F	51.21	31.22	0.20	13.90	3.32	0.23	100.08	69.8
G	287.0	C	02	F	51.38	30.20	0.24	13.58	3.69	0.17	99.26	67.0
F	288.0	C	15	F	49.60	31.93	0.32	15.55	2.54	0.23	100.17	77.2
F	289.0	C	08	F	50.22	31.89	0.17	14.43	2.87	0.18	99.76	73.5
F	291.0	C	10	F	50.03	32.19	0.18	15.06	2.74	0.18	100.38	75.2
F	295.0	C	13	F	50.98	31.38	0.23	13.99	3.34	0.18	100.10	69.8
F	300.0	C	15	F	50.79	31.01	0.20	13.89	3.41	0.18	99.48	69.2
F	304.0	C	09	F	51.74	31.12	0.22	13.09	3.64	0.22	100.03	66.5
F	306.0	C	14	F	51.58	30.66	0.26	13.61	3.55	0.22	99.88	67.9
F	310.0	C	13	F	51.29	30.75	0.24	14.00	3.43	0.23	99.94	69.3
K	2.0	R	08	F	49.52	32.51	0.21	15.29	2.74	0.15	100.42	75.5
K	8.0	R	10	F	50.12	31.34	0.24	14.72	3.09	0.22	99.73	72.5
K	15.0	R	11	F	50.92	31.20	0.26	14.69	3.20	0.24	100.51	71.7
K	20.4	R	11	F	50.38	31.35	0.24	14.82	3.10	0.18	100.07	72.5
K	20.5	R	12	F	50.88	31.17	0.20	14.74	3.17	0.21	100.37	72.0
K	26.0	R	10	F	51.19	30.75	0.25	14.06	3.37	0.29	99.91	69.7
K	32.0	R	11	F	50.66	30.87	0.25	14.67	3.18	0.21	99.84	71.8
J	37.0	R	11	F	50.87	31.15	0.31	14.25	3.14	0.27	99.99	71.5
J	43.0	R	07	F	50.69	31.95	0.29	14.72	3.16	0.23	101.04	72.0
J	49.0	R	10	F	50.61	31.49	0.26	14.66	3.13	0.23	100.38	72.1
J	55.0	R	10	F	50.04	31.57	0.23	14.81	2.90	0.24	99.79	73.8
J	60.0	R	14	F	50.93	31.14	0.25	13.98	3.24	0.27	99.81	70.5
J	66.0	R	09	F	50.99	31.03	0.24	14.32	3.21	0.29	100.08	71.1
J	72.0	R	08	F	50.80	31.35	0.26	14.55	3.29	0.29	100.54	71.0
J	77.0	R	09	F	50.71	31.72	0.27	14.73	2.92	0.22	100.57	73.6
J	83.0	R	08	F	50.59	31.87	0.24	15.12	2.87	0.22	100.91	74.4
J	88.0	R	09	F	50.19	31.58	0.27	14.81	2.96	0.22	100.03	73.4
J	90.0	R	09	F	50.43	31.68	0.25	15.00	2.92	0.21	100.49	73.9
J	95.0	R	07	F	49.93	32.42	0.29	15.12	2.94	0.19	100.89	74.0
J	96.0	R	10	F	50.83	30.68	0.26	14.39	3.18	0.30	99.64	71.4
J	98.0	R	07	F	49.93	32.21	0.26	14.42	2.91	0.20	99.93	73.2
J	99.0	R	10	F	50.46	32.12	0.28	14.96	2.95	0.20	100.97	73.7
J	100.0	R	10	F	49.86	32.65	0.28	15.30	2.75	0.20	101.04	75.5
J	102.0	R	12	F	49.93	32.35	0.27	14.70	2.81	0.22	100.28	74.3
J	103.0	R	10	F	50.34	31.71	0.34	14.41	3.08	0.22	100.10	72.1
J	105.0	R	07	F	50.07	32.41	0.33	14.81	2.91	0.19	100.72	73.8
J	109.0	R	14	F	49.33	32.03	0.30	14.90	2.81	0.22	99.59	74.6
J	111.0	R	09	F	50.09	31.79	0.29	14.80	2.99	0.25	100.21	73.2
J	113.0	R	11	F	50.17	31.95	0.25	14.88	3.07	0.25	100.57	72.8
J	115.0	R	12	F	49.93	31.98	0.29	14.90	2.89	0.23	100.22	74.0
J	117.0	R	06	F	50.35	31.81	0.30	14.82	3.07	0.26	100.61	72.7
J	120.0	R	09	F	50.58	31.71	0.27	14.71	3.07	0.21	100.55	72.6
J	122.0	R	10	F	50.11	32.00	0.29	14.64	3.04	0.24	100.32	72.7
J	125.0	R	11	F	50.11	31.71	0.29	14.95	2.99	0.22	100.27	73.4
J	127.0	R	10	F	50.54	31.88	0.25	14.83	3.06	0.27	100.83	72.8
J	129.0	R	08	F	50.25	31.99	0.24	14.66	2.94	0.23	100.31	73.4
J	134.0	R	10	F	49.70	31.06	0.24	14.79	2.88	0.24	98.91	73.9
J	139.0	R	10	F	49.56	31.41	0.25	15.30	2.67	0.22	99.41	76.0
J	144.0	R	09	F	50.04	31.46	0.26	15.07	2.86	0.21	99.90	74.4
J	147.0	R	06	F	49.70	32.39	0.25	14.88	2.95	0.22	100.39	73.6
J	152.0	R	10	F	49.82	31.85	0.30	15.16	2.71	0.23	100.07	75.6
J	158.0	R	10	F	50.01	31.82	0.24	15.34	2.79	0.21	100.41	75.2
J	166.0	R	09	F	50.13	31.45	0.25	14.93	2.88	0.23	99.87	74.1
J	172.0	R	08	F	50.28	31.99	0.25	14.82	2.93	0.23	100.50	73.6
J	179.0	R	07	F	50.39	32.04	0.28	15.53	2.84	0.23	101.31	75.1
J	185.0	R	09	F	50.39	31.56	0.24	14.93	2.81	0.20	100.13	74.6
J	191.0	R	08	F	50.22	31.89	0.24	15.27	2.82	0.20	100.64	75.0
J	196.0	R	10	F	50.07	31.81	0.24	15.17	2.95	0.22	100.46	74.0
J	202.0	R	07	F	50.50	31.90	0.23	15.00	2.94	0.23	100.80	73.8
J	210.0	R	09	F	50.77	31.83	0.20	14.95	2.98	0.20	100.93	73.5
J	215.0	R	07	F	50.66	31.90	0.23	15.34	3.03	0.23	101.39	73.7
H	219.0	R	10	F	49.62	31.88	0.19	15.20	2.76	0.21	99.86	75.3
H	223.0	R	08	F	49.21	31.79	0.24	15.15	2.61	0.21	99.21	76.2
H	227.0	R	11	F	49.71	32.41	0.24	14.83	2.70	0.21	100.10	75.2
H	229.0	R	08	F	49.24	32.31	0.21	15.00	2.70	0.18	99.64	75.4
G	231.0	R	10	F	49.96	31.15	0.18	14.85	2.99	0.20	99.33	73.3
G	233.0	R	09	F	49.88	31.54	0.19	14.53	2.94	0.21	99.29	73.2

MDH 29 PLAGIOCLASE ANALYSES - continued -

U	SH	C/R	N	F/E	SiO_2	Al_2O_3	FeO	CaO	Na_2O	K_2O	Total	An%
G	240.0	R	12	F	50.86	31.17	0.21	14.38	3.10	0.25	99.97	71.9
G	247.0	R	09	F	50.29	31.58	0.26	15.09	2.94	0.23	100.39	73.9
G	250.0	R	09	F	49.23	32.19	0.27	14.97	2.81	0.19	99.66	74.6
G	254.0	R	10	F	50.03	31.97	0.32	15.37	2.79	0.22	100.70	75.3
G	260.0	R	08	F	49.65	31.92	0.26	15.26	2.70	0.23	100.02	75.7
G	269.0	R	12	F	51.07	31.62	0.21	14.83	3.17	0.24	101.14	72.1
G	273.0	R	06	F	50.06	31.55	0.28	14.23	3.10	0.21	99.43	71.7
G	276.0	R	08	F	51.83	30.23	0.18	13.49	3.62	0.30	99.65	67.3
G	278.0	R	08	F	51.66	30.29	0.19	13.08	3.72	0.28	99.22	66.0
G	284.0	R	08	F	51.33	30.83	0.22	13.92	3.41	0.26	99.97	69.3
G	286.0	R	13	F	51.43	30.87	0.20	13.58	3.48	0.25	99.81	68.3
F	288.0	R	13	F	49.66	31.83	0.31	15.35	2.57	0.23	99.95	76.7
F	289.0	R	07	F	50.40	31.90	0.21	14.47	2.89	0.20	100.07	73.5
F	291.0	R	08	F	49.59	32.53	0.17	15.42	2.60	0.18	100.49	76.6
F	295.0	R	14	F	51.13	31.41	0.24	13.81	3.34	0.18	100.11	69.6
F	300.0	R	15	F	50.59	31.04	0.20	13.90	3.47	0.19	99.39	68.9
F	304.0	R	08	F	52.16	30.80	0.27	13.01	3.89	0.23	100.36	64.9
F	306.0	R	13	F	51.23	30.98	0.26	13.76	3.50	0.21	99.94	68.5
F	310.0	R	12	F	51.31	30.67	0.24	13.78	3.48	0.23	99.71	68.6
K	2.0	C	05	E	50.02	32.17	0.24	15.13	2.89	0.21	100.66	74.3
K	8.0	C	12	E	50.65	31.47	0.24	14.65	3.13	0.24	100.38	72.1
K	15.0	C	10	E	50.98	31.39	0.27	14.51	3.11	0.25	100.51	72.1
K	20.4	C	12	E	50.37	30.89	0.31	14.72	3.05	0.19	99.53	72.7
K	20.5	C	13	E	51.02	31.25	0.26	14.70	3.18	0.18	100.59	71.9
K	26.0	C	09	E	51.75	30.37	0.26	13.71	3.52	0.32	99.93	68.3
K	32.0	C	13	E	50.12	31.00	0.31	14.83	3.06	0.25	99.57	72.8
J	37.0	C	09	E	50.90	31.37	0.35	14.69	3.08	0.28	100.67	72.5
J	43.0	C	08	E	50.41	31.36	0.33	14.33	3.30	0.23	99.96	70.6
J	49.0	C	09	E	50.52	31.27	0.36	14.53	3.29	0.23	100.20	70.9
J	55.0	C	10	E	51.11	31.14	0.36	14.52	3.23	0.24	100.60	71.3
J	60.0	C	15	E	51.29	31.00	0.35	14.27	3.24	0.28	100.43	70.9
J	66.0	C	09	E	51.08	31.13	0.34	14.36	3.35	0.23	100.49	70.3
J	72.0	C	08	E	51.50	31.34	0.34	14.41	3.33	0.25	101.17	70.5
J	77.0	C	09	E	51.03	31.74	0.30	14.64	3.02	0.24	100.97	72.8
J	83.0	C	08	E	50.63	31.82	0.32	15.10	2.96	0.22	101.05	73.8
J	88.0	C	08	E	50.48	31.77	0.36	14.80	2.94	0.22	100.57	73.6
J	90.0	C	08	E	50.09	31.49	0.35	15.19	2.88	0.19	100.19	74.5
J	95.0	C	08	E	49.78	32.08	0.38	14.91	2.99	0.20	100.34	73.4
J	96.0	C	08	E	50.62	30.39	0.36	14.29	3.25	0.27	99.18	70.8
J	98.0	C	08	E	50.57	32.14	0.35	15.11	3.06	0.23	101.46	73.2
J	99.0	C	10	E	50.61	31.92	0.36	15.01	2.99	0.22	101.11	73.5
J	100.0	C	09	E	50.18	32.24	0.36	14.73	3.03	0.18	100.72	72.9
J	102.0	C	12	E	50.17	31.88	0.37	14.74	3.04	0.22	100.42	72.8
J	103.0	C	12	E	50.31	32.02	0.39	14.52	3.09	0.23	100.56	72.2
J	105.0	C	08	E	50.04	32.25	0.38	14.74	3.07	0.22	100.70	72.6
J	109.0	C	13	E	49.48	31.81	0.42	14.31	2.89	0.21	99.12	73.2
J	111.0	C	10	E	50.39	31.59	0.38	14.63	3.18	0.27	100.44	71.8
J	113.0	C	06	E	50.66	31.70	0.38	14.66	2.99	0.22	100.61	73.0
J	115.0	C	08	E	50.75	31.51	0.39	14.82	3.06	0.21	100.74	72.8
J	117.0	C	06	E	50.70	31.73	0.36	14.12	3.23	0.24	100.38	70.7
J	120.0	C	10	E	50.74	31.54	0.28	14.50	3.30	0.23	100.59	70.8
J	122.0	C	09	E	50.86	30.96	0.36	14.56	2.96	0.25	99.95	73.1
J	125.0	C	10	E	50.42	32.01	0.32	14.47	3.02	0.22	100.46	72.6
J	127.0	C	12	E	50.40	32.02	0.38	14.68	3.07	0.24	100.79	72.5
J	129.0	C	08	E	49.76	31.84	0.37	14.16	3.04	0.25	99.42	72.0
J	134.0	C	10	E	49.79	31.25	0.31	14.85	2.94	0.21	99.35	73.6
J	139.0	C	10	E	49.84	31.46	0.35	14.97	2.82	0.20	99.64	74.6
J	144.0	C	07	E	50.11	31.45	0.34	14.64	2.89	0.22	99.65	73.7
J	147.0	C	05	E	49.46	32.16	0.34	14.67	3.02	0.18	99.83	72.9
J	152.0	C	14	E	50.27	32.21	0.34	14.44	2.94	0.18	100.38	73.1
J	158.0	C	10	E	50.17	31.51	0.30	14.92	2.95	0.22	100.07	73.6
J	166.0	C	09	E	50.56	31.43	0.31	14.72	3.02	0.18	100.22	72.9
J	172.0	C	08	E	50.55	31.77	0.31	14.78	2.97	0.20	100.58	73.3
J	179.0	C	07	E	50.62	31.97	0.38	14.75	2.94	0.19	100.85	73.5
J	185.0	C	10	E	50.72	31.63	0.31	14.44	3.08	0.21	100.39	72.2
J	191.0	C	08	E	50.73	31.50	0.33	15.13	3.00	0.18	100.87	73.6
J	196.0	C	09	E	50.15	31.79	0.35	14.81	3.08	0.18	100.36	72.7
J	202.0	C	10	E	50.79	31.92	0.36	14.58	3.07	0.21	100.93	72.4

MDH 29 PLAGIOCLASE ANALYSES - continued -

U	SH	C/R	N	F/E	SiO_2	Al_2O_3	FeO	CaO	Na_2O	K_2O	Total	An%
J	210.0	C	10	E	50.27	32.10	0.37	14.62	3.10	0.21	100.67	72.3
J	215.0	C	08	E	49.41	31.82	0.37	15.20	2.94	0.19	99.93	74.1
H	219.0	C	06	E	49.93	31.90	0.32	15.22	2.72	0.21	100.30	75.6
H	223.0	C	08	E	49.19	31.90	0.33	15.39	2.74	0.20	99.75	75.6
H	227.0	C	16	E	49.36	32.02	0.34	15.27	2.70	0.20	99.89	75.8
H	229.0	C	08	E	49.40	31.89	0.31	15.30	2.73	0.20	99.83	75.6
G	231.0	C	10	E	50.12	31.36	0.32	14.58	3.07	0.22	99.67	72.4
G	233.0	C	05	E	50.11	31.54	0.30	14.61	3.01	0.20	99.77	72.8
G	240.0	C	14	E	51.13	31.04	0.34	14.30	3.25	0.22	100.28	70.9
G	247.0	C	09	E	49.99	31.40	0.38	15.05	2.84	0.21	99.87	74.5
G	254.0	C	10	E	49.67	31.25	0.41	15.17	2.83	0.21	99.54	74.8
G	260.0	C	08	E	49.66	31.76	0.33	15.47	2.69	0.20	100.11	76.1
G	269.0	C	05	E	51.68	30.87	0.34	14.62	3.36	0.24	101.11	70.6
G	273.0	C	05	E	50.66	31.64	0.29	14.25	3.30	0.20	100.34	70.5
G	276.0	C	07	E	51.62	30.74	0.37	13.56	3.56	0.27	100.12	67.8
G	284.0	C	05	E	51.17	31.28	0.29	14.37	3.31	0.23	100.65	70.6
G	286.0	C	14	E	51.83	30.67	0.30	13.91	3.41	0.23	100.35	69.3
F	289.0	C	02	E	50.42	31.98	0.35	14.53	2.82	0.20	100.30	74.0
F	295.0	C	14	E	51.32	31.37	0.37	13.82	3.38	0.20	100.46	69.3
F	300.0	C	14	E	51.53	30.77	0.33	13.92	3.58	0.20	100.33	68.2
F	306.0	C	12	E	52.50	30.01	0.35	13.34	3.65	0.26	100.11	66.9
F	310.0	C	14	E	52.08	30.69	0.37	13.56	3.64	0.24	100.58	67.3
K	2.0	R	05	E	50.66	31.93	0.34	14.65	3.14	0.25	100.97	72.1
K	8.0	R	10	E	50.78	31.39	0.25	14.50	3.22	0.26	100.40	71.3
K	15.0	R	10	E	50.96	31.27	0.28	14.48	3.14	0.24	100.37	71.8
K	20.4	R	10	E	50.27	30.93	0.31	14.82	3.07	0.18	99.58	72.7
K	20.5	R	12	E	50.92	31.28	0.26	14.67	3.18	0.18	100.49	71.8
K	26.0	R	08	E	51.84	30.51	0.29	13.69	3.56	0.31	100.20	68.0
K	32.0	R	10	E	49.88	31.09	0.33	14.94	3.00	0.24	99.48	73.3
J	37.0	R	10	E	51.17	31.33	0.37	14.55	3.17	0.29	100.88	71.7
J	43.0	R	08	E	49.99	31.38	0.37	14.35	3.28	0.22	99.59	70.7
J	49.0	R	09	E	50.64	31.25	0.34	14.59	3.31	0.25	100.38	70.9
J	55.0	R	10	E	50.95	31.24	0.36	14.56	3.21	0.24	100.56	71.5
J	60.0	R	12	E	51.33	31.12	0.39	14.23	3.26	0.26	100.59	70.7
J	66.0	R	10	E	51.14	31.14	0.34	14.43	3.35	0.24	100.64	70.4
J	72.0	R	07	E	51.68	31.43	0.34	14.37	3.42	0.24	101.48	69.9
J	77.0	R	09	E	50.95	31.68	0.32	14.79	3.06	0.24	101.04	72.8
J	83.0	R	08	E	50.31	31.78	0.36	15.16	2.94	0.22	100.77	74.0
J	88.0	R	09	E	50.42	31.56	0.40	14.84	2.96	0.23	100.41	73.5
J	90.0	R	06	E	49.86	31.53	0.39	15.38	2.82	0.21	100.19	75.1
J	95.0	R	07	E	49.53	32.49	0.40	14.95	2.91	0.23	100.51	74.0
J	96.0	R	08	E	50.76	30.23	0.38	14.11	3.29	0.27	99.04	70.3
J	98.0	R	08	E	50.63	32.13	0.37	14.99	3.12	0.22	101.46	72.6
J	99.0	R	09	E	50.43	32.03	0.41	14.99	2.95	0.23	101.04	73.7
J	100.0	R	10	E	50.31	32.14	0.37	14.79	3.03	0.19	100.83	73.0
J	102.0	R	10	E	50.34	32.01	0.41	14.73	3.08	0.20	100.77	72.5
J	103.0	R	08	E	50.49	31.95	0.43	14.37	3.15	0.21	100.60	71.6
J	105.0	R	07	E	48.91	32.42	0.38	14.93	2.90	0.19	99.73	74.0
J	109.0	R	12	E	49.44	31.92	0.42	14.41	2.81	0.20	99.20	73.9
J	111.0	R	10	E	50.42	31.62	0.38	14.53	3.18	0.28	100.41	71.6
J	113.0	R	06	E	50.71	31.72	0.38	14.55	3.12	0.22	100.70	72.0
J	115.0	R	09	E	50.61	31.62	0.39	14.84	3.04	0.21	100.71	73.0
J	117.0	R	05	E	50.42	32.02	0.38	14.11	3.13	0.25	100.31	71.4
J	120.0	R	10	E	50.67	31.62	0.30	14.42	3.24	0.24	100.49	71.1
J	122.0	R	08	E	50.94	30.93	0.38	14.54	3.02	0.25	100.06	72.7
J	125.0	R	09	E	50.52	31.95	0.38	14.48	3.06	0.21	100.60	72.3
J	127.0	R	09	E	50.58	32.00	0.40	14.52	3.13	0.24	100.87	71.9
J	129.0	R	09	E	49.80	32.01	0.40	14.21	2.95	0.24	99.61	72.7
J	134.0	R	09	E	49.64	31.32	0.32	14.89	2.96	0.23	99.36	73.5
J	139.0	R	09	E	49.74	31.46	0.35	15.00	2.81	0.20	99.56	74.7
J	144.0	R	07	E	50.07	31.64	0.35	14.73	2.95	0.19	99.93	73.4
J	147.0	R	05	E	49.62	32.22	0.36	14.34	3.00	0.20	99.74	72.5
J	152.0	R	12	E	50.20	32.41	0.36	14.52	2.86	0.19	100.54	73.7
J	158.0	R	08	E	50.29	31.48	0.30	14.53	3.11	0.22	99.93	72.1
J	166.0	R	07	E	50.48	31.46	0.31	14.78	2.98	0.20	100.21	73.3
J	172.0	R	07	E	50.41	31.80	0.34	14.79	3.06	0.20	100.60	72.8
J	179.0	R	07	E	50.76	31.84	0.40	14.87	3.04	0.18	101.09	73.0
J	185.0	R	10	E	50.83	31.50	0.33	14.44	3.12	0.21	100.43	71.9

MDH 29 PLAGIOCLASE ANALYSES - continued -

U	SH	C/R	N	F/E	SiO_2	Al_2O_3	FeO	CaO	Na_2O	K_2O	Total	An%
J	191.0	R	08	E	50.84	31.44	0.33	15.05	3.09	0.20	100.95	72.9
J	196.0	R	08	E	50.30	31.66	0.36	14.70	3.16	0.18	100.36	72.0
J	202.0	R	07	E	50.64	32.02	0.35	14.68	2.99	0.21	100.89	73.1
J	210.0	R	08	E	50.19	32.20	0.38	14.77	3.06	0.21	100.81	72.7
J	215.0	R	05	E	49.52	31.78	0.36	15.21	2.92	0.22	100.01	74.2
H	219.0	R	05	E	49.77	31.78	0.32	15.20	2.73	0.20	100.00	75.5
H	223.0	R	08	E	49.03	31.91	0.35	15.39	2.72	0.20	99.60	75.8
H	227.0	R	12	E	49.51	32.06	0.33	15.19	2.76	0.20	100.05	75.3
H	229.0	R	06	E	49.62	32.02	0.34	15.03	2.78	0.19	99.98	74.9
G	231.0	R	10	E	50.24	31.33	0.33	14.55	3.09	0.22	99.76	72.2
G	233.0	R	06	E	50.22	31.60	0.32	14.72	3.10	0.21	100.17	72.4
G	240.0	R	14	E	51.07	31.08	0.34	14.40	3.29	0.22	100.40	70.7
G	247.0	R	07	E	49.91	31.59	0.37	14.98	2.84	0.21	99.90	74.5
G	254.0	R	09	E	49.70	31.45	0.41	14.97	2.83	0.21	99.57	74.5
G	260.0	R	08	E	49.78	31.59	0.39	15.45	2.75	0.19	100.15	75.6
G	269.0	R	04	E	51.18	31.06	0.36	15.20	3.23	0.23	101.26	72.2
G	273.0	R	05	E	50.49	31.62	0.34	14.19	3.36	0.22	100.22	70.0
G	276.0	R	07	E	51.94	30.47	0.35	13.47	3.72	0.31	100.26	66.7
G	284.0	R	04	E	51.26	30.83	0.35	14.03	3.39	0.32	100.18	69.6
G	286.0	R	11	E	51.82	30.83	0.32	14.23	3.38	0.27	100.85	69.9
F	289.0	R	02	E	50.45	31.83	0.38	14.32	2.92	0.20	100.10	73.0
F	295.0	R	12	E	51.48	31.32	0.38	13.81	3.44	0.20	100.63	68.9
F	300.0	R	11	E	51.76	30.51	0.38	13.69	3.64	0.21	100.19	67.5
F	306.0	R	10	E	52.61	29.93	0.40	13.25	3.72	0.26	100.17	66.3
F	310.0	R	14	E	52.18	30.28	0.40	13.33	3.74	0.25	100.18	66.3

MDH 29 PLAGIOCLASE ANALYSES - continued -

UNIT - STRATIGRAPHIC HEIGHT - CORE/RIM - NUMBER OF ANALYSES

U	SH	C/R	N	SiO_2	Al_2O_3	FeO	CaO	Na_2O	K_2O	Total	An%
E	311.5	C	06	51.30	30.48	0.17	13.50	3.58	0.07	99.08	67.5
E	311.8	C	24	52.43	30.33	0.21	13.02	4.03	0.29	100.32	64.1
E	313.0	C	10	50.09	31.53	0.19	14.54	2.90	0.21	99.47	73.5
E	315.0	C	13	50.39	31.25	0.20	14.54	3.27	0.19	99.84	71.1
E	316.8	C	10	50.29	31.18	0.18	14.37	3.38	0.03	99.44	70.2
E	317.0	C	09	52.15	29.72	0.16	12.75	3.87	0.26	98.91	64.5
E	319.1	C	11	52.76	29.44	0.19	12.55	4.40	0.11	99.41	61.2
E	319.8	C	08	55.58	27.74	0.11	10.33	5.58	0.34	99.67	50.6
E	321.0	C	10	51.85	31.09	0.18	13.47	3.57	0.21	100.37	67.6
E	325.0	C	22	51.94	30.12	0.19	13.28	3.80	0.21	99.54	65.9
E	327.0	C	08	57.86	25.87	0.13	8.55	6.66	0.33	99.40	41.5
E	330.0	C	22	50.11	31.54	0.19	14.97	3.03	0.15	99.95	73.2
E	333.0	C	20	50.97	30.29	0.20	13.81	3.52	0.23	99.03	68.4
E	335.0	C	19	54.23	28.72	0.17	11.34	4.94	0.16	99.57	55.9
E	339.0	C	16	53.18	29.13	0.19	12.03	4.59	0.19	99.30	59.1
E	342.0	C	19	49.51	32.19	0.19	15.54	2.79	0.12	100.34	75.5
E	345.0	C	10	52.08	29.96	0.15	12.84	3.95	0.19	99.16	64.2
E	347.0	C	20	49.94	31.25	0.18	14.89	3.01	0.14	99.40	73.2
E	349.0	C	14	56.52	27.47	0.12	9.69	5.90	0.27	99.96	47.6
E	350.0	C	09	52.15	30.08	0.16	13.39	3.81	0.17	99.76	66.0
E	351.0	C	13	55.95	27.49	0.07	10.12	5.73	0.28	99.64	49.4
E	353.0	C	12	60.19	24.99	0.10	6.90	7.46	0.38	100.03	33.8
E	355.0	C	09	59.10	25.32	0.10	7.95	6.97	0.31	99.74	38.7
E	357.0	C	10	55.03	28.00	0.14	11.07	5.10	0.28	99.62	54.5
E	359.0	C	10	52.21	29.56	0.16	12.57	4.19	0.26	98.94	62.4
E	362.0	C	08	51.76	30.44	0.19	13.57	3.81	0.15	99.94	66.3
E	367.0	C	10	53.95	28.73	0.12	11.16	4.95	0.23	99.14	55.5
E	369.0	C	10	57.35	27.04	0.12	8.76	6.39	0.29	99.96	43.1
E	373.0	C	10	53.20	29.97	0.18	12.82	4.15	0.24	100.59	63.1
E	377.0	C	14	49.99	31.43	0.16	14.41	3.21	0.19	99.39	71.3
E	379.0	C	09	55.17	28.54	0.10	10.77	5.29	0.25	100.13	52.9
E	381.0	C	09	56.96	27.06	0.11	9.24	5.99	0.31	99.68	46.0

MDH 29 PLAGIOCLASE ANALYSES - continued -

U	SH	C/R	N	SiO_2	Al_2O_3	FeO	CaO	Na_2O	K_2O	Total	An%
E	383.0	C	15	51.25	30.60	0.19	13.95	3.67	0.19	99.85	67.7
E	386.0	C	10	54.71	28.64	0.17	11.22	5.02	0.27	100.03	55.3
E	390.0	C	19	51.79	30.44	0.14	13.48	3.78	0.22	99.86	66.4
E	392.0	C	10	53.36	29.29	0.14	11.96	4.50	0.28	99.54	59.5
E	395.0	C	10	50.56	30.99	0.14	14.24	3.26	0.20	99.39	70.7
E	397.0	C	10	57.14	27.26	0.11	8.34	6.21	0.25	99.31	42.6
E	401.0	C	10	50.40	31.02	0.20	14.45	3.30	0.20	99.57	70.8
E	406.0	C	10	53.92	29.00	0.14	11.68	4.68	0.32	99.74	58.0
E	410.0	C	13	53.14	29.06	0.12	11.88	4.46	0.30	98.97	59.6
E	413.0	C	10	55.75	27.83	0.14	10.05	5.68	0.31	99.76	49.4
E	415.0	C	10	51.50	30.71	0.17	13.59	3.67	0.22	99.85	67.1
E	418.0	C	09	50.75	30.63	0.18	14.20	3.30	0.18	99.24	70.4
E	421.0	C	10	50.71	31.55	0.16	14.17	3.30	0.22	100.11	70.4
E	425.0	C	10	50.18	31.61	0.20	14.91	3.00	0.19	100.10	73.3
E	427.0	C	08	55.08	28.31	0.12	10.47	5.24	0.35	99.58	52.5
E	430.0	C	19	51.68	30.21	0.18	13.43	3.72	0.25	99.46	66.6
E	433.0	C	10	50.93	30.69	0.21	13.55	3.27	0.23	98.87	69.6
E	433.8	C	05	49.93	31.01	0.23	14.57	3.09	0.01	98.85	72.3
E	435.0	C	09	50.82	30.90	0.20	14.33	3.31	0.22	99.78	70.5
E	437.0	C	08	52.01	29.99	0.20	13.44	3.82	0.25	99.71	66.0
E	439.0	C	10	50.13	31.73	0.19	14.72	3.03	0.22	100.02	72.8
E	442.0	C	24	50.25	31.20	0.20	14.39	3.12	0.21	99.36	71.8
E	444.0	C	07	50.11	30.85	0.17	14.50	3.29	0.17	99.10	70.9
E	445.0	C	09	51.54	29.93	0.15	13.80	3.48	0.21	99.11	68.7
E	446.0	C	15	51.55	30.27	0.17	13.83	3.62	0.22	99.66	67.8
E	447.0	C	09	56.14	27.49	0.12	9.57	5.76	0.29	99.37	47.9
E	450.0	C	10	55.64	27.72	0.11	10.67	5.47	0.22	99.83	51.9
E	453.0	C	19	49.99	31.58	0.18	14.97	2.98	0.16	99.86	73.5
E	455.0	C	10	53.50	29.12	0.13	12.55	4.18	0.24	99.71	62.4
E	457.0	C	10	49.76	31.35	0.20	14.84	3.16	0.14	99.44	72.2
E	459.0	C	10	51.09	30.56	0.16	13.61	3.68	0.22	99.32	67.2
E	461.0	C	10	51.22	31.03	0.17	13.69	3.28	0.16	99.55	69.8
E	464.0	C	11	49.44	32.16	0.17	15.87	2.69	0.15	100.49	76.5
E	466.0	C	08	56.29	27.91	0.13	10.05	5.72	0.30	100.40	49.3
E	468.0	C	11	50.42	31.46	0.18	14.78	3.21	0.20	100.25	71.8
D	471.0	C	10	50.33	31.19	0.19	14.11	3.45	0.04	99.30	69.4
D	473.0	C	16	52.31	30.12	0.16	13.33	4.00	0.20	100.14	64.8
D	474.0	C	07	54.55	28.36	0.14	11.11	5.19	0.19	99.53	54.2
D	477.0	C	06	52.21	29.56	0.16	12.58	4.00	0.24	98.73	63.5
E	311.5	R	05	51.56	30.41	0.17	12.93	3.66	0.08	98.83	66.1
E	311.8	R	24	53.13	29.98	0.23	12.56	4.30	0.32	100.53	61.7
E	313.0	R	10	53.71	29.28	0.26	11.75	4.43	0.38	99.81	59.5
E	315.0	R	12	50.95	30.95	0.17	14.24	3.45	0.20	99.95	69.5
E	316.8	R	10	50.48	31.07	0.16	14.32	3.48	0.03	99.54	69.5
E	317.0	R	10	54.18	28.36	0.21	11.15	4.69	0.31	98.90	56.8
E	319.1	R	09	53.09	29.32	0.18	12.19	4.55	0.12	99.50	59.7
E	319.8	R	10	56.58	27.06	0.15	9.42	5.96	0.36	99.54	46.6
E	321.0	R	10	54.60	29.41	0.21	11.41	4.69	0.32	100.63	57.4
E	325.0	R	16	51.99	30.09	0.21	13.22	3.80	0.22	99.53	65.8
E	327.0	R	07	57.76	26.04	0.17	8.55	6.64	0.27	99.46	41.6
E	330.0	R	18	49.56	31.74	0.20	15.35	2.87	0.13	99.84	74.7
E	333.0	R	20	51.09	30.20	0.24	13.79	3.58	0.23	99.17	68.0
E	335.0	R	19	54.22	28.72	0.17	11.31	4.95	0.18	99.59	55.8
E	339.0	R	18	53.62	28.72	0.24	11.49	4.89	0.19	99.18	56.5
E	342.0	R	16	50.41	31.62	0.19	14.78	3.18	0.16	100.35	72.0
E	345.0	R	10	52.97	29.40	0.17	12.17	4.34	0.20	99.26	60.8
E	347.0	R	20	51.03	30.65	0.23	14.12	3.44	0.17	99.63	69.4
E	349.0	R	15	57.90	26.49	0.18	8.47	6.56	0.27	99.86	41.6
E	350.0	R	09	53.33	29.12	0.20	12.30	4.40	0.19	99.54	60.7
E	351.0	R	07	56.47	27.40	0.14	9.72	5.88	0.28	99.89	47.7
E	353.0	R	09	61.43	24.17	0.11	5.75	8.10	0.31	99.87	28.2
E	355.0	R	08	59.03	25.31	0.14	7.83	7.05	0.27	99.63	38.0
E	357.0	R	10	56.67	26.75	0.19	9.66	5.90	0.31	99.47	47.5
E	359.0	R	10	53.28	28.84	0.19	11.63	4.60	0.32	98.85	58.3
E	362.0	R	12	52.46	29.98	0.20	13.05	4.12	0.18	99.99	63.6
E	367.0	R	10	54.77	28.18	0.21	10.58	5.33	0.25	99.31	52.3
E	369.0	R	10	58.51	26.16	0.18	7.83	6.94	0.28	99.89	38.4
E	373.0	R	10	53.02	29.85	0.20	12.83	4.21	0.21	100.30	62.7

MDH 29 PLAGIOCLASE ANALYSES - continued -

U	SH	C/R	N	SiO_2	Al_2O_3	FeO	CaO	Na_2O	K_2O	Total	An%
E	377.0	R	14	52.17	29.86	0.22	12.84	4.06	0.24	99.41	63.6
E	379.0	R	09	57.01	27.39	0.17	9.25	6.15	0.30	100.26	45.4
E	381.0	R	09	57.64	26.71	0.17	8.68	6.33	0.31	99.84	43.1
E	383.0	R	15	51.54	30.42	0.20	13.64	3.80	0.21	99.81	66.5
E	386.0	R	10	56.14	27.58	0.23	9.96	5.71	0.33	99.95	49.1
E	390.0	R	16	53.19	29.49	0.21	12.35	4.41	0.28	99.92	60.7
E	392.0	R	10	54.51	28.46	0.21	10.99	5.12	0.31	99.60	54.3
E	395.0	R	09	50.94	30.71	0.19	13.86	3.52	0.23	99.44	68.5
E	397.0	R	08	57.99	26.84	0.23	7.60	6.56	0.28	99.49	39.0
E	401.0	R	10	51.39	30.62	0.25	13.86	3.65	0.23	100.00	67.7
E	406.0	R	09	55.76	27.80	0.22	10.17	5.45	0.36	99.76	50.8
E	410.0	R	15	54.85	27.89	0.17	10.55	5.21	0.35	99.01	52.8
E	413.0	R	09	56.10	27.54	0.22	9.74	5.85	0.30	99.77	48.0
E	415.0	R	10	53.21	29.79	0.28	12.24	4.40	0.26	100.17	60.6
E	418.0	R	08	51.57	30.19	0.27	13.45	3.63	0.19	99.30	67.2
E	421.0	R	10	52.20	30.50	0.26	12.88	3.95	0.29	100.07	64.3
E	425.0	R	10	50.12	31.50	0.27	14.85	3.04	0.19	99.97	73.0
E	427.0	R	07	54.91	28.17	0.25	10.44	5.22	0.34	99.34	52.5
E	430.0	R	18	52.52	29.60	0.26	12.68	4.13	0.29	99.48	62.9
E	433.0	R	07	51.34	30.51	0.30	13.56	3.45	0.21	99.38	68.5
E	433.8	R	04	49.98	31.15	0.21	14.57	3.05	0.02	98.98	72.5
E	435.0	R	10	51.17	30.68	0.23	14.10	3.46	0.23	99.86	69.3
E	437.0	R	07	53.24	29.45	0.32	12.46	4.15	0.28	99.91	62.4
E	439.0	R	10	50.49	31.38	0.22	14.10	3.28	0.22	99.69	70.4
E	442.0	R	20	50.77	30.87	0.25	13.83	3.38	0.23	99.34	69.3
E	444.0	R	07	51.60	30.29	0.22	13.46	3.93	0.20	99.69	65.4
E	445.0	R	10	52.92	29.22	0.23	12.85	4.05	0.24	99.51	63.7
E	446.0	R	15	52.33	29.89	0.24	13.29	3.95	0.23	99.93	65.0
E	447.0	R	08	57.34	26.85	0.23	8.78	6.28	0.29	99.76	43.6
E	450.0	R	09	56.44	27.22	0.14	10.01	5.85	0.21	99.86	48.6
E	453.0	R	19	51.07	30.97	0.23	14.22	3.45	0.20	100.14	69.5
E	455.0	R	10	55.12	27.96	0.19	11.15	4.82	0.29	99.53	56.1
E	457.0	R	10	50.69	31.06	0.23	14.57	3.40	0.15	100.10	70.3
E	459.0	R	10	52.52	29.78	0.17	12.41	4.26	0.26	99.41	61.7
E	461.0	R	09	52.99	29.95	0.21	12.30	4.07	0.24	99.75	62.5
E	464.0	R	14	50.10	31.80	0.21	15.37	2.97	0.18	100.64	74.1
E	466.0	R	08	56.76	27.46	0.20	9.55	5.97	0.32	100.25	46.9
E	468.0	R	09	51.68	30.69	0.22	13.86	3.72	0.24	100.40	67.3
D	471.0	R	08	50.51	31.13	0.19	13.77	3.51	0.04	99.18	68.4
D	473.0	R	16	52.92	29.86	0.18	13.00	4.21	0.24	100.42	63.1
D	474.0	R	08	55.12	27.98	0.16	10.62	5.62	0.19	99.69	51.1
D	477.0	R	06	52.43	29.54	0.16	12.36	4.09	0.28	98.86	62.6

WHOLE ROCK ANALYSES

BOREHOLE DEPTH (sample number) - STRATIGRAPHIC HEIGHT (relative to the E/F boundary)

B D (m)	82.0	85.0	88.0	91.0	94.0	103.0	104.0	107.0	109.0	114.0	118.0	120.0
UNIT	M	M	M	M	M	M	M	M	M	M	M	M
S H (m)	533.0	530.0	527.0	524.0	521.0	512.0	511.0	508.0	506.0	501.0	497.0	495.0
SiO_2	50.85	49.98	50.32	50.49	50.53	50.24	51.23	50.79	50.10	49.46	50.64	50.04
TiO_2	0.04	0.04	0.05	0.04	0.05	0.05	0.04	0.04	0.03	0.01	0.03	0.04
Al_2O_3	18.36	18.70	19.75	18.93	19.47	18.06	18.32	18.44	24.17	25.85	19.96	23.85
Fe_2O_3	6.29	5.94	5.46	5.94	5.88	6.62	6.08	6.05	3.07	1.91	5.17	3.10
MnO	0.14	0.14	0.12	0.14	0.12	0.15	0.14	0.14	0.06	0.03	0.12	0.06
MgO	9.12	8.33	7.65	8.30	8.57	8.93	9.12	9.26	5.18	4.56	8.10	5.33
CaO	11.85	12.01	12.28	11.96	11.20	11.61	12.08	11.77	13.23	13.50	12.49	12.99
Na_2O	1.95	2.00	2.09	2.02	2.08	2.00	2.00	2.01	2.29	2.38	1.97	2.31
K_2O	0.06	0.07	0.10	0.07	0.10	0.08	0.06	0.06	0.11	0.13	0.08	0.15
P_2O_5	0.09	0.09	0.09	0.09	0.09	0.09	0.09	0.09	0.09	0.08	0.09	0.08
Total	98.75	97.30	97.91	97.98	98.09	97.83	99.16	98.65	98.33	97.91	98.65	97.95
Zn	33	34	28	36	34	36	32	31	18	5	41	21
Cu	-	-	-	-	-	-	-	-	-	-	-	-
Ni	209	198	186	198	201	219	216	219	96	49	196	98
Co	111	47	45	44	49	48	52	49	26	22	44	29
Ga	14	13	15	12	14	16	13	17	23	21	16	19
Zr	5	3	4	4	5	3	3	3	4	4	7	6
Y	5	-	3	4	3	3	3	-	3	-	4	3
Sr	280	294	303	293	303	269	269	274	384	434	296	389
Rb	-	2	3	-	2	-	-	2	2	3	-	4
Pb	-	-	-	-	-	-	-	-	-	-	-	-
Cr	835	780	776	792	742	915	937	942	439	179	867	418
V	64	79	66	82	62	77	72	94	14	12	69	26
Ba	47	60	55	55	56	23	39	34	45	72	42	98
Sc	11	16	18	12	16	15	12	23	12	12	22	12
S	na	na	na	na	na	na	na	na	na	na	na	na

B D	122.0	125.0	128.0	131.0	134.0	137.0	139.0	142.0	145.0	149.0	151.0	154.0
UNIT	M	M	M	M	M	M	M	M	M	M	M	M
S H	493.0	490.0	487.0	484.0	481.0	478.0	476.0	473.0	470.0	466.0	464.0	461.0
SiO_2	50.07	50.40	50.30	50.26	50.94	49.34	49.74	50.98	50.44	50.17	49.98	50.73
TiO_2	0.04	0.05	0.05	0.05	0.08	-	0.03	0.10	0.06	0.10	0.03	0.05
Al_2O_3	20.60	20.57	20.98	20.01	17.44	30.41	24.98	15.73	20.14	15.06	23.42	18.96
Fe_2O_3	5.15	5.09	5.12	5.77	6.98	0.88	3.74	8.19	5.75	8.99	3.36	5.83
MnO	0.11	0.11	0.11	0.12	0.14	-	0.08	0.16	0.12	0.18	0.07	0.13
MgO	7.83	7.91	7.66	8.44	11.10	0.28	5.12	12.91	8.24	13.04	4.79	8.61
CaO	11.78	11.92	11.70	11.34	10.59	14.55	12.40	9.78	11.27	9.16	12.87	11.94
Na_2O	1.98	1.97	2.02	1.95	1.72	2.63	2.22	1.55	1.98	1.54	2.29	2.01
K_2O	0.09	0.10	0.11	0.10	0.09	0.14	0.12	0.07	0.12	0.10	0.12	0.08
P_2O_5	0.09	0.08	0.09	0.09	0.09	0.09	0.08	0.09	0.09	0.08	0.08	0.08
Total	97.74	98.20	98.14	98.13	99.17	98.32	98.51	99.56	98.21	98.42	97.01	98.42
Zn	27	29	29	31	41	7	21	54	32	54	16	29
Cu	-	-	-	-	5	-	-	7	5	5	-	-
Ni	188	185	179	207	257	4	120	303	197	320	109	207
Co	42	46	48	49	118	22	33	66	47	70	29	45
Ga	18	18	15	15	11	22	16	10	13	9	15	12
Zr	4	4	5	4	8	-	5	10	4	8	3	4
Y	3	-	3	3	5	-	-	6	3	5	-	3
Sr	308	321	324	297	264	478	369	219	307	211	377	285
Rb	2	-	2	2	2	2	4	3	3	-	2	-
Pb	5	-	-	-	-	-	-	-	-	-	-	-
Cr	888	921	836	921	1152	16	532	1242	821	1234	435	816
V	74	60	49	72	82	12	53	86	77	97	31	72
Ba	96	85	46	64	46	34	61	60	52	48	50	39
Sc	12	17	12	11	28	13	12	13	16	17	12	15
S	na	na	na	na	na	na	na	na	na	na	na	na

WHOLE ROCK ANALYSES - continued -

B D	158.0	162.0	165.0	168.0	170.0	173.0	177.0	181.0	184.0	188.0	191.0	194.0
UNIT	M	M	M	M	M	M	M	M	M	M	M	M
S H	457.0	453.0	450.0	447.0	445.0	442.0	438.0	434.0	431.0	427.0	424.0	421.0
SiO_2	50.63	50.54	50.71	50.46	50.05	49.74	50.03	49.91	50.18	49.83	49.42	49.31
TiO_2	0.05	0.05	0.04	0.05	0.03	0.03	0.03	0.04	0.08	0.04	0.01	0.02
Al_2O_3	21.99	19.50	18.66	19.48	23.98	23.93	25.08	23.83	15.95	21.66	25.50	25.40
Fe_2O_3	4.11	5.58	5.90	5.66	3.65	3.29	2.64	3.28	8.70	4.96	2.52	2.49
MnO	0.08	0.12	0.14	0.12	0.07	0.06	0.05	0.06	0.18	0.10	0.05	0.05
MgO	6.72	8.14	9.02	8.35	5.52	5.11	4.27	5.23	12.63	6.95	4.52	4.22
CaO	12.68	12.14	12.01	12.31	12.61	13.11	13.29	13.27	9.49	11.90	13.30	13.12
Na_2O	2.24	2.06	1.96	1.97	2.25	2.27	2.36	2.25	1.53	2.10	2.40	2.41
K_2O	0.13	0.09	0.06	0.05	0.11	0.12	0.11	0.10	0.04	0.05	0.07	0.08
P_2O_5	0.08	0.08	0.09	0.09	0.09	0.08	0.08	0.09	0.09	0.09	0.08	0.08
Total	98.71	98.30	98.59	98.54	98.36	97.70	97.94	98.06	98.87	97.68	97.87	97.18
Zn	23	30	30	30	29	20	10	23	50	30	16	27
Cu	-	-	-	-	-	-	-	-	-	-	-	-
Ni	131	201	216	209	109	101	73	99	305	167	71	63
Co	35	42	89	46	32	31	82	31	66	49	26	24
Ga	12	13	9	12	16	15	16	16	11	15	14	17
Zr	5	3	-	4	6	5	3	4	5	4	-	-
Y	3	3	-	-	3	3	-	-	4	3	-	-
Sr	351	290	283	285.	376	382	412	384	223	334	423	422
Rb	-	2	3	2	-	-	4	-	2	2	2	-
Pb	-	-	-	-	-	-	-	-	-	-	-	-
Cr	508	814	850	974	423	485	332	509	1264	671	234	188
V	59	73	75	69	12	25	37	41	101	48	27	15
Ba	89	60	78	58	72	45	73	80	21	41	52	23
Sc	12	35	12	25	12	25	12	12	35	12	12	12
S	na	na	na	na	na	na	na	na	na	na	na	na

B D	197.0	200.0	203.0	205.0	207.0	210.0	213.0	216.0	218.0	221.0	224.0	227.0
UNIT	M	M	M	M	M	M	M	M	M	M	M	M
S H	418.0	415.0	412.0	410.0	408.0	405.0	402.0	399.0	397.0	394.0	391.0	388.0
SiO_2	51.10	49.24	50.67	50.71	50.56	50.28	50.53	50.65	51.15	50.07	50.96	50.17
TiO_2	0.08	0.03	0.06	0.06	0.06	0.06	0.07	0.08	0.11	0.10	0.11	0.11
Al_2O_3	17.13	21.53	19.89	19.67	20.80	19.48	19.84	18.77	13.33	11.79	13.20	12.28
Fe_2O_3	7.31	4.82	5.16	5.60	5.13	5.67	5.53	6.38	9.48	11.10	10.00	10.64
MnO	0.16	0.11	0.11	0.12	0.11	0.12	0.11	0.13	0.19	0.21	0.19	0.20
MgO	11.41	7.36	7.79	8.23	7.20	8.36	7.87	9.51	15.57	17.85	16.47	17.07
CaO	10.42	12.31	12.35	11.95	11.98	11.89	11.93	11.04	8.39	6.92	7.56	7.18
Na_2O	1.79	1.87	2.13	2.09	2.20	2.04	2.12	1.97	1.42	1.05	1.38	1.20
K_2O	0.05	0.04	0.08	0.07	0.08	0.06	0.09	0.08	0.05	0.01	0.02	-
P_2O_5	0.08	0.09	0.09	0.08	0.09	0.08	0.09	0.09	0.09	0.09	0.09	0.09
Total	99.53	97.40	98.33	98.58	98.21	98.04	98.18	98.70	99.78	99.19	99.98	98.94
Zn	45	24	26	29	26	30	28	34	60	78	58	64
Cu	-	9	-	-	-	-	5	-	8	11	-	-
Ni	269	186	187	199	173	205	196	225	371	457	394	428
Co	65	40	45	44	42	45	46	90	84	97	89	89
Ga	10	14	11	13	14	12	13	12	7	6	8	5
Zr	5	3	4	4	6	3	6	7	5	4	5	4
Y	3	-	3	3	3	3	3	4	5	4	4	-
Sr	256	344	310	303	332	305	315	294	178	153	182	161
Rb	-	-	-	-	2	-	2	-	-	3	3	2
Pb	-	-	-	-	-	-	-	-	-	-	-	-
Cr	919	631	754	753	615	730	719	944	1617	1876	1711	1857
V	108	44	62	70	83	86	69	85	107	142	104	104
Ba	32	39	42	27	77	36	46	63	21	20	31	25
Sc	19	12	12	14	12	12	27	26	31	18	13	14
S	na	na	na	na	na	na	na	na	na	na	na	na

WHOLE ROCK ANALYSES - continued -

B D	229.0	232.0	235.0	238.0	241.0	244.0	248.0	251.0	254.0	256.0	259.0	263.0
UNIT	M	M	M	M	M	M	M	M	M	M	M	M
S H	386.0	383.0	380.0	377.0	374.0	371.0	367.0	364.0	361.0	359.0	356.0	352.0
SiO_2	50.89	50.59	50.16	50.14	51.23	49.84	49.68	50.77	50.97	48.70	49.69	50.98
TiO_2	0.14	0.10	0.05	0.08	0.15	0.02	0.04	0.07	0.09	0.03	0.04	0.05
Al_2O_3	9.85	14.18	25.75	20.64	14.71	28.96	25.31	23.78	20.79	20.74	21.98	20.15
Fe_2O_3	11.40	9.15	4.15	6.54	9.50	2.27	4.31	4.92	6.46	6.26	5.83	6.21
MnO	0.21	0.18	0.09	0.14	0.19	0.04	0.10	0.10	0.14	0.13	0.13	0.13
MgO	19.49	15.74	7.00	11.88	16.95	3.05	8.14	8.98	10.92	12.67	11.04	12.61
CaO	6.37	7.96	12.11	10.38	7.93	13.40	11.98	11.45	10.16	10.49	10.63	9.95
Na_2O	0.97	1.39	2.25	1.70	1.38	2.50	1.98	2.11	1.89	1.19	1.54	1.92
K_2O	0.02	0.04	0.07	0.04	0.03	0.08	0.06	0.11	0.09	0.03	0.04	0.06
P_2O_5	0.09	0.09	0.06	0.05	0.05	0.07	0.06	0.06	0.06	0.05	0.05	0.05
Total	99.43	99.42	101.69	101.59	102.12	100.23	101.66	102.35	101.57	100.29	100.97	102.11
Zn	74	55	22	38	59	9	23	30	40	34	34	35
Cu	-	-	-	25	8	-	-	-	5	-	-	-
Ni	485	380	153	290	401	77	184	205	281	302	271	283
Co	100	87	38	59	86	32	40	48	57	51	55	107
Ga	5	8	16	13	11	19	15	15	13	14	13	13
Zr	5	4	3	-	4	-	4	3	6	3	4	3
Y	4	4	-	-	4	-	-	-	6	-	-	-
Sr	123	198	367	280	177	447	361	338	288	281	302	269
Rb	3	-	2	-	-	2	-	2	-	-	-	2
Pb	-	-	-	-	-	-	-	-	-	-	-	-
Cr	2193	1783	713	1268	1964	361	941	1045	1400	1557	1423	1503
V	116	104	27	57	111	12	25	52	67	68	51	67
Ba	20	20	48	29	20	40	47	68	34	46	41	42
Sc	41	14	12	28	19	12	12	14	11	11	22	12
S	na	na	na	na	na	na	na	na	na	na	na	na

B D	265.0	268.0	271.0	274.0	277.0	281.0	284.0	286.0	288.0	290.0	293.0	294.0
UNIT	L	L	L	L	L	L	L	L	L	L	L	L
S H	350.0	347.0	344.0	341.0	338.0	334.0	331.0	329.0	327.0	325.0	322.0	321.0
SiO_2	52.24	51.54	51.79	51.23	42.10	52.36	51.42	40.90	48.25	41.64	50.82	51.53
TiO_2	0.17	0.15	0.10	0.14	0.53	0.15	0.15	0.55	0.25	0.52	0.07	0.07
Al_2O_3	5.00	5.77	11.01	6.29	8.03	1.81	2.19	4.39	5.74	6.71	16.77	17.20
Fe_2O_3	13.99	13.41	10.64	13.65	15.49	14.63	14.94	16.92	13.89	16.12	7.79	7.76
MnO	0.23	0.23	0.20	0.23	0.30	0.23	0.24	0.32	0.25	0.31	0.17	0.16
MgO	24.24	24.09	20.47	23.33	19.02	28.15	27.34	22.33	23.65	20.13	15.87	15.49
CaO	4.40	4.07	6.17	4.50	3.51	2.21	2.37	2.08	4.13	2.77	8.41	8.51
Na_2O	0.51	0.65	1.19	0.57	0.68	0.14	0.16	0.13	0.33	0.49	1.54	1.71
K_2O	-	-	0.03	0.01	-	-	-	-	-	-	0.05	0.07
P_2O_5	0.03	0.04	0.04	0.04	0.01	0.03	0.03	-	0.02	0.01	0.05	0.05
Total	100.81	99.95	101.64	99.99	89.67	99.71	98.84	87.62	96.51	88.70	101.54	102.55
Zn	92	81	66	79	200	87	86	235	107	206	43	45
Cu	9	-	-	13	5	5	-	10	-	5	-	-
Ni	587	553	457	527	538	616	599	619	533	547	329	324
Co	120	166	95	153	138	137	153	154	127	151	114	79
Ga	6	7	7	6	16	4	3	17	8	18	11	11
Zr	4	4	6	6	5	3	3	5	-	5	4	4
Y	4	5	6	6	9	5	5	-	6	7	3	-
Sr	51	60	120	69	65	9	11	8	37	41	207	206
Rb	-	-	-	-	-	-	-	-	-	-	-	-
Pb	-	-	-	-	-	-	-	-	-	-	-	-
Cr	3106	3270	2336	3579	84890	4144	3988	83527	25180	84923	1849	1657
V	153	142	76	146	789	178	151	994	390	1038	86	87
Ba	23	23	20	19	18	18	18	17	18	18	41	48
Sc	40	34	22	34	21	19	29	21	10	24	19	22
S	na	na	na	na	na	na	na	na	na	na	na	na

WHOLE ROCK ANALYSES - continued -

B D	296.0	300.0	304.0	304.5	304.7	305.0	307.0	2.0	309.0	8.0	15.0	20.4
UNIT	L	L	K	K	K	K	K	K *	K	K *	K *	K *
S H	319.0	315.0	311.0	310.5	310.3	310.0	309.0	308.0	306.0	302.0	295.0	289.6
SiO_2	52.36	51.90	50.13	50.11	40.82	47.52	50.09	48.34	49.95	48.64	49.09	49.52
TiO_2	0.12	0.16	0.06	0.03	0.42	0.09	0.06	0.07	0.07	0.10	0.10	0.06
Al_2O_3	8.48	3.96	17.52	19.32	9.28	22.80	21.81	24.59	21.01	16.12	16.13	18.35
Fe_2O_3	11.53	14.07	7.65	7.13	15.00	5.70	6.19	4.84	6.59	9.29	9.27	7.75
MnO	0.21	0.24	0.17	0.16	0.30	0.13	0.14	0.10	0.14	0.19	0.19	0.17
MgO	22.75	26.01	14.73	14.94	18.64	10.53	10.57	6.67	11.08	15.07	15.15	13.29
CaO	5.14	3.24	8.73	9.54	3.95	11.62	10.26	11.59	9.95	8.11	8.08	9.09
Na_2O	0.93	0.41	1.54	1.22	0.52	1.32	2.06	2.27	1.97	1.58	1.68	1.89
K_2O	0.02	-	0.05	0.02	-	0.03	0.07	0.11	0.08	0.06	0.07	0.05
P_2O_5	0.04	0.03	0.03	0.05	-	0.05	0.05	-	0.05	-	-	-
Total	101.58	100.01	100.61	102.52	88.92	99.79	101.30	98.58	100.89	99.16	99.75	100.16
Zn	72	86	56	37	203	61	36	52	43	63	61	48
Cu	-	-	-	-	-	-	-	6	-	9	9	6
Ni	489	581	328	321	515	217	233	174	240	339	327	280
Co	113	189	67	79	135	96	58	78	59	113	120	110
Ga	7	4	9	11	17	16	14	17	12	9	14	11
Zr	4	6	-	4	3	-	3	-	4	5	7	5
Y	3	6	4	-	3	3	3	3	-	3	3	3
Sr	91	36	224	224	68	292	279	344	265	198	202	238
Rb	2	2	-	-	2	-	-	3	-	2	2	-
Pb	-	-	-	-	-	-	-	-	-	-	-	-
Cr	2865	4451	1972	2664	84661	19027	5433	12699	5665	5727	4046	1442
V	112	166	103	91	993	246	101	176	100	128	142	88
Ba	19	18	-	21	25	39	40	39	46	20	38	31
Sc	33	29	40	11	13	11	11	11	11	21	22	11
S	na	na	na	na	na	na	na	na	na	na	na	na

B D	20.5	26.0	32.0	37.0	49.0	55.0	60.0	66.0	72.0	77.0	83.0	87.0
UNIT	K *	K *	K *	J *	J *	J *	J *	J *	J *	J *	J *	J *
S H	289.5	284.0	278.0	273.0	261.0	255.0	250.0	244.0	238.0	233.0	227.0	223.0
SiO_2	49.13	49.74	49.02	49.18	49.71	51.03	49.25	49.68	50.84	49.69	49.57	50.36
TiO_2	0.06	0.15	0.08	0.11	0.12	0.13	0.14	0.14	0.14	0.09	0.09	0.13
Al_2O_3	20.32	10.93	18.73	13.48	13.67	12.80	11.65	11.28	11.68	16.28	16.24	13.73
Fe_2O_3	6.64	11.48	7.17	10.71	10.51	10.42	11.51	11.52	10.85	8.76	8.75	9.64
MnO	0.15	0.21	0.15	0.20	0.20	0.20	0.21	0.21	0.21	0.17	0.17	0.20
MgO	10.80	18.16	12.10	17.03	16.99	18.13	18.49	19.57	19.03	15.64	15.67	17.69
CaO	10.23	7.04	10.18	7.21	7.09	6.92	6.35	6.13	6.04	8.29	8.22	6.97
Na_2O	2.05	1.25	1.84	1.34	1.44	1.40	1.23	1.19	1.14	1.57	1.54	1.23
K_2O	0.07	0.11	0.07	0.07	0.11	0.09	0.08	0.07	0.06	0.06	0.06	0.06
P_2O_5	-	0.01	-	-	-	-	-	-	-	-	-	-
Total	99.45	99.08	99.34	99.33	99.84	101.11	99.09	99.79	100.00	100.55	100.31	100.00
Zn	43	85	43	64	66	68	71	74	83	57	71	72
Cu	11	15	8	11	11	16	17	11	14	6	8	10
Ni	220	397	262	374	383	394	404	420	437	337	341	417
Co	95	161	121	124	121	157	121	129	126	113	103	105
Ga	13	11	10	9	6	8	9	9	14	12	9	15
Zr	5	15	4	6	9	8	8	5	8	5	4	10
Y	4	5	-	5	6	3	8	4	6	4	4	4
Sr	277	134	241	162	164	158	139	136	119	198	196	141
Rb	-	3	-	2	-	4	-	2	2	-	-	3
Pb	-	-	-	-	-	-	-	-	-	-	-	-
Cr	1253	2872	2719	2405	2232	2387	2606	2427	2570	2093	2376	2878
V	78	121	90	100	103	96	126	128	137	90	78	129
Ba	27	32	52	20	61	25	43	39	20	37	23	20
Sc	11	38	25	34	22	27	34	27	25	26	15	20
S	na	na	na	na	na	na	na	na	na	na	na	na

WHOLE ROCK ANALYSES - continued -

B D	90.0	94.0	96.0	99.0	100.0	103.0	111.0	120.0	127.0	134.0	144.0	147.0
UNIT	J *	J *	J *	J *	J *	J *	J *	J *	J *	J *	J *	J *
S H	220.0	216.0	214.0	211.0	210.0	207.0	199.0	190.0	183.0	176.0	166.0	163.0
SiO_2	49.15	50.11	50.65	50.30	49.81	50.30	50.15	50.39	50.14	50.04	50.90	49.87
TiO_2	0.11	0.12	0.21	0.14	0.10	0.13	0.15	0.15	0.12	0.12	0.11	0.10
Al_2O_3	13.65	13.33	3.53	12.64	14.30	10.10	10.27	10.64	12.66	13.45	14.94	15.99
Fe_2O_3	9.95	9.87	15.20	10.54	9.72	11.60	11.79	11.46	10.46	10.19	9.05	8.90
MnO	0.19	0.20	0.24	0.21	0.19	0.21	0.21	0.21	0.20	0.20	0.18	0.18
MgO	17.90	18.50	25.61	18.54	17.62	21.01	20.00	20.36	18.82	18.01	16.77	15.97
CaO	7.30	6.65	3.28	6.46	7.47	6.02	6.24	5.90	6.90	7.19	7.93	8.11
Na_2O	1.26	1.16	0.35	1.10	1.32	1.00	1.03	1.04	1.25	1.30	1.41	1.54
K_2O	0.05	0.04	0.05	0.07	0.04	0.03	0.06	0.07	0.06	0.08	0.07	0.08
P_2O_5	-	-	-	-	-	-	0.01	0.01	-	-	-	-
Total	99.55	100.00	99.16	100.00	100.56	100.39	99.91	100.23	100.61	100.58	101.25	100.74
Zn	61	75	113	80	65	75	76	73	73	66	60	57
Cu	10	7	12	11	5	10	14	10	7	7	10	8
Ni	386	437	575	437	385	451	447	441	412	398	367	347
Co	101	100	159	120	110	142	117	127	110	104	133	91
Ga	11	13	4	11	9	8	7	7	8	11	10	8
Zr	4	7	13	8	5	7	13	13	8	7	8	8
Y	5	4	6	4	3	6	3	5	5	5	-	3
Sr	167	133	28	122	169	116	117	128	148	157	187	199
Rb	-	-	3	-	-	-	3	4	-	2	3	4
Pb	-	-	-	-	-	-	-	-	-	-	-	-
Cr	2512	2769	3675	3018	2611	3198	3085	3061	2912	3086	2275	2065
V	86	123	179	127	104	128	135	130	90	96	115	109
Ba	20	20	20	20	26	26	30	19	42	40	32	44
Sc	27	26	31	25	29	25	29	36	28	34	27	18
S	na	na	na	na	na	na	na	na	na	na	na	na

B D	152.0	158.0	166.0	172.0	179.0	185.0	191.0	196.0	200.0	205.0	210.0	213.0
UNIT	J *	J *	J *	J *	J *	J *	J *	J *	J *	J *	J *	J *
S H	158.0	152.0	144.0	138.0	131.0	125.0	119.0	114.0	110.0	105.0	100.0	97.0
SiO_2	49.60	50.35	50.07	51.12	51.45	51.52	51.54	51.90	51.47	51.09	51.78	50.63
TiO_2	0.10	0.13	0.13	0.12	0.13	0.13	0.18	0.16	0.17	0.14	0.18	0.18
Al_2O_3	16.58	15.34	16.04	17.16	16.61	17.00	14.23	16.78	15.85	18.88	16.02	17.03
Fe_2O_3	8.62	9.21	9.00	8.08	8.21	8.12	9.30	8.05	8.73	7.43	8.55	8.47
MnO	0.17	0.18	0.18	0.16	0.17	0.16	0.18	0.16	0.17	0.15	0.17	0.17
MgO	15.16	16.02	15.10	13.74	14.32	14.10	15.81	14.01	14.52	11.86	14.60	13.19
CaO	8.38	7.94	8.26	8.63	8.44	8.50	7.54	8.56	8.31	9.29	8.24	8.56
Na_2O	1.58	1.48	1.56	1.50	1.42	1.45	1.20	1.47	1.38	1.63	1.35	1.43
K_2O	0.10	0.12	0.15	0.13	0.15	0.14	0.18	0.17	0.18	0.20	0.21	0.15
P_2O_5	-	0.01	0.01	0.06	0.07	0.05	0.06	0.06	0.07	0.07	0.06	0.06
Total	100.29	100.78	100.50	100.70	100.97	101.17	100.22	101.32	100.85	100.74	101.16	99.87
Zn	61	69	62	65	58	62	65	60	68	57	61	67
Cu	8	13	12	12	8	13	13	14	18	13	19	13
Ni	336	361	339	318	322	325	368	313	341	284	340	337
Co	94	100	88	83	71	97	106	90	70	76	77	96
Ga	13	11	9	10	10	14	9	10	13	12	13	9
Zr	7	12	15	11	14	13	22	16	18	15	20	16
Y	3	3	7	6	4	5	5	4	5	5	7	7
Sr	208	191	197	212	207	214	179	209	194	233	197	207
Rb	-	2	3	-	4	4	7	5	5	5	9	-
Pb	-	-	-	5	7	-	-	6	6	10	-	5
Cr	1996	2005	1858	1728	1793	1752	2001	1769	2073	1736	3941	6065
V	103	110	93	56	84	63	109	68	96	72	103	134
Ba	41	38	66	17	15	16	31	-	25	47	32	-
Sc	11	15	18	27	21	18	15	24	29	20	29	25
S	na	na	na	na	na	na	na	na	na	50	60	60

WHOLE ROCK ANALYSES - continued -

B D	215.0	219.0	223.0	228.0	231.5	231.7	233.0	235.0	240.0	242.0	247.0	250.0
UNIT	J *	H *	H *	H *	G *	G *	G *	G *	G *	G *	G *	G *
S H	95.0	91.0	87.0	82.0	78.4	78.3	77.0	75.0	70.0	68.0	63.0	60.0
SiO_2	51.75	49.78	50.21	41.32	47.81	50.55	52.06	52.23	51.97	50.83	51.81	52.85
TiO_2	0.15	0.13	0.14	0.39	0.29	0.23	0.18	0.18	0.17	0.14	0.13	0.15
Al_2O_3	14.36	21.95	21.59	23.99	12.59	11.62	9.98	10.40	10.06	12.04	9.75	8.64
Fe_2O_3	9.35	5.41	6.34	7.79	11.15	11.08	11.28	11.17	11.17	10.57	11.09	11.38
MnO	0.19	0.11	0.13	0.16	0.22	0.21	0.21	0.21	0.21	0.21	0.21	0.21
MgO	16.49	7.89	9.69	5.93	17.11	18.36	19.71	19.63	20.25	18.94	21.07	22.09
CaO	7.48	11.08	10.30	9.76	6.26	5.96	5.74	6.08	5.69	6.30	5.56	5.27
Na_2O	1.22	1.80	1.75	1.89	1.00	0.99	0.96	1.01	0.90	0.95	0.81	0.72
K_2O	0.11	0.16	0.17	0.13	0.07	0.12	0.14	0.11	0.08	0.04	0.03	0.06
P_2O_5	0.06	0.06	0.06	0.05	0.06	0.08	0.06	0.06	0.05	0.06	0.05	0.06
Total	101.16	98.37	100.38	91.41	96.56	99.20	100.32	101.08	100.55	100.08	100.55	101.43
Zn	68	50	58	213	129	94	72	82	79	79	73	79
Cu	13	17	12	18	20	16	13	14	12	10	9	9
Ni	384	185	234	313	470	440	446	445	447	450	466	485
Co	81	102	58	100	104	109	160	116	96	102	100	109
Ga	12	19	15	32	14	12	4	10	7	11	10	9
Zr	14	12	10	10	14	17	14	13	10	6	6	10
Y	6	5	4	4	6	6	6	6	6	4	4	7
Sr	168	320	282	294	133	122	114	109	110	125	105	85
Rb	2	5	4	-	3	2	6	5	2	-	3	4
Pb	-	7	-	-	-	-	-	-	-	-	-	-
Cr	2657	8176	8778	79532	33101	14459	3140	2942	4144	6643	2722	2759
V	81	132	122	877	453	230	122	127	137	166	140	134
Ba	18	35	-	28	-	15	-	17	17	17	19	15
Sc	17	13	13	10	24	22	24	21	37	11	28	27
S	50	40	50	30	na	30	40	40	30	30	40	40

B D	254.0	260.0	264.0	269.0	273.0	276.0	278.0	281.0	284.0	288.0	289.0	290.0
UNIT	G *	G *	G *	G *	G *	G *	G *	G *	G *	F *	F *	F *
S H	56.0	50.0	46.0	41.0	37.0	34.0	32.0	29.0	26.0	23.0	21.0	20.0
SiO_2	51.73	51.88	51.96	52.77	52.65	52.63	53.25	53.01	52.60	48.28	46.07	47.87
TiO_2	0.14	0.14	0.15	0.19	0.20	0.20	0.22	0.24	0.23	0.23	0.35	0.24
Al_2O_3	8.93	8.55	10.46	8.10	7.81	7.59	6.87	6.48	7.84	25.95	26.31	27.20
Fe_2O_3	11.19	11.28	10.63	11.35	11.37	11.64	11.84	12.17	11.94	4.88	5.72	4.38
MnO	0.21	0.21	0.20	0.21	0.20	0.21	0.21	0.21	0.21	0.09	0.11	0.09
MgO	21.90	22.42	20.75	22.45	22.55	22.60	22.80	22.82	21.25	5.46	5.81	5.71
CaO	5.34	5.17	5.72	4.88	4.93	4.69	4.58	4.54	5.23	12.21	11.66	12.17
Na_2O	0.69	0.65	0.86	0.76	0.72	0.79	0.74	0.57	0.77	2.15	2.21	2.03
K_2O	0.03	0.02	0.06	0.09	0.07	0.06	0.11	0.13	0.14	0.30	0.27	0.28
P_2O_5	0.06	0.05	0.05	0.06	0.06	0.05	0.06	0.06	0.07	0.07	0.06	0.06
Total	100.22	100.37	100.84	100.86	100.56	100.46	100.68	100.23	100.28	99.68	98.07	100.06
Zn	76	75	77	82	82	80	81	80	91	77	121	77
Cu	12	11	19	11	14	20	19	21	19	23	32	24
Ni	492	508	476	492	518	512	513	507	495	120	154	123
Co	153	122	88	106	98	115	102	105	127	90	94	56
Ga	8	6	5	7	8	8	8	9	8	24	29	23
Zr	6	6	6	11	12	11	15	17	17	18	15	18
Y	3	4	4	8	4	5	6	8	9	8	7	6
Sr	93	81	98	77	77	79	69	54	81	344	341	365
Rb	2	-	-	-	5	4	3	5	5	4	3	5
Pb	-	-	8	-	7	9	-	-	-	12	6	-
Cr	2877	2941	2918	3353	3457	3668	3647	4616	6442	24163	43769	25004
V	146	126	115	140	129	138	109	148	152	206	459	260
Ba	18	18	16	36	17	15	17	17	41	69	67	66
Sc	35	32	24	20	24	15	27	25	29	10	13	14
S	50	50	40	50	60	60	60	140	70	60	na	90

WHOLE ROCK ANALYSES - continued -

B D	291.0	295.0	297.0	300.0	304.0	306.0	310.0	311.8	313.0	315.0	317.0	319.0
UNIT	F *	F *	F *	F *	F *	F *	F *	E *	E *	E *	E *	E *
S H	19.0	15.0	13.0	10.0	6.0	4.0	0.0	-1.0	-3.0	-5.0	-7.0	-9.0
SiO_2	50.01	52.97	53.46	54.48	53.66	53.46	52.63	52.85	53.00	42.81	53.25	40.75
TiO_2	0.13	0.21	0.23	0.28	0.23	0.23	0.23	0.24	0.23	0.44	0.16	0.56
Al_2O_3	24.37	14.90	12.71	8.65	10.22	9.70	7.11	7.39	7.60	9.05	8.29	5.96
Fe_2O_3	4.66	9.71	10.78	11.97	11.48	11.50	12.80	12.26	11.56	13.85	10.40	16.21
MnO	0.10	0.18	0.20	0.21	0.21	0.21	0.22	0.22	0.20	0.28	0.19	0.31
MgO	5.87	14.51	16.64	18.83	18.85	19.00	21.46	21.10	21.29	19.09	21.73	19.32
CaO	11.84	7.82	6.45	5.82	5.95	6.02	4.74	4.64	4.93	3.68	5.56	2.98
Na_2O	1.97	1.46	1.43	0.89	1.06	0.99	0.69	0.83	0.89	0.69	0.90	0.50
K_2O	0.24	0.24	0.29	0.31	0.24	0.22	0.13	0.23	0.25	0.03	0.11	0.04
P_2O_5	0.07	0.09	0.07	0.09	0.08	0.08	0.06	0.06	0.08	0.05	0.05	0.07
Total	99.30	102.09	102.26	101.53	101.98	101.41	100.07	99.82	100.03	89.97	100.64	86.65
Zn	48	69	78	86	85	82	94	87	81	190	75	230
Cu	18	18	21	24	17	23	18	17	15	44	25	46
Ni	131	311	364	406	415	410	474	499	458	649	480	740
Co	35	91	82	162	91	114	123	175	115	124	89	184
Ga	18	13	10	8	8	6	7	9	7	15	9	19
Zr	14	26	18	38	25	23	17	24	24	9	12	10
Y	5	8	6	10	7	7	7	9	10	3	9	4
Sr	344	179	145	98	108	108	81	75	79	70	83	38
Rb	6	8	6	13	8	9	6	5	6	3	6	4
Pb	8	6	7	-	5	8	7	-	-	-	-	-
Cr	10476	2061	1886	2186	2216	2532	3566	5966	3750	69349	3978	85390
V	150	107	115	167	133	133	121	121	106	528	74	633
Ba	71	38	47	32	37	46	59	23	28	16	27	12
Sc	18	22	20	43	29	30	37	24	24	24	21	32
S	70	90	80	90	70	60	60	100	80	120	160	230

B D	320.0	321.0	325.0	327.0	330.0	333.0	335.0	339.0	342.0	345.0	347.0	350.0
UNIT	E *	E *	E *	E *	E *	E *	E *	E *	E *	E *	E *	E *
S H	-10.0	-11.0	-15.0	-17.0	-20.0	-23.0	-25.0	-29.0	-32.0	-35.0	-37.0	-40.0
SiO_2	52.76	53.01	51.69	53.12	48.28	50.38	44.61	48.44	53.39	53.31	52.78	53.16
TiO_2	0.18	0.13	0.20	0.41	0.25	0.24	0.52	0.32	0.14	0.21	0.16	0.16
Al_2O_3	8.27	9.53	6.85	3.37	8.40	9.41	5.54	5.25	10.17	8.27	9.70	9.25
Fe_2O_3	10.80	9.95	11.04	12.84	11.25	10.57	14.06	13.61	9.13	10.25	9.33	9.67
MnO	0.20	0.19	0.20	0.21	0.22	0.21	0.27	0.24	0.18	0.19	0.18	0.18
MgO	22.10	21.49	22.67	24.53	22.01	21.66	21.99	22.94	22.30	22.82	22.84	22.55
CaO	4.59	5.42	5.22	1.77	4.26	4.53	2.78	3.13	5.38	4.72	4.84	5.11
Na_2O	1.02	1.08	0.74	0.31	0.72	0.90	0.46	0.61	0.98	0.99	0.90	0.91
K_2O	0.10	0.07	0.05	0.70	0.03	0.04	0.02	0.04	0.04	0.04	0.04	0.04
P_2O_5	0.15	0.07	0.04	0.09	0.05	0.05	0.06	0.07	0.06	0.05	0.06	0.06
Total	100.17	100.94	98.70	97.35	95.47	97.99	90.31	94.80	101.77	100.85	100.83	101.09
Zn	75	68	84	111	113	102	170	136	67	82	81	74
Cu	28	18	24	31	28	20	30	32	26	28	16	17
Ni	497	472	529	640	620	558	721	651	514	531	543	525
Co	143	100	118	122	209	111	168	159	105	97	140	89
Ga	6	9	7	6	10	11	9	15	6	7	8	6
Zr	13	6	10	48	7	9	10	11	8	8	9	6
Y	7	4	5	9	6	8	8	9	6	7	3	4
Sr	88	106	68	9	78	94	33	44	105	94	91	98
Rb	-	3	4	26	-	-	-	-	-	2	3	-
Pb	-	5	8	5	-	-	6	5	-	-	-	6
Cr	5348	3036	14951	23596	33197	24278	60004	34335	6280	7917	11311	6230
V	90	86	179	229	257	212	433	325	86	111	103	102
Ba	67	-	17	136	17	-	17	16	17	-	17	18
Sc	27	25	22	34	17	10	24	29	23	32	28	19
S	180	150	170	230	180	150	210	250	130	210	90	110

WHOLE ROCK ANALYSES - continued -

B D	351.0	353.0	355.0	357.0	359.0	362.0	363.0	367.0	369.0	372.0	373.0	377.0
UNIT	E *	E *	E *	E *	E *	E *	E *	E *	E *	E *	E *	E *
S H	-41.0	-43.0	-45.0	-47.0	-49.0	-52.0	-53.0	-57.0	-59.0	-62.0	-63.0	-67.0
SiO_2	55.97	57.58	54.73	55.46	54.79	51.66	55.30	54.81	57.66	56.15	53.36	53.81
TiO_2	0.33	0.41	0.27	0.31	0.23	0.27	0.30	0.24	0.37	0.40	0.18	0.16
Al_2O_3	4.57	3.20	5.63	5.68	6.81	8.69	3.91	5.78	3.71	3.04	7.25	8.52
Fe_2O_3	11.01	11.34	11.32	10.96	10.50	10.45	11.22	10.81	10.93	11.68	10.57	9.42
MnO	0.18	0.18	0.19	0.19	0.19	0.19	0.18	0.18	0.17	0.18	0.19	0.18
MgO	24.14	24.68	23.89	23.89	23.37	21.88	25.86	23.99	25.13	24.24	23.32	23.53
CaO	4.17	3.05	3.81	3.89	4.46	5.15	3.95	4.41	2.91	2.87	4.36	4.78
Na_2O	0.60	0.38	0.84	0.82	0.94	0.94	0.52	0.85	0.55	0.27	0.90	0.84
K_2O	0.31	0.67	0.13	0.20	0.10	0.03	0.11	0.08	0.42	0.77	0.04	0.05
P_2O_5	0.06	0.20	0.06	0.10	0.08	0.05	0.09	0.05	0.07	0.07	0.05	0.06
Total	101.34	101.69	100.87	101.50	101.47	99.31	101.44	101.20	101.92	99.70	100.22	101.35
Zn	83	88	84	81	79	97	80	85	82	84	78	67
Cu	30	17	49	27	34	31	32	45	22	5	30	19
Ni	565	570	568	554	513	542	561	542	531	521	509	487
Co	125	160	121	104	113	111	107	109	135	95	124	156
Ga	7	4	7	9	9	12	4	6	7	7	6	4
Zr	32	68	22	27	14	8	22	15	50	56	8	13
Y	7	12	9	8	9	5	7	10	11	10	5	5
Sr	39	13	55	53	74	96	35	58	24	6	84	87
Rb	11	26	5	7	2	3	6	2	17	28	5	2
Pb	-	7	-	-	8	-	7	7	7	-	5	6
Cr	5310	5351	4296	4159	3133	17852	3250	3032	3210	3153	2986	2953
V	130	152	127	121	82	206	102	99	127	138	98	61
Ba	27	28	-	29	25	18	18	-	41	52	-	16
Sc	34	41	30	25	27	34	31	35	21	32	27	25
S	320	310	320	230	210	210	210	270	310	410	170	140

B D	379.0	381.0	383.0	386.0	388.0	390.0	392.0	395.0	397.0	401.0	404.0	406.0
UNIT	E *	E *	E *	E *	E *	E *	E *	E *	E *	E *	E *	E *
S H	-69.0	-71.0	-73.0	-76.0	-78.0	-80.0	-82.0	-85.0	-87.0	-91.0	-94.0	-96.0
SiO_2	56.14	54.24	54.54	55.34	56.64	54.60	54.50	54.11	56.19	55.06	54.12	53.93
TiO_2	0.30	0.26	0.19	0.25	0.35	0.20	0.17	0.16	0.32	0.17	0.16	0.19
Al_2O_3	5.11	4.56	7.69	5.41	3.70	7.33	6.83	8.01	3.06	7.84	8.65	7.34
Fe_2O_3	10.47	11.22	9.69	10.76	11.13	9.87	9.86	9.44	10.97	9.26	9.53	10.02
MnO	0.18	0.19	0.18	0.19	0.18	0.18	0.18	0.18	0.18	0.17	0.18	0.18
MgO	24.38	24.18	23.13	24.81	24.95	23.62	24.69	23.73	25.62	24.64	23.65	23.35
CaO	3.99	4.59	5.00	3.57	2.81	4.62	4.57	4.96	3.63	4.57	4.83	4.93
Na_2O	0.66	0.61	0.85	0.77	0.51	0.83	0.74	0.78	0.40	0.75	0.83	0.75
K_2O	0.27	0.12	0.11	0.11	0.42	0.11	0.02	0.05	0.24	0.06	0.05	0.09
P_2O_5	0.08	0.06	0.06	0.07	0.10	0.06	0.06	0.07	0.09	0.05	0.05	0.06
Total	101.58	100.03	101.44	101.28	100.79	101.42	101.62	101.49	100.70	102.57	102.05	100.84
Zn	80	78	99	76	85	70	71	72	77	69	69	84
Cu	39	37	28	29	16	29	32	19	16	21	30	12
Ni	529	553	496	505	533	509	524	520	558	512	502	494
Co	119	101	117	98	100	92	122	90	120	157	102	93
Ga	9	4	5	6	4	8	4	3	5	4	5	6
Zr	29	16	15	15	37	18	5	11	30	11	8	12
Y	8	8	7	5	11	5	4	6	7	5	7	5
Sr	47	41	79	54	19	74	70	75	18	77	74	71
Rb	10	3	4	4	15	4	-	3	12	-	2	3
Pb	-	5	-	-	6	5	-	-	5	-	-	-
Cr	3124	3261	2989	3069	3201	2985	3169	3135	3590	3135	3100	3043
V	100	98	93	97	108	83	70	78	134	75	68	61
Ba	29	25	15	24	111	-	17	15	25	17	18	-
Sc	19	32	18	25	22	31	24	22	24	25	20	25
S	320	260	210	200	230	170	170	130	270	120	140	110

WHOLE ROCK ANALYSES - continued -

B D	410.0	413.0	415.0	418.0	421.0	423.0	425.0	427.0	430.0	433.0	435.0	437.0
UNIT	E *	E *	E *	E *	E *	E *	E *	E *	E *	E *	E *	E *
S H	-100.0	-103.0	-105.0	-108.0	-111.0	-113.0	-115.0	-117.0	-120.0	-123.0	-125.0	-127.0
SiO_2	55.46	56.12	54.36	55.21	53.93	53.95	51.45	54.70	54.61	51.77	53.57	53.48
TiO_2	0.24	0.24	0.17	0.18	0.17	0.16	0.14	0.19	0.16	0.18	0.22	0.17
Al_2O_3	4.65	4.79	6.24	4.75	6.24	6.30	4.86	2.38	4.48	7.46	4.39	2.93
Fe_2O_3	10.53	10.42	10.41	10.60	10.43	10.68	11.95	12.58	11.76	11.18	12.14	12.60
MnO	0.18	0.18	0.18	0.18	0.19	0.19	0.21	0.20	0.20	0.22	0.21	0.22
MgO	25.41	24.94	24.42	25.57	24.18	25.09	26.57	26.81	25.84	23.07	24.47	26.19
CaO	4.02	3.95	4.25	3.54	4.45	3.91	3.60	2.67	3.49	4.40	3.53	3.00
Na_2O	0.58	0.54	0.71	0.51	0.61	0.57	0.48	0.20	0.40	0.60	0.46	0.25
K_2O	0.10	0.21	0.06	0.12	0.08	0.03	0.02	0.08	0.02	0.05	0.11	0.03
P_2O_5	0.07	0.08	0.05	0.07	0.06	0.05	0.04	0.06	0.05	0.05	0.14	0.06
Total	101.24	101.47	100.85	100.73	100.34	100.93	99.32	99.87	101.01	98.98	99.24	98.93
Zn	77	77	75	77	74	80	80	86	87	95	93	90
Cu	23	32	36	23	12	22	25	12	24	19	21	10
Ni	532	525	522	525	520	538	542	562	591	578	557	577
Co	189	91	121	101	110	75	189	111	120	109	125	104
Ga	7	7	4	6	6	4	3	7	6	3	7	5
Zr	13	23	8	13	11	9	5	11	7	9	17	7
Y	6	7	7	7	4	6	6	8	5	6	8	6
Sr	43	39	58	37	57	49	45	11	36	56	26	17
Rb	5	9	2	3	3	-	-	2	-	-	1	1
Pb	-	5	7	-	5	-	-	-	-	11	6	-
Cr	3390	3252	3226	3448	3401	3483	3527	3744	3571	19165	11731	4981
V	79	116	84	90	85	79	89	70	92	214	213	133
Ba	19	26	-	17	-	16	18	16	17	-	15	17
Sc	31	21	19	20	28	30	21	32	40	30	46	42
S	140	170	160	130	110	70	100	90	90	110	130	70

B D	439.0	440.0	442.0	444.0	445.0	446.0	447.0	450.0	453.0	455.0	457.0	459.0
UNIT	E *	E *	E *	E *	E *	E *	E *	E *	E *	E *	E *	E *
S H	-129.0	-130.0	-132.0	-134.0	-135.0	-136.0	-137.0	-140.0	-143.0	-145.0	-147.0	-149.0
SiO_2	53.96	53.71	51.29	53.32	53.36	54.62	58.96	53.53	50.56	52.18	50.93	51.13
TiO_2	0.14	0.17	0.21	0.18	0.14	0.16	0.28	0.29	0.13	0.22	0.14	0.15
Al_2O_3	5.22	5.46	7.07	6.22	6.97	6.28	3.15	3.13	7.09	4.39	6.15	6.57
Fe_2O_3	11.30	11.60	11.41	11.40	11.06	11.29	11.43	12.87	11.06	12.27	11.70	11.21
MnO	0.20	0.21	0.22	0.21	0.21	0.21	0.19	0.21	0.21	0.22	0.22	0.21
MgO	25.80	24.84	23.45	23.54	24.19	24.09	24.17	24.80	23.73	24.80	24.01	23.46
CaO	3.49	3.71	3.88	4.33	4.04	3.70	2.89	2.32	4.78	3.39	4.35	4.54
Na_2O	0.44	0.52	0.57	0.64	0.65	0.73	0.34	0.42	0.75	0.67	0.75	0.79
K_2O	0.01	0.05	0.02	0.04	0.01	0.06	0.59	0.45	0.03	0.12	0.06	0.09
P_2O_5	0.06	0.06	0.06	0.05	0.05	0.05	0.05	0.06	0.04	0.06	0.05	0.06
Total	100.62	100.33	98.18	99.93	100.68	101.19	102.11	98.08	98.38	98.32	98.36	98.21
Zn	84	86	100	93	86	84	85	90	81	88	86	81
Cu	17	18	18	22	21	17	17	19	19	19	17	19
Ni	544	535	514	526	516	475	468	493	482	490	484	472
Co	113	106	216	113	118	116	156	105	127	123	121	105
Ga	3	7	9	6	6	7	5	6	6	4	7	6
Zr	6	9	7	8	5	10	40	35	5	17	8	14
Y	5	7	3	6	5	7	8	8	5	7	7	6
Sr	42	42	59	54	58	59	14	17	73	39	62	71
Rb	-	2	-	2	-	2	20	16	-	3	2	2
Pb	5	9	-	-	6	5	-	5	-	9	-	-
Cr	4682	4136	22001	10460	7442	3547	3735	4478	5025	5451	4383	3802
V	140	128	271	194	155	127	163	170	140	156	141	155
Ba	17	18	-	16	17	16	137	57	18	29	15	16
Sc	39	36	28	40	26	41	43	31	42	35	20	36
S	80	170	110	120	130	100	170	170	110	160	140	140

WHOLE ROCK ANALYSES - continued -

B D	461.0	464.0	466.0	468.0	473.0	474.0	477.0
UNIT	E *	E *	E *	E *	D *	D *	D *
S H	-151.0	-154.0	-156.0	-158.0	-163.0	-164.0	-167.0
SiO_2	50.37	50.16	51.36	47.37	49.47	50.78	48.83
TiO_2	0.14	0.14	0.25	0.24	0.18	0.29	0.27
Al_2O_3	7.18	6.75	2.68	6.24	7.14	3.82	6.17
Fe_2O_3	11.24	11.33	12.97	11.73	11.06	12.98	12.49
MnO	0.21	0.22	0.23	0.24	0.22	0.23	0.23
MgO	23.26	23.74	25.57	23.90	23.79	25.17	23.24
CaO	4.64	4.37	2.50	3.60	4.30	2.43	4.18
Na_2O	0.82	0.69	0.34	0.55	0.71	0.52	0.73
K_2O	0.06	0.03	0.23	0.01	0.06	0.29	0.11
P_2O_5	0.04	0.04	0.09	0.03	0.05	0.14	0.06
Total	97.96	97.47	96.22	93.86	96.98	96.65	96.31
Zn	79	82	94	115	99	103	120
Cu	13	16	18	19	20	25	39
Ni	477	504	552	547	474	531	607
Co	123	208	150	124	176	130	169
Ga	6	6	5	12	10	6	10
Zr	7	8	20	6	8	24	16
Y	5	3	7	5	5	7	6
Sr	72	68	17	54	66	24	55
Rb	2	-	10	-	2	9	5
Pb	-	-	9	-	8	6	8
Cr	4154	9095	11117	33216	23911	23017	24467
V	134	174	193	298	229	266	262
Ba	16	18	24	16	16	66	-
Sc	26	34	24	29	33	38	38
S	90	50	180	160	110	140	200

Samples marked with * are from borehole MDH 29, all others are from MDH 23

S concentrations were determined by infrared absorption spectrometry

Total iron expressed as Fe_2O_3

na = not analysed

\- = below detection limit (see chapter A.II)